ISSN 2078-7405

MINISTRY OF EDUCATION & SCIENCE OF UKRAINE

CUTTING & TOOLS

In Technological System

97'2022

МІНІСТЕРСТВО ОСВІТИ ТА НАУКИ УКРАЇНИ

НАЦІОНАЛЬНИЙ ТЕХНІЧНИЙ УНІВЕРСИТЕТ
«ХАРКІВСЬКИЙ ПОЛІТЕХНІЧНИЙ ІНСТИТУТ»

Ministry of Education & Science of Ukraine
National Technical University
«Kharkiv Polytechnic Institute»

РІЗАННЯ ТА ІНСТРУМЕНТИ в технологічних системах

CUTTING & TOOLS IN TECHNOLOGICAL SYSTEM

Міжнародний науково-технічний збірник
International Scientific-Technical Collection

Заснований у 1966 р. М. Ф. Семко
Found by M. F. Semko in 1966

ВИПУСК № 97
Edition № 97

Харків НТУ «ХПІ» – 2022 – Kharkiv NTU «KhPI»

BBC 34.63
UDC 621.91

State Publication
Certificate of the State Committee of Television and Radio Broadcasting of Ukraine
KB No. 7840 of September 8, 2003
Published by the decision of the Academic Council of NTU "KhPI",
Minutes No. 9 dated November 25, 2022

The collection presents scientific articles that consider topical issues in the field of machining of various modern materials using high-performance technologies, new techniques, measuring devices for quality control of treated surfaces and high-performance cutting tools. Aspects of optimization and mathematical modeling at different stages of the technological process are considered.

For engineers and researchers working in the field of mechanical engineering technology, material cutting, design of cutting tools in technological systems.

The scientific collection "Cutting and tools in technological systems" is included in the List of professional publications of Ukraine of category "B", order of the Ministry of Education and Science of Ukraine dated 17.03.2020, No. 409

R34 Cutting and Tools in Technological Systems: International Scientific and Technical Collection – Kharkiv: NTU "KhPI", 2022. – Vol. – 174 p. : ill.

Address of the Editorial Board: 2 Kyrpychova Str., Kharkiv, 61002, National Technical University "Kharkiv Polytechnic Institute", Department of "Integrated Technologies of Mechanical Engineering named after M.F. Semko, tel. +38 (057) 706-41-43.

BBC 34.63
Materials reproduced from author's originals
NTU "KhPI", 2022

UDC 658.511 **doi: 10.20998/2078-7405.2022.97.01**

P. Telek, Miskolc, Hungary

COMPARISON ANALYSIS OF MATERIAL HANDLING SOLUTIONS OF PRODUCTION WORKPLACES

Abstract: *Production and assembling workplaces can be different in manufacturing and physical environment characterisations, or internal structure, involving the applied material handling solutions, which must be suited to the workplace specifications. The general objective of my research is to develop a model which can help to select the most suitable material handling equipment for production workplaces. The topic presented in this paper deals with the comparison of the different handling solutions. After the overview of the material handling model and the handling equipment selection procedure of production workplaces, a comparison analysis of the applicable handling solutions will be introduced. The last chapter of the paper contains an example for the comparison analysis of a given workplace.*

Keywords: *workplace handling; modeling; material handling equipment; comparison.*

1. INTRODUCTION

The role of the industrial processes is more and more important in the everyday life of people living in everywhere in the World. We use many items for different purposes, most of them are manufactured in special workplaces, so their structure and operation parameters are very important to reach the suitable consumption parameters (quality, price, etc.). Production and assembling workplaces can be different in manufacturing and physical environment characterisations, or internal structure, involving the applied material handling solutions, which must be suited to the workplace specifications. The general objective of my research is to develop a model which can help to select the most suitable material handling equipment for production workplaces. The topic presented in this paper deals with the comparison of the different handling solutions.

This paper presents the material handling model of production workplaces, an overview about the handling equipment selection process for workplaces and the comparison analysis of the applicable handling solutions. To show the applicability of the conception an example will also be presented.

2. MATERIAL HANDLING IN WORKPLACES

2.1. Production workplaces

Production workplace means an object where a given production operation can be realized. There are many types of workplaces which can be different in physical, production, handling, or other aspects [1].

In the international literature, we can find different categories for workplaces based on manufacturing activities, product types, workplace elements, workplace structure, working environment, job characteristics, manufacturing characteristics, operation types, etc.

A **manufacturing activity** means an operation group realized on one element of a production workplace, which can be very different in complexity [2]. There are lot of activities using in a production process depend on the manufacturing characteristics (assembling, cutting, filling, pushing, etc.). A production procedure of a given **product type** requires many different manufacturing activities and working environment [3], and the linking of the activities also determines the workplace parameters (e. g. parallel or linear processes). All manufacturing activity must be realized on suitable **workplace elements**, which also can be different, depend on the applied activity types (manufacturing machines, assembly tables, etc.) [4]. The **workplace structure** defines the relations among the different workplace elements [5], involving the manufacturing and handling activities (U-shape, linear, parallel, etc.). The **working environment** affects the human operators and the machines which realize the activities [6], the most important influencing factors are the temperature, noise, lighting and other parameters (e. g. social and comfort environment). Another important category is the **job characteristics**, which depends on the job type of the human or machine workforce (e. g. baker, painter, woodworker) [7]. The widest category is the **manufacturing characteristics** [8], which involves all production and service sector of the economy and define only some main characteristics (e. g. textile industry, transportation). The **operation type** is also an important parameter because different workplaces must be used for manual, mechanized, full automated or assisted systems [1].

If we build a workplace, all categories must be taken into consideration, however; this research deals only the material handling aspects of the workplaces, so only the types which significantly influence the material handling parameters are important from this aspect.

2.2. Material handling model

Material handling means a simple task to move units from a source object to a destination point. Naturally, the characterizations of the given task can be very different, and the realization process can also be very complicated. If we link some material handling tasks suited to certain logic and take them together into account, we get material handling process as a result [9]. The realization of a given task involved in a handling process always influences all other tasks in the process.

The workplace handling is the smallest part of the material handling system of a manufacturing process. It involves only the handling of input materials and elements, the internal handling of elements and processed units, and the handling of output products of a given workplace [10]. Realization of the workplace handling depends on the physical environment, which contains different functional areas: production, operator, storage, loading, transport, inspection, etc. areas [6], but in this research the model defined in paper [11] was use taking 3 different areas into account: production, operator and storage areas.

The number, size and location of the individual areas can be different depending on the characterisation of the given workplace. In the aspect of the handling process, different workplace variations (head-type, through-flow, complex handling, etc.) can be described based on the external and the internal handling processes [11].

For the analysis of the handling processes of the workplaces a material handling model must be used. If we add vertical sizes to the workplace areas, a prismatic volume is formed [11], which involves the related handling activities as individual points (Fig. 1).

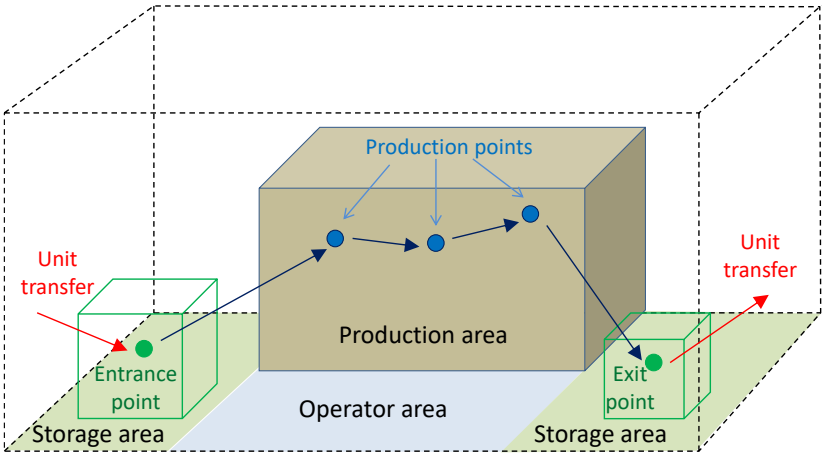

Figure 1 – Simple handling model of workplaces [11]

As Fig. 1 shows, the internal handling process is a chain of different handling operations (blue arrows), which starts at the entrance point, involves different production points (operation, picking and storing points) and is stopped at the exit point. The different steps can be realized individually or combined with others.

Based on the workplace and unit parameters, the general model can be simplified or more complex depending on the given tasks (one-point, two-point, three-point model, etc., see [10]).

3. MATERIAL HANDLING EQUIPMENT SELECTION FOR WORKPLACES

3.1. Planning of material handling

During the planning of material handling, we are looking for suitable equipment and procedure to satisfy the supplying requirements of production processes. The planning process can be realized by system-based or task-based approaching.

The system-based approaching analyses the whole production and handling system and based on the system relations [12]. The most important element of the planning process is the comparison of different handling systems in objects, in devices, in handling tasks or in technology processes. Result of the planning is the adapting of a similar handling system (e. g. similar production firms of multinational companies) [13]. The application of this approach is limited because of the complexity of the material handling systems and the lack of reference handling systems (general databases).

The task-based approaching [14] follows a given or iterative order of different planning subtasks. The optimal solution for the task-based approach, if we realize all required subtasks together, in a predefined order. This integrated planning concept cannot be used in generally, because of the volume, complexity and iterative manner of the different tasks. In the practice, it can be solved only at simple planning cases [15]. Other possibility is the simplification of the integrated planning process to single-task-planning, augmented-planning or complex-planning [9].

There are many solution techniques and methods to solve single planning tasks [16], but their results are limited. During augmented planning the focus is on a single task, but some parameters of other subtasks are also taken into consideration. Complex-planning combines 2-3 subtasks, which are linked by a certain aspect (e. g. technology), its complexity depends on the involved subtasks [17].

According to the increasing of the computational performance and to the development of optimization methods, the integrated planning can be applied more and more complex handling systems, but because of the complexity of the required methods and software applications, users can hardly understand the procedures so they cannot easily accept its using [18]. To avoid this black-box effect, new research concepts started during the last years, e. g. the process-based planning,

which does not target to find the global optimum, but search a suitable and understandable solution using an easier logic [9].

We can see that the planning of material handling is a complex and hard process, but the equipment selection is a very important element of the traditional, the integrated and the process-based planning. In our research the focus is on the application of the equipment selection for the production workplaces.

3.2. Material handling equipment selection

Main objective of the equipment selection is to find the best material handling solution for all handling relations. During the selection process the optimal solution is searched along a given objective function with the comparison of the parameters of the material handling devices and the handling relations.

Materials handling relation means a special connection between two objects which contains any kind of handling activity. Handling relations can be defined by the two linked objects and one handling parameter existing among them [19]. The most important parameters used in handling relations are the types and quantities of the goods, the distances and routes among the objects, the handling costs, the handling time requirements, the handling circumstances and conditions, the disturbing objects and problems, etc. [14].

At the other side the handling machines also have different parameters (e. g. capacities, velocities, loading and transport capabilities) which must take into consideration during the selection process [20].

The equipment selection procedure can be segmented into different steps depends on the compared parameter types, which can be exclusion-type, limitation-type, or numerical parameters [20]. Exclusion-type parameters can exclude the application of certain equipment types (for example: roller conveyor cannot be used for bulk solids). They can be unambiguous exclusions (function, goods type, etc.) and definable exclusions (operation characteristic, handling method, track-line, etc.). Limitation-type parameters do not exclude equipment types, but they can narrow their practical application field (e. g. forklifts cannot be used for individual handling of small boxes). They can be numerical limitations (goods parameters, task parameters, etc.) and not numerical limitations (object parameters, track parameters, etc.). Numerical parameters are the bases of the analytic design process, their values can be different for the individual materials handling machines (route length, energy consumption, etc.).

Based on the different parameter types, the equipment selection procedure has three phases:

1. Exclusion of the non-suitable solutions
2. Taking the limitations into account
3. Comparison of the applicable machine types

In this paper only the third phase is analysed comparing the applicable material handling machine types.

3.3. Equipment selection for workplace handling

The workplace handling is separated into two different parts in the aspect of the equipment: internal and external handling. The task of the external handling machine is to transport goods into the entrance point and take off goods from the exit point. The internal handling machine takes the goods at the entrance point, moves them among the production points and leaves them on the exit point (Fig. 1). There are three different possibilities for the realization of the handling process in the aspect of the workplace handling machine types:

1. Using separate machines for the internal and external handling
2. Using only an external handling machine which also realizes the internal tasks (e. g. forklift)
3. Using only an internal handling machine which can handle the goods on the entrance and exit points, the external machine is only a transporter without loading possibility (e. g. pallet car)

There are different equipment selection steps for the above-mentioned cases, in the first case two independent or parallel procedures must be applied, in the other two situations one complex selection process is required, but in the third case in two parts (the internal handling is the dominant).

In this paper we describe a general equipment selection procedure which can be applied in all three cases using suitable parameter set.

The equipment selection procedure defined in the previous chapter has the next phases for production workplaces:

1. Exclusion of the solutions which are not suitable for workplace handling of the given goods [11]
2. Taking the physical parameters and manufacturing environments of the workplace into account (e. g. safe mounting of crane structure, see [10])
3. Comparison of the applicable handling solutions

This paper deals only with phase 3, where the theoretical principles and methods, or rather the practical application will be presented.

4. COMPARISON ANALYSIS OF HANDLING MACHINES FOR WORKPLACES

After the first two phases of the selection procedure, we can get three different results: only one machine type is usable, there are more than one machines which is applicable or there is no suitable machine type for the tasks. We can use the third phase in all three cases, but the aims are different. If we have only one usable machine, the methods applied for the comparison will be the bases of

the dimensioning process, or the possible subtypes can also be compared. In case of more than one suitable machine types, the comparison procedure is obvious. If we could not find any suitable machine, we must modify the handling parameters and make new handling environment for repeating the first two phases. For the modifications, we can also use the mathematical methods of the comparison phase.

The comparison procedure is based on one or more numerical parameters in every case, the most important ones are the transport distances (vertical, horizontal, etc.), the operation times (transport, loading, waiting, etc.), the predefined limits (e. g. production start time), the machine parameters (capacities, utilizations, etc.), etc.

Some of the above-mentioned parameters cannot be previously defined (e. g. waiting times), so such comparison methods are required which can take the complex and stochastic effects into consideration.

4.1. Comparison methods

The production workplaces and the material handling solutions can be very different, so lot of methods can be used for the comparison analysis [21]: Analytic methods, Mathematic software, Optimisation methods, Simulation methods or Virtual reality software.

For simple comparison we can use **analytic methods** to find the best handling solution, but they can be used only for well determined, special cases (e. g. optimization of transport capacities).

Much more exact comparison can be realized by the using of **mathematic software**, which are also limited in task types, but they can analyse much more versions. Important conditions of their application are the mathematical describability (suitable models and formulas) and the knowledge of the suitable software (MathCAD [22], MatLab [23], etc.).

Optimisation is a new and effective technique to find the best solution for a given task or process. During the optimisation process we create different variations and analyse their efficiency to find an optimal solution. The increasing of the computing capacities and calculation speed of the computers resulted many new methods and algorithms in the practice [24], but this device mainly suit for increasing the operation efficiency.

Simulation methods are the most often used devices for the comparison of different solutions. As this paper will use one of them in the next chapter so their description can be found there.

Another possibility for the comparison of handling machines is the using of **virtual reality software** (VR). There are different definitions for virtual reality [25], but in the aspect of the planning of material handling we can define virtual reality solutions as devices for presentation of simulated 3D objects and their environment. In practice, VR solutions can be used for planning or teaching of

handling processes. In the aspect of the equipment selection, we can use them for virtual comparison of different machines and their behaviours.

4.2. Simulation methods

Simulation is a device to model real processes and evaluate their states, changings and other process elements [14]. Simulation methods usually applicable for modelling of given processes, however they can be adapted for different similar process variations setting their parameters in.

Types and characterisations of the applied simulation process depend on the model, the calculation schemes, the environment and the parameters are taken into account. Based on the large variation of the methods, a huge number of simulation software has been developed during the last decades.

There are also several simulation methods used for the material handling and logistic processes, modelling different elements of the handling procedure [26]. The main application field of simulation software in material handling is the examination of the operation and taking the effects of stochastic changing parameters into consideration. Another important application of the simulation is the preliminary analysis of the designed machines and systems, involving the comparison of alternative solutions.

The most often used simulation methods in material handling are PlantSimulation [27], FlexSim [28], ExtendSim [29], Enterprise Dynamics [30], etc.

Demonstrating the comparison process of the handling variations, a simulation analysis was made using Technomatix Plant Simulation software [27], presented in the next chapter.

5. SCENARIO FOR THE COMPARISON ANALYSIS

5.1. The example workplace

To demonstrate the comparison phase of the material handling equipment selection process, an example production workplace was created. In the example, the model described in [10] was applied with six handling points presented in Fig. 2 and 3, their physical and functional data are involved into Table 1.

Table 1 – Data of the predefined handling points of the example workplace

Handling points	Coordinates			Function	Location
	X	Y	Z		
Point 1	1	1	1	Entrance	Left side
Point 2	3	2	1,5	Production	Front side
Point 3	4	3	1	Production	Inside
Point 4	6	3	1,5	Production	Right side

Point 5	4	4	1,5	Production	Back side
Point 6	1	3	0,5	Exit	Left side

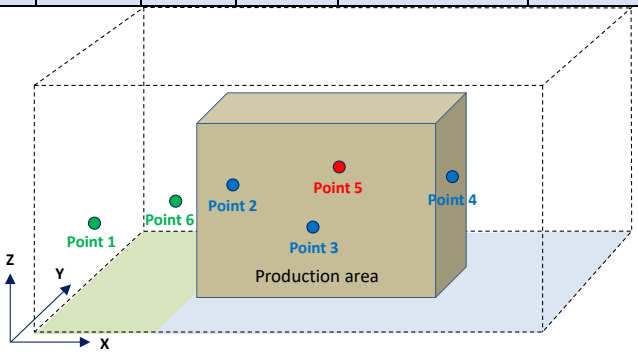

Figure 2 – Structure and handling points of the example workplace

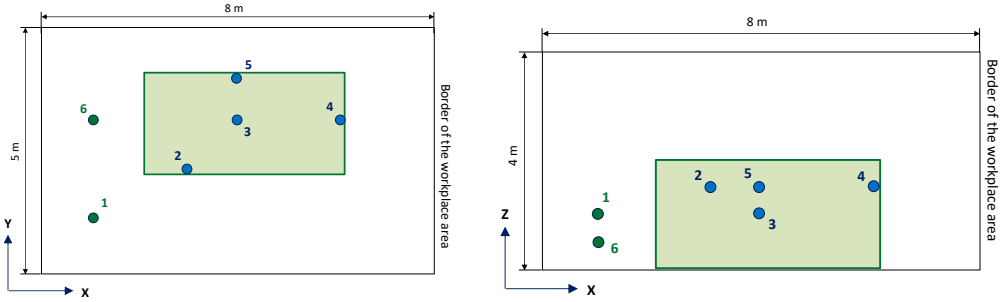

Figure 3 – Horizontal and vertical locations of the handling points

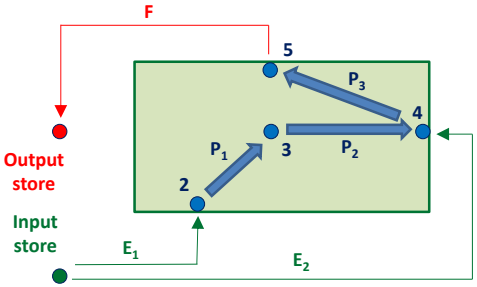

Figure 4 – Manufacturing operations and material flow of the process
(E_1, E_2 –elements transport, P_1, P_2, P_3 –processed units handling, F –finished units transport)

In the production procedure two different elements (single pieces) enter into point 1 in unit loads and are transported individually among the other handling points. Element 1 starts the process in Point 2 as the main part, then moves into Point 3 and 4. Element 2 starts in Point 4 where it is built into the main part. After the union the main part moves to Point 5 and leaves the workplace at Point 6, in another unit load (see Fig. 4).

5.2. The suitable handling machines

Based on the analysis in [10] there are 5 applicable material handling equipment types which suitable for internal handling of small, individual production workplaces (conveyors, running hoists, linear manipulators, jib cranes and articulated robots).

After the previous selection based on the exclusion and limitation type parameters, articulated robots are not suitable for the example because it is hard to reach 3 different sides of an area from outside direction. Linear manipulators are also not so efficient, because they have complex and expansive structure and operation which is not required in this simple case. Running hoists are suitable, however the alternate moving along a long line (near 12 m) is not effective (individual transport of the two elements and the main part). The real solutions are the using of conveyors and jib cranes.

Different conveyor types can be considered for the workplace handling, but the chain driven variations (e. g. trolley-, tow-conveyors) are too complex for small areas. At single piece handling the most usable types are the roller and belt conveyors, however, the frequent changing of the directions can be better realized by rollers (Fig. 5.a).

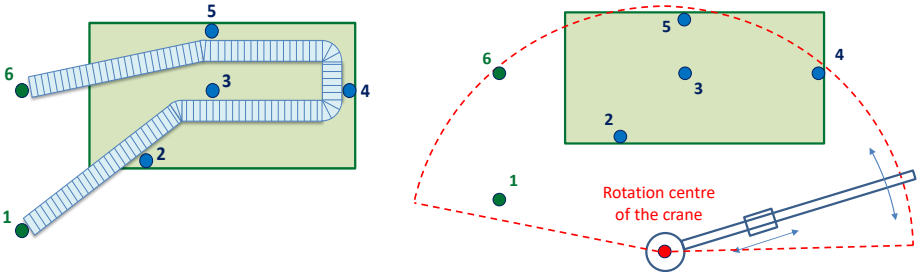

a) Roller conveyor line b) Wall-mounted jib crane

Figure 5 – Handling machine variations

The other possibility is the using of jib cranes, where the workplace determines the application of a wall-mounted crane with a 4-meter-long jib. The location and handling area of the crane are presented in Fig. 5.b.

In the simulation analysis the parameters of these two machines and the manual handling as a reference will be compared (Version A: conveyor, Version B: jib crane and Version C: manual handling).

5.3. The simulation model

To realise the handling process, a simulation model was made in Technomatix Plant Simulation environment, which contains different simulation elements for the handling variations suited to the applied software: production stations, transfer objects, transport line sections, sources and drains (input and output), handling solutions (conveyors, cranes, human resources), buffers and stores, etc.

4 production stations were applied at points 2, 3, 4, 5 (point 4 is an assembling station) for all cases, the handling variations differs mainly in the transfer specifications (represented in the loading time), the number and length of the transport lines and some specification of the handling solutions. Table 2. presents the details of the basic simulation model.

Table 2 – Base data of the simulation model

MODEL PARAMETERS	Version A	Version B	Version C
Handling solution	Roller conveyor	1 jib crane (4m jib)	1 human person
Process times for all stations	120 s	120 s	120 s
Loading operations	Automatic transfer	Lifting and clutching	Manual handling
Loading times for all operations	10 s	10 s	10 s
Transport operations	Continuous moving on conveyor sections	Jib rotation + hoist movement	Manual transport
Transport speed	0,5 m/s	1 m/s	1 m/s
Transport sections	5	11	6+6
Sources	1 input store	1 input store	1 input store
Drains	1 output store	1 output store	1 output store
Internal stores	Only buffers	Only buffers	Only buffers

The number and length of the transport sections of the handling solutions depend on the applied machines and strategies. In case of the roller conveyor, only 5 line-sections (1→2, 2→3, 3→4, 4→5, 5→6) were used which link the stations directly and the 1→2, 2→3 and 3→4 sections were used together for the transport of the elements from the source store to station 4 (see Fig. 5.a).

For the jib crane, passive moving sections also must be defined beside the active transport phases, because the crane must change its position among the loaded activities. The number of the active sections is 6 (1→2, 2→3, 3→4, 4→5, 5→6, 1→4), the theoretical number of the empty movement sections is 13, however it depends on the working strategy, in this case a simple strategy is applied with 5 empty movements (2→1, 3→1, 4→1, 5→1, 6→1). Fig. 6.a presents the applied movement sections for the crane.

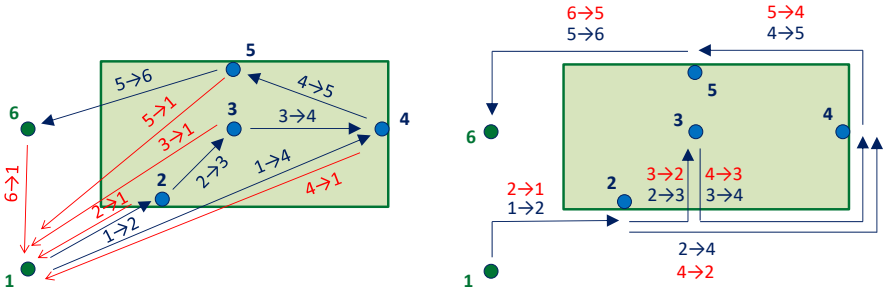

a) Crane handling b) Manual handling

Figure 6 – Transport lines for the workplace
(blue lines –transport sections, red lines – empty movement sections)

There are also exist passive movement sections at human handling solutions, however the number and lengths of them depend on the handling specifications of the workplace. In this case the input and output points are separated, so the human worker must move along an open line and use the active sections for the empty returns (see Fig. 6.b). Because of it, the 5 active sections are obviously (1→2, 2→3, 3→4, 4→5, 5→6), but one relation (1→4) is special, because in the sections 2→3 and 3→4 the worker must step into the production area, which is not needed for the 1→4 relation. To solve this problem, a section 2→4 was created and used sections 1→2 and 2→4 together for transport the elements in relation 1→4. In case of the passive movements the worker must use the active sections in invert directions.

5.4. Simulation results of the versions at the basic model

After running the simulation for all versions with the basic data, the results of the different handling solutions can be compared. During the research the production performance, the transport capacities and the waiting times were used as comparison parameters (Table 3).

Table 3 – Simulation results of the different versions

COMPARISON PARAMETERS	Version A	Version B	Version C
Simulation time [min]	120	120	120
Produced quantity [pcs]	55	44	39
Total waiting times of the handling [%]	72	0	0
Average waiting times of the stations [%]	3,3	20,4	27,9
Total transport distance [m]	952	1412	1945
Average buffer levels [pcs]	1,1	2,5	2,5
Maximum buffer level [pcs]	2	7	7
Loaded handling routes [%]	28	51	50,6
Rise time [s]	603	760	809
Cycle time [s]	120	148	164

The most important cause of the differences among the versions is that at the continuous handling the loading and transport operations are independent from each other because the transport can be parallel. At discontinuous handling the operations directly affect each other in case of one handling machine. If we change the basic handling parameters (loading times and transport velocities) the results will be different (Fig. 7).

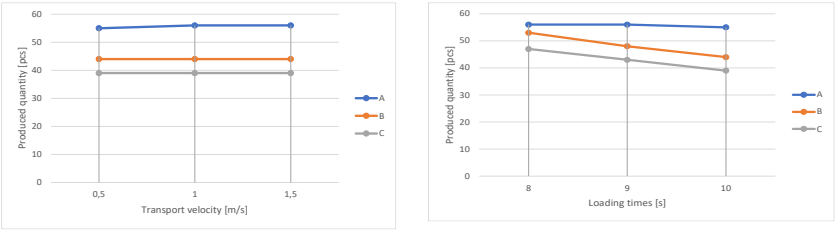

a) handling velocity b) loading times

Figure 7 – Effects of the parameters to the production performance

Fig. 7.a presents that the transport speed has no significant influence on the production process, in all analysed cases the production quantity is almost the same for all versions. However, the loading times are much more important for the production process in case of discontinuous handling machines. The cause of this situation that the model contains 12 loading operations, and the total time of the loading is much more than the total time of the transport operations (at limited workplace area).

As we can see on Fig. 7.b, the reduction of the loading times do not cause noticeable changes for the conveyor, but significantly increases the production performance in the other two cases. The changing is 20% in the production quantity between 10s and 8s loading times, during 2 hours production.

The changing of the loading time also affects the other simulation parameters, Table 4 presents some data in case of 8 s loading times.

Table 4 – Simulation results of the different versions (8 s loading times)

COMPARISON PARAMETERS	Version A	Version B	Version C
Produced quantity [pcs]	56	53	47
Average waiting times of the stations [%]	3,2	6,2	15,5
Rise time [s]	583	644	693
Cycle time [s]	120	124	140

Based on Table 4 we can say that the reduction of the loading time also reduces the cycle time, and a limit value can be calculated where the cycle time reaches the minimum value and the transportation fits to the production time (limit values: 6,3s for manual handling and 7,7s for crane handling). Below the limit value the handling machine must wait at the loading points, above the limit the parts must wait on the buffers which increase the cycle time (Fig 8).

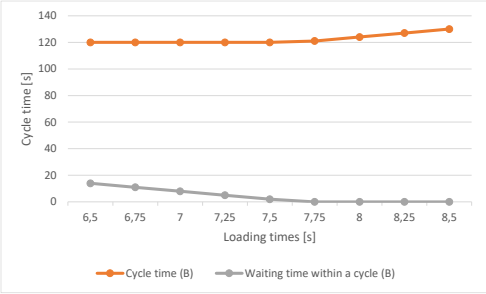

Figure 8 – Effects of the loading times to the cycle time
and the waiting time of the handling machine

5.5. Analysis of the modified production process

Another important parameter for material handling solutions, how it can fulfil the requirements of the changeable production process. Fig. 9.a presents the production quantities of the versions if the process time is changing. It can be seen, that discontinuous machines can not adapt the changing only the conveyor can react and result suitable quantities.

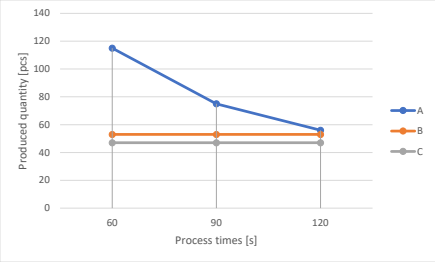

a) Effects to the production

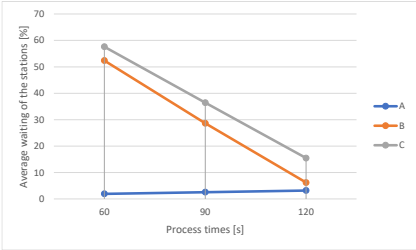

b) Effects to the waiting times

Figure 9 – Effects of the changing of the process times to the versions

The handling solutions in Version B and C are not enough flexible to adapt the changing, their scheduling is determined and cannot be easily modified. In this case, the changing of the process appearing at the stations as waiting times (see Fig. 9.b).

Of course, we can increase the number of the discontinuous machines and it will result better handling process, however this solution is not so easy for cranes in this limited area. Much more usable possibility is the increasing of the number of the human workers, but it requires more complex routing to avoid the disturbances.

5.6. Conclusions of the simulation analysis

Summarising the results of the above detailed analysis of the workplace handling solutions, we can say that

- using of continuous handling machines for workplace handling is effective and flexible solution, but expensive and has continuous energy consumption and maintenance requirement,
- application of discontinuous handling equipment is simple, cheap and effective, but requires exact parameter setting for the optimal operation, which limits its flexibility,

- using of manual workforces is also simple and effective, the handling system can be flexible if the number of the workers is optimized, however in complex cases the route-planning can be hard task.

Another important observation is the importance of the loading times in small, limited areas, which determines the cycle times of the discontinuous handling solutions.

Of course, these consequences are general statements, the actual parameters of the workplace environment can modify the application characteristics of the individual handling solutions.

6. SUMMARY

People use many items for different purposes, most of them are manufactured in different workplaces, so their structure and operation parameters are very important to reach the suitable consumption parameters. There are many material handling solutions can be used in the production workplaces depending on the workplace specifications. The main objective of the research presented in this paper was to compare the different handling solutions of production workplaces. After the overview of the material handling model and the handling equipment selection procedure of production workplaces, a comparison analysis of the applicable handling solutions was introduced. The last chapter of the paper presented an example for the comparison analysis of a given workplace.

As a result of the analysis some statements were described, which can be considered during the planning process of production workplaces.

Of course, the results presented in this paper are only some small parts of the research related to the material handling equipment selection process, and the consequences are general statements, the actual parameters of the workplace environment can modify the application characteristics of the individual handling solutions.

References: 1. *Mark B. G., Rauch E. & Matt D. T.* (2022). Systematic selection methodology for worker assistance systems in manufacturing. *Computers and Industrial Engineering*, **166**, art. no. 107982, https://doi.org/10.1016/j.cie.2022.107982, **2.** *Brankamp, K.* (1980). Gyártási és szerelési kézikönyv. Műszaki könyvkiadó, Budapest, **3.** *Boothroyd, G. & Redford, A. H.* (1968). Mechanized assembly. McGraw-Hill, London, **4.** *Stephens, M. P. & Meyers, F. E.* (2010). Manufacturing Facilities Design & Material Handling. Pearson Education, New Jersey, **5.** *Prabir, J. & Manoj, T.* (2021). Lean Tools in Apparel Manufacturing, Woodhead Publishing, Duxford. **6.** *Dilworth, J. B.* (1979). Production and Operations Management: Manufacturing and Nonmanufacturing. Random House, New York, Toronto, **7.** Bureau of Labor Statistics. "Production Occupations" https://www.bls.gov/ooh/production/home.htm, **8.** Census Bureau. "Definition: NAICS 31-33, Manufacturing", https://www.census.gov/naics/?input=31&year=2017&details=31, **9.** *Telek, P.:* Process-based planning of material handling in manufacturing systems. IOP Conference Series: Materials Science and Engineering 448, 012018. (2018). https://doi.org/10.1088/1757-899X/448/1/012018, **10.** *Telek, P.:* Material handling model of production workplaces. Advanced

Logistic Systems - Theory and Practice 16(1), 51-62, (2022). https://doi.org/10.32971/als.2022.005, **11.** *Telek, P.:* Role of workplace handling parameters in the material handling equipment selection. Journal of Production Engineering 25(1), 53-58, (2022). http://doi.org/10.24867/JPE-2022-01-053, **12.** *Bányai, T.* (2012). Integrált anyagáramlási rendszerek strukturált modellezése. GÉP 63(4), 83-86, **13.** *Telek, P., Cservenák, Á.* (2019). Planning of material handling - literature review. Advanced Logistic Systems - Theory and Practice 13(2), 29-44. https://doi.org/10.32971/als.2020.003, **14.** *Cselényi, J., Illés, B. (ed.)* (2006). Anyagáramlási rendszerek tervezése és irányítása I. Miskolci Egyetemi Kiadó, Miskolc, **15.** *Telek, P.* (2013). Equipment preselection for integrated design of materials handling systems. Advanced Logistic Systems - Theory and Practice 7(2), 57-66, **16.** *Jiang, S., Nee, A. Y. C.* (2013). A novel facility layout planning and optimization methodology. CIRP Annals - Manufacturing Techn. 62, 483-86. https://doi.org/10.1016/j.cirp.2013.03.133, **17.** *Ortner-Pichler, A., Landschützer, C.* (2017). Improving geometry manipulation capabilities of Knowledge-based Engineering applications by the versatile integration of 3D-CAD sys-tems. In CD proc. of MultiScience - XXXI. microCAD Int. Multidiscipl. Sci. Conf. (C1: 3.), University of Miskolc https://doi.org/10.26649/musci.2017.044, **18.** *Welgama, P. S., Gibson, P. R.* (1995). A Hybrid Knowledge Based/Optimisation System for automated Selection of Materials Handling System. Computers Ind. Engng. 28(2), 205-217. https://doi.org/10.1016/0360-8352(94)00200-7, **19.** *Telek P.* (2016). Material flow relations in the design process of materials handling. Advanced Logistic Systems - Theory and Practice 10(1), 53-64, **20.** *Telek P.* (2014). Application of device-preselection for discontinuous unit handling. Advanced Logistic Systems - Theory and Practice 8(1), 93-102, **21.** *Telek P.* & Trummer, W. (2018). Introduction of Demo3D into the scientific education of material handling. Advanced Logistic Systems - Theory and Practice 12(1), 61-76. https://doi.org/10.32971/als.2019.005, **22.** MathCad official website. Retrieved from https://www.mathcad.com/en/, **23.** MatLab official website. Retrieved from https://www.mathworks.com/products/matlab.html, **24.** *Bányai, A., Bányai, T. & Illés, B.* (2017). Optimization of Consignment-Store-Based Supply Chain with Black Hole Algorithm. *COMPLEXITY 2017*, 6038973. https://doi.org/10.1155/2017/6038973 , **25.** *Parisi, T.* (2016). *Learning Virtual Reality*. O'Reilly Media, 1005 Gravenstein Highway North, Sebastopol, CA, USA, **26.** *Tamás, P.* (2017). Decision Support Simulation Method for Process Improvement of Intermittent Production Systems. *Appl. Sci., 7*(9), 950. https://doi.org/10.3390/app7090950, **27.** Plant Simulation official website. Retrieved from https://www.plm.automation.siemens.com/store/en-nl/plant-simulation, **28.** FlexSim official website. Retrieved from https://www.flexsim.com/, **29.** ExtendSim official website. Retrieved from https://www.extendsim.com/, **30.** Enterprise Dynamics official website. Retrieved from https://www.incontrolsim.com/software/enterprise-dynamics/

Петер Телек, Мішкольц, Угорщина

ПОРІВНЯЛЬНИЙ АНАЛІЗ РІШЕНЬ ПО ПЕРЕМІЩЕННЮ МАТЕРІАЛІВ НА ВИРОБНИЧИХ РОБОЧИХ МІСЦЯХ

Анотація. *Загальна мета дослідження — розробка моделі, яка допоможе вибрати найбільш підходяще вантажно-розвантажувальне устаткування для виробничих робочих місць. Тема статті стосується порівняння різних рішень по обробці. Щоб показати застосовність концепції, був наведений приклад. Основною метою вибору устаткування є пошук найкращого рішення для всіх видів вантажно-розвантажувальних робіт. У процесі вибору здійснюється пошук оптимального рішення по заданій цільовій функції з порівнянням параметрів вантажопідйомних пристроїв і вантажно-розвантажувальних відносин. Залежно від типів параметрів процедура вибору устаткування складається із трьох етапів: виключення невідповідних рішень, врахування обмежень і порівняння застосовних типів машин. У цій статті аналізується тільки третій етап, порівняння застосовних типів вантажно-розвантажувальних машин. Процедура порівняння в кожному випадку заснована на одному або*

декількох числових параметрах, найбільш важливими з яких є транспортні відстані (вертикальні, горизонтальні і т.п.), час роботи (транспортування, навантаження, очікування і т.п.), визначені межі (наприклад, час початку виробництва), параметри машини (продуктивність, використання і т.п.). Для реалізації процесу обробки була створена імітаційна модель у середовищі Technomatix Plant Simulation, яка містить різні елементи моделювання варіантів обробки, що підходять для прикладного програмного забезпечення: виробничі станції, об'єкти перевантаження, ділянки транспортних ліній, джерела й стоки (вхід і вихід), вантажно-розвантажувальні рішення (конвеєри, крани, персонал), буфери й склади і т.д. У ході дослідження як параметри порівняння використовувалися продуктивність виробництва, транспортні потужності й час очікування. Підводячи підсумок можна сказати, що використання машин безперервної дії для вантажно-розвантажувальних робіт на робочому місці є ефективним і гнучким рішенням, але дорогим і вимагає постійного енергоспоживання й технічного обслуговування, застосування переривчастого вантажно-розвантажувального устаткування просто, дешево й ефективно, але вимагає точного настроювання параметрів для оптимальної роботи, що обмежує його гнучкість, використання ручної праці також просто й ефективно, система вантажно-розвантажувальних робіт може бути гнучкою, якщо кількість робітників оптимізована, однак у складних випадках планування маршруту може бути складним завданням. У результаті аналізу були описані деякі положення, які можна враховувати при плануванні виробничих робочих місць.

Ключові слова: *робота на робочому місці; моделювання; вантажно-розвантажувальне устаткування; порівняння.*

UDC 669.058+533.924 **doi: 10.20998/2078-7405.2022.97.02**

S. Klymenko, S.An. Klymenko, A. Manokhin, Kyiv, Ukraine,
V. Stolbovoy, V. Beresnev, Kharkiv, Ukraine,
F. Šiška, Z. Chlup, Brno, Czech Republic

STRUCTURE, COMPOSITION AND MECHANICAL PROPERTIES OF MULTI-LAYER VACUUM-ARC NITRIDE COATINGS

Abstract. *The conditions of application of multilayer vacuum-arc nitride coatings on a substrate made from polycrystalline cubic boron nitride (PCBN) are considered using the samples of (TiAlCrY)N/ZrN, (TiZr/TiSi)N, (TiAlSiY)N/CrN compositions. A schematic diagram of a vacuum-arc installation for applying similar coatings is presented, and the technological conditions of coating formation are considered. The structure and composition of the coatings were studied during diffractometric studies, and the performance of coated tools was examined when turning hardened steel. A large amount of the droplet phase in the (TiAlCrY)N/ZrN coating was established. The lattice parameters of two nitrides with an fcc crystal lattice were determined: ZrN – 4.590 Å, TiAlCrYN – 4.203 Å. CSR (coherent-scattering region) of the ZrN phase is 5.4 nm at the microstrain level* $\varepsilon = 4.79 \cdot 10^{-3}$. *High homogeneity and low defects in the thickness of the (TiZr)N/(TiSi)N coating were established – the amount of droplet phase is insignificant. The CSR of the coating is 24.2 nm at the level of microstrain* $\varepsilon = 5.76 \cdot 10^{-3}$, *and the predominant texture orientation is (111). A small amount of the droplet phase was found in the (TiAlCrY)N/CrN coating. Both coating layers are characterized by the formation of phases with a cubic (fcc) crystal lattice, and a strong (111) texture occurs. The crystallographic planes (111) of the phase grains are mainly oriented parallel to the coating interface. The size of the CSR is 14.6 nm. It is shown that multilayer vacuum-arc coatings lead to an increase in the tool life of PCBN cutting tools by reducing the effect of adhesive sticking of the processed material and reducing the intensity of chemical interaction in the cutting zone.*

Keywords: *vacuum-arc technology; multilayer nitride coatings; composition and mechanical properties of coatings; PVD coatings; PCBN cutting tool.*

Introduction. In the engineering industry one of the most important priority directions is surface strengthening and the application of strengthening protective coatings on machine parts, cutting and forming tools, and technological equipment [1]. Increasing the volume of surface strengthening treatment is one of the trends in world practice.

Analyzing modern materials for PVD coatings can be identified two trends in the development of materials for coatings [2–4]. The first consists of creating multi-layer coatings. Each layer performs its own function and ensures a smooth transition of the physical and mechanical properties of the coating from the surface to the base. The second trend is to create multi-component layers.

Protective coatings make it possible to repeatedly increase the durability of machine parts, providing the possibility of intensification of many production processes [5].

Vacuum-arc technologies make it possible to apply hard, dense coatings on the surface of various materials, including non-metallic ones, with high adhesion [6]. The technology allows the application of multi-layer coatings (with a total thickness of up to 50 μm) with unique properties. At the same time, corrosion and erosion resistance, wear and heat resistance, and fatigue strength of products increase [7].

Multi-layer coatings can enhance the stability of tools by 25–200% compared to single-layer TiC and TiCN coatings [8].

During the intermittent cutting of difficult-to-process materials, tools with multilayer coatings, in which «soft» and «hard» layers alternate, showed the best resistance [9].

Multilayer coatings are generally multifunctional [10]. They combine high hardness, wear resistance, resistance to oxidation and adhesive interaction with the contacting material, low friction coefficient, and increased resistance to abrasive wear and oxidation at elevated temperatures.

A new generation of multilayer coatings, consisting of a large number of very thin (~ 10 μm) layers with a composition that continuously changes in thickness and properties, allow solving the problem of the difference in coefficients of thermal expansion and the effect of residual stresses, therefore, avoiding adhesive peeling from the substrate [11, 12].

Multilayer nitride coatings, along with high hardness, have greater plasticity compared to single-layer coatings, making them effective when working under dynamic contact load conditions [13].

The presence of protective coatings on the contact surfaces of products leads to changes in the mechanics and physico-chemistry of the contact interaction [14]. The first is determined by the redistribution of stresses on the surfaces of the parts, a change in the friction coefficient and, as a result, acting forces and temperature. The second is related to the fact that in order to ensure the most optimal conditions for the operation of parts or tools, in each specific case it is necessary to choose such a coating that ensures the minimization or absence of effects that negatively affect their performance. The protective coating should also play the role of a passive protector, which prevents the mechanical interaction of the product and the tool in the contact zone or play a certain role, changing the conditions of direct chemical interaction of their materials [15].

In this regard, the composition and properties of protective coatings can affect the conditions of interaction in the contact zone and thus increase the efficiency of the coated products [16].

In this work, on the example of the compositions (TiAlCrY)N/ZrN, (TiZr)N/(TiSi)N, (TiAlSiY)N/CrN, the conditions for the formation of vacuum-arc multilayer nitride coatings on a substrate of polycrystalline cubic boron nitride (PCBN) are considered, and they are investigated composition and properties.

Methods of research. Vacuum-arc nitride coatings were applied in a modified BULAT-6 installation, the schematic diagram of which is shown in Fig. 1. RNUN 070300 indexable inserts made of polycrystalline cubic boron nitride (PCNB) of the «Borsinit» brand as substrates for deposition. The samples were placed on a metal flat holder located at a distance of 500 mm from the evaporator.

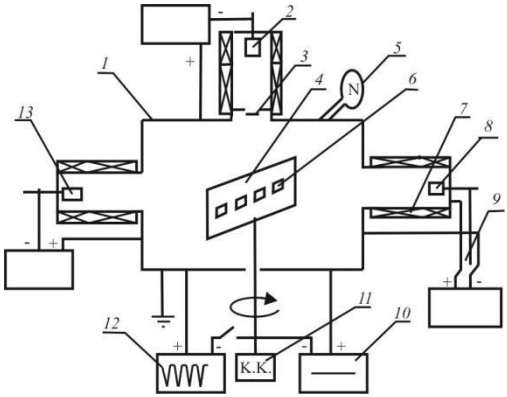

Figure 1 – Schematic diagram of a vacuum-arc installation of the "BULAT-6" type for deposition of nitride coatings with preliminary cleaning in a gas discharge: 1 – vacuum chamber; 2 – vacuum-arc evaporator; 3 – a metal screen that does not allow vaporized metal ions to pass through; 4 – screen-holder of substrates; 5 – nitrogen injector; 6 – samples; 7 – vacuum-arc evaporator housing – anode for gas discharge; 8 – cathode of the same material; 9 – switching relay; 10 – constant voltage source; 11 – command-controller; 12 – pulse voltage source; 13 – cathode of the second material

The vacuum chamber was previously pumped to a pressure of $P = 0.3 \cdot 10^{-3}$ Pa, and ion cleaning and surface activation of the substrates were performed in a gas vacuum-arc discharge. Electrical indicators during the preparation of the substrate for deposition: – current on the cathode I_k = -70 A, current on the anode I_A = 100 A, voltage on the rotary mechanism U_P = -1100 V, voltage from the high-voltage pulse source U_I = -2000 V, frequency 7– 12 kHz. Nitrogen pressure in the vacuum-arc chamber during cleaning P_H = 0.6 Pa. The temperature on the samples was 550–590 °C, the cleaning time in all experiments was 10 min.

After cleaning in a vacuum and heating the samples, a layer of clean cathode material was applied for 1 min.

Deposition of vacuum-arc nitride nanolayer coatings was performed within 60 min. Nitrogen pressure in the vacuum chamber during deposition of coatings P_N = 0.05–0.60 Pa, and the negative potential on the substrate U_P = -100– -200 V was used. Deposition of nanolayer vacuum-arc coatings was carried out using a

command-controller. The vaporizers work simultaneously for 7 seconds and will periodically turn off during the 180° rotation of the substrate by the electric motor. This mode is intended for applying two-phase coatings on flat substrates. Both evaporators, operating for a given time, are turned on at the same time, which determines the thickness of the coating nanolayer, and the rotation system is turned off. On the surface of the substrate, nitrides of the material of cathode 1 are deposited on one side, and materials of cathode 2 are deposited on the other side.

Diffractometric studies were carried out on a DRON-4-07 X-ray diffractometer in copper Cu-Kα radiation using a nickel selectively absorbing filter. The diffracted rays were recorded by a scintillation detector. The characteristics of the diffraction maxima – angular position 2θ, the intensity *I*, and integral half-width *B*, were determined.

The analysis of the substructural characteristics (the size of the regions of coherent scattering *L* and the level of microdeformations ε) was carried out by the integral width of the diffraction lines.

A scanning electron microscope LYRA 3 XMU FEG/SEMxFIB (Tescan, Czech Republic) equipped with an EDS analyser Ultimmax with software Aztec (Oxford Instruments, UK) was used for microstructure observation and elemental analysis of coatings. The surface roughness was calculated from 3D reconstructed surfaces measured by a laser confocal microscope Lext OLS3100 (Olympus, Japan).

Mechanical properties of the coatings (determined by indentation of the interface of the coatings in the polished state) – microhardness and Young's modulus were determined using a universal nanomechanical testing machine Zwick ZHN (Zwick/Roell, Germany) at a load on the indenter of 490.3 mN.

Polishing of the coating interface was performed using a suspension based on ASM 1/0 synthetic diamond powder to obtain a roughness of R_a 0.05.

Testing of cutting tools with polished coatings was carried out during finishing turning with an impact of a sample made of ShKh15 steel (60–62 HRC). Cutting modes: cutting speed v = 140 m/min, feed and cutting depth S = 0.06 mm/rev, t = 0.15 mm. The rake angle of the cutting tool γ = -10°. The width of the flank wear chamfer on the rear surface was measured with a microscope installed on the machine bed with an error of ± 4 μm.

Results and discussion

(TiAlCrY)N/ZrN coating. The surface morphology of the vacuum-arc nanolayer (TiAlCrY)N/ZrN coating shows a rather large amount of the droplet phase of the cathode material (Fig. 2, *a*, *b*). Such a large number of droplets is due to the relatively poor thermal conductivity of the TiAlCrY cathode/target.

A large amount of the droplet phase leads to an increase in the percentage content of elements Ti, Al, Cr, and Y in the coating. At the same time, a bcc

structure was formed that did not form a nitride, which is unfavourable for the coating working on the tool. Likewise, the droplet phase creates difficulties when conducting mechanical tests, in particular, microhardness.

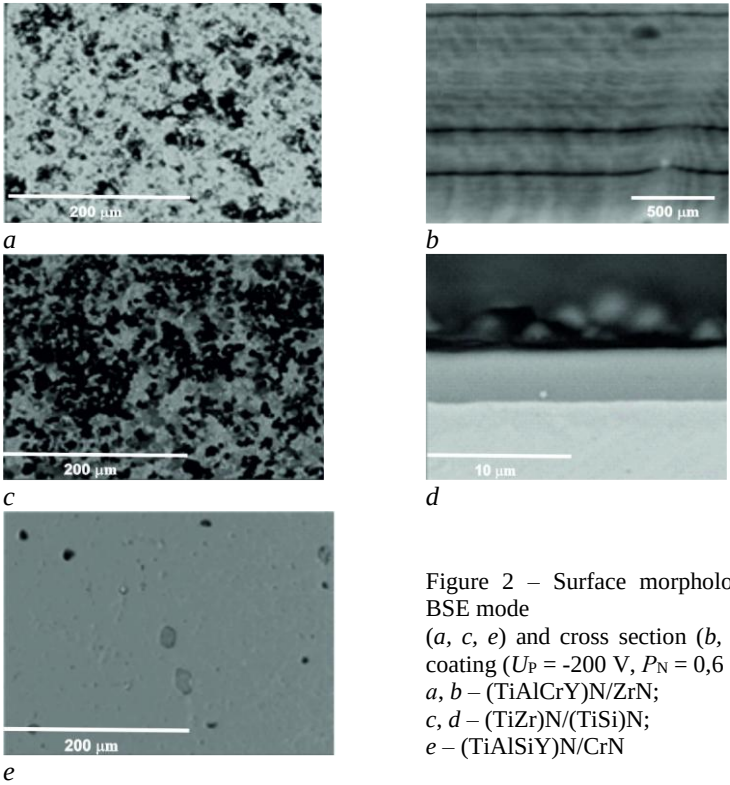

a *b* *c* *d* *e*

Figure 2 – Surface morphology SEM BSE mode
(*a, c, e*) and cross section (*b, d*) of the coating (U_P = -200 V, P_N = 0,6 Pa):
a, *b* – (TiAlCrY)N/ZrN;
c, *d* – (TiZr)N/(TiSi)N;
e – (TiAlSiY)N/CrN

In Fig. 3, the characteristic energy dispersive spectr a of the coating is given. As can be seen, the entire elemental composition of the two cathodes is revealed in the coating.

Considering that the concentration of yttrium in the target was about 1%, this element is not observed in the spectrum of the coatings, since its concentration is most likely below 0.1%.

The microgeometry of the coating interface after its formation (from R_a 0.59 to R_z 3.48) (Fig. 4, *a*), due to the droplet phase, leads to limitations and accuracy of microhardness measurement and research by scratch testing.

Such a developed surface, due to the droplet phase, can negatively affect the wear resistance of a cutting tool with such a coating due to brittle destruction by softer drops.

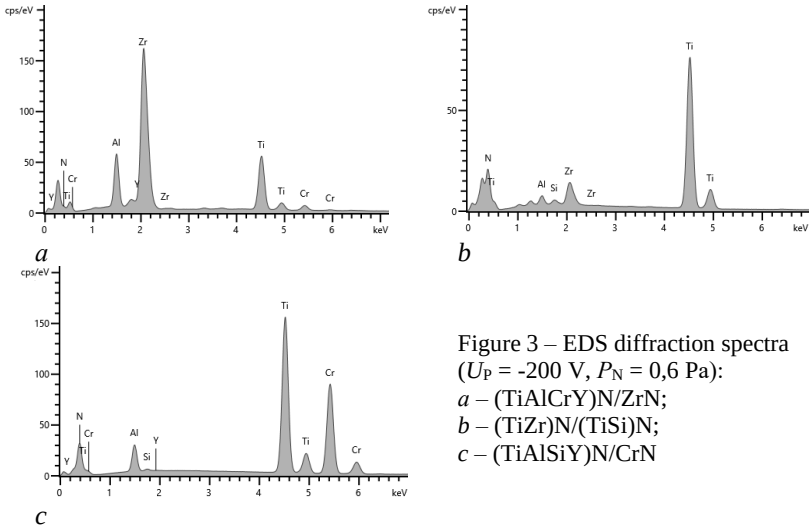

Figure 3 – EDS diffraction spectra (U_P = -200 V, P_N = 0,6 Pa):
a – (TiAlCrY)N/ZrN;
b – (TiZr)N/(TiSi)N;
c – (TiAlSiY)N/CrN

The results of X-ray structural studies and the phase composition of (TiAlCrY)N/ZrN coatings showed the presence of two nitrides with an fcc crystal lattice, ZrN and TiAlCrYN (Fig. 5, *a*). The lattice parameter of ZrN nitride a = 4.590 Å, the size of the coherent-scattering regions of this phase is D = 5.4 nm, and the level of microstrain $\varepsilon = 4.79 \cdot 10^{-3}$. The lattice parameter of vacuum-arc coating TiAlCrYN a = 4.203 Å.

(TiZr)N/(TiSi)N coating. Vacuum-arc deposition of multilayer nitride (TiZr)N/(TiSi)N coatings was carried out from two different TiZr and TiSi cathodes. The period of the (TiZr)N/(TiSi)N layers is 20–30 nm with a total coating thickness of ~ 4 μm. Cathode materials have good thermal conductivity, so the amount of droplet phase on the surface of the tested sample is insignificant. However, the use of silicon in the cathode leads to possible inhomogeneities on the surface of the coating, which is shown in Fig. 2.

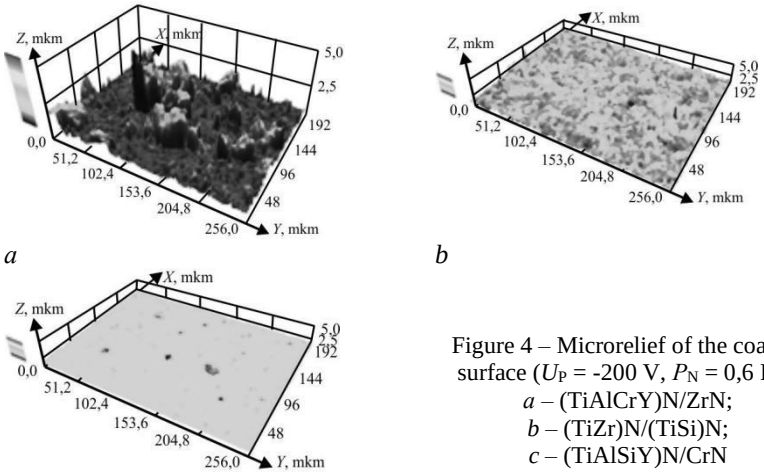

Figure 4 – Microrelief of the coating surface (U_P = -200 V, P_N = 0,6 Pa):
a – (TiAlCrY)N/ZrN;
b – (TiZr)N/(TiSi)N;
c – (TiAlSiY)N/CrN

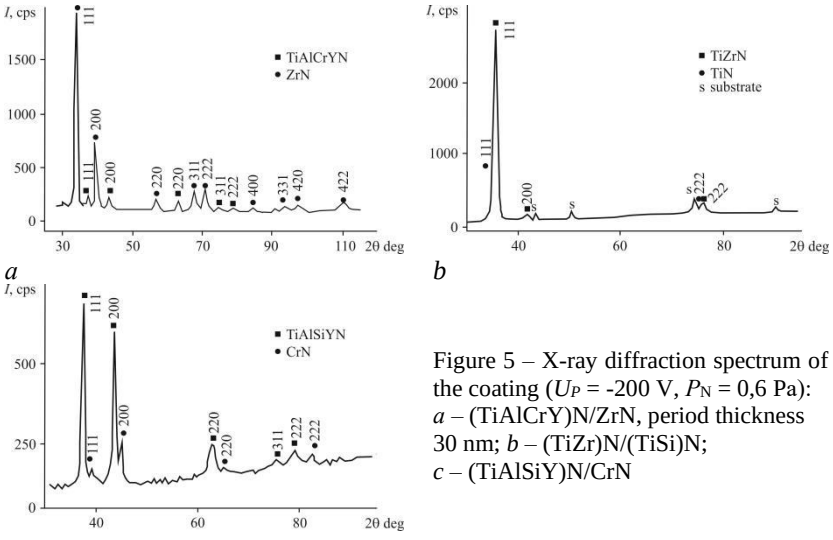

Figure 5 – X-ray diffraction spectrum of the coating (U_P = -200 V, P_N = 0,6 Pa):
a – (TiAlCrY)N/ZrN, period thickness 30 nm; *b* – (TiZr)N/(TiSi)N;
c – (TiAlSiY)N/CrN

As can be seen from fig. 3, *b*, the composition of the coating includes all components of cathodes.

The image of the polished cross-section of the vacuum-arc (TiZr)N/(TiSi)N coating shows high uniformity and low defects throughout the thickness of the

coating (Fig. 2, *d*). This is visible from the analysis of the microrelief of the coating interface after its formation (from R_a 0.1091 to R_z 0.8365) (Fig. 4, *b*).

A decrease in the concentration of lighter elements, especially silicon, was determined in the coating material (Fig. 5, *b*). The CSR size for such a coating is 24.2 nm at the level of microstresses $\varepsilon = 5{,}76 \cdot 10^{-3}$. The intensity analysis and the results of structural studies indicate the predominant orientation of the texture [111], the silicon nitride phase was not detected.

(TiAlSiY)N/CrN coating. On the surface of the (TiAlSiY)N/CrN coating, an insignificant content of the droplet phase was determined, which was deleted after polishing (Fig. 2, *e*).

In Fig. 3, the characteristic energy dispersive spectrum of the coating is shown. It was determined that the formed coating has an almost stoichiometric structure. The chemical composition of the coating corresponds to the elements included in the cathode material, except for yttrium, which was not detected (the reason is described above).

The roughness of the (TiAlSiY)N/CrN coating interface after its formation is low (from R_a 0.0628 to R_z 0.5638) (Fig. 4, *c*), due to the use of cathode materials with good thermal conductivity.

Analysis of the diffraction spectrum (Fig. 5, *c*) shows that the resulting coating is characterized by the formation of phases with a cubic (fcc) crystal lattice in both layers of the multilayer coating.

A disordered solid solution (TiAlSiY)N with crystal lattices of structural type NaCl and CrN is formed in the nitride coating layers. The intensity of the lines in the X-ray spectrum indicates the presence of a strong (111) texture in multi-element nitride and chromium nitride. The grains of these phases are mainly oriented so that their crystallographic planes (111) are parallel to the surface of the sample. The size of the CSR is 14.6 nm.

Mechanical properties of coatings. The microhardness and Young's modulus of coatings are given in the Table. 1.

Table 1 – Mechanical properties of coatings

Coating	Microhardness, GPa	Young's modulus, GPa
(TiAlCrY)N/ZrN	32,3–38,0	395–415
(TiZr)N/(TiSi)N	26,5–28,2	380–430
(TiAlSiY)N/CrN	30,4–36,0	300

Depending on the deposition conditions, the microhardness of the investigated coatings varies in a wide range. It should be noted that the microhardness of coatings can be significantly greater than the microhardness of nitrides (single-layer coatings) included in them. For example, TiAlSiYN coating has a microhardness of 34 GPa, CrN coating – 26 GPa.

When examining the surface of the coatings, no chips or cracks were detected, which reduces the likelihood of defects and cracks forming during thermobaric loading of the coatings when they are used in a cutting tool.

Testing of coatings in a cutting tool. To determine the most promising composition for further research, testing of tools with vacuum-arc coatings of compositions (TiAlCrY)N/ZrN, (TiZr)N/(TiSi)N, (TiAlSiY)N/CrN was carried out. The test results are shown in Fig. 6, where the results obtained for the uncoated tool are also presented for comparison.

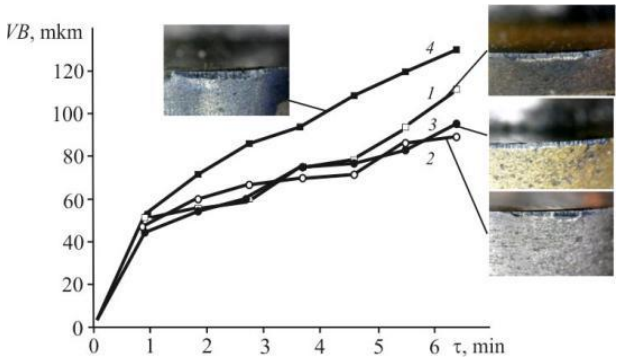

Figure 6 – Dependence of the tool wear on cutting time and contact areas of coated tools (cutting time 6.5 min): *1* – (TiAlCrY)N/ZrN; *2* – (TiZr)N/(TiSi)N; *3* – (TiAlSiY)N/CrN; *4* – without coating

As can be seen, all multi-layer vacuum-arc coatings deposited on the PCBN leads to an increase in the tool life compared to a cutting tool without coating. Coatings perform the role of protection against abrasion, they reduce the effect of adhesive sticking of the processed material, decline chemical interaction intensity in the cutting zone at high temperature conditions, most often protective coating efficency is associated also with a decrease in the coefficient of friction due to formation of thin oxide films on its surfaces. Moreover, they reduce the probability of tool breakage under dynamic load conditions, especially at the stage of the cutting tool penetration into the processed part. Fig. 6 shows the worn areas of the tools, where the width of the flank wear zones of the tools without coating and with nano-layer vacuum-arc coatings is visually different.

Conclusions. On the example of the compositions (TiAlCrY)N/ZrN, (TiZr)N/(TiSi)N, (TiAlSiY)N/CrN, the formation of vacuum-arc multilayer nitride coatings on a polycrystalline cubic boron nitride substrate was considered, their structural features, composition and mechanical properties, the possibility of use in cutting tools when processing hardened steel.

The selection of components for multi-layer coatings allows the development of protective wear-resistant layers on the surface of the cutting tool, the system of which has a hardness of up to 38 GPa.

References: 1. Selinder, T. Performance of PVD TiN/TaN and TiN/NbN superlattice coated cemented carbide tools in stainless steel machining / T. Selinder, M. Sjöstrand, M. Nordin et al. // Surf. Coat. Technol. – 1998. – vol. 105. – № 1–2. – pp. 51–55; **2**. Caliskan, H. Study of nanolayer AlTiN/TiN coating deposition on cemented carbide and its performance as a cutting tool / H. Caliskan, E. Altas, P. Panjan // J. Nano Res. – 2017. – vol. 47. – pp. 1–10; **3.** Veprek, S. Different approaches to superhard coatings and nanocomposites, / S. Veprek, M. Veprek-Heijman, P. Karvankova, J. Prochazka //ThinSolidFilms. – 200. – vol. 476. pp. 1–29; **4.** Hultman, L. Synthesis, structure, and properties of super-hard superlattice coatings, in Nanostructured Coatings / L. Hultman. – New York: Springer-Verlag, 2006. – pp. 539–554; **5**. Vereschaka, A.A. Influence of nanolayer thickness on the performance properties of multilayer composite nano-structured modified coatings for metal-cutting tools / A.A. Vereschaka, J.I., Bublikov, N.N., Sitnikov et al. // Int. J. Adv. Manuf. Technol. – 2018. – vol. 95. – pp. 2625–2640; **6.** Uhlmann, E. Investigation of wear resistance of coated PcBN turning tools for hard machining / E. Uhlmann, H. Riemer, D. Schröter et al. // Int. J. Refract. Met. Hard Mater. – 2018. – vol. 72. – pp. 270–275; **7.** Zhu, D. Tool wear characteristics in machining of nickel-based superalloys / D. Zhu, X. Zhang, H. Ding // Int. J. of Mach. Tools and Manuf. – 2013. – 64. – pp. 60–77; **8.** Manokhin, A.S. Wear Rate of PcBN Cutting Tools Equipped with Nanolayered Protective Coatings / A.S. Manokhin, S.A. Klimenko, V.M. Beresnev et al. // J. of Superhard Mat. – 2020. – vol. 42, № 6. – pp. 423–431; **9.** Manokhin, A.S. Promising types of coatings for PCBN tools / A.S. Manokhin, S.A. Klimenko, S.An.Klimenko, V.M. Beresnev // J. of Superhard Mat. – 2018. – vol. 40, № 6. – pp. 424–431; **10.** Kauffmann, F. Mirostructural size effects on the hardness of nanocrystalline TiN/amophous-SiNx coatings prepared by magnetronsputtering / F. Kauffmann, G. Dehm, V. Schier et al. // Thin Solid Films. – 2005. – vol. 473. – pp. 114–122; **11.** Dobrzański, L.A. Structure and mechanical properties of gradient PVD coatings / L.A. Dobrzański, L.W. Żukowska, J. Mikuła et al. // J. of Mat. Proc. Technol. – 2008. – vol. 201, №. 1–3; **12.** Nanostructured Coatings for High Performance Tools. Reprint // Werkzeug Technik. – 2003. – № 77; **13.** Wang, Chen. Toughness enhancement of nanostructured hard coatings: Design strategies and toughness measurement techniques / Chen Wang, Kaicheng Shi, Cameron Gross et al. // Surf. and Coat. Technol. – 2014. – vol. 257. – pp. 206–212; **14.** Manokhin, A. To the Question of the Mechanism of the Effect of Coating on the Durability of Tools from PCBN / A. Manokhin, S. Klymenko, V. Beresnev et al. // Advanced Manufacturing Processes. – Springer International Publishing, 2020. – pp. 206–215; **15.** Franz, R. Vanadium containing self-adaptive low-friction hard coatings for high-temperature applications : A review / R. Franz, C. Mitterer // Surf. and Coat. Technol. – 2013. – vol. 228. – pp. 1–13; **16.** Tadahiro, W. Tool wear of (Ti, Al) N-coated polycrystalline cubic boron nitride compact in cutting of hardened steel / W. Tadahiro, H. Hiroyuki // IOP Conf. Ser. : Mat. Sci. Eng. – 2017.– 264. – pp. 1–8.

Сергій Клименко, Сергій Анатолійович Клименко,
Андрій Манохін, Київ, Україна,
В'ячеслав Столбовий, В'ячеслав Береснєв, Харків, Україна,
Філіп Шишка, Зденек Хлуп, Брно, Чехія

СТРУКТУРА, СКЛАД ТА МЕХАНІЧНІ ВЛАСТИВОСТІ БАГАТОШАРОВИХ ВАКУУМНО-ДУГОВИХ НІТРИДНИХ ПОКРИТТІВ

Анотація. *Розглянуто умови нанесення багатошарових вакуумно-дугових нітридних покриттів на підкладку з полікристалічного кубічного нітриду бору (ПКНБ) на прикладі композицій (TiAlCrY)N/ZrN, (TiZr/TiSi)N, (TiAlSiY)N/CrN. Наведено принципова схема вакуумно-дугової установки для нанесення подібних покриттів, розглянуто технологічні умови формування покриттів, запропоновано діаграма режиму роботи випарників та обертання підкладки. Структура і склад покриттів вивчено при дифрактометричних дослідженнях, механічні властивості оцінені з використанням нанотвердоміру «Micron-gamma» з індентором Берковича, працездатність інструментів з покриттям розглянута при точінні загартованої сталі. Встановлено велика кількість краплинної фази у покритті (TiAlCrY)N/ZrN. Визначено параметри гратки двох нітридів з ГЦК кристалічною решіткою: ZrN – 4,590 Å, TiAlCrYN – 4,203 Å. ДКР фази ZrN 5,4 нм при рівні мікронапружень $\varepsilon = 4{,}79 \cdot 10^{-3}$. Встановлена висока однорідність і мала дефектність по товщині покриття (TiZr)**N**/(TiSi)N – кількість краплинної фази незначна. ДКР покриття становить 24,2 нм при рівні мікронапружень $\varepsilon = 5{,}76 \cdot 10^{-3}$, переважна орієнтація текстури (111). Встановлена незначна кількість краплинної фази у покритті (TiAlCrY)N/CrN. У обох шарах покриття характерним є утворення фаз с кубічною (ГЦК) кристалічною решіткою, має місце сильна текстура (111). Кристалографічні площини (111) зерна фаз переважно орієнтовані паралельно інтерфейсу покриття. Розмір ДКР становить 14,6 нм. Показано, що багатошарові вакуумно-дугові покриття призводять до збільшення ресурсу роботи різальних інструментів з ПКНБ за рахунок зниження впливу адгезійного налипання оброблюваного матеріалу та зниження інтенсивності хімічної взаємодії в зоні різання та впливі кисню повітря.*

Ключеві слова: *вакуумно-дугова технологія; багатошарові нітридні покриття; склад і механічні властивості покриттів.*

UDC 621.914.22 **doi: 10.20998/2078-7405.2022.97.03**

S. Dyadya, O. Kozlova, D. Karamushka,
E. Kushnir, Zaporozhye, Ukraine

CAUSES OF DIFFERENT WAVES OF MACHINED SURFACES AFTER UP AND DOWN END-MILLING

Abstract. *In modern industry, among the methods of surface treatment is widely used end-milling. Under certain conditions of its use there are self-oscillations, which significantly affect the quality of the treated surface. Various techniques are used to study this influence, in particular, the comparison of the basic fragments of the oscillogram obtained by cutting with the treated surface. It is established that it is formed by the first and last wave of self-oscillations during up and down milling, respectively. But depending on the direction of feed step and the height of the waviness on it have different meanings. Therefore, it is important to determine the reasons that lead to this result. This paper considers the features of each direction of supply that affect the formation of the treated surface. When superimposing fragments of the oscillogram obtained by up milling, it is seen that the deviation of the first wave of self-oscillations from the position of elastic equilibrium starts from the point of incision of the cutter in the part. Therefore, the pitch of the wave on the treated surface depends on the feed and the number of cuts required to cut the first protrusion on the cutting surface. The paper presents a formula for determining the length of the base of this speech. When using it, the discrepancy between the calculated wave step on the treated surface and the measured one does not exceed 4%. In the case of down milling, the last section with waviness on the cutting surface, which is cut and affects the shape of the treated surface, has a shorter base length than the opposite. This is the first reason why the pitch of the wave in the down milling is smaller than in the up. Also at formation of wave on the processed surface at down milling the feature in the form of shift on a phase of waves of self-oscillations on each following cut is observed. This increases the cutting time and the length of the cutting surface. Each subsequent forming depression is shifted towards the treated surface with a decrease in its deviation from the position of elastic equilibrium. However, the phase shift direction is opposite to the feed direction. This is the second reason why the pitch of the wave on the machined surface after the down milling is less than after the up. The calculation of the step of the wave of the treated surface after the down milling according to the results of the study of fragments of oscillograms shows that the error does not exceed 12% compared to the measured one.*
Keywords: *milling; self-oscillation; waviness; pitch; height; cutting surface.*

1. INTRODUCTION

To control the accuracy of machining on metal-cutting machines, it is necessary to know the mechanism for the formation of a machined surface. The results of research in this direction are reflected in publications [1-6, etc.]. For cylindrical end-milling, it is known that the machined surface is formed by sections of the cutting surface that are not sheared after the feed motion.

2. EXPERIMENTS AND DISCUSSION OF RESULTS

Depending on the speed zone of oscillations [7] and the feed direction, the machined surfaces have distinctive features. The presence of waviness on it is typical for milling in the third high-speed zone. However, in it, with the same milling modes, the step Sw and the height Wz of the waviness with counter feed are greater than with the associated one (Fig. 1).

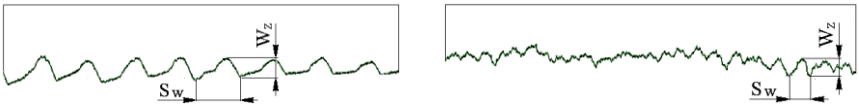

a b

Figure 1 – Profile of machined surfaces after up (a) and down (b) milling

This is confirmed by their values given in table 1. They were obtained after milling samples of Steel 3 on a special stand [8] at a spindle speed n = 280 rpm, a radial depth a_e = 0.5 mm, an axial cutting depth a_p = 3 mm, feed per tooth S_z = 0.1 mm with a single-tooth carbide cutter ∅50 mm.

Table 1 – Step and height of waviness after up and down milling

Feed direction	Waviness step, S_w, mm	Waviness height, W_z, mm
Up milling	2,6	0,103
Down milling	1,08	0,075

The height of the waviness after down milling is 1.37 times, and the step of waviness is 2.4 times less than after the down milling. It was shown in [9-11] that during down milling, the deviations from the position of elastic equilibrium (PEE) on the last wave of self-oscillations, which form the height of waviness on the machined surface, are less than the deviations from PEE on the first wave of self-oscillations during up milling. This explains the differences in waviness heights for different feed directions. To explain the differences in the pitch of the waviness, it is necessary to consider the features of each feed direction during milling.

First of all, it should be noted that up and down milling takes place under different cutting conditions. With up milling, cutting begins with the smallest thickness of the cut layer, with associated milling - with the largest. When milling with self-oscillations, this feature is reflected in the beginning of their occurrence. In up milling, self-oscillations begin immediately after the cutter cuts in, while in

down milling, after a certain time, when the thickness of the cut layer decreases (Fig. 2).

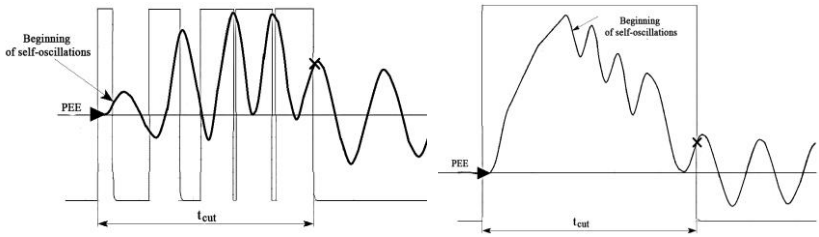

a b

► – inserting a cutter into a workpiece; ×– exit of the cutter from the part;
$t_{рез}$ – cutting time, PEE – position of elastic equilibrium

Figure 2 – Fragments of oscillograms obtained during up (a) and down (b) milling

This feature in both feed directions affects the fact that the profiling zone of the machined surface is always subject to self-oscillations. With up milling, it is formed on the first wave of self-oscillations, with down milling, on the last wave of self-oscillations. A wavy profile on the machined surface is obtained in the form of heredity after cutting off the protrusions on the cutting surface [9-11]. In up milling during the feed movement, the sheared protrusion increases the thickness of the sheared layer and reduces the deviation from the PEE on the first wave of self-oscillations. On Figure 3 shows the overlay of successive fragments of oscillograms that form one wave on the machined surface (for better clarity, fragments of 1, 5, 10, 15, 20, 25 and 27 cuts are shown out of 27 fragments of oscillograms).

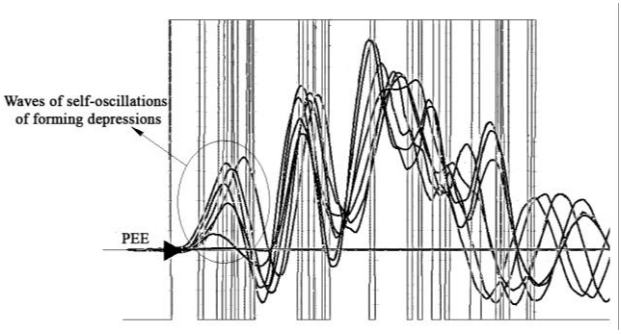

Figure 3 – Overlay of fragments of oscillograms after up and down milling

From Figure 3 shows that all deviations from the PEE of the first wave of self-oscillations start from the point of entry. This means that the step of waviness on the machined surface is formed during the feed movement and cutting off the first protrusion on the cutting surface. The length of the base of the protrusion – L can be calculated by the formula:

$$L = \frac{\pi dnt}{60}, \quad (1)$$

where d – the cutter diameter, mm;

n – spindle speed, rpm;

t – the time from the plunge of the tool into the part and to the cavity behind the first ledge, determined from the oscillogram.

In ongoing research for up milling $t = 3.6 \cdot 10^{-3}$s. Therefore, the sheared protrusion on the cutting surface will have a base length $L = 2.63$ mm. When applied to the tooth $S_z = 0.1$ mm, to cut it, you will need 27 cuts and the step of the waviness will be equal to $S_w = 2.7$ mm, which is close to the measured value. The error between the calculated and measured waviness pitch does not exceed 4%.

In contrast to up-and-down milling, the machined surface is formed at the exit of the cutter. Here, the cut off wavy section of the cutting surface has a shorter base length than with the opposite one. Its length can be calculated by formula (1) based on the time t determined from the last wave of self-oscillations on the down milling waveform. In ongoing research $t = 1.32 \cdot 10^{-3}$ s. In this case, the calculated length of the cut section will be equal to $L = 0.96$ mm. Removing it will require fewer cuts. This is one of the reasons why the undulation pitch is smaller in up milling than in down milling. It should also be noted that the period of self-oscillations during up milling is longer than during down milling (in the ongoing studies, $1.75 \cdot 10^{-3}$ s (571 Hz) and $1.52 \cdot 10^{-3}$ s (657 Hz), respectively). When waviness is formed on the machined surface after down milling, a feature appears in the form of a phase shift – $\Delta\varphi_{1\text{-}2}$ self-oscillation waves on each subsequent cut (Fig. 4).

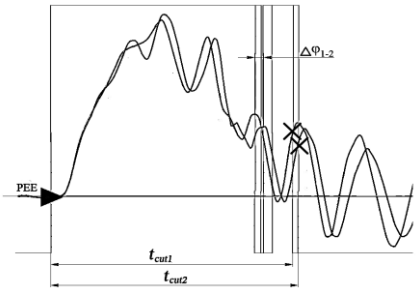

Figure 4 – Phase shift of self-oscillation waves during down milling $\Delta\varphi_{1\text{-}2}$ on the subsequent cut

This leads to an increase in cutting time and the length of the cutting surface. Each subsequent shaping cavity is displaced towards the machined surface with a decrease in its deviation from the PEE. Seventh cut with longest cutting time t_{cut7} (Fig. 5 a), cuts the valley closest to the PEE. It will be one of the peaks of the waviness on the treated surface. The phase shift between cuts had the following values: $\Delta\varphi_{1\text{-}2}$ = 0.175 mm, $\Delta\varphi_{2\text{-}3}$ = 0.117 mm, $\Delta\varphi_{3\text{-}4}$ = 0.087 mm, $\Delta\varphi_{4\text{-}5}$ = 0.204 mm, $\Delta\varphi_{5\text{-}6}$ = 0.2 mm, $\Delta\varphi_{6\text{-}7}$ = 0.2 mm. Total shift $\Delta\varphi_{1\text{-}7}$ = 0.983 mm (Fig. 5 a). In down milling, the direction of feed is opposite to the direction of the phase shift. Therefore, the actual distance between the first and seventh depressions remaining on the machined surface when feeding S_z = 0.1 mm/tooth will be equal to 0.383 mm. The presence of a phase shift in the direction opposite to the feed is the second reason why the step of waviness in down milling is smaller than in up milling. It should also be noted that the depressions from the first to the seventh cut form only half of the waviness pitch. After cutting off the last protrusion from the cutting surface, subsequent cutting begins the formation of the second half of the waviness step.

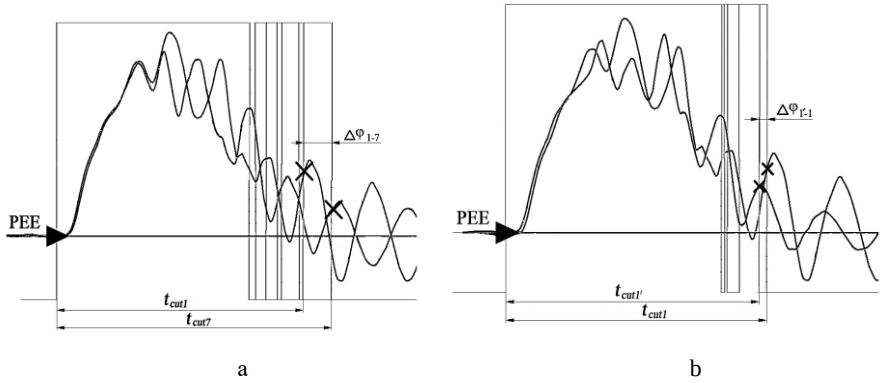

a b

Figure 5 – Overlay of fragments of oscillograms after down milling

During the previous cuts during the feed movement, the workpiece moved by 0.7 mm. The new largest cavity in the machined surface left from the cutting surface formed over time $t_{cut1'} = 8.3 \cdot 10^{-3}$ s, will be at a distance of 0.95 mm from the previous largest cavity left from the cutting surface formed during cutting $t_{cut1} = 8.64 \cdot 10^{-3}$ s (Fig. 5 b). After that, cutting with a phase shift begins and the formation of a new waviness height. With three cuts and a total shift of 0.6 mm, the calculated waviness pitch will be 0.96 mm. The error between the calculated value of the waviness step on the machined surface after down milling and the measured one does not exceed 12%.

3. CONCLUSIONS

1. The common thing in the formation of waviness on the machined surface after up and down milling is cutting off the protrusions on the cutting surface. But with up milling, they are at the beginning of the cutting surface, and with down milling, at its end.

2. In up milling, the length of the base of the protrusion cut off from the cutting surface, which affects the step of waviness on the machined surface, is greater than the length of the base of a similar protrusion during down milling. This is the first reason why the step of the waviness after down milling is smaller than after the up milling.

3. The wavy pitch in up milling depends on the amount of feed and the number of cuts made by the tool when cutting off the first protrusion on the cutting surface.

4. The undulation step in down milling depends on the amount of feed, the number of cuts of the cutter when cutting off the last protrusion on the cutting surface, and the phase shift between subsequent cuts, directed in the direction opposite to the feed direction. This is the second reason why the step of waviness after down milling is smaller than after up milling.

References: 1. *Sokolovskij A.P.* Tochnost' obrabotki na metallorezhushhih stankah. Moscow : Mashgiz, 1952. 289 p. **2.** *Korsakov V.S.* Tochnost' mehanicheskoj obrabotki. Moscow: Mashgiz; 1961. 378 p. **3.** *Kedrov S.S.* Kolebanija metallorezhushhih stankov. Moscow: Mashinostroenie; 1978. 200 p. **4.** *Matalin A.A.* Tehnologija mehanicheskoj obrabotki. Leningrad: Mashinostroenij; 1977. 464 p. **5.** *Reshetov D.N., Portman V.T.* Tochnost' metallorezhushhih stankov. Moscow: Mashinostroenie; 1986. 336 p. **6.** *Kolev K.S. Rosev L.M.* Tochnost' obrabotki i rezhimy rezanija. Moscow: Mashinostroenie; 1976. 144 p. **7.** *Dyaya S.I, Kozlova Ye.B, Kondratyuk E.V, Zubarev A.E, Krishtal V.A.* Systematization of vibrations during end milling of thin-walled elements of parts. Engine Building Bulletin. 2016;1:68-71. **8**. *Vnukov Yu.N, Dyaya S.I, Kozlova Ye.B, Logominov V.A, Chernovol N.N.* Self-oscillations when milling thin-walled elements of parts. Zaporizhzhia: ZNTU; 2017. 208 p. **9.** *Dyaya S.I, Kozlova Ye.B, Germashev A.I, Kuchugurov M.V.* Influence of the self-oscillation period on the formation of the profile of the machined surface during end cylindrical milling. Cutting & Tools in Technological Systems. 2019;91: pp. 24–36. **10.** *Mozgovoy V.F, Dyaya S.I., Kozlova Ye.B, Logominov V.A, Zubarev A.E.* Formation of the profile of the machined surface during end cylindrical milling under conditions of self-oscillation. Bulletin of Engine Building. 2018;1: pp. 92–100. **11.** *Dyaya S, Kozlova Ye, Germashev A, Leschenko A.* Features of Peripheral End milling: Formation of Machined Surface Profile. Advances in Engineering Research. 2019; 188: pp. 184–188.

Сергій Дядя, Олена Козлова, Дар'я Карамушка,
Євгеній Кушнір, Запоріжжя, Україна

ПРИЧИНИ РІЗНОЇ ХВИЛЯСТОСТІ ОБРОБЛЕНИХ ПОВЕРХНОНЬ ПІСЛЯ ЗУСТРІЧНОГО І ПОПУТНОГО КІНЦЕВОГО ФРЕЗУВАННЯ

Анотація. *У сучасній промисловості серед методів обробки поверхонь широко застосовується кінцеве фрезерування. За певних умов його використання виникають автоколивання, які істотно впливають на якість обробленої поверхні. Для дослідження цього впливу використовуються різні методики, зокрема, зіставлення отриманих при різанні базових фрагментів осцилограми з*

обробленою поверхнею. Встановлено, що вона формується першою та останньою хвилею автоколивань при зустрічному та попутному фрезеруванні відповідно. Але в залежності від напрямку подачі крок та висота хвилястості на ній мають різні значення. Тому актуальним є визначення причин, що призводять до такого результату. У цій роботі розглядаються особливості кожного напряму подачі, що впливають на формування обробленої поверхні. При накладанні фрагментів осцилограми, отриманих при зустрічному фрезеруванні, видно, що відхилення першої хвилі автоколивань від положення пружної рівноваги починається від точки врізання фрези в деталь. Тому крок хвилястості на обробленій поверхні залежить від подачі та кількості різів, необхідних для зрізання першого виступу на поверхні різання. У роботі наведено формулу для визначення довжини основи цього виступу. При її використанні розбіжність між розрахованим кроком хвилястості на обробленій поверхні та виміряним не перевищує 4%. При попутному фрезеруванні остання ділянка з хвилястістю на поверхні різання, що зрізається та впливає на форму обробленої поверхні, має меншу довжину основи, ніж при зустрічному. Це перша причина, чому крок хвилястості при попутному фрезеруванні менший, ніж при зустрічному. Також при формуванні хвилястості на обробленій поверхні при попутному фрезеруванні спостерігається особливість у вигляді зсуву по фазі хвиль автоколивань на кожному наступному різі. Це призводить до збільшення часу різання та довжини поверхні різання. Кожна наступна формоутворююча западина зміщується у бік обробленої поверхні із зменшенням її відхилення від положення пружної рівноваги. Однак напрямок зсуву по фазі протилежний напрямку подачі. Це друга причина, через яку крок хвилястості на обробленій поверхні після попутного фрезерування менший, ніж після зустрічного. Розрахунок кроку хвилястості обробленої поверхні після попутного фрезерування за результатами дослідження фрагментів осцилограм показує, що похибка не перевищує 12% порівняно з виміряним.

Ключові слова: *фрезерування; автоколивання; хвилястість; крок; висота; поверхня різання.*

UDC 621.923 **doi: 10.20998/2078-7405.2022.97.04**

V. Lavrinenko, V. Poltoratskiy, O. Bochechka, Kyiv, Ukraine
V. Solod, Kamianske, Ukraine,
Ye. Ostroverkh, V. Fedorovich, Kharkiv, Ukraine

SURFACE MODIFICATION OF SYNTHETIC GRINDING POWDERS DIAMOND WITH HEAT-RESISTANT OXIDES AND CHLORIDES LIQUID PHASE APPLICATION METHOD

Abstract. *The restrictions to the selection of oxides, which may be interesting in the modification of forging heat-resistant oxides of the surface of diamond grinding powders, are defined. It is shown that the first group of the most efficient applied for modifying the surface of the diamond grinding powders includes the following oxides – B_2O_3, TiO_2, SiO_2 and Al_2O_3. The second group, less effective – ZnO, BaO and CaO. To achieve an additional positive effect from the modification it is possible to consider a double modification of surface of diamond grains with a mixture of oxides of the first group and chloride ($CaCl_2$, NaCl). The process of grain surface modification of synthetic diamond grinding powders by heat-resistant oxides and chlorides of metals and non-metals by liquid phase application has been studied. The structural characteristics of the external structure have been studied and the quantitative elemental composition of the surface of modified powders has been determined. It is established that to achieve a guaranteed increase in wear resistance of diamond wheels when grinding hard alloys at least 2 times it is recommended to modify the surface of diamond grains with a combination of oxides: B_2O_3 grain surface modification (50 % grain) and Al_2O_3 grain surface modification (50 %).*

Keywords: *modification; method of liquid-phase deposition, thermal stability; oxides; physical properties; modification of oxides; diamond grinding powders.*

Introduction

Oxygen in cutting processes is an important factor in changing the tribotechnical characteristics of contact surfaces [1]. Oxide layers formed under the action of oxygen or its compounds on contact surfaces significantly reduce friction. And the higher the chemical activity of the metal to oxygen, the more friction is reduced. It is known that in all cases of friction, the presence of oxide film translates the tribosystem into the area of least dangerous oxidative wear.

The protective properties of the oxide film depend on its composition, thickness, hardness of the substrate, etc. [2].

The presence of such an effect is also important for the grinding processes of wheels made of superhard materials (SHM). In [1] the authors determined that to increase the efficiency of grinding processes with wheels with SHM it is possible to apply the following conditions for the delivery of oxygen to the treatment area:

- the bond of the working layer of the wheel must contain materials that are quite actively oxidized (Al, Si, Sn, Cu, Ti, etc.), and it is necessary to create conditions for their oxidation during processing;
- additional, for example, plasma, impact on the working surface of the wheel should be such that oxide films are formed on the bond and on the grains of SHM;
- as supporting elements in the working layer of the circle can be effectively used oxide granular mineral concentrates, especially oxide rutile (TiO_2) concentrates;
- abrasive materials in the form of counterfeit oxide (Al_2O_3) tool ceramics can be effectively used in wheels when processing polymeric materials and cast irons.

Other options for introducing oxygen into the treatment area, as an example, are the use of 0.5% solution of hydrogen peroxide in water [3], i.e. the use of special lubricating and cooling process medium (LCPM). The participation of oxygen as a component of the external environment is the most significant in the lubricating effect of LCPM. The lubricating effect of moist air increases when it is sprayed. Mineral oil enhances the effect of oxygen, as it delivers oxygen to the treatment area, as some hydrocarbon compounds are able to dissolve oxygen in an amount of up to 50 %. When spraying oils, the processes of formation of their oxidation products are activated, which easily give atomic oxygen to the metal surface. The role of oxygen-containing compounds increases with increasing cutting speed. In the case of using oils as lubricants, three factors are important: the oxidative activity of the gaseous medium and its humidity, the oxidation of carbon compounds, the conditions of transfer of molecular oxygen to the friction zones.

Consider what we know from recent scientific publications in this area. Oxygen on the surface of diamonds can be caused by normal oxidation. In [4] it was shown that microcrystalline and nanocrystalline diamond layers behave differently during oxidation. In general, microcrystalline samples were more easily oxidized, and this may be due to the fact that in such a sample with larger diamond grains there is a certain ordering of the amorphous carbon phase, indicating the graphitization of sp^2/sp^3.

In [5] the morphological and structural evolution that occurs during the graphitization of microcrystals of synthetic diamond of cubic octahedral shape at a temperature of 1600 °C in the process of vacuum annealing is studied. It is established that graphitization begins with the vertices and edges of crystals. Octahedral faces {111} are more prone to graphitization than cubic ones {100}. The graphite structures formed during the complete graphitization of diamond microcrystals retained the shape of the original crystals.

The authors [6] investigated the graphitization of diamond under the additional presence of metal, namely titanium during its scribing with diamond.

The diamond graphitization wear is ascribed to the catalytic effect of titanium atoms on crystal structure transformation. When the temperature reached up to 1100 K, Raman shifts peak of graphite corresponding to 1544 cm^{-1} was detected to illustrate the graphite transformation of diamond crystal structure, and the existence of TiO_2 and C–O bond were confirmed to explain the oxidation wear of diamond grain at the atmosphere of air medium.

Let's pay attention to this C–O bond. The possibility of its use was proved by works [7, 8] through graphene oxide. In paper [7], a novel method with addition of graphene in diamond slurry is proposed to conduct CMP lapping of sapphire wafer. Two kinds of graphenes are added including graphene oxide (GO), reduced graphene oxide (RGO). Results indicate that addition of graphene in diamond slurry can significantly increase material removal rate (MRR) of sapphire wafer. MRR of sapphire wafer is proportional to graphene weight fraction. At higher weight fraction, GO/diamond slurry leads to higher MRR than RGO/diamond slurry does.

The tribological properties of oxidized wood-derived nanocarbons (oWNCs), which have the same surface chemical composition as graphene oxide (GO), were investigated as additives in water-based lubricants [8]. WNCs were synthesized from four kinds of Japanese wood powder by metal-catalyzed carbonization, and were strongly oxidized by a modified Hummer's method. The four oWNCs have aggregated chain-like nanostructures and maintain graphitic layers. In particular, the aqueous dispersion of the oWNC derived from Japanese cedar (J. Cedar) wood powder showed a very low friction coefficient and formed a thick tribofilm on the plate surface.

Now let's look at how a diamond reacts to the presence of metals in contact with it. Electroless composite plating is a valuable way to prepare diamond magnetic abrasives [9]. Diamond magnetic abrasives were prepared by the electroless composite plating method using iron particles and micro diamond particles. The experimental results show the adsorption rate of microdiamond particles on iron powder substrate can be forecasted by the established formula.

The above, as well as data on titanium [6], indicate the importance of taking into account the reaction of diamonds with metals, as discussed in [10]. To explore the difficulty of diamond reacting with different kinds of metals and metal oxides, the activation energies of the reaction between diamond and metals, as well as between diamond and metal oxides, were obtained by first-principle calculation. For the transition metals in the fourth period of the Periodic Table of the Elements, when they react with diamond and form corresponding metal carbides, the order of activation energy from low to high is Mn, Fe, V, Ti, Cr, Co, Ni, Zn, and Cu. The calculated results are in accord with unpaired "*d*" electrons theory and previous studies. And when diamond reacts with MnO, FeO, CoO, NiO, and CuO to form

metals and CO, the calculated activation energy in descending order is MnO, FeO, CoO, NiO, and CuO.

As we see, some attention is paid to oxides by researchers, so let's consider it more specifically. Let's start with CuO [11]. Surface morphologies showed that diamond coating can deposit on the substrate with CuO particles. However, CuO particles can lead to the formation of the amorphous carbons with high Raman bands.

In the work [12] W-containing coatings were deposited on the surface of diamond microcrystals by hot pressing using WO_3 as a metal source. After treatment of the mixture at 850 °C for 15 min, WO_2 and $W_{18}O_{49}$ were found on the diamond surface. During the coating formation, the deposition selectivity with regard to the diamond facet was observed. The {100} facets of diamond were preferentially coated. The coating developed through the formation and coalescence of islands, which were of square shape on the {100} facets and of triangular shape on the {111} facets of diamond. In [13] filed the behavior of another refractory compound – V. During sintering, vanadium ions in the bond was enriched on the diamond surface and combined with the unsaturated carbon atom existed on the surface of diamond to form abrasive. Разом з тим, results showed that the refractoriness of the vitrified bond with 4 wt. % V_2O_5 reached 555 °C, 17 °C lower than that of the vitrified bond without V_2O_5.

In the work [14] diamond was modified by coating SiO_2 layer through isothermal hydrolysis method. Diamond abrasives with three different micro-nanoscale particle sizes were chosen to be modified. The results show that SiO_2 thin film is uniformly grafted onto the diamond surface. The results of polishing tests show that the SiO_2-modified diamond abrasives exhibit higher material removal rate and better polishing quality than that of unmodified diamond abrasives.

Given a certain positive from the modification of SiO_2 in a number of works [15–17] another heat-resistant oxide - Al_2O_3 was considered.

In the work [15] diamond powders have been coated with thin layers of Al_2O_3 by atomic layer deposition with the aim of prevent its thermal oxidation. it was found that the weight loss onset temperatures (T_{onset}), that denotes the temperature at which decomposition diamond to CO_2 begins, shifted towards higher temperatures (an increment of ≈ 50 K) as result of protective effect of the Al_2O_3 layer.

Understanding and rationally controlling the interfacial electronic states of the Al_2O_3/diamond (Al_2O_3(001)/C(001)) appears to be crucial in the next generation oxide-semiconductor devices on the basis of diamond. In the work [16] the density functional theory computations are used to systematically elucidate the effects of the different terminated planar of Al_2O_3 and diamond on the electronic properties of the Al_2O_3/diamond interfaces.

Ще один приклад застосування Al_2O_3 поданий в статті [17]. A Cu-Ni-Sn matrix reinforced by Al_2O_3 particles (referred as $CuNiSn/Al_2O_3$) has been developed as a potential substitute for cobalt to fabricate diamond-cutting tools. The new $CuNiSn/Al_2O_3$ matrix is promising for fabricating diamond tools with low cost, high processing efficiency and long service life.

At the end of our review we will also pay attention to some exotic but interesting options for grain surface modification, such as boron - with the formation of B2O3 on the grain surface [18], activation of NaCl [19] and diamond coating with hydrogen [20].

It was demonstrated that the properties of diamond can be improved by surface engineering [15]. It is also important to modify the surface of diamond grains with oxides [21], because it will allow to deliver oxygen to the treatment area.

In this setting, this problem is little studied, and the possibility of their implementation is discussed in this article. Synthetic diamond-polished grinding powders modified with heat-resistant oxides were used as abrasive powders in the working layer of the abrasive tool. This allowed to efficiently deliver the oxides directly to the area of treatment with diamond grains, i.e. directed oxides to the surface of diamond grains. The functions that must be performed by oxides in the treatment area are as follows: to calm the oxidation processes of diamond; to influence the facilitation of plastic deformation of the processed material; change the friction processes in the treatment area; reduce the temperature in the treatment area.

In the first stage, we determined which oxides can perform these functions. At one time, [22] investigated the loss of mass of diamond grains in a mixture with various metals or oxides when heated in air at 900 ± 10 °C for 20 min. It was found that the investigated metals in the experimental conditions are oxidized to form oxides, and therefore the decisive influence on the heat resistance of diamonds are no longer the metals themselves, but their oxides.

It has also been shown that the loss of diamond grains is the lowest in the presence of boric anhydride (B_2O_3), tungsten or tungsten anhydride (WO_3), and zinc oxide (ZnO). Manganese and silicon dioxide (SiO_2) almost do not change the weight loss of diamond grains, and cobalt, copper, nickel and their oxides Co_3O_4, CuO, NiO significantly impair the heat resistance of diamond. From [22] it can also be concluded that in order to achieve the quenching condition of the diamond oxidation process, it is desirable to have metals or oxides in contact with it with low melting points. In addition, since diamonds are compressed in the bond of the working layer of the wheel, it is desirable that the oxides do not have large values of coefficient of thermal expansion and specific heat.

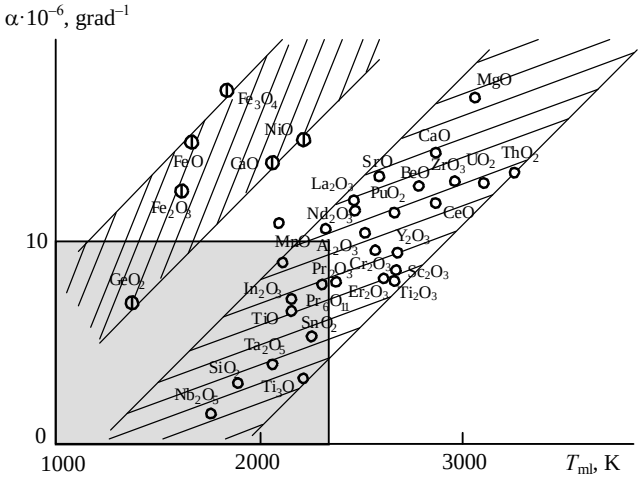

Figure 1 – Correlation between melting point and CLTE of oxides

We analyze the relationship between data on thermal expansion and other properties of oxides and carbides, given in [23, 24]. It is known [25] that thermal expansion is closely related to the parameters characterizing the state of a solid, and there are such dependences for metals, but the authors of this article did not find similar generalized data for oxides and carbides. It is known [26] that for metals the coefficient of linear thermal expansion (CLTE) is the lower, the higher the melting point of the metal. For oxides, as we found in the analysis of the data set [23, 24], there is an inverse relationship: with increasing melting point (T_{ml}) of oxides, their CLTE increases (Fig. 1). In fig. 1 shows that the oxides of metals of group VIII – iron, cobalt and nickel, as well as germanium occupy a separate area parallel to the main.

A similar grouping is observed in the analysis of the relationship between CLTE and standard molar heat capacity of oxides (Fig. 2). Analysis of the relationship between density and heat capacity shows that with increasing oxide density, the standard heat capacity increases slightly (see Figure 2). Significant growth is observed for oxides containing Me_2O_3. In general, the above-described grouping by valence of the metal oxide is observed. Therefore, oxides have a number of characteristic features, the analysis of which can be useful, for example, in explaining the behavior of ceramics in heating or the choice of oxides for modification of oxides on the grain surface.

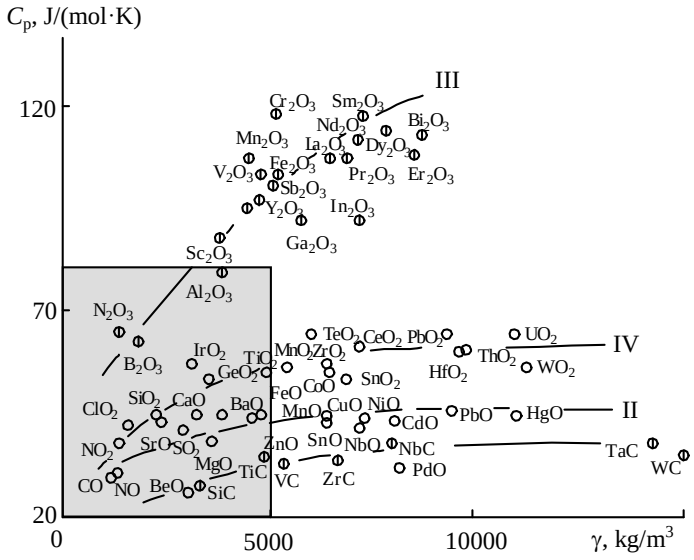

Figure 2 – Correlation between density and specific molar heat capacity of oxides and carbides; Roman numerals indicate the valence of oxide metals

Taking into account the experimental data obtained by the authors [1] on the introduction of oxides in the contact zone of the grinding wheel and the workpiece and the above correlations, it was determined that for the modification of grinding grains impractical. Other restrictions, according to the authors, are restrictions on the melting temperature of such oxides – no more than 2300 K (see Fig. 1), on the specific molar heat capacity – no more than 80 J/(mol·K) (see Fig. 2) and by the density of oxides - no more than $5 \cdot 10^3$ kg/m^3 (see Fig. 2). Given the above limitations, the oxides that can be used in the modification of heat-resistant oxides of the surface of diamond grains include a significant part of the oxides of the group MeO_2 (TiO_2, SiO_2, GeO_2, SnO_2). Oxides of Me_2O_3 (N_2O_3, B_2O_3, Al_2O_3), as well as MeO (TiO, BaO, BeO, CaO) can be used to a lesser extent. According to the authors, the use of Me_2O_5 oxides for modification is inexpedient. In addition, beryllium oxide (BeO) should be excluded, as it, like other beryllium compounds, is a carcinogen.

Now let's look at the following. Aqueous solutions of LCPM based on alkali metal salts (electrolyte solutions) are often used in the process of diamond-abrasive grinding of hard alloys and tool steels and ceramics. High grinding temperatures do not exclude the possibility of simultaneous presence in the treatment area of both saturated saline solutions and alkali metal oxides. Sufficient oxygen, air, water and

thermal decomposition products of LCPM elements promote rapid oxidation of the metal surface. The growth of oxidation products is facilitated not only by high temperatures in the cutting zone by the grinding wheel, but also by the accumulation of electric discharges on the treated surface with a positive potential relative to the mass of the machine arising from abrasive grains on metal (thermoelectric effect). In this case, there are conditions for electrochemical reactions of anodic dissolution on the entire surface to be treated [27]. In the case of LCPM diamond treatment, impurities, often organic, containing chemically active elements: sulfur, chlorine, phosphorus, iodine, etc., which are released mainly in the contact zones during thermal decomposition of impurities, are introduced to increase the lubricating effect. The mechanism of lubricating action of impurities is based on their ability to form in the contact zones solid lubricating layers of the corresponding inorganic metal salts, thereby chemically modifying the surface. Combined impurities containing sulfur, chlorine and phosphorus are used simultaneously to expand the capabilities of LCPM [27]. Of these impurities can be considered salts of chlorides – $CaCl_2$, NaCl, $BaCl_2$, $MgCl_2$, $FeCl_3$, KC1, of which the most environmentally friendly are $CaCl_2$ and NaCl.

In general, this suggests that by analogy with the described action of LCPM can also be considered a double modification of the grain surface of diamond grinding powders with a mixture of oxides and chlorides, which can give an additional effect when modifying the surface of diamonds.

Therefore, the analysis of the above allowed us to draw the following conclusion. The first group, of most effectively used to modify the grain surface of diamond grinding powders, include the following oxides: B_2O_3, TiO_2, SiO_2 and Al_2O_3, the second group, less effective - ZnO, BaO and CaO. To achieve an additional positive effect from the modification, we can consider double modification of the surface of diamond grains with a mixture of oxides of the first group and chlorides ($CaCl_2$, NaCl).

Indirectly, our conclusions are confirmed by the data of [28], where it is shown that the addition of ZnO promotes the formation of oxygen polyhedra and at the same time a large amount of lean oxygen in the glass mesh, which leads to increased wettability of glazed bonds and the formation of –C=O, –O–H and –C–H bond on the surface of diamond grains.

Now, in the second stage, we will understand the issues of surface modification of diamond grain grinding powders.

Our previous studies [21] found that it is promising to modify the grain surface of diamond grinding powders with heat-resistant inorganic non-metallic coatings (oxides and chlorides of metals and non-metals) by liquid-phase application. The most economically advantageous method is the liquid-phase application of the modifier - from aqueous solutions of oxides and chlorides of metals and non-metals.

Materials and methods of research

For research, average samples of raw materials were selected: grinding powders of synthetic diamonds: AC6 125/100 and AC15 250/200, metallized Ni. The grain surface of the powders was modified by the isothermal method of liquid-phase application from saturated solutions of both heat-resistant oxides (B_2O_3), chlorides ($CaCl_2$, NaCl, $MgCl_2$, $FeCl_3$) and their mixtures (B_2O_3 + $CaCl_2$, B_2O_3 + NaCl).

Determination of structural and morphological characteristics of the external structure and quantitative elemental composition of modified powders was performed using a scanning electron microscope (SEM) ZEISS EVO 50XVP, equipped with energy-dispersive X-ray spectrum analyzer INCA ENERGY 450.

Modification of the surface of powder materials by the method of liquid-phase application is the process of precipitation of the modifier substance released (crystallized) from the solution in the form of crystals or films on the surface of a solid (in our case, diamond grinding powder).

The fixation of the modifier on the grains of this powder is due to the process of physical adsorption, the phenomenon of absorption by some solids of gases, salts, etc. substances from solutions. The active centers that exist on the surface of synthetic diamond grains are the primary fixation centers of the modifier [13]. We point out the following features of physical adsorption: first, it is a weak type of interaction, because it is not caused by electronic transitions, but only by changing the nature of electron motion in adsorbent and adsorbate particles, and secondly, adsorbed particles retain their molecular nature. that is, they are chemically unchanged. Therefore, this interaction is considered molecular [29]. In our process of physical adsorption (modification) the adsorbent was synthetic diamond grinding powder, the adsorbate was a precipitated layer of the modifier substance (B_2O_3/NaCl/$CaCl_2$/ ...), the adsorbent was a saturated solution of the modifier substance.

In the liquid-phase method of forming a precipitated layer from a solution of heat-resistant compounds (for example, B_2O_3, $CaCl_2$, $MgCl_2$, $FeCl_3$, etc.), when a substance is deposited on the grain surface of a powder material, its crystallization occurs. This is the case for a saturated solution and is positive because it helps to achieve a sufficient thickness of the precipitated layer. According to our research, even with a short duration of the modification process, the size of the crystals formed is much smaller (by one or two orders of magnitude) compared to the size of diamond grains.

Discussion of experimental results

The investigated powder - synthetic diamond grinding powder (25 ct) was mixed with 10–15 ml of saturated solution of the modifier substance using a

magnetic stirrer for 10 minutes under normal conditions. Excess solution was drained and the remaining mixture was filtered. The obtained wet mass of powder was dried with stirring at a temperature of 120 ºC to a dry homogeneous state. After coating by gravimetry, the relative amount of the modifier was determined, as well as the change in heat resistance of the modified powders. Heat treatment of both original and modified samples was carried out in air in a tubular furnace at a temperature of 800–900 ºC for 30 minutes. The coefficient of heat resistance K_{ml} was determined by the loss of mass of the samples (Table 1).

Table 1 – The results of modification of synthetic diamond grinding powders with saturated solutions of heat-resistant oxides and chlorides

№	Samples	Modifier	The amount of modifier,%	K_{ml}
1	AC6 125/100	$CaCl_2$ (*)	8.2	0.95
2	AC6 125/100	NaCl	9.7	0.98
3	AC6 125/100	B_2O_3	6.3	0.98
4	AC6 125/100	B_2O_3 (тричі)	7.4	0.98
5	AC6 125/100	$MgCl_2$ (*)	6.0	0.92
6	AC6 125/100	$FeCl_3$ (*) (5 мл р-ну)	5.2	0.97
7	AC6 125/100	B_2O_3+$CaCl_2$ (*)	8.7	0.94
8	AC6 125/100	B_2O_3+NaCl	9.2	0.98
9	AC15 250/200 (Ni)	B_2O_3	5.9	0.95
10	AC6 125/100 output			0.91

** Hygroscopic powders*

The degree of coverage of diamond grains, for example, with boron oxide (B_2O_3) is on average 5.64% (B_2O_3 density – 2.55 g/cm^3, diamond density – 3.56 g/cm^3).

From the data in Table 1, we pay attention to the fact that virtually all grinding powders with grains that have undergone surface modification have a coefficient of heat resistance higher than the original diamond powder. Moreover, the largest values of the coefficient are characteristic of the conditions of grain surface modification with boron oxide (B_2O_3).

In Figure 3 shows a sample of grinding powder of diamond AC6 125/100, three times modified with B_2O_3 oxide – sample № 4 (see Table 1), and shows the areas in which the elemental composition of the grain surfaces of the sample was determined by local X-ray spectral (LRS) analysis.

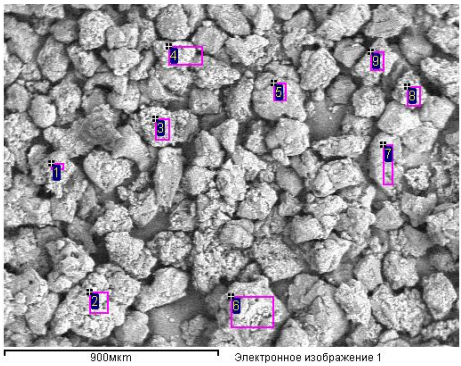

Figure 3 – Areas subjected to elemental analysis on the grain surface of sample № 4 and their quantitative elemental composition % wt.:

Spectrum	Researched elements		
	B	*C*	*O*
1	10.05	28.63	61.32
2	12.53	19.69	67.79
3	4.85	41.01	54.14
4	8.87	28.78	62.35
5	0.00	34.53	65.47
6	7.16	37.88	54.96
7	5.17	72.26	22.58
8	9.44	41.60	48.97
9	8.52	26.96	64.52

As you can see, the results of quantitative LRS analysis of sample № 4 (three times modified B_2O_3) show the content of carbon (diamond) from 72.26 to 19.69 %, boron from 0.0 to 12.53 %, oxygen from 22.58 to 67.79 %.

Thus, we have described above the features of surface modification of synthetic diamond grinding powders both separately with heat-resistant oxide (B_2O_3) and in combination with chlorides (NaCl, $CaCl_2$).

In the future, we studied the performance characteristics of diamond wheels with grinding powders of synthetic diamond brand AC6 with the above surface modifications.

Heavily machined tungsten-titanium-cobalt hard alloy brand T15K6 with sample sizes 63x15x7 mm was selected for processing. Grinding modes: wheel rotation speed - 18 m/s, transverse feed – 0.05 mm/double stroke, longitudinal feed – 0.57 m/min (for processing productivity of 200 mm^3/min) and 1.14 m/min (for processing productivity of 400 mm^3/min). Grinding was carried out without

cooling, so as not to introduce additional disturbances in the processing process, as it is unknown at this time the possibility of possible interaction of chlorides with the components of the process fluid, which may be the subject of further research. The wear resistance of the grinding tool was evaluated according to the relative consumption of diamonds (q) and the roughness of the treated surface according to (R_a). The test results are given in table. 2.

Table 2 – Performance of diamond grinding wheels on a polymer bond B2-08 with a relative grain concentration of 100% with different options for surface modification of diamond grains brand AC6 125/100

Modification of a surface of diamond grains in a working layer of diamond wheels 12A2-45° 125x5x3x32	Processing productivity:			
	200 mm^3/min		400 mm^3/min	
	q, mg/g	R_a, mkm	q, mg/g	R_a, mkm
Modification of B_2O_3 grain surface (50 % of grains) and modification of Al_2O_3 grain surface (50 %)	7	0.37	17	0.43
Modification of $CaCl_2$ grain surface (100 %)	9	0.37	20	0.41
Modification of B_2O_3 grain surface (50 % of grains) and modification of $MgCl_2$ of grain surface (50 %)	12	0.40	24	0.41
Modification of $FeCl_3$ grain surface (100 %)	15	0.48	26	0.43
AC6 125/100 B2-08 100 without modifying the surface of the grains	**17**	**0.31**	**37**	**0.52**
Modification of NaCl grain surface (100 %)	17	0.33	46	0.44
Modification of B_2O_3 grain surface (100 %)	25	0.45	32	0.49
Modification of a mixture (B_2O_3 + $CaCl_2$) of grain surface (100 %)	22	0.45	43	0.40
Modification of the mixture (B_2O_3 + NaCl) of the grain surface (100 %)	343	0.36	–	–

Let's analyze the results of table. 2. First in terms of wear resistance of the diamond tool. At once we will pay attention that 100% modification of a surface of diamond grains by pure oxide B_2O_3 and its mix with chlorides of $CaCl_2$ or NaCl on productivity of processing of 200 mm^3/min only increases the wear of the wheel. Note that the modification of the grain surface exclusively NaCl does not actually

affect the wear of the wheel, but such modification in a mixture with B_2O_3 is unacceptable, because it immediately translates the wear of the wheel in the area of catastrophic wear, which does not allow research on such a wheel min. (see Table 2).

And what modification allows to increase wear resistance of a diamond wheel?

First, it is pure chlorides of $CaCl_2$ and $FeCl_3$.

Second, combined modification, when 50 % of the grains are modified with B_2O_3 oxide and the other 50 % of the grains are modified with $MgCl_2$, chloride or Al_2O_3 oxide. We place the specified modification in a row as wear resistance increases:

$$No\ modification - FeCl_3 - B_2O_3/MgCl_2 - CaCl_2 - B_2O_3/Al_2O_3.$$

The difference in wear resistance for the first (without modification) and the last (for B_2O_3/Al_2O_3) link of this series is 2.43, i.e. the wear resistance of the diamond wheel when modified with a combination of B_2O_3/Al_2O_3 increases by 2.43 times. This range for a productivity of 200 mm^3/min.

And what will happen with a 2-fold increase in productivity? In fact, the location of this series has not changed, but it included modifying the surface of the grains with B_2O_3 oxide, and here this series looks like this:

$$No\ modification - B_2O_3 - FeCl_3 - B_2O_3/MgCl_2 - CaCl_2 - B_2O_3/Al_2O_3.$$

For higher processing productivity of 400 mm^3/min the difference in wear resistance for the first (without modification) and the last (for B_2O_3/Al_2O_3) link of this series is already 2.18, i.e. the wear resistance of the diamond wheel when modified with a combination of B_2O_3/Al_2O_3 increases by 2.18 times. That is, modification of the surface of diamond grains with a combination of B_2O_3/Al_2O_3 is guaranteed to double the wear resistance of diamond wheels, both at low and high processing productivity.

An indirect conclusion from the above is that at low processing productivity chlorides occur in the above series three times, and B_2O_3 oxide – twice. With increasing productivity of processing chlorides and the specified oxide already occur equally - three times. In both cases of productive processing, it is best to modify the surface of diamond grains with a combination of B_2O_3/Al_2O_3.

From the table 2 also shows that the modification of the diamond surface with NaCl chloride, both alone and in a mixture with B_2O_3, is negative and the use of these two modifications for diamond powders is unacceptable. Note also that the modification of the mixture ($B_2O_3 + CaCl_2$) of the grain surface also does not give a positive effect.

Now, before considering the impact of grain surface modification on the roughness of the treated surface, let's pay attention to the state of the cutting layer

of diamond wheels in different modifications, because this is what determines the roughness.

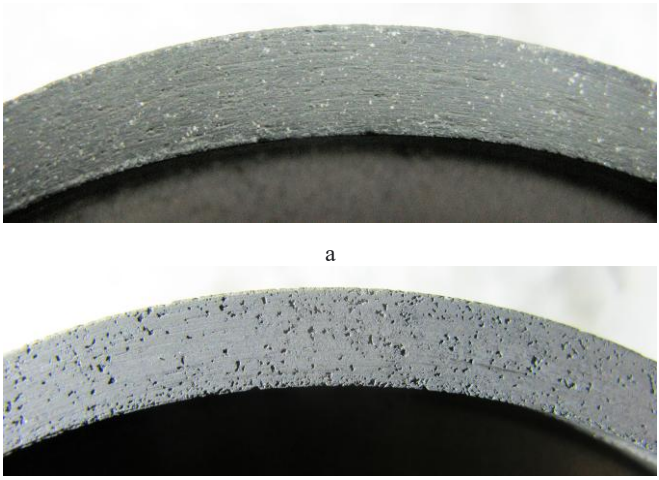

a

b

Figure 3 – Condition of the cutting surface of a circle with diamond grains with modification of their surface with a mixture of – (B_2O_3 + $CaCl_2$): a – in the initial state, b – after grinding a hard alloy with a capacity of 400 mm^3/min

In the case of modification of the surface of diamond grains with the use of chlorides, certain disturbances occur on the cutting surface. Thus, if we compare the cutting surface of the circle, for example, when modifying the surface of diamond grains with a mixture (B_2O_3 + $CaCl_2$) in the initial state (Fig. 3, a) and after grinding hard alloy T15K6 (Fig. 3, b), we see that many wells appear on the cutting surface, probably from torn diamond grains, i.e. the diamond content here is deteriorating. Similar surfaces are formed when modified with the participation of other chlorides: NaCl, FeCl3 and mixtures – (B_2O_3 + $CaCl_2$) and (B_2O_3 + NaCl). The reason for this effect of chlorides on the cutting surface of the wheel is unclear and requires further research. Perhaps the peculiarities of diamond content of chloride-modified diamond grains contribute here.

Of course, such changes in the cutting surface can not but affect the roughness of the treated surface, which we will consider below. Note that the productivity of grinding has a significant impact. If at low productivity in 200 mm^3/min grinding wheel with diamond grains without surface modification gives the lowest value of the roughness of the treated surface according to the parameter R_a (Table 3), then at a much higher productivity of 400 mm^3/min the same wheel already gives the largest values of roughness on the parameter R_a (Table 4). In this

case, in the first case, close to the original wheel (within 20 % deviation) indicators for the parameter R_a (see Table 3) have wheels with subsequent surface modifications of diamond grains (in a row as the parameter R_a increases):

No modification – NaCl – B_2O_3/NaCl – ($CaCl_2$ – B_2O_3/Al_2O_3).

In turn, for productivity of 400 mm^3/min roughness indices differ less (see table. 4) and those that differ the least, it is possible to arrange in a row as the parameter R_a:

No modification – ($CaCl_2$ – B_2O_3/$MgCl_2$) – ($FeCl_3$ – B_2O_3/Al_2O_3) – NaCl.

We also pay attention to how the fullness of the rough surface differs according to such a parameter of the support surface curve as *t50*. The larger the value of *t50*, the better the roughness of the rough surface.

Table 3 – Roughness of the treated surface of the hard alloy T15K6 diamond grinding wheels on a polymer bond B2-08 with a relative grain concentration of 100 % with different options for modification of the surface of diamond grains brand AC6 125/100 (with a productivity of 200 mm^3/min)

Modification of a surface of diamond grains in a working layer of diamond wheels 12A2-45° 125x5x3x32	Roughness indicators:			
	R_a, mkm	R_{max}, mkm	S_m, mkm	*t50*, %
AC6 125/100 B2-08 100 without modifying the surface of the grains	**0.31**	**2.27**	**72**	**48.92**
Modification of NaCl grain surface (100 %)	0.33	2.51	56	67.17
Modification of the mixture (B_2O_3 + NaCl) of the grain surface (100 %)	0.36	2.78	47	48.56
Modification of B_2O_3 grain surface (50 % of grains) and modification of Al_2O_3 grain surface (50 %)	0.37	1.94	50	57.08
Modification of $CaCl_2$ grain surface (100 %)	0.37	2.28	53	43.82
Modification of B_2O_3 grain surface (50 % of grains) and modification of $MgCl_2$ of grain surface (50 %)	0.40	2.16	175	68.13
Modification of B_2O_3 grain surface (100 %)	0.45	3.26	63	57.26
Modification of a mixture (B_2O_3 + $CaCl_2$) of grain surface (100 %)	0.45	2.89	64	50.36
Modification of $FeCl_3$ grain surface (100 %)	0.48	4.09	75	56.48

Table 4 – Roughness of the treated surface of the hard alloy T15K6 diamond grinding wheels on a polymer bond B2-08 with a relative grain concentration of 100 % with different options for modification of the surface of diamond grains brand AC6 125/100 (with a productivity of 400 mm^3/min)

Modification of a surface of diamond grains in a working layer of diamond wheels 12A2-45° 125x5x3x32	Roughness indicators:			
	R_a, mkm	R_{max}, mkm	S_m, mkm	*t50*, %
Modification of a mixture (B_2O_3 + $CaCl_2$) of grain surface (100 %)	0.40	3.47	53	69.33
Modification of B_2O_3 grain surface (50 % of grains) and modification of $MgCl_2$ of grain surface (50 %)	0.41	3.03	68	57.38
Modification of $CaCl_2$ grain surface (100 %)	0.41	3.00	95	50.00
Modification of B_2O_3 grain surface (50 % of grains) and modification of Al_2O_3 grain surface (50 %)	0.43	4.73	96	90.14
Modification of $FeCl_3$ grain surface (100 %)	0.43	3.65	61	51.14
Modification of NaCl grain surface (100 %)	0.44	3.37	69	27.79
Modification of B_2O_3 grain surface (100 %)	0.49	3.45	63	45.50
AC6 125/100 B2-08 100 without modifying the surface of the grains	**0.52**	**3.67**	**72**	**64.23**

For processing productivity of 200 mm^3/min this figure varies within 25 % (see table. 3), and for 400 mm^3/min this difference is already 63 % (see Table 4).

In more detail, the features of the supporting surfaces of the rough surface are presented in Fig. 4. That is, if necessary, changing the surface modifier of diamond grains from $CaCl_2$ to NaCl can not affect the bearing capacity of the rough surface obtained by grinding, in this case to increase it by the parameter *t50* from 43 % to 70 %.

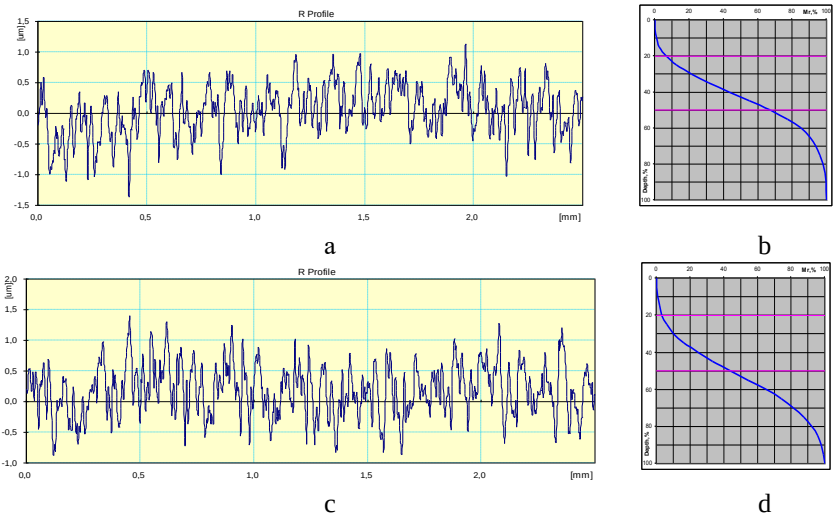

Figure 4 – Profilograms (a, c) and curves of the relative reference length of the profile (b, d) of the surface treated with a wheel with modified surface of NaCl grains (a, b) and a wheel with modified surface of $CaCl_2$ grains (c, d) when grinding hard alloy with a productivity of 200 mm^3/min

Conclusions

1. The possibility of directed modification of the surface of diamond grinding powders with heat-resistant oxides and chlorides of metals and non-metals is shown.

2. Modification of the surface of diamond grains with oxides and chlorides increases the heat resistance of synthetic diamond grinding powders. The best result was obtained by modifying the surface of diamond grains with boric anhydride (B_2O_3).

3. It is established that to achieve a guaranteed increase in wear resistance of diamond wheels when grinding hard alloys at least 2 times it is recommended to modify the surface of diamond grains with a combination of oxides: B_2O_3 grain surface modification (50 % grain) and Al_2O_3 grain surface modification (50 %). Modification of the surface of diamond grains with $CaCl_2$ chloride increases the wear resistance of diamond wheels by a maximum of 1.8 times. A third acceptable option is grain surface modification by a combination of oxide and chloride: grain surface B_2O_3 modification (50 % grain) and grain surface $MgCl_2$ modification (50 %). This modification makes it possible to increase the wear resistance of the wheels by 1.4-1.5 times.

4. It was found that diamond grains modified with sodium chloride or modified with a mixture (B_2O_3 + NaCl) should be used to achieve the minimum roughness during finishing grinding operations. As grinding productivity increases, this relationship disappears and it is recommended to use diamond grains modified with calcium chloride or modified with a mixture (B_2O_3 + $CaCl_2$).

5. It was found that if we have the condition to achieve a rough surface with the highest bearing capacity, then the use of diamond grains with chloride modification is unacceptable, and it is necessary to use diamond grains in wheels with surface modification combination B_2O_3/Al_2O_3.

References: **1.** *Lavrinenko V.I., Solod V.Yu.* Oxidation or oxide materials in the machining zone in superabrasive grinding–a factor of influence on the grinding performance. J. Superhard Mater. 2016. vol. 38, no. 6. pp. 417–422. **2.** *Lyubarskiy I.M., Palatnik L.S.* Metallofizika treniya [Metal Physics of Friction] (in Russian). Moscow: Metallurgiya, 1976. 176 p. **3.** *Latyishev V.N., Naumov A.G.* Ob effektivnosti ispolzovaniya kisloroda v protsesse rezaniya [On the efficiency of oxygen use in the cutting process] (in Russian). Rezanie i instrument v tehnologicheskih sistemah. 2001. № 60. pp. 121–127. **4.** The effect of UV and thermally induced oxidation on the surface and structural properties of CVD diamond layers with different grain sizes / Anna Dychalska, Marek Trzcinski, Kazimierz Fabisiak, Kazimierz Paprocki, ... Mirosław Szybowicz. (2022) Diamond and Related Materials. V. 121. 108739. **5.** Graphitization of synthetic diamond crystals: A morphological study / Boris B.Bokhonov, Dina V.Dudina, Marat R.Sharafutdinov. (2021) Diamond and Related Materials. V. 118. 108583. **6.** Investigation on abrasive wear mechanism of single diamond grain in flexible scribing titanium alloy / Qinghong Wan Lai, Zou Shiqi Liu, Tingting Wang, Shengtian Chen, Yun Huang. (2021) Diamond and Related Materials. V. 120. 108631. **7.** Diamond Lapping of Sapphire Wafer with Addition of Graphene in Slurry / Hsien-Kuang Liu, Chao-Chang A.Chen, Wei-Chung Chen. (2017) Procedia Engineering. V. 184. pp. 156-162. **8.** Tribological properties of oxidized wood-derived nanocarbons with same surface chemical composition as graphene oxide for additives in water-based lubricants / Hiroshi Kinoshita, Kyoko Suzuki, Tsutomu Suzuki, Yuta Nishina. (2018) Diamond and Related Materials. V. 90. pp. 101-108. **9.** Adsorption and deposition of micro diamond particles in preparing diamond magnetic abrasives by electroless composite plating / Bin Yang, Wenzhuang Lu, Wei Feng, Xu Yang, Dunwen Zuo. (2017) Diamond and Related Materials. V. 73. pp. 137-142. **10.** Exploring the activation energy of diamond reacting with metals and metal oxides by first-principle calculation/ Ao Deng, Jing Lu, Dongxu Li, Yanhui Wang. (2021) Diamond and Related Materials. V. 118. 108522. **11.** Growth and characterization of chemical vapor deposition diamond coating incorporated amorphous carbon with high Raman bands induced by CuO particles / Naichao Chen, Fasong Ju, Fan Zhou, Shuai Chen, Kun Wei, Ping He. (2021) Diamond and Related Materials. V. 116. 108387. **12.** Morphological features and phase composition of W-containing coatings formed on diamond via its interaction with WO_3 / A.V. Ukhina, D.V. Dudina, B.B. Bokhonov, D.V. Savintseva, D.A.Samoshkin, S.V. Stankus. (2022) Diamond and Related Materials. V. 123. 108876. **13.** Effect of V_2O_5 addition on the wettability of vitrified bond to diamond abrasive and grinding performance of diamond wheels / Shuai-peng Chen, Xiao-pan Liu, Long Wan, Peng-zhao Gao, Wei Zhang, Zhi-qiang Hou. (2019) Diamond and Related Materials. V. 102. 107672. **14.** The effects of SiO_2 coating on diamond abrasives in sol-gel tool for SiC

substrate polishing / Jing Lu, Yongchao Xu, Yunhe Zhang, Xipeng Xu. (2017) Diamond and Related Materials. V. 76. pp. 123-131. **15.** Enhancing the oxidation resistance of diamond powder by the application of Al_2O_3 conformal coat by atomic layer deposition / D.Dominguez , H.Tiznado, H.A.Borbon-Nuñez, F.Muñoz-Muñoz, J.M.Romo-Herrera, G.Soto. (2016) Diamond and Related Materials. V. 69. pp. 108-113. **16.** Two-dimensional hole gas formed at diamond surface by Al_2O_3/diamond interface engineering Kongping Wu, Yong Zhang, Jianli Ma, Zhifen Fu, Changzhao Chen. (2020) Diamond and Related Materials. V. 105. 107807. **17.** Preparation and properties of Al_2O_3-reinforced Cu-Ni-Sn metallic matrix for applications in diamond-cutting tools/ Feng Chen, Zhiqiao Yan, Zhenpeng Liu, Ying Long, Naike Fu, Fenglin Zhang, Bin Liu, Yong Liu. (2020) Diamond and Related Materials. V. 109. 108025. **18.** Thermal stability of polycrystalline diamond compact sintered with boron-coated diamond particles / Xiaohua Sha, Wen Yue, Haichao Zhang, Wenbo Qin, Dingshun She, Chengbiao Wang. (2020) Diamond and Related Materials. V. 104. 107753. **19.** Effect and corresponding mechanism of NaCl additive on boron carbide powder synthesis via carbothermal reduction / Xin Li, Shuai Wang Dan, Nie Kun Liu, Shu Yan, Pengfei Xing. (2019) Diamond and Related Materials. V. 97. 107458. **20.** Temperature and defect effects on the mechanical properties of pentadiamond / Huasong Qin, Guoqiang Zhang, Yingyan Zhang, Lang Qin, Yilun Liu,Qing-Xiang Pei. (2021) Diamond and Related Materials. V. 118. 108523. **21.** *Poltoratskiy V.G., Bochechka A.A., Lavrinenko V.I., Tkach V.N., Petasyuk G.A., Bilochenko V.A., Leschenko O.V., Grischenko G.S.* Modifitsirovanie shlifporoshkov sinteticheskogo almaza i kompaktov na osnove mikroporoshkov cBN termostoykimi oksidami i hloridami metodom jidkofaznogo naneseniya. [Modification of synthetic diamond grinding powders and compacts based on CBN micropowders with heat-resistant oxides and chlorides by liquid-phase deposition] (in Russian). Porodorazrushayuschiy i metalloobrabatyivayuschiy instrument – tehnika i tehnologiya ego izgotovleniya i primeneniya: Sb. nauch. tr. Vyip. 22. Kyiv: ISM im. V. N. Bakulya, 2019. pp. 317–327. ISSN 2223-3938. **22.** *Murovskiy V.A., Kutsovskaya A.M., Chistyakov E.M.* Vliyanie sredyi na intensivnost goreniya almaza [The influence of the environment on the intensity of diamond burning] (in Russian). Sinteticheskie almazyi. 1971. № 5. pp. 31–33. **23.** *Samsonov G.V., Vinitskiy I.M.* Tugoplavkie soedineniya [Refractory compounds] (in Russian). Moskow: Metallurgiya, 1985. 560 p. **24.** Fiziko-himicheskie svoystva okislov: Spravochnik [Physical and chemical properties of oxides: Handbook] / pod red. G.V. Samsonova. Moskow: Metallurgiya, 1978. 472 p. **25.** *Novikova S.I.* Teplovoe rasshirenie tverdyih tel [Thermal expansion of solids] (in Russian). Moskow: Nauka, 1974. 294 p. **26.** *Lifshits B.G., Kraposhin V.S., Linetskiy Ya.L.* Fizicheskie svoystva metallov i splavov [Physical properties of metals and alloys] (in Russian). Moskow: Metallurgiya, 1980. 320 p. **27.** Lavrinenko, V.I., Solod, V.Yu., Kashynskyi, I.S., Dobroskok V.L. Determination of oxides intended for the surface modification of diamond grains by the functional characteristics. Journal of Superhard Materials, 2020, Vol. 42, No. 6, pp. 417–422. **28.** *P.F. Wang, Zh.H. Li, J. Li, Y.M. Zhu.* Effect of ZnO on the interfacial bonding between Na_2O–B_2O_3–SiO_2 vitrified bond and diamond. Solid State Sciences. 2009. V. 11, Is. 8. P. 1427-1432. **29.** *Karnauhov A.P.* Adsorbtsiya. Tekstura dispersnyih i poristyih materialov [Texture of dispersed and porous materials] (in Russian). – Novosibirsk: Nauka. Sibirskoe predpriyatie RAN, 1999. – 470 p.

Валерій Лавриненко, Володимир Полторацький, Олександр Бочечка, Київ, Україна
Володимир Солод, Кам'янське, Україна
Євгеній Островерх, Володимир Федорович, Харків, Україна

МОДИФІКАЦІЯ ПОВЕРХНІ СИНТЕТИЧНИХ АЛМАЗНИХ ШЛІФПОРОШКІВ ЖАРОСТІЙКИМИ ОКСИДАМИ І ХЛОРИДАМИ РІДКОФАЗНИМ МЕТОДОМ НАНЕСЕННЯ

Анотація. *Визначено обмеження на вибір оксидів, які можуть становити інтерес при модифікуванні штампувальними жаростійкими оксидами поверхні алмазних шліфпорошків. Досліджено процес модифікації поверхні зерен синтетичних алмазних шліфпорошків термостійкими оксидами та хлоридами металів та неметалів методом рідкофазного нанесення. Досліджено структурні характеристики зовнішньої структури та визначено кількісний елементний склад поверхні модифікованих порошків. Показано можливість спрямованого модифікування поверхні алмазних шліфпорошків термостійкими оксидами та хлоридами металів та неметалів. Модифікація поверхні алмазних зерен оксидами та хлоридами підвищує термостійкість синтетичних алмазних шліфпорошків. Встановлено, що для досягнення гарантованого підвищення зносостійкості алмазних кругів при шліфуванні твердих сплавів не менше ніж у 2 рази рекомендується модифікувати поверхню алмазних зерен комбінацією оксидів: B_2O_3 (50% зерна) та Al_2O_3 (50 %). Модифікація поверхні алмазних зерен хлоридом $CaCl_2$ підвищує зносостійкість алмазних кругів максимум в 1,8 рази. Третім прийнятним варіантом є модифікація поверхні зерна комбінацією оксиду та хлориду: модифікація поверхні зерна B_2O_3 (50% зерна) та модифікація поверхні зерна $MgCl_2$ (50%). Дана модифікація дозволяє підвищити зносостійкість кругів у 1,4-1,5 рази. Встановлено, що для досягнення мінімальної шорсткості при чистовому шліфуванні слід використовувати алмазні зерна, модифіковані хлоридом натрію або сумішшю (B_2O_3 + NaCl). Зі збільшенням продуктивності шліфування ця залежність зникає і рекомендується використовувати алмазні зерна, модифіковані хлоридом кальцію або сумішшю (B_2O_3 + $CaCl_2$). Встановлено, що якщо є умова отримання шорсткої поверхні з найбільшою несучою здатністю, використання алмазних зерен з хлоридною модифікацією неприпустимо, і необхідно використовувати алмазні зерна в кругах з комбінацією модифікації поверхні B_2O_3/ Al_2O_3.*

Ключові слова: *модифікація; метод рідкофазного осадження; термічна стабільність; оксиди; фізичні властивості; модифікація оксидів; алмазні шліфувальні порошки.*

УДК 621.9.01 **doi: 10.20998/2078-7405.2022.97.05**

O. Manovytskyi, S. Klymenko, V. Burykin, Kiyv, Ukraine

CALCULATION OF SHEAR ANGLE WHEN CUTTING WITH A TOOL OF A NEGATIVE RAKE ANGLE

Abstract. *The article considers the results of the study of the cutting process in order to obtain the calculated dependences of the shear angle oF the physical and mechanical properties of hard-worked iron-carbon steels and alloys in thermobaric conditions of the cutting process and the value of the negative rake angle which is a typical tool for processing with polycrystalline superhard materials (PSHM) cutting tools. When cutting, the formation of chips occurs in the plastic flow of metal in the area of cutting or fracture with the formation and subsequent development of cracks and the subsequent separation of elemental or stepped chips. A well-known chip shaping scheme with one plane shift and the value of the contact area of the front surfaces of the cutting elements with the allowable material to be removed are used to describe the contact phenomena in the chip forming zone and calculate the shear angle in this plane. It is established that the inverse relationship between the shear angle and the negative rake angle of the cutting element indicates that the increase in the negative value of the rake angle leads to a decrease in the shear angle. The specific elongation and shortening of the processed material at the cutting temperature are defined by the authors as the characteristics of shear plasticity and selected for use in the calculation of the values of shear angles during blade processing. As a result of this work, the calculated dependences of the shear angle values on the physical and mechanical properties of heavy-duty ferro-carbon steels and alloys in thermobaric conditions of the cutting process and the value of the negative rake angle, which is characteristic of machining with tools of PSHM equipped.*

Keywords: *cutting process; rake angle; chip shrinkage; iron-carbon alloys; relative plastic characteristics; shear angle.*

Introduction. In single point cutting with chip removal: milling, turning or boring, drilling, drawing, etc., the characteristics of both cutting and machining materials are important, and most importantly – their ratio. In the case of milling or interrutting turning, there are also impulse loads on the cutting edge. However, the basis for understanding the process of chip formation, stress-strain state, the load on the cutting edge in any method of machining are natural processes occurring in the cutting zone.

Depending on the ductility of the metal during cutting, the formation of chips occurs in the plastic flow of metal in the zone of cutting or destruction with the formation and subsequent development of cracks and subsequent separation of elemental or stepped chips [1, 2].

Known methods for assessing the nature of deformation in the cutting zone can effectively solve the problem of deformation-stress state, but this is not always enough to fully disclose the physical nature of phenomena and quantify processes [3–5].

One of the main provisions of the science of metal cutting is the dependence of chip shrinkage on the degree of deformation of the layer of allowance material. Chip shrinkage is one of the main characteristics that allows to recognize the phenomena in the cutting zone, to make numerical calculations using this indicator [2].

However, it is well known that measuring the length and width of chips, weighing them and obtaining the final results of calculations of the actual values of shrinkage of chips are high complexity, have significant errors and are extremely inconvenient in practice in research and industrial production.

It is especially difficult to obtain the value of chip shrinkage in the formation of elemental and articular types of chips, the total length of which is almost impossible to determine without errors [1].

Using the well-known chip shaping scheme with one plane shift and knowing the contact area of the front (rake) surfaces of the cutting elements with the allowable material to be removed, we can describe the contact phenomena in the chip formation zone and calculate cutting forces [3]. As is known [6], the separation of the metal occurs in the cutting zone, where it received a final deformation, which is extreme, and if the tension is equal to the ultimate strength of the compacted metal.

When in contact with the rake surface of the cutter, the stress in the chips will also reach its limits. The author [7] believes that chips are formed as a result of the occur and development of cracks in the immediate vicinity of the cutting edge of the tool.

The aim of this work was to obtain the calculated dependences of the shear angle values of the physical and mechanical properties of heavy-duty iron-carbon steels and alloys in thermobaric conditions of the cutting process and the value of the negative rake angle, which is a typical tool for processing, equipped with polycrystalline superhard materials (PSHM).

Research methodology. In fig. 1 shows a textured chip root – a micro section of the chip-forming element, the texture of which depends on the location in the cutting zone.

The direction of the texture leads to the end of the plane in which the metal is extremely hardened and subject to shear, which separates the allowance material and turns it into chips.

The consequence of the contact interaction of the chips with the rake surface of the cutter is additional heating of the chips due to its friction on the front surface of the cutter and internal friction and subsequently the texture of softened chips already formed by the rake surface of the tool and the internal friction of the chips [9].

There are several modern models of the deformation zone during turning, both with one and with several shear planes, which reflect the process of chip formation as a result of plastic deformation shear of the allowance material.

Conditionally, according to the limit values of fluidity and strength, ferrocarbon materials can be divided into highly plastic at $\sigma_т(\sigma_{0,2})/\sigma_в$ = 0,45–0,55; plastic at $\sigma_т/\sigma_в$ = 0,55–0,70; $\sigma_т/\sigma_в$ = 0,55–0,70; low-plastic, having a ratio of $\sigma_т/\sigma_в$ = 0,70–0,90 and brittle, which practically do not correlate with each other [10].

Despite the fact that the model with a developed deformation zone looks more realistic, analytical studies using models with a displacement in one plane have a fairly complete view and when using high-speed turning and milling finishes are still more acceptable. This is especially evident when working with brittle and low-plastic materials [1].

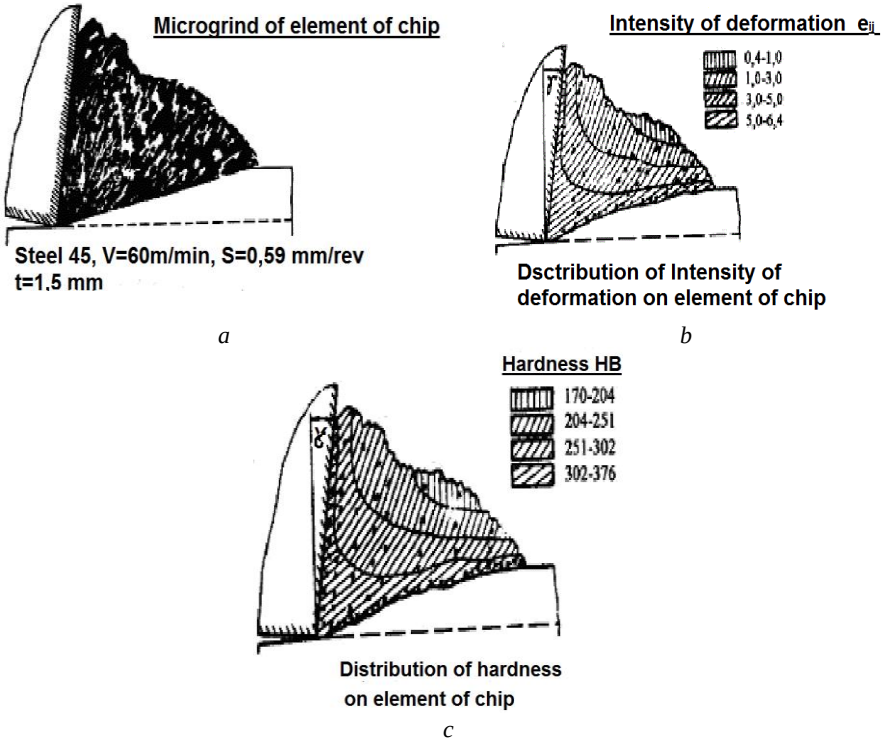

Figure 1 – Microgrind of a detachable chip element with the formed texture and hardness of the chip element [8]

Images of the deformation zone, the corners of the texture of the root chips with their measured values are shown in fig. 2, which shows a cutter with a zero rake angle that was used during processing.

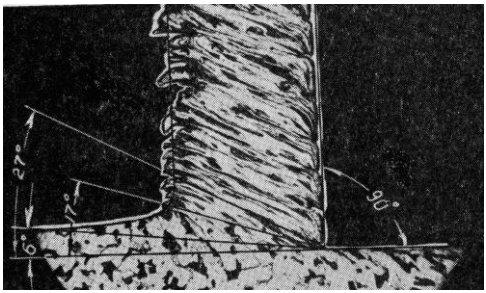

Figure 2 – Image of the boundaries of the deformation zone in the formation of chips and the angle of the texture when free rectangular cutting of steel 20H; velocity v = 0,7 m/min, slice thickness a = 0,065 mm [2]

Numerous microgrinds that reveal the texture of the shear line that passes to the chips, as best described in [2]. The sequence of deformation of the allowance and the formation of the chip element, when processing steel type 20H in the records, high-speed film camera with a frequency of 1500 frames per second are shown in fig. 3.

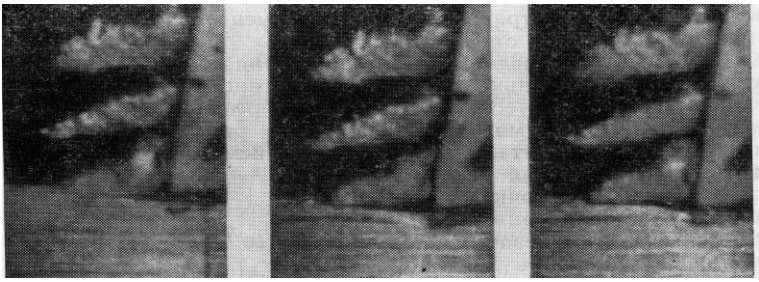

Figure 3 – The sequence of formation of elements of chips and textures with a frequency of high-speed filming of 1500 frames per second when processing cold-formed steel type 20G. The thickness of the cut is 0,25 mm

According to these indicators, almost all hardened steels, bleached and high-alloy cast irons, heat-resistant and similar alloys should be classified as low-plastic materials.

High-speed turning, shown in fig. 3, orthogonal rectangular free cutting of steel type 20H with a cutting speed of 40 m/min and a cut thickness of 0,25 mm, allowed to trace the main sequences of the chip formation process. At the stage of formation of the chip element in the material to be separated, the texture lines are visible and more clearly observed in the individual chip elements. In this case, the

direction of the shift lines is the same. As long as the normal stresses in the elementary volume of the deformable material are balanced by tangential stresses on the rake surface of the cutter, movement does not occur, the allowance material is plastically deformed and applied to the rake surface of the cutter, but not yet separated in the form of chips. As soon as the compressive stresses reach the strength of the material, the deformed allowance material is shifted along the shear lines forming a texture, moved along the rake (front) surface of the cutter and then separated as a chip element. [10].

As rightly insisted [12], the force of chip formation during cutting initiates significant compressive stresses and, as a consequence, elastic-plastic deformations of the metal to be cut, followed by plastic shear.

Consider a modified negative front angle Merchant scheme [1], which illustrates the relationship between the cutting angle, shear angle and rake angle of the cutter, as well as the thickness of the cut in orthogonal rectangular cutting, as shown in fig. 4.

Taking into account the fact that the displaced metal is of constant density and neglecting lateral deformations across the width of the section, the condition of continuity can be represented in equal volumes of derived metal before its deformation and deformed immediately before its shift [13].

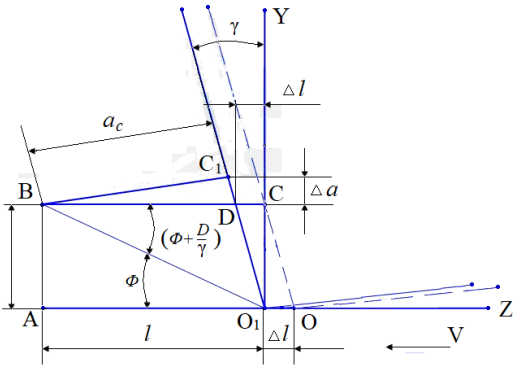

Figure 4 – Scheme for determining the relationship between the shear angle, the front angle of the cutter, the thickening and shortening of the allowance metal, which is deformed during chip formation; Δa – thickening of the metal along the thickness of the cut; Δl – shortening of the metal along the length of the cut

Assuming the constancy and invariance of the cut width and taking into account the constant density of the metal passing into the chips, we can proceed to the equality of the planes of quadrilaterals OABC and O_1ABC_1.

The area of the OABC quadrilateral will be

$$S_{OABC} = a \cdot l \ + 0{,}5a \cdot \Delta l \ . \tag{1}$$

And the area of the quadrilateral $O_1ABC_1$is equal to

$$S_{O_1ABC_1} = S_{O_1ABC} + S_{DBC} - S_{DBC_1} \cdot \tag{2}$$

The area of a rectangle and triangles together will be equal to:

$$S_{O_1ABC_1} = a \cdot l + \frac{0{,}5 \cdot \Delta a \cdot l \cdot \cos(\Phi + \gamma)}{\cos\gamma \cdot \cos\Phi} - 0{,}5a \cdot \Delta l \cdot \tag{3}$$

After reduction we have

$$\frac{0{,}5l \cdot \Delta a \cdot \cos(\Phi + \gamma)}{\cos\Phi \cdot \cos\gamma} = 0 \cdot \tag{4}$$

After revealing the sum of angles and transformations, we have

$$\frac{\sin\Phi \cdot \sin\gamma}{\cos\Phi \cdot \cos\gamma} = 1 \tag{5}$$

or

$$tg\Phi = ctg\gamma \tag{6}$$

As shown in fig. 3 and 4, subject to continuity will be the following

$$\frac{a}{l} = \frac{\Delta a}{\Delta l} = tg\Phi \tag{7}$$

From the resulting equation (6) the obvious inverse relationship between the shear angle and the negative rake angle of the cutting element indicates that an increase in the negative value of the front angle leads to a decrease in shear angle, ie, assuming that the machined material is completely plastic and there is no friction on the surfaces in contact with the cutting tool, if there was a zero front angle, the deformation of the section thickness would reach infinity and stresses on the thickness and length of the section would be equal when assigning the rake angle $\gamma = 45°$.

However, structural and tool materials are not ideal and have certain properties that are manifested in their plastic deformation, including milling in high temperatures.

There are many studies of the characteristics of materials at temperatures close to the turning temperature results. These data are contained both in the standard documentation for most steels and alloys (state standards, specifications) and in numerous references.

But it is extremely difficult to determine the actual local temperature in the contact zone during turning, drilling or milling. Heat release is the result of

deformation in the cutting area, as well as the friction of the cutter tooth against the rear surface and the chips running on the rake surface of the cutting element.

Direct methods of measuring the temperature in the area of the shear zone estimate the temperature values depending on the temperature of the workpiece, chips and tool is too inaccurate, because in this case there is a fairly high temperature gradient. There are modeling methods for determining the temperature in the deformation zone, based on the similarity theory proposed in [12].

Fig. 5 shows graphical images illustrating the dependence of temperature in the movement zone and the temperature on the front surface of the cutter depending on the cutting speed of different tool materials by complex criterion *F* taking into account the effect of tool geometry and thermal conductivity ratio of tool and workpiece material.

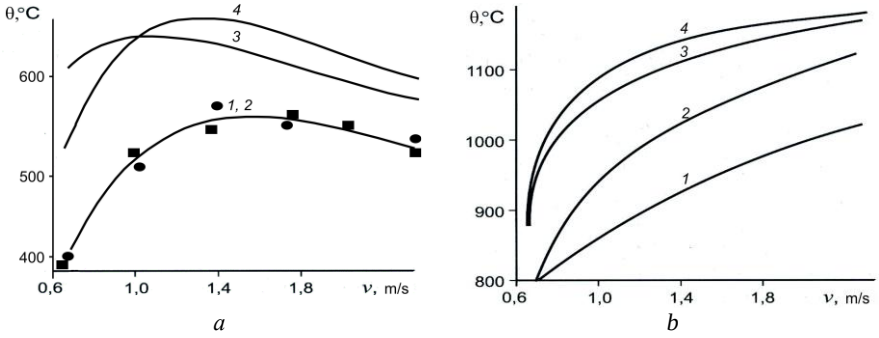

Figure 5 – Dependence of the temperature in the shear plane (*a*) and the temperature on the front surface of the cutter (*b*) on the cutting speed [10]

The study shows that the temperature on the rake surface of the cutting element varies from 800 to 1200 °C (depending on the tool used) and the shear temperature at the optimum cutting speed of the tool – from 500 to 700 °C, and for the type of polycrystalline cubic Boron Nitride (PcBN) cyborite – narrower range from 500 to 550 °C [14].

Taking into account the relationship between longitudinal and transverse deformations in equation (7), based on the conditions of continuity (scheme in fig. 4), and analyzing the relationship between longitudinal and transverse deformations when testing the strength of machined materials, we can assume that longitudinal deformation Δl when cutting will be proportional to the relative narrowing δ, and the deformation in the thickness of the cut Δa is proportional to the relative elongation ψ in static or dynamic test, in addition, in a certain

temperature range, these characteristics are almost identical [14]. In this case, equation (7) can be represented as follows

$$\frac{a}{l} = \frac{\Delta a}{\Delta l} = \frac{\delta}{\psi} = tg\Phi \tag{8}$$

Based on the scheme for determining the ratio of the thickness of the cut and the thickness of the chips depending on the value of the shear angle (fig. 4) we obtain: the equation (8) can be represented as follows

$$\frac{a}{\sin\Phi} \cdot \cos(\Phi + \gamma) = a_c \tag{9}$$

a – slice thickness; a_c – chip thickness.

The ratio of the thickness of the cut to the thickness of the chips will be the shrinkage of the chips

$$\frac{a_c}{a} = \frac{\cos(\Phi + \gamma)}{\sin\Phi} = \xi \tag{10}$$

Taking into account the dependence of the shear angle, friction angle and rake angle of the cutter according to Merchant's equation

$$\Phi = \frac{\pi}{4} - 0{,}5(\eta - \gamma) \tag{11}$$

or according to Oxley's equation:

$$\Phi = 50^0 - 0{,}8(\eta - \gamma) \tag{12}$$

we can find the friction angle for known values of the shear angle and the specified rake angle of the cutter.

The table shows the reference values of relative strain values at appropriate shear zone temperatures for some types of alloy and tool steels to be machined by cutting in the hardened state and calculated by the above formulas to determine chip shrinkage and friction angle. The obtained values of the shear angle are used when finding the friction angle by formulas (11) or (12).

The table summarizes the data obtained as a result of calculations according to the method proposed on the quantitative characteristics of shear angles, coefficients of friction and shrinkage of chips in the processing of typical representatives of hardened to high hardness low-alloy, medium-alloy, tool and high-alloy steels. Indicators of relative elongation and relative narrowing are given from the reference data of the properties of steels [7].

Fig. 6 shows graphs of the dependence of chip shrinkage from the hardness of the steel being processed and the cutting speed.

Table – Shear angles, friction angle, coefficients of friction and shrinkage of chips in steel processing

Steel brand		Test temperature, °C	Relative		Angle		Coefficient of friction μ	Shrinkage of chips ζ
			lengthening δ, %	narrowing ψ, %	shear angle Φ, degree	friction η, degree (γ = = –10°)		
Medium alloyed	20H	500	26	75	19°07'	41°46'	0,9105	2,67
		600	35	77	24°34'	30°52'	0,5977	1,99
		800	51	90	29°02'	21°54'	0,4090	1,60
	30H	600	32	90	19°35'	40°50'	0,8642	2,60
		650	35	90,5	21°11'	39°48'	0,8282	2,15
		800	48	79	31°27'	17°06'	0,3060	1,44
	40H	500	25	78	17°46'	44°32'	0,9838	2,90
		600	26	81	17°48'	44°24'	0,9850	2,90
		800	48	94	27°48'	24°44'	0,4606	1,70
	40HGN	500	25	78	17°46'	44°32'	0,9838	2,90
		600	27	85	17°37'	44°46'	0.9925	2,91
		800	57	96	30°52'	18°16'	0,3496	1,51
	12HN3A	500	26	75	19°08'	41°42'	0,8909	2,66
		600	35	65	28°08'	23°42'	0,4390	1,67
		700	43	67	32°42'	14°36'	0,2606	1,36
Tooi steels	ShH-15	614	13	37	19°22'	41°04'	0,8714	2,33
		650	14,5	48	17°48'	44°24'	0,9737	2,19
		695	21	50	22°47'	34°26'	0,6856	2,17
	U8A	500	40	77	27°28'	25°04'	0,4677	1,72
		600	48	85	29°24'	21°06'	0,3859	1,57
		800	58	100	30°07'	19°46'	0,3594	1,52
	U10A	500	38	77	26°17'	27°26'	0,5191	1,89
		600	46	85	28°24'	23°12'	0,4286	1,62
		800	52	100	31°20'	17°20'	0,3121	1,44
	U12A	500	32	68	27°28'	25°04'	0,4677	1,72
		600	44	82	28°23'	23°14'	0,4259	1,65
		800	52	96	32°48'	14°24'	0,2567	1,33
High alloyed	12H13	600	41	80	28°17'	23°26'	0,4338	1,66
		800	62	98	32°19'	15°22'	0,2748	1,38
	12H18N9T	650	17	43	21°24'	37°12'	0,7590	2,26
		800	24	51,5	24°59'	32°02'	0,6253	1,94

Chip shrinkage is calculated by equation (10).

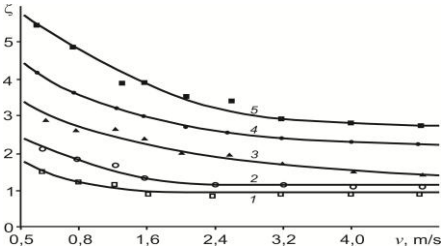

Figure 6 – Dependence of chip shrinkage on the initial hardness of the processed HVG steel and the cutting speed of PcBN ismit [13]: γ = –5°, φ = 45°, cutting depth *t* = 0,2 mm, feed *S* = 0,084 mm/rev; *1* – 61 HRC, *2* – 55 HRC, *3* – 45 HRC, *4* – 37 HRC, *5* – 23 HRC

Research results. If we compare the value of the texture angle shown in fig. 2, obtained by M. M. Zorev when turning steel 20H, with calculated data for this grade of steel, shown in the table, the arithmetic mean of the shear angle, calculated for the temperature in the conditional shear plane in the range from 600 to 800 °C, it almost coincides with that shown in fig. 2. As can be seen from fig. 5, the temperature in the conditional shear plane is in the range from 500 to 750–800 °C, and shown in fig. 6 dependences of chip shrinkage on the cutting speed when processing steels of high (curves *1*, *2*) and medium (curve *3*) hardness are just close to those calculated by formula (10) and are in the range of values from 2.5 to asymptotically close to one.

Thus, we have practically proven conclusions about the legitimacy of the application of the relative plasticity characteristics of the processed iron-carbon materials at a temperature equal to the cutting temperature to calculate the shear angle, which is an extremely important characteristic of the cutting process. Confirmation of this legitimacy are the approximate values obtained experimentally and calculated using the obtained values of the shear angles of the values of shrinkage of chips.

References: 1. *Armarego, I. Dzh. A.* Obrabotka metallov rezaniyem / I. Dzh. A. Armarego, R. Kh. Braun. – M. : Mashinostroyeniye, 1977. – 326 s. **2.** *Zorev, N. N.* Voprosy mekhaniki protsessa rezaniya metallov / N. N. Zorev. – M. : Mashgiz, 1956. – 364 s. **3.** *Mazur, M. P.* Osnovi teoríí rízannya materíalív : pídruchnik / M. P. Mazur, Yu. M. Vnukov, V. L. Dobroskok ta ín. – L'vív : Noviy Svít-2000, 2010. – 422 s. **4.** *Chou, Y. Kevin.* Experimental investigation on CBN turning of hardened AISI 52100 steel / Y. Kevin Chou, Chris J. Evans, Moshe M. Barash // J. of Mater. Proc. Technology. – 2002. – № 124. – P. 274–283. **5.** *Petrusenko, L. A.* Raschot napryazheniy, voznikayushchikh v opasnoy zone lezviynoy chasti rezhushchego instrumenta / L. A. Petrusenko, V. S. Antonyuk // Vísnik NTU Ukraíni «Kíívs'kiy polítekhníchniy ínstitut». Mashinobuduvannya – K. : NTU Ukraíni «KPÍ», 2016. – Vyp. 77. – S. 147–156. **6.** Fiziko-matematicheskaya teoriya protsessov obrabotki materialov i tekhnologii mashinostroyeniya : v 10 t. – T. 3 : Rezaniye materialov lezviynymi instrumentami / F. V. Novikov i dr. – Odessa : ONPU, 2003/ – 546 s. **7.** *Poletika, M. F.* Matematicheskoye modelirovaniye protsessa rezaniya / M. F. Poletika, M. G. Gol'dshmidt, Yu. P. Stefanov // Vopr. mekhaniki i fiziki protsessov rezaniya i kholodnogo plasticheskogo deformirovaniya : sb. nauch. tr. – K. : ISM im. V. N. Bakulya NAN Ukrainy, 2002. – S. 33–43. **8.** *Rozenberg, Yu. A.* Rezaniye materialov : ucheb. dlya tekhn. vuzov / Yu. A. Rozenberg. – Kurgan : Poligraf kombinat, Zaural'ye, 2007. – 294 s. **9.** *Ostaf'yev, V. A.* Fizicheskiye osnovy protsessa rezaniya. / V. A. Ostaf'yev,

V. S. Antonyuk, S. P. Visloukh i dr. – K. : Vishcha shk., 1976. – 136 s. **10.** *Korolev, P. N.* Soprotivleniye materialov : sprav. po raschetno-proyekt. rab. / P. N. Korolev. – K. : Vishcha shk., 1974. – 288 s. **11.** *Novikov, N. V.* Raschet sily struzhkoobrazovaniya pri slozhnoprofil'nom tochenii reztsami, osnashchennymi kruglymi plastinami / N. V. Novikov, A. S. Manovitskiy, S. A. Klimenko // Nadezhnost' instrumenta i optimizatsiya tekhnologicheskikh sistem : sb. nauch. tr. – Kramatorsk : DGMA, 2008. – Vyp. № 23 – S. 3–11. **12.** *Silin, S. S.* Metod podobiya pri rezanii materialov / S. S. Silin. – M. : Mashinostroyeniye, 1979. – 152 s. **13.** *Polukhin, P. I.* Soprotivleniye plasticheskoy deformatsii metallov i splavov / P. I. Polukhin, G. Ya. Gun, A. M. Galkin. – M.: Metallurgiya, 1976. – 488 s. **14.** Sverkhtverdyye materialy. Polucheniye i primeneniye : v 6 t. / pod obshchey red. N. V. Novikova. – T. 5 : Obrabotka materialov lezviynym instrumentom / pod red. S. A. Klimenko. – K. : ISM im. V. N. Bakulya, IPTS «ALKON» NAN Ukraíni, 2006. – 316 s.

Олександр Мановицький, Сергій Клименко, Віталій Бурикін, Київ, Україна

РОЗРАХУНОК КУТА ЗСУВУ ПРИ РІЗАННІ ІНСТРУМЕНТОМ З ВІД'ЄМНИМ ПЕРЕДНІМ КУТОМ

Анотація. *У статті розглядаються результати дослідження процесу різання з метою отримання розрахункових залежностей значень кута зсуву від фізико-механічних властивостей важкооброблюваних залізо-вуглецевих сталей і сплавів в термобаричних умовах процесу різання та величини негативного переднього кута, що є характерним при обробці інструментом, оснащеним полікристалічними надтвердими матеріалами (ПНТМ). При обробці різанням, утворення стружки відбувається в пластичному потоці металу в зоні різання або руйнування з утворенням і подальшим розвитком тріщин і наступним відділенням елементної або ступінчастої стружки. Одним з основних положень науки про різання металів є залежність усадки стружки від ступеня деформації шару матеріалу припуску. Усадка стружки - одна з основних характеристик, яка дозволяє розпізнати явища в зоні різання, зробити числовії розрахунки з використанням цього показника, проте визначення дійсної довжини та ширини стружки, її зважування та отримання остаточних результатів розрахунків фактичних величин усадки стружки пов'язані з високою трудомісткістю, мають значні похибки та надзвичайно незручні при практичному застосуванні при проведенні досліджень та в промисловому виробництві, особливо - елементних та суглобистих типів стружок. Використана загальновідома схема формування стружки з одним площинним зсувом та значення площі контакту передніх поверхонь ріжучих елементів з матеріалом припуску, що підлягає видаленню, для надання опису контактних явищ в зоні формування стружки та розрахунку кута зсуву у цій площині. Встановлено, що наявнв зворотна залежність між кутом зсуву і негативним переднім кутом ріжучого елемента вказує, що зростання в негативному значенні переднього кута веде до зменшення кута зсуву, тобто, матеріал, підданий механічній обробці, не є ідеальним і має певні властивості, які проявляються при його пластичному деформуванні, в тому числі при фрезеруванні в умовах високих температур. Питоме подовження та вкорочення оброблюваного матеріалу при температурі різання визначені авторами, як характеристики пластичності при зсуві і обрані для використання в розрахунках значень кутів зсуву при лезовій обробці. Внаслідок виконання даної роботи було отримано розрахункові залежності значень кута зсуву від фізико-механічних властивостей важкооброблюваних залізо-вуглецевих сталей і сплавів в термобаричних умовах процесу різання та величини негативного переднього кута, що є характерним при обробці інструментом, оснащеним ПНТМ.*

Ключові слова: *процес різання; передній кут; усадка стружки; залізо-вуглецеві сплави; відносні пластичні характеристики; кут зсуву*.

UDC 621.914.1 **doi: 10.20998/2078-7405.2022.97.06**

A. Nagy, G. Varga, Miskolc, Hungary

ANALYZING THE EFFECT OF THE TOOL PASS NUMBER AND THE DIRECTION OF SLIDING BURNISHING ON SURFACE ROUGHNESS

Abstract. *Nowadays, the concern of environmental protection is becoming more and more important in production as well. They often contribute to this by reducing or eliminating the amount of coolants and lubricants, or by using alternative machining methods. One of them is burnishing, which makes a positive effect on surface integrity, while reduces the environmental load. In this paper we examined the change in surface roughness achieved by burnishing after turning on a corrosion-resistant steel workpiece, where the number of burnishing passes and burnishing direction were changed. The results showed increased smoothness, bearing capacity and dimensional stability by increasing the number of passes from 1 to 2, however, the 3 times repetition did not show any additional favorable improvement on the surfaces. In case of the forward-backward-forward burnishing directions, further chipping occurred, in other cases the effect of the directions was negligible on the amplitude roughness parameters, but considerable on the parameters characterizing the roughness peak. The greatest improvement was achieved with the backward-forward settings.*
Keywords: *turning; burnishing; surface roughness; environmentally friendly machining.*

1 INTRODUCTION

Nowadays, the concern of environmental protection is becoming increasingly important in construction, energy sources and use, waste management, and industries as well, in which this issue is particularly significant in the design and manufacture of products. During machining the workpiece loses a part of its volume which becomes waste, and it must be treated and recycled. The tools, molds do not last forever, and are thrown away as they wear out, deform. During production, the use of auxiliary materials (coolants and/or lubricants) is also a crucial issue in terms of environmental protection, as it can reduce the possibility to recycle the waste (e.g. contaminated chips, sludge, which is produced during grinding), and is also harmful to the health and the environment; some cutting fluids are also responsible for the development of skin diseases and respiratory problems, and are therefore classified as hazardous waste [1].

Increasingly strict national and international environment protection laws are passed, which manufacturers must comply with. Due to restrictions imposed by law, some manufacturing processes involve additional costs; thus, it is necessary to develop new methods to replace the older ones. This is not only a technological challenge for researchers and engineers, but also increases the importance of ecological characteristics in the comparison of different machining processes. One approach to this is environmentally conscious design and manufacturing, which aims to reduce or recycle the by-products of a process. For this, such technologies are developed that are

less harmful to the environment, but at the same time the improvement of product quality, cost reduction and productivity increase are facilitated [1,2].

One of the most frequently studied and used methods of environmental protection in production is the reduction of the used amount of cooling-lubricating fluids or its abandonment. The latter, i.e. dry or "green" machining is considered a better approach not only from an ecological point of view, but also in economic respect [1]. Varga et al. investigated the effect of the cutting data and the flow rate of cutting fluid on 3D roughness on turned surfaces with the aim of how this method of reducing the environmental load influences the roughness values [2]. With a full factorial experimental design, empirical formulas for the relationship between technological data and surface roughness were given, based on which optimal cutting data could be selected [3]. In another paper [2], they studied the effect of changing several cutting data on the surface roughness of holes made with environmentally friendly technology in cast burnishing workpieces. They found that the roughness values of the surfaces machined with cooling-lubricating fluid were almost the same or smaller. Furthermore, the consequence of abandonment of cooling-lubrication was investigated on roughness and cylindricity on turned surfaces [4]. The results showed that it had the smallest, negligible effect after feed and cutting speed. Kundrák et al. examined hard turning and combined machining (turning, grinding) as finishing of the bore of case-hardened steel gears. While the same roughness value was achieved on the machined surfaces, hard turning was found to result shorter machining time and lower costs, and the chip did not become contaminated (its composition did not change) with the cutting fluid, so it could be used in metallurgical processes or recycling [1,5]. Application of untraditional turning procedures can also lead to better surface roughness, as showed by Sztankovics et al. [6].

In the production of components, some finishing processes can be replaced by burnishing, which reduces the environmental load by not producing chip, and at the same time improves the integrity of the surface. The turned surface layer has tensile stress. During burnishing, the surface material layer is compressed, resulting in a functionally favorable surface. On the one hand, it creates microstructural compression which generates compressive stress in the surface layer, as well as increases its microhardness, and thereby also improves surface strength, wear resistance and fatigue life [7,8]. Furthermore, the bearing surface characteristics are improved by the indentation of the surface topography, including wear resistance and dimensional stability, without significant changes in the ability to retain the lubricant. Due to the multiple positive effects, it attracts the attention of engineers and researchers both in industry [9] and in research, which is investigated worldwide. We provide a brief overview of them.

Grzesik et al. investigated to what extent the superfinishing and burnishing after hard turning on a hardened Cr-steel workpiece changes the values of 2D and 3D roughness parameters and improves the functional properties of the machined

surfaces [10]. Based on their results, smoother surfaces can be achieved with both types of procedures, with lower roughness values and better bearing characteristics.

During burnishing, the burnishing speed, feed, force, and number of passes can be adjusted on the machine tool. By changing these parameters, Ferencsik and Varga analyzed their effect on the surface microhardness and the residual stress of the surface layer [7], as well as on the surface roughness [11,12]. With the application of the full factorial experimental design, formulas were given for the correlations of the adjusted and measured parameters, which can be used to select optimal machining values in the studied ranges. Analyzing the differences in the roughness of the turned and then burnished surfaces for R_a, R_q, R_z and R_t parameters, they found that the increase of the force acting on the low-hardness aluminum alloy from 10N to 20N has a negative effect and increasing the feed at a pass number of 3 is beneficial, while 1 pass has a negative impact on roughness. By increasing the number of passes from 1 to 3, further significant changes were measured in roughness, in case of feed rates above 0.003 mm/rev. Rami et al. stated in their literature review [13] that the burnishing force and the diamond ball diameter mostly affect the plastic deformation, i.e. the roughness decreases, the hardness and the compressive stress increase. All of these increase the resistance of the part to fatigue, corrosion and wear. In addition, the number of passes also improves the surface quality, but only up to a certain limit. Then, due to the large-scale plastic deformation of the metal surface, it will be overhardened, which causes an increasing demand for compressive force during further deformations and flaking on the surface, without a noticeable change in hardness [14]. On AISI 4140 alloy steel, the average roughness R_a decreased in case of setting a maximum of 100N burnishing force, above which material separation was observed and the roughness value increased. When increasing the ball diameter, R_a decreased, which is related to the fact that the depth of the indentations decreases with the same feed. The smallest roughness was achieved with a small feed, low burnishing force, and a large ball diameter, which R_a value was similar to that typical for grinding. However, with the minimum diameter and maximum force, they were able to achieve the highest residual compressive stress in the surface layer [13].

When burnishing, the Workpiece-Fixture-Machine-Tool system can vibrate with a large-diameter tool (in the case of a large contact surface). This was studied for a straight-edged wiper insert tool (which burnished the surface as well) [15]. The regenerative chatter in case of the studied cutting parameters was investigated.

Alshareef et al. analyzed the integrity of turned and subsequently burnished surfaces, including residual stress, surface microstructure and roughness on acid-resistant steel [16]. It was found that the residual stress is mainly determined by surface pressure (burnishing force and ball diameter) and feed, and burnishing speed has negligible effect on it. The large amount of tensile stress in the turned surface layer was significantly reduced during burnishing and compressive stress was generated. The thickness of the changed microstructural layer was about 15 μm. The

values of R_a and R_z parameters decreased by more than 60%. Surface integrity characteristics were investigated [17] on austenitic corrosion-resistant steel during ultrasonic burnishing with a ball and a roller, varying the burnishing speed, force, and number of passes. The optimal parameter values for roughness, microhardness and residual stress were determined in the studied ranges. It was observed that with rolling, the parameters showed better results due to the greater overlapping ratio. The most favorable roughness results were experienced for 3 times burnishing, after that the roughness of the surface topography deteriorated with repetition.

Based on the literature review, it can be concluded that burnishing can be recommended to be used as a finishing, primarily because of its effect on improving surface integrity characteristics, but also as an environmentally friendly alternative. It was found that burnishing influences the microhardness, residual stress, and roughness of the surface. The aim of this supplementary paper is to determine how and to what extent burnishing affects the roughness of turned surfaces on corrosion-resistant steel, if the number of passes and the burnishing direction are changed.

2 EXPERIMENTAL CONDITIONS

For the investigation, experiments were performed on an E400 universal lathe. During these, the cylindrical X5CrNi18-10 (1.4301) grade corrosion-resistant steel workpiece was clamped in a three-jaw chuck, on which the surface was segmented to 5 smaller parts. On each segment two different burnishing settings were applied, marked with A and B letters (Table 1 and Fig. 1). The turned diameter was Ø49.5 mm, and the length of the five sections was 26 mm each (Fig. 1). We first carried out turning with the same cutting parameters (n = 375 1/min, f = 0.0812 mm/rev, a_p = 0.5 mm) with a new CNMG 120408-MP cutting insert. During this a 4% emulsion of Rhenus FU71 T (oil viscosity: 160 mm^2/s) cutting fluid was used, which was dripped onto the workpiece in a small amount (flow rate: V_p = 150 ml/min). After that, we performed the burnishing on the prepared surfaces with f = 0.05 mm/rev feed, n = 375 1/min spindle speed and F_b = 10 N burnishing force. The diameter of the diamond ball was Ø3 mm. Burnishing was carried out in different ways on the surfaces by changing the number and direction of the burnishing passes, where "forward" direction is identical to the feed direction in turning, and "backward" is the opposite of that (Table 1). The choice of the variations are based on our preliminary practical experience.

Table 1 – Tool pass number and direction of burnishing on the sections

No.	1st pass	2nd pass	3rd pass	No.	1st pass	2nd pass	3rd pass
1A	forward	-	-	**3B**	forward	forward	backward
1B	forward	forward	-	**4A**	forward	backward	forward
2A	forward	backward	-	**4B**	forward	backward	backward
2B	backward	forward	-	**5A**	backward	forward	forward
3A	forward	forward	forward	**5B**	backward	forward	backward

After the experiments, the roughness of the surfaces was measured on the AltiSurf 520 three-dimensional topography measuring device with a CL2 confocal chromatic sensor, which has a vertical resolution of 0.012 μm. The 2D profile (red line) and 3D areal (red square) roughness measurements on the surfaces were performed at 3 rotated locations on the surfaces, the reported results are their arithmetic mean (Fig. 1). During the evaluation, at first the nominal (cylindrical) surface shape was extracted, then the evaluation (1.25 mm) and cut-off (0.25 mm) lengths specified in ISO 21920:2021 and ISO 25178-3:2012 standards were set according to the turned topographies. In case of the 3D measurements, the topographies had an area of 1.25 × 1.25 mm^2 (Fig. 1). For R_{mr} and S_{mr} material ratio parameters, a cut-off depth of c = 1 μm from the highest peak point was set.

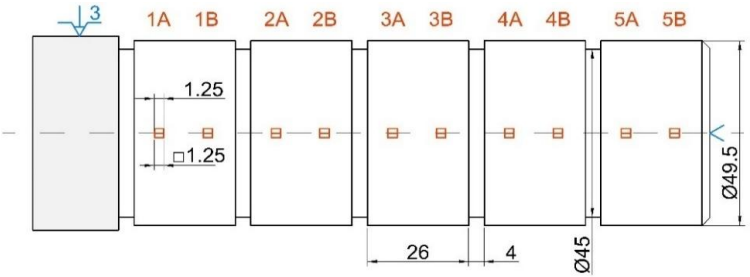

Figure 1 – Measurement locations for surface roughness analysis

3 RESULTS AND DISCUSSION

The roughness measurement results for the following parameters are given for the turned surfaces in Table 2 and for the burnished surfaces in Table 3:

Table 2 – Roughness values measured on the turned surfaces

No.	R_a	R_z	R_{pk}	R_{mr}	R_{sk}	R_{ku}	S_a	S_z	S_{pk}	S_{mr}	S_{sk}	S_{ku}
	[μm]	[μm]	[μm]	[%]	[-]	[-]	[μm]	[μm]	[μm]	[%]	[-]	[-]
1A	1.81	8.36	1.15	2.92	0.04	2.04	1.85	11.20	1.15	0.11	0.05	2.07
1B	1.81	8.33	1.14	2.91	0.02	2.03	1.85	11.16	1.14	0.11	0.05	2.06
2A	1.83	8.46	1.16	2.95	0.03	2.06	1.88	11.33	1.16	0.11	0.05	2.09
2B	1.80	8.29	1.14	2.89	-0.01	2.02	1.84	11.11	1.14	0.11	0.05	2.05
3A	1.81	8.34	1.15	2.91	-0.03	2.03	1.85	11.17	1.14	0.11	0.05	2.06
3B	1.84	8.47	1.16	2.95	0.02	2.06	1.88	11.34	1.16	0.11	0.05	2.09
4A	1.84	8.50	1.17	2.97	-0.01	2.07	1.89	11.39	1.17	0.11	0.05	2.10
4B	1.81	8.33	1.14	2.91	0.04	2.03	1.85	11.17	1.14	0.11	0.05	2.06
5A	1.80	8.28	1.14	2.89	0.00	2.02	1.84	11.09	1.13	0.11	0.05	2.05
5B	1.85	8.53	1.17	2.98	0.02	2.08	1.89	11.42	1.17	0.11	0.05	2.11

- Arithmetic mean height of profile (R_a) or surface (S_a)
- Maximum height of profile (R_z) or surface (S_z)
- Material ratio of profile (R_{mr}), Surface bearing area ratio (S_{mr})
- Reduced peak height of profile (R_{pk}) or surface (S_{pk})
- Skewness of profile (R_{sk}) or surface (S_{sk})
- Kurtosis of profile (R_{ku}) or surface (S_{ku})

Table 3 – Roughness values measured on the burnished surfaces

No.	R_a	R_z	R_{pk}	R_{mr}	R_{sk}	R_{ku}	S_a	S_z	S_{pk}	S_{mr}	S_{sk}	S_{ku}
	[μm]	[μm]	[μm]	[%]	[-]	[-]	[μm]	[μm]	[μm]	[%]	[-]	[-]
1A	1.69	7.36	0.57	10.82	-1.01	2.74	1.76	10.18	0.47	0.51	-0.97	2.60
1B	1.15	6.09	0.67	12.96	-1.30	3.85	1.15	8.64	0.54	1.51	-1.33	4.04
2A	0.96	5.41	0.78	3.86	-1.00	3.64	0.97	7.65	0.72	2.23	-1.02	3.89
2B	0.87	5.06	0.43	20.70	-1.29	4.12	0.91	7.49	0.42	3.08	-1.32	4.36
3A	0.88	5.24	0.67	12.60	-1.27	4.26	0.93	7.50	0.54	1.91	-1.30	4.27
3B	0.90	5.47	0.50	14.76	-1.36	4.48	0.93	7.51	0.56	2.60	-1.30	4.23
4A	1.62	8.01	2.00	1.65	0.38	2.78	1.70	17.90	3.45	0.27	0.76	4.31
4B	0.89	5.17	0.68	5.23	-1.36	4.25	0.91	7.88	0.60	1.05	-1.44	4.67
5A	0.86	4.91	0.45	20.14	-1.4	4.33	0.85	6.85	0.35	2.9	-1.45	4.6
5B	0.78	5.32	0.78	7.54	-1.22	4.72	0.79	7.19	0.69	3.15	-1.42	5.36

In Table 4 the degree of decrease of the roughness values (ΔR_i and ΔS_i) on the surfaces are summarized based on Equations 1 and 2, where *i* denotes the index of the given roughness parameter. Therefore, a negative value in the table expresses a deterioration of roughness. In the case of R_{mr} and S_{mr} parameters, the value increase is displayed as a multiplication factor.

$$\Delta R_i = \frac{R_i^{turned} - R_i^{burnished}}{R_i^{turned}} \cdot 100\ [\%] \quad (1)$$

$$\Delta S_i = \frac{S_i^{turned} - S_i^{burnished}}{S_i^{turned}} \cdot 100\ [\%] \quad (2)$$

During burnishing with setting 4A, material separation occurred, so the beneficial effects from a functional point of view – reduction of roughness values, increase of bearing capability, compressive residual stress – were absent. Regarding the roughness values in Table 4, the experimental results confirm the opposite effects; although the decrease in the values of parameters R_a and S_a is negligible (approx. 7-10%), we experienced the lowest, mostly negative rates for

the other examined parameters. Due to the different characters of roughness changes, we analyze the results and the degree of changes without section 4A.

In Table 4, results show that a favorable effect can be achieved with burnishing on the surfaces for all studied combinations of number of passes and direction. In case of the average roughness parameters, this means minimum 6.65% and maximum 57.9% value decrease for R_a, and 5.23-58% improvement for S_a. The decrease in the value of the maximum height parameters is between 11.9% and 42.3% for R_z, and between 9.12% and 39.8% for S_z. Since the peaks of the topography is flattened and rounded during burnishing, we expect a decrease in value for the reduced peak parameters; the thickness decreases of the upper material layer, which wears off quickly during the initial usage. This is confirmed by the experimental results with rates between 33.1% and 62% for R_{pk} and between 38.2% and 70.2% for S_{pk}. On the other hand, an increase is expected in the material ratio parameters, measured at the same cut level; the 1.31–7.16 times increase for R_{mr} and 4.51–27.66 times for S_{mr} also confirm the expectation.

Table 4 – Rate of change in roughness values by burnishing

No.	R_a	R_z	R_{pk}	R_{mr}	S_a	S_z	S_{pk}	S_{mr}
1A	6.65%	11.9%	50.2%	3.71×	5.23%	9.12%	59.3%	4.51×
1B	36.4%	26.9%	41.7%	4.46×	38.0%	22.6%	52.9%	13.45×
2A	47.7%	36.0%	33.1%	1.31×	48.3%	32.5%	38.2%	19.60×
2B	51.4%	39.0%	62.0%	7.16×	50.5%	32.6%	63.2%	27.66×
3A	51.4%	37.2%	41.5%	4.33×	49.6%	32.9%	53.0%	17.02×
3B	50.9%	35.4%	57.3%	5.00×	50.7%	33.8%	52.1%	22.88×
4A	10.0%	3.22%	-76.0%	0.57×	7.50%	-61.3%	-204%	2.42×
4B	50.8%	38.0%	40.7%	1.80×	51.0%	29.4%	47.1%	9.36×
5A	53.4%	42.3%	61.3%	6.79×	54.9%	39.8%	70.2%	25.39×
5B	57.9%	37.6%	33.5%	2.54×	58.0%	37.1%	40.5%	27.50×

In the following, we compare the roughness of the cylindrical surfaces machined with the same number of passes. The values of the parameters in Tables 2-3 are illustrated in bar diagrams in Fig. 2, where the burnishing directions are shown below the columns in chronological order. The arrows on the diagrams show the direction, where "→" means forward, "←" means backward.

Fig. 2a shows the average roughness R_a values, while Fig. 2b illustrates the maximum height R_z values. The two diagrams show a very similar nature, so both are characterized simultaneously, together with their 3D counterparts, S_a and S_z. It can be seen that similar turning and burnishing values were measured for each pass numbers, regardless of the burnishing directions. After turning, with negligible differences, approx. R_a = 1.8 μm, S_a = 1.85 μm, R_z = 8.4 μm and S_z = 11.2 μm were measured,

while on the burnished surfaces at i = 1 pass number (on surface 1B) the improvement ratio is 6.7% for R_a, 5.2% for S_a, 11.9% for R_z, 9.1% for S_z, at i = 2; the rate is between 36.4–51.4% for R_a, 38–50.5% for S_a, 26.9–39% for R_z, 22.6–32.6% for S_z, in the case of i = 3 number of passes, we experienced a decrease of between 50.8–57.9% for R_a, 49.6–58% for S_a, 35.4–42.3% for R_z, and 29.4–39.8% for S_z. The differences between the improvement rates are small, at i = 2; the rate is 15% for R_a, 12.5% for S_a, 12% for R_z, 10% for S_z, and every value is smaller at i = 3; 7% for R_a, 8.4% for S_a, 7% for R_z, 10.4% for S_z. In the case of i = 2 number of passes, the highest improvement rate was found on section 2B, while in the case of i = 3, the highest rate was on section 5B based on R_a values, and on section 5A based on R_z values, which have a common in the initial backward-forward directions.

Considerable differences were observed between the R_{pk} (Fig. 2c) and S_{pk} parameters. While on the turned surfaces approx. $R_{pk} = S_{pk} = 1.15$ μm values were obtained, during burnishing the reduction of these values on surface 1B (i = 1) was 50.2% for R_{pk} and 59.3% for S_{pk}, at i = 2 passes the value of R_{pk} between 33.1% and 62%, and S_{pk} between 38.2% and 63.2% during reinforcement with; during reinforcement with i = 3 passes, the value of R_{pk} decreased between 33.5–61.3% and S_{pk} between 40.5–70.2%. The differences between the improvement rates are no longer negligible; for i = 2 number of passes, 29% for R_{pk}, 25% for S_{pk}; For i = 3 number of passes, 27.8% for R_{pk}, 29.7% for S_{pk}. From the functional – load capability and dimensional stability – point of view, the best result was again shown by section 2B in the case of i = 2, while section 5A in the case of i = 3, where the initial directions are in the same; backward-forward.

Similar functional properties (including wear resistance and dimensional stability) can also be expressed with the material ratio parameters, the values of which are shown in Fig. 2d. During turning, the values of R_{mr} are typically 2.95%, and the values of S_{mr} are equally 0.11%. After burnishing, multiples of these values can be measured on the surfaces; at number of passes i = 1, it is 3.7 times for R_{mr} and 4.5 times for S_{mr}, in the case of i = 2, it is 1.3...7.2 times for R_{mr}, 13.5...27.7 times for $S_{mr,}$ at i = 3, there is 1.8–6.8 times increase in R_{mr} and 9.4–27.5 times increase in S_{mr}. The significant differences between the rates indicate the sensitivity of these parameters to a change in the machining conditions, compared to e.g. R_a, S_a and R_z, S_z. Based on the results, the maximum R_{mr} and S_{mr} values were also achieved in the case of i = 2 on section 2B and in the case of i = 3 on section 5A, where the initial burnishing directions are as mentioned before.

Overall, based on the values of the 8 roughness parameters considered, to achieve the best functional properties, we recommend burnishing with backward-forward directions in case of 2 passes, or an additional pass in forward direction in case of 3 passes.

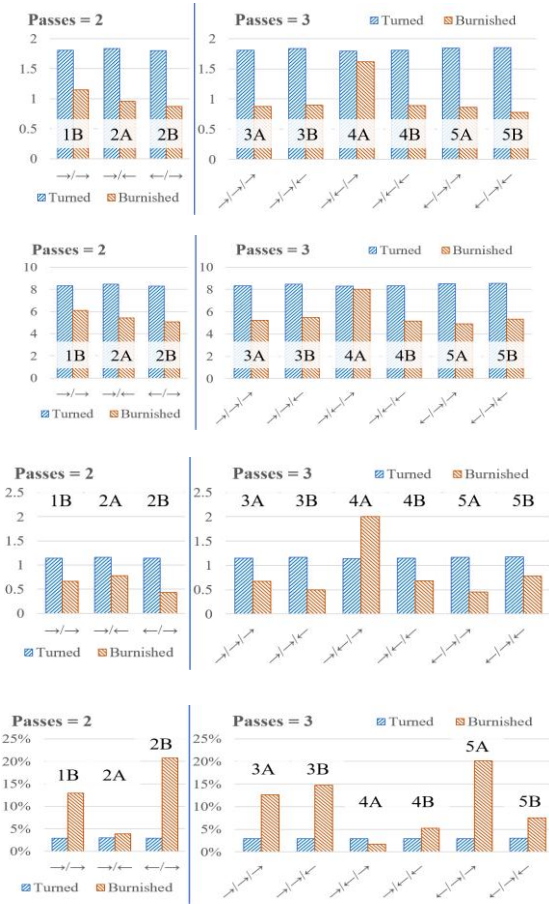

Figure 2 – Comparison of roughness values of R_a (a), R_z (b), R_{pk} (c), R_{mr} (d) by number of passes

After that, we compare the effects of the number of passes with roughness parameters. For this, we consider the most favorable values from a functional point of view for each number of passes, which are also shown in the diagrams in Figure 3, where MR means "material ratio". The R_a (Fig. 3a) and R_z (Fig. 3b) parameter values show similarly that, compared to the values of the turned surface, a slight improvement can be achieved with 1 pass, there is a significant additional improvement in case of 2 passes, and with 3 passes a further minimal improvement can be achieved. Different characteristics from this show the R_{pk} (Fig. 3c) and R_{mr}

(Fig. 3d) parameter values, where a significant improvement is experienced even with 1 pass, then a further large positive change for 2 passes, but a minimal deterioration for an additional repetition. Presumably, with 3 passes we reached the limit where the surface roughness characteristics no longer improve, as described in the literature [14]. Therefore, we recommend the use of i = 2 passes on corrosion-resistant steel, because in the case of i = 3, the overall small improvement no longer compensates for the significant decrease in productivity.

Figure 3 – Roughness values of R_a (a), R_z (b), R_{pk} (c), R_{mr} (d) as a function of number of passes

In the study, the measured values of the R_{sk} skewness and R_{ku} kurtosis indices are analyzed. These can be coupled and placed as points on a topological map, which cover different ranges on the R_{sk}–R_{ku} plane (Fig. 4a). These are typical for each machining method, and thus the characteristic properties of the created surface topographies can be identified [18]. Fig. 4a shows the expected ranges of turning and burnishing. In this plane the measured results are illustrated on a diagram (Fig. 4b). The R_{sk}–R_{ku} value pairs measured on the turned surfaces indicate the nature of the profiles; their peaks and valleys are generally at almost the same distance from the center line, and their sharpness is characteristic of turning. Compared to these, on the burnished surfaces the measured R_{sk} values are smaller (negative values); the profiles have flattened and rounded peaks and narrow, relatively deep valleys, and by increasing the number of passes, these characteristics of the peaks and valleys further increase a little. The R_{ku} values are unexpectedly high and become higher with the increase of number of passes, i.e. the sharpness of the profiles increases. For this, one reason may be the relatively small spaces between turning marks on the profile due to the small feed, another possible reason is the narrowing of the turned roughness valleys during the further deformation of the surface layer during several passes of burnishing.

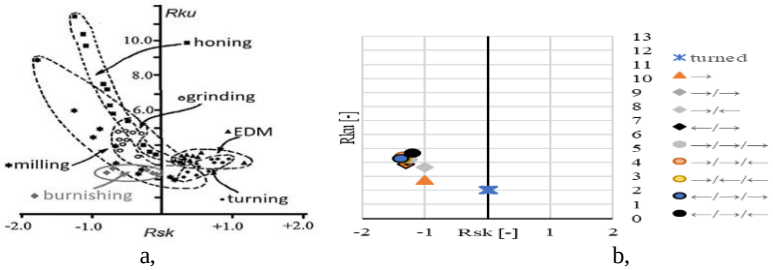

Figure 4 – Topological map of machined surfaces [19] (a) and of the experimental results (b)

4 CONCLUSIONS

In the present paper, we investigated the effect of burnishing on the surface topography of X5CrNi18-10 grade alloyed corrosion-resistant steel after turning, where the number of burnishing passes and directions were changed while the burnishing force, feed and speed were constant. Our findings are as follows.

Based on experimental roughness results, burnishing of turned surfaces resulted in an improvement in a single pass from a functional point of view – smoothness, bearing capability, quickly-wearing upper layer –, and further improvement in the case of 2 number of passes. However, we did not experience any significant changes in roughness in case of 3 passes, besides the reduction of productivity. Based on

these, we recommend the use of 2 passes burnishing on the examined material quality and burnishing force.

Within a given number of passes, changing the burnishing directions resulted in almost identical amplitude roughness values, but significant differences in the degree of value changes of R_{pk}, S_{pk} and R_{mr}, S_{mr} parameters characterizing the roughness peak. Compared to the turning feed direction, the greatest improvement was achieved by the backward-forward directions in the case of 2 passes, and by the backward-forward-forward strategy in the case of the 3 times repetition, so we recommend their use. During burnishing with 3 passes in forward-backward-forward directions (on surface 4A), material separation occurred, which deteriorated the surface roughness properties, so it is recommended not to use this setting.

ACKNOWLEDGEMENTS

Project no. NKFI-125117 has been implemented with the support provided from the National Research, Development and Innovation Fund of Hungary, financed under the K_17 funding scheme.

References: 1. *Kundrák, J., Mamalis, A.G., Gyáni, K., Markopoulos, A.:* Environmentally friendly precision machining, Materials and manufacturing processes vol.21(1) (2006) pp.29-37. **2.** *Varga, Gy., Szigeti, F., Kovács, A.:* Analysis of Surface Roughness of Holes Machined by Environmentally Friendly Way (in Hungarian). Műszaki Tudomány az Észak-kelet Magyarországi Régióban 2012. MTA Debreceni Akadémiai Bizottság, Debrecen, Hungary, 2012, pp. 433-442. **3.** *Varga, G., Sovilj, B., Jakubowicz, M., Babič, M.:* Experimental Examination of Surface Roughness in Low-Environmental-Load Machining of External Cylindrical Workpieces. International Scientific-Technical Conference MANUFACTURING, Springer, Cham, 2019, pp. 307-321. **4.** *Antal, N., Gyula, V.:* Effect of abandonment of cooling and lubrication on surface roughness and cylindricity in turning of steel, Multidiszciplináris Tudományok vol.11(4) (2021) pp.395-407. **5.** *Kundrák, J., Varga, G., Deszpoth, I.:* Analysis of Extent of Environment Load in Alternative Manufacturing Procedures. WSEAS Transactions on Environment and Development vol.14 (2018) pp.313-320. **6.** *Sztankovics, I., Kundrak, J.:* Theoretical Value and Experimental Study of Arithmetic Mean Deviation in Rotational Turning. Rezanie I Instrumenty V Tekhnologicheskih Sistemah vol.96 (2022) pp.73-81. **7.** *Ferencsik, V., Varga, G.:* Examination of surface state-change on diamond burnished aluminium components. Proceedings of the International Symposium for Production Research 2019, Springer, Cham, 2020, pp.535-544. **8.** *Stephenson, D.A., Agapiou, J.S.:* Metal cutting theory and practice. CRC press, 2018. **9.** *Maheshwari, A.S., Gawande, R.R.:* The role of burnishing process in manufacturing industry - A state-of-the-art survey, International Journal of Engineering Research and Development vol.13 (2017) pp.50-60. **10.** *Grzesik, W., Zak, K.:* Modification of surface finish produced by hard turning using superfinishing and burnishing operations, Journal of Materials Processing Technology vol.212(1) (2012) pp.315-322. **11.** *Varga, G., Ferencsik, V.:* Analysis of surface topography of diamond burnished aluminium alloy components. Vehicle and Automotive Engineering, Springer, Cham, 2017, pp.143-154. **12.** *Ferencsik, V., Varga, G.:* The Influence of Diamond Burnishing Process Parameters on Surface Roughness of Low-Alloyed Aluminium Workpieces, Machines vol.10(7) (2022) ArtNo.:564. **13.** *Rami, A., Gharbi, F., Sghaier, S., Hamdi, H.:* Some insights on combined turning-burnishing (CoTuB) process on workpiece surface integrity, International Journal of Precision Engineering and Manufacturing vol.19(1) (2018) pp.67-78. **14.** *Hassan, A.M., Al-Dhifi, S.Z.:* Improvement in the Wear Resistance of Brass Components by the Ball Burnishing Process, Journal of Materials Processing Technology vol. 96(1) (1999) pp.73-80. **15.** *Hirose, M., Hayasaka, T., Shamoto, E.:* Unique regenerative chatter in wiper-turning operation with burnishing process, Part 1: Prediction and analytical investigation of generation mechanism,

critical stability, and characteristics, Precision Engineering vol.71 (2021) pp.304-312. **16.** *Alshareef, A.J., Marinescu, I.D., Basudan, I.M., Alqahtani, B.M., Tharwan, M.Y.:* Ball-burnishing factors affecting residual stress of AISI 8620 steel, The International Journal of Advanced Manufacturing Technology vol.107(3) (2020) pp.1387-1397. **17.** *Shi, Y.L., Shen, X.H., Xu, G.F., Xu, C.H., Wang, B.L., Su, G.S.:* Surface integrity enhancement of austenitic stainless steel treated by ultrasonic burnishing with two burnishing tips, Archives of Civil and Mechanical Engineering vol.20(3) (2020) pp.1-17. **18.** *Molnár, V., Sztankovics I.:* Analysis of Roughness Parameters Determining Tribological Properties in Hard Turned Surfaces. Hungarian Journal Of Industry And Chemistry vol.49(2) (2021) pp.77-84. **19.** *Kovács, Z.F., Viharos, Z.J., Kodácsy, J.:* Improvements of surface tribological properties by magnetic assisted ball burnishing, Surface and Coatings Technology vol.437 (2022) ArtNo.:128317.

Антал Надь, Дьюла Варга, Мішкольц, Угорщина

АНАЛІЗ ВПЛИВУ КІЛЬКОСТІ ПРОХОДІВ ІНСТРУМЕНТУ ТА ЙОГО НАПРЯМКУ ПРИ ВИГЛАДЖУВАННІ НА ШОРСТКІСТЬ ПОВЕРХНІ

Анотація. *В даний час піклування про охорону навколишнього середовища стає все більш важливим і у виробництві. Цьому часто сприяють, зменшуючи чи усуваючи кількість охолоджуючих рідин та мастильних матеріалів або використовуючи альтернативні методи обробки. Один з них – вигладжування, що позитивно впливає на цілісність поверхні та знижує навантаження на навколишнє середовище. У цій роботі автори розглянули зміну шорсткості поверхні, що досягається при вигладжуванні після токарної обробки заготовки з корозійностійкої сталі, де кількість проходів вигладжування та напрямок вигладжування змінювалися. Для дослідження були проведені досліди на універсальному токарному верстаті. При цьому циліндрична заготовка з корозійностійкої сталі затискалася в трикулачковому патроні, на якому поверхня сегментувалася на 5 дрібніших частин. До кожного сегменту застосовувалися два різні налаштування полірування. При цьому використовувалася емульсія мастильно-охолоджувальної рідини, яку капали на заготівку в невеликій кількості. Після цього проводили вигладжування на підготовлених поверхнях з подачею f = 0,05 мм/об, частотою обертання шпинделя n = 375 1/хв і зусиллям вигладжування F_b = 10 Н. Діаметр алмазної кулі становив Ø3 мм. Вигладжування проводилося різними способами на поверхнях шляхом зміни числа і напрямку проходів, що вигладжують, де напрямок «вперед» ідентичний напрямку подачі при точінні, а «назад» протилежно йому. На підставі експериментальних результатів шорсткості автори роблять висновок про те, що вигладжування точених поверхонь призвело до поліпшення за один прохід з функціональної точки зору – гладкість, несуча здатність, верхній шар, що зношується, – і подальше поліпшення у разі 2-х проходів. Однак суттєвих змін шорсткості за 3 проходи, крім зниження продуктивності, вони не помітили. Виходячи з цього, автори рекомендують використовувати 2 проходи полірування в залежності від якості досліджуваного матеріалу та сили полірування. Протягом заданого числа проходів зміна напрямку вигладжування призводить до практично однакових значень амплітуди шорсткості, але суттєвим відмінностям у ступені зміни значень параметрів R_{pk}, S_{pk} та R_{mr}, S_{mr}, що характеризують пік шорсткості. У порівнянні з токарним напрямом подачі найбільшого поліпшення було досягнуто при використанні напрямків «назад–вперед» у разі 2 проходів та стратегії «назад–вперед–вперед» у разі 3-кратного повторення, тому автори рекомендують їх використання. При вигладжуванні за 3 проходи в напрямках «вперед–назад–вперед» відбувається розшарування матеріалу, що погіршує шорсткість поверхні, тому це настроювання використовувати не рекомендується.*

Ключові слова: *токарна обробка; вигладжування; шорсткість поверхні; екологічно чисте оброблення.*

UDK 621.923.7 **doi: 10.20998/2078-7405.2022.97.07**

V. Ferencsik, G. Varga, Miskolc, Hungary

THE EFFECT OF BURNISHING PROCESS ON SKEWNESS AND KURTOSIS OF THE SCALE LIMITED SURFACE

Abstract. *In this paper roughness examination and analysis on burnished low alloyed aluminium surfaces are reported, highlighting 2 parameters from the vertical deviations of the roughness profile from the mean line. From the input parameters of the burnishing process, the effect of burnishing force, feed rate, speed and number of passes are investigated. Measurements of the surface topography – before and after burnishing – are conducted on an Altisurf 520 3D measuring device. The generated and calculated values of the machined surface roughness are analysed in detail with the drawing of the conclusions as well.*

Keywords: *low-alloy aluminum; smoothing; surface roughness; parameters of the 3D topography of the surface.*

1. INTRODUCTION

The quality of the machined surface is crucial for mechanical parts as, it is an indicator of surface integrity, thus it has a direct impact on the properties and complete lifetime of the product [1]. For this reason, measuring and evaluating the surface roughness of machined parts is a widely used method in industry [2–4]. As a result of the ever-higher requirements, many measurement methods and techniques have been developed which are partly contained in standards [5, 6], and partly in the literature that provide new possibilities.

The cornerstone of the 3D evaluation technique was laid by Stout et al., when they interpreted 3D surface roughness and defined 3D metrics in their publication [7]. The scientific interest in surface topography is due to the fact that it enables a significantly more realistic analysis of the surface [8], so many researchers have dealt with investigation of this topic.

Dzionk et al. investigated and compared different 3D amplitude roughness parameters on burnished hardened C53 material shafts when the tool was Si_3N_4 ceramic ball [9]. In certain cases they managed to achieve 3.5 times better roughness values. Skoczylas et al. [10], beyond surface micro-hardness, examined S_a and S_z parameters and according to the results the values of these were effected by mostly the burnishing force. In contrast, Luo et al. [11] experienced that higher burnishing depth and speed cause higher improvement when non-ferrous materials (LY12 aluminium alloy and H62 brass) were burnished with PCD tool. In this paper, we study the effect of burnishing force (F), feed (f), speed (v), and number passes (i) on 2 kinds of 3D roughness parameters (S_{sk}, S_{ku}) investigating the correlation between these setting parameters on low alloyed aluminium workpieces.

2. IMPLEMENTATION OF BURNISHING PROCESS

Burnishing is one of the cold plastic forming procedures which utilizes the mechanics of mechanical deformation and it is suitable for machining external cylindrical surfaces. The process has many advantages: it reduces surface roughness, increases micro-hardness, while causes compressive residual stress, improves shape correctness and it is environmentally friendly because it does not require a high amount of coolant and lubricant [12–16].

The mechanism of burnishing is shown in Fig. 1., in which a rigid ball with certain parameters and defined force passes on the surface of the rotating workpiece while performing a rectilinear movement.

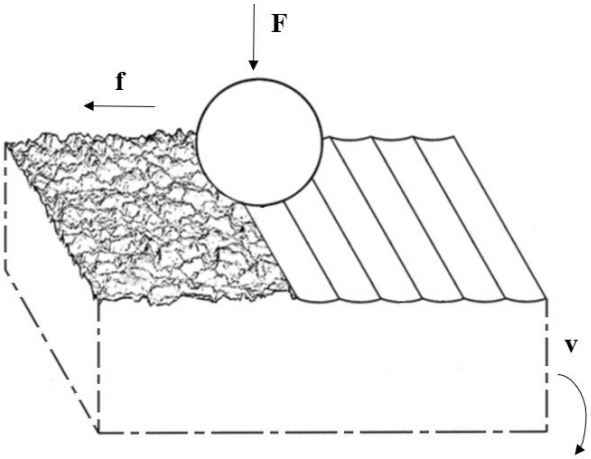

Figure 1 – Schematic illustration of burnishing [17]

In this study, the material of the examined cylindrical workpieces was EN AW-2011 grade low alloyed aluminium as extending the exact knowledge of machinability of non-ferrous materials is a major field in many industries (automotive, aeronautics, aerospace) due to their low density and good mechanical properties [18–20].

Before burnishing, finish turnings were carried out set at f_1 = 0.2 mm/rev, than f_2 = 0.15 mm/rev. Burnishing process was realized with the same machine (E400 universal lathe) using r = 3.5 mm radius PCD spherical tool. The kinematic viscosity of the manually dosed oil was ν = 70 mm^2/s.

Table 1. contains the adjusted burnishing parameters, which were determined based on preliminary experimental work.

Table 1 – Applied burnishing parameters

No	*F* [N]	*f* [mm/rev]	*v* [m/min]	*i* [-]
1	15	0.05	50.54	2
2	25	0.05	50.54	2
3	35	0.05	50.54	2
4	25	0.01	50.54	2
5	25	0.1	50.54	2
6	25	0.05	35.71	2
7	25	0.05	71.43	2
8	25	0.05	50.54	1
9	25	0.05	50.54	3

3. MEASURING OF THE 3D SURFACE ROUGHNESS

Many methods and techniques are known for characterizing surfaces and measuring surface roughness. It is important and necessary to review the measurement practice, the setting and standardization requirements of the measurement conditions, especially in the case of 3D topographic measurement and evaluation [21].

In this experiment, measurements of 3 areas of 2x2 mm rotated by 120° were implemented with an Altisurf 520 3D surface topography measuring device before and after burnishing. CL2 confocal chromatic sensor was used, the cut-off was 0.8 mm and Gauss filter was applied.

Results were evaluated with Altimap Premium software, Fig. 2 shows a state during measuring process.

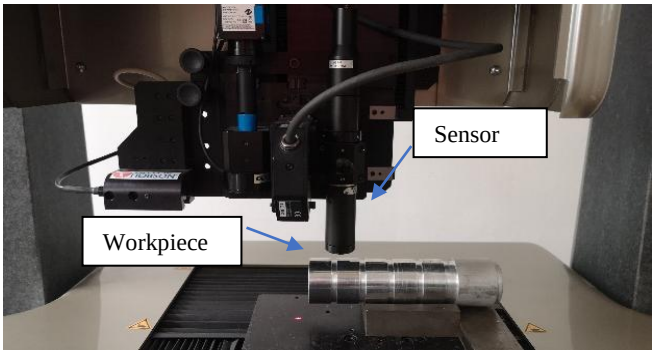

Figure 2 – Working area of the measuring device

The 3D roughness parameters can be classified into 6 groups, one of them is the amplitude parameters [22], Table 2 includes which 2 parameters from those were examined.

Table 2 – Examined 3D roughness parameters according to EN ISO 25178 [23]

Mark	Name	Definition	Formula
S_{sk}	Skewness of the scale limited surfaces	Represents the degree of bias of the roughness shape (asperity)	$\frac{1}{{S_q}^3}\left[\frac{1}{A}\iint_A Z^3(x,y)dxdy\right]$
S_{ku}	Kurtosis of the scale limited surface	The value of it is a measure of sharpness of the roughness profile	$\frac{1}{{S_q}^4}\left[\frac{1}{A}\iint_A Z^4(x,y)dxdy\right]$

4. RESULTS

Table 3–4 summarizes the averaged values of the measured roughness parameters and contains dimensionless ratios that were created to make more illustrative the changes.

For S_{sk} parameter the calculations were made according to El-Taweel and El-Axir [24]:

$$\Delta\rho_{S_{sk}}\% = \left(\frac{S_{sk_{before}} - S_{sk_{after}}}{S_{sk_{before}}}\right) \cdot 100\%, \quad (1)$$

where:

$S_{sk\ \text{before}}$ — Surface roughness parameter measured after turning,
$S_{sk\ \text{after}}$ — Surface roughness parameter measured after burnishing,
$\Delta\rho S_{sk}\%$ — Percentage value of the calculated ratio.

Table 3 – The results of S_{sk} with the calculated ratios of the experiment

No.	S_{sk} [µm]		$\Delta\rho_{S_{sk}}$ [%]
	before	after	
1	0.4033	-0.5941	247.31
2	0.3373	-0.4502	233.47
3	-0.5299	0.2204	-141.59
4	-0.1326	-0.1361	2.64
5	0.0988	0.5335	-439.98
6	0.5559	-0.0160	102.88
7	0.5461	0.0015	99.73
8	0.3335	-0.3031	190.88
9	0.2222	-0.0068	103.06

The smaller the value of S_{sk} become, the better the change, because in the case of a negative S_{sk}, it is a surface with good bearing properties and wear-resistant. In the case of a positive value of S_{sk}, there are sharp peaks on the surface, which result in very fast initial wear.

As S_{ku} expresses the dispersion range of the topography, and for Gaussian surfaces S_{ku} = 3 [25], therefore, the ratios express the deviation from this value, as the closer $\Delta_{S_{ku}}$ is to zero, the better its value due to burnishing. Measurement results of S_{ku} before and burnishing are shown in Table 4 as an illustration.

$$\Delta S_{ku} = 3 - S_{ku\_b/a} \quad (2)$$

Table 4 – The results of S_{ku} with the calculated ratios of the experiment

No.	S_{ku} [µm] before	$\Delta S_{ku\ b}$ [µm]	S_{ku} [µm] after	$\Delta S_{ku\ a}$ [µm]
1	2.5835	0.4165	3.0478	-0.0478
2	2.7854	0.2146	3.7455	-0.7455
3	6.4683	-3.4683	3.9387	-0.9387
4	3.3558	-0.3558	3.0667	-0.0667
5	3.7699	-0.7699	4.3709	-1.3709
6	2.7839	0.2161	3.2129	-0.2129
7	2.6563	0.3437	3.0571	-0.0571
8	2.6515	0.3485	3.4251	-0.4251
9	2.5508	0.4492	4.9857	-1.9857

The influences of investigated burnishing parameters (horizontal axis) on calculated ratios and deviations (vertical axis) are presented in diagrams (Diagram 1-4).

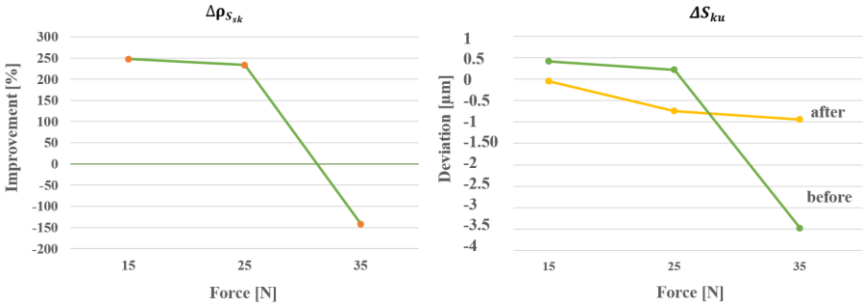

Diagram 1 – The effect of burnishing force on the analysed parameters

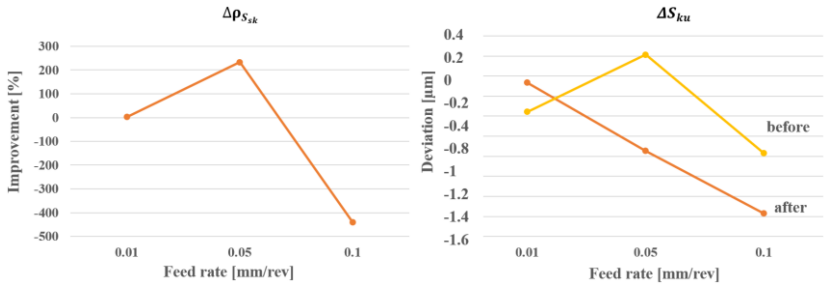

Diagram 2 – The impression of feed rate on the analysed parameters

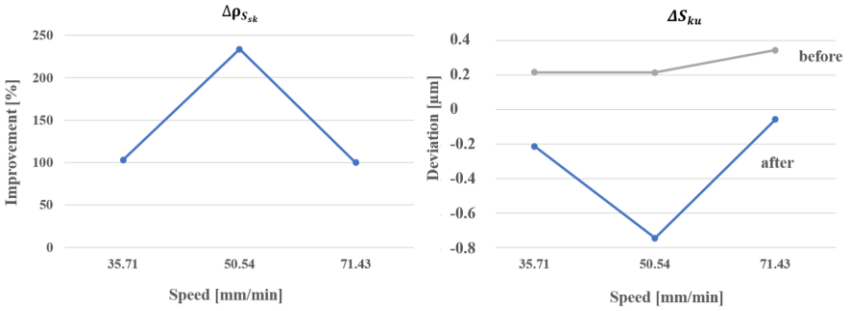

Diagram 3 – The impression of speed on the analysed parameters

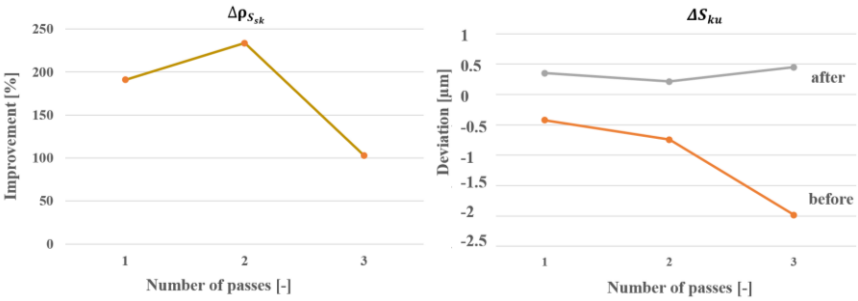

Diagram 4 – The impression of number of passes on the analysed parameters

The calculated results and the diagrams clearly show that the most advantageous parameter setting was in the case of marked 1 surface. So, applying F = 15 N burnishing force with f = 0.05 mm/rev feed rate, and 50.54 m/min speed with i = 2 number of passes produces the most preferred surface roughness values.

5. SUMMARY

This paper analysed the burnishing process on low alloyed aluminium cylindrical workpieces, where the considered parameters were burnishing force, feed rate, speed and number of passes. From the 3D amplitude roughness parameters the skewness and kurtosis of the scale limited surface were tested. According to the measured and calculated results, following conclusions can be made:

- The most approving changing in surface roughness was experienced in case of marked 1 surface and further results demonstrate that setting of F = 15 N force with f = 0.05 mm feed rate is the most beneficial.
- The numerical experiment results also obviously prove that the higher feed rate and speed adversely affect the change in surface roughness as, in case of 5 marked surface all 3D roughness parameters deteriorated to a great extent.
- Our future plans include investigating further 3D roughness parameters in order to better understand the process taking place during machining.

ACKNOWLEDGEMENTS

"Project no. NKFI-125117 has been implemented with the support provided from the National Research, Development and Innovation Fund of Hungary, financed under the K_17 funding scheme."

References: 1. *J. Kundrák, A. Nagy, A.P. Markopoulos, N.E. Karkalos*: Investigation of surface roughness on face milled parts with round insert in planes parallel to the feed at various cutting speeds, Rezanie I Instrumenty V Tekhnologicheskih Sistemah 91, (2019) 87-96. **2.** *G. N. Tóth, Á. Drégelyi-Kiss, B. Palásti-Kovács:* Analysis of the microgeometric parameters of cut surfaces, Pollack Periodica: an international journal for engineering and information sciences vol. 8 (2013). 55-66. **3.** *Á. Drégelyi-Kiss, Á. Czifra, B. Palásti-Kovács:* Comparison of capability calculations of surface roughness measurement in automotive industry, Proceedings of the ISMQC (2013) 1-8. **4.** *V. Molnár, I. Sztankovics:* Analysis of Roughness Parameters Determining Tribological Properties in Hard Turned Surfaces, Hungarian Journal Of Industry And Chemistry 49:2 (2021) 77-84. **5.** EN ISO 4287 Geometrical Product Specification (GPS) - Surface texture: Profile method. Terms, definitions and surface texture parameters (1997). **6.** ISO/DIS 25178-2: Geometrical product specification (GPS) - Surface texture: Areal - Part 2. Terms, definitions and surface texture parameters (2012). **7.** *G. Farkas:* Esztergált műszaki műanyag felületek mikrotopográfiai jellemzői, Ph.D. értekezés, (2010) 1-138. **8.** *J. Kundrák, I. Sztankovics, V. Molnár*: Accuracy and topography analysis of hard machined surfaces, Manufacturing Technology 21:4, (2021) 512-519. **9.** *S. Dzionk, B. Scibiorski, W. Przybylski*: Surface texture analysis of hardened shafts after ceramic ball burnishing, Materials vol. 204, (2019) 1-15. **10.** *A. Skoczylas, K. Zaleski:* Selected properties of the surface layer of C45 steel parts subjected to laser cutting and ball burnishing, Materials 3429, (2020) 1-19. **11**. *H. Luo, J. Liu, L. Wang, Q. Zhong:* Investigation of the burnishing process with PCD tool on non-ferrous metals, Int. J. Adv. Manuf. Technol. 25, (2005) 454-459. **12.** *G. Varga, B. Sovilj, I. Pasztor:* Experimental Analysis of Sliding Burnishing, Academic Journal of Manufacturing Engineering 11, (2013) 6-11. **13.** *MR. Stalin John, P. Suresh, D. Raguramand, BK. Vinayagam:* Surface characteristics of low plasticity burnishing for different materials using lathe, Arab J Sci Eng. 39, (2014) 3209–3216. **14.** *A. Akkurt:* Comparison of roller burnishing and other methods of finishing treatment of the surface of openings in parts from tool steel D3 for cold forming, Metal Science and Heat Treatment 53, (2011)145-150. **15.** *L. Luca, S. Neagu-Ventzel, I. Marinescu:* Effects of working parameters on surface finish in ball-burnishing of hardened steels, Precision Engineering 29, (2005) 253-256. **16.** *W. Grzeski, B. Kruszynski, A. Ruszaj:* Surface integrity of machined surfaces, Materials Science (2010) 143-179. **17.** *C. Cao, J. Zhu, T. Tanaka, D.N. Pham:* Invetsigation of corrosion resistance enhancemet for biodegradable magnesium alloy by ball burnishing process, Int. J. of Automation Technology 14, (2020) 175-183. **18.** *R. Horváth, Á. Drégely-Kiss, Gy.*

Mátyási: The examination of surface roughness parameters in the fine turning of hypereutectic aluminium alloys, U. P. B. Sci. Bull., Series D 77, (2015) 205-216. **19.** *Varga, G.:* Effects of technological parameters on the surface texture of burnished surfaces, Key Engineering Materials 581, (2014), 403-408. **20.** *D. Toboła, P. Rusek, K. Czechowski, T. Miller, K. Duda:* New Indicators of Burnished Surface Evaluation – Reasons of Application, Metrol Meas Syst 12, (2015), 263–274. **21.** *G. Farkas, K. B Palásti, G. Kalácska:* Műszaki felületek mikrogeometriai vizsgálata, MTA Agrárműszaki Bizottság, XXIX. Kutatási és Fejlesztési Tanácskozás, (2005), 113-117. **22.** *R. Deltombe, M. Kubiakk, R. Krzysztof, M. Bigerelle:* How to select the most relevant 3D roughness parameters of a surface, Scanning 36, (2014), 150-160. **23**. ISO 22081:2021, Geometrical product specifications (GPS) – Geometrical tolerancing – General geometrical specifications and general size specifications, (2021), https://www.iso.org/standard/72514.html (Viewed: 01/06/22). **24.** *T.A. El-Taweel, M.H. El-Axir:* Analysis and optimization of the ball burnishing process through the Taguchi technique, International Journal of Advanced Manufacturing Technologies 41, (2009), 301-310. **25.** *K. B. Palásti:* Gépalkatrészek minősége. Tervezés, gyártás, minősítés. BMF BGK, Főiskolai jegyzet (2001) 10-25.

Вікторія Ференчик, Дьюла Варга, Мішкольц, Угорщина

ВПЛИВ ПРОЦЕСУ ВИГЛАДЖУВАННЯ НА АСИМЕТРІЮ І ЕКСЦЕС ПОВЕРХНІ ОБМЕЖЕНОГО МАСШТАБУ

Анотація: *У цій статті повідомляється про дослідження та аналіз шорсткості полірованих поверхонь із низьколегованого алюмінію з виділенням двох параметрів вертикальних відхилень профілю шорсткості від середньої лінії. Оздоблювальне накочування (галтівка) сталевими кульками - це одна з процедур холодного пластичного формування, в якому використовується механіка механічної деформації і яка підходить для обробки зовнішніх циліндричних поверхонь. Процес має багато переваг: зменшує шорсткість поверхні, підвищує мікротвердість, при цьому викликає залишкові напруження стиснення, покращує правильність форми і є екологічно чистим, оскільки не вимагає великої кількості рідини, що охолоджує, і мастила. У цьому дослідженні матеріалом циліндричних заготовок був низьколегований алюміній, оскільки розширення точних знань про оброблюваність кольорових металів є основною областю в багатьох галузях промисловості (автомобільній, авіаційній, аерокосмічній) через їх низьку щільність і хороші механічні властивості. Перед вигладжуванням виконували чистову токарну обробку. Процес вигладжування здійснювався на тому ж верстаті з використанням сферичного інструменту полікристалічного алмазу радіусом r = 3,5 мм. Кінематична в'язкість масла, що дозується вручну, становила = 70 мм2/с. За параметрами тривимірної амплітуди шорсткості було протестовано асиметрію та ексцес поверхні, обмеженої масштабом. За результатами вимірювань і розрахунків були зроблені такі висновки: найбільш сприятливу зміну шорсткості поверхні було відзначено у випадку поверхні з маркуванням №1, і подальші результати показують, що встановлення сили F = 15 Н з подачею f = 0,05 мм є найбільш сприятливим; результати чисельного експерименту також очевидно доводять, що вищі швидкість обробки і швидкість подачі несприятливо впливають на зміну шорсткості поверхні, оскільки у разі розміченої поверхні №5 всі параметри тривимірної шорсткості значно погіршилися. У плани авторів на майбутнє входить вивчення додаткових тривимірних параметрів шорсткості, щоб краще зрозуміти процес, що відбувається під час обробки.*

Ключові слова: *низьколегований алюміній; вигладжування; шорсткість поверхні; параметри 3D-топографії поверхні.*

UDC 620.169.1 **doi: 10.20998/2078-7405.2022.97.08**

Z. Mehdiyev, C. Felhő,
M. Berkes Maros, Miskolc, Hungary

INVESTIGATION ON PRODUCTION PARAMETERS OF ADDITIVELY MANUFACTURED ABS POLYMER GEARS

Abstract. *The amount of wear and the load-bearing capabilities are important factors in the lifespan performance of gears. And those factors can be influenced by different 3D printing parameters in production. The objective of the research work was to analyze the material behaviour of printed Acrylonitrile butadiene styrene (ABS) polymers for gears according to production parameters. Each printed specimen was tested several times and summarised the results by determining the average values. While the wear performance of the samples was highly influenced by the "Layer height" parameter, the load-bearing capacities of the printed samples were highly influenced by the amount of the "Infill pattern" production parameter. Finally, based on the carried out experimental tests, the ideal 3D printing parameters were decided to provide the highest load-bearing capacity and the lowest friction coefficient under compressive forces for 3D printed ABS polymer gears.*
Keywords: *3D printing; ABS; FDM and printing parameters.*

1. INTRODUCTION

Polymer gears have replaced metal gears in a variety of industrial applications in recent times. Because of the advantages that polymer gears have over metal gears, their use has significantly increased in the last few years. Some examples of plastic gears field applications include the automobile industry, office equipment, and household utensils, as well as food and textile machinery [1–4]. Polymer gears offer some advantages compared to metal gears, particularly, in terms of their high specific mechanical properties (high size-weight ratio), good tribological efficiency (low friction coefficient, self-lubrication), high resistance against impact loading due to the elasticity of the material, ability to absorb and damp vibration, etc.
On the other hand, polymer gears have several disadvantages, such as a reduction in load-carrying capability and low operating temperatures if compared to metal gears, relatively high dimensional variations due to temperature and humidity conditions, etc. [5]. In addition, unlike metal gears, polymer gears are usually run with no lubricant [6].

Nowadays polymer gears are mainly produced by Additive Manufacturing (3D printing) technologies because this technology is quite different from traditional techniques, and it offers so many advantages comparing with others such as the digital nature of the fabrication process.

Additive manufacturing (AM) also known as 3D printing, is getting more interest because of the significant increase in the requisition for high-performance materials and increased functionalities and complexities in a geometrical design.

In the last years, additive manufacturing has been considered an effective production technology, and it got a major position in the manufacturing sector with the development of technology. The fundamental principle of this technology is that a model initially created layer-by-layer using a 3D Computer - Aided Design system, can be produced directly without the requirement for process planning [2, 7–11].

There are many kinds of 3D printing technologies on the market, with their own capabilities and limitations. Among them all, the Fused Deposition Modelling (FDM) technique appears to be more practical for general use because it produces the objects with the filament itself while in other 3D printing techniques the use of resin-based material is a necessity [12–14]. In this method, the polymer filament is pushed onto a surface through a heated nozzle, at first it melts, and then solidifies upon touching the surface, and thus a structure is built up layer by layer [15].

There are several printing parameters such as temperature, infill pattern, layer height, printing speed, etc. that should be defined before the FDM production process. The mentioned production parameters can influence the accuracy, material and mechanical properties of the printed part, and printing time.

Because of the mentioned facts above, load-carrying capability and amount of wear are critical factors in the production process of polymer gears, and several production parameters should be investigated for this purpose.

The current paper gives a summary of the analysis carried-out on additively manufactured acrylonitrile butadiene styrene polymers used for gears, characterizing the material behaviour with ball-on-disk and compression laboratory tests.

2. SAMPLE PROCESSING

The specimens (Figure 1) were produced from ABS thermoplastics by using the "Ultimaker Original +" 3D printer (Figure 2) to perform experimental wear tests. The same 3D printer was used to print all the specimens for the current research work.

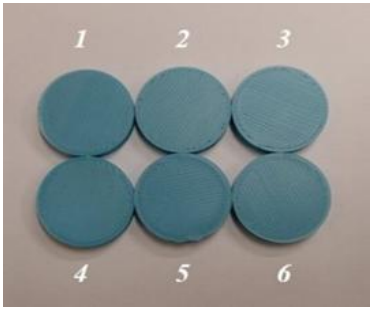

Figure 1 – 3D printed ABS samples for ball-on-disk test

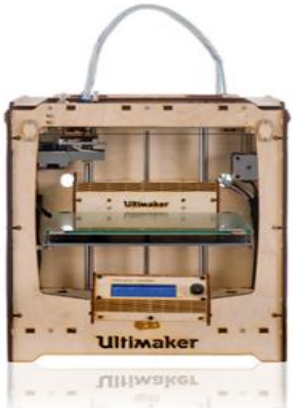

Figure 2 – Ultimaker Original +" 3D printer [16]

From Table 1 it is seen, that ball-on-disk test samples are produced with different processing parameters, providing the possibility to investigate the effect of the layer height (0.2 mm or 0.4 mm), the printing speed (30; 50 or 80 mm/s), and the number of base layers and top layers (1; 3 or 5).

Table 1 – Printing parameters of the 3D printed specimens for ball-on-disk wear tests

Material	Sample No	Temp. (^{0}C)	Layer height (mm)	Printing Speed (mm/s)	Number of Contours	Base layers	Top layers	Infill pattern, %
ABS	1	220	0.2	50	2	3	3	100
	2		0.4	50		3	3	100
	3		0.2	30		3	3	100
	4		0.2	80		3	3	100
	5		0.2	50		1	1	25
	6		0.2	50		5	5	50

The samples (Figure 3) for the experimental compression tests were produced from ABS thermoplastic in a small cube form with dimensions of 10x10x10 mm. Different printing parameter combinations (illustrated in Table 2) were used to

print all the samples, providing the possibility to investigate the influence of the temperature (190; 210; 220 or 230 ℃), layer height (0.2 mm or 0.4 mm), Infill pattern (25; 50 or 100 %). Every 3 samples were produced with the same material and the same printing parameters to determine the average test results.

Figure 3 – 3D printed ABS samples for compression test

Table 2 – The used 3D printing parameters of ABS samples for compression test:

Material	Sample No.		Temp. (^{0}C)	Layer height (mm)	Printing Speed (mm/s)	Number of Contours	Base layers	Top layers	Infill pattern, %
ABS	1	1-1.1-1.2	210	0.2	50	2	3	3	100
	2	2-2.1-2.2	220	0.2					100
	3	3-3.1-3.2	230	0.2					100
	4	4-4.1-4.2	220	0.4					100
	5	5-5.1-5.2	220	0.2					25
	6	6-6.1-6.2	220	0.2					50

3. MATERIAL TESTING METHODS

Ball-on-disk test

The standardized ball-on-disk test method is particularly well suited to analyze the relationships between the wear resistance, wear mechanisms, and loading parameters such as sliding velocity, contact pressure, and environmental conditions.

The specimens were cleaned and dried prior to the testing and measuring processes. Non-chlorinated, non-film-forming cleaning agents and solvents were

used to remove all dirt and foreign substance from the specimens. Then the required parameters were set and started the test. When the desired number of revolutions was reached, the test was stopped. As the last step, the specimens were removed and cleaned off from any loose wear debris [17]. Sometimes this last operation is neglected if the wear debris morphology would be analyzed that provides valuable information about the wear mechanism.

CETR – UNMT1 Universal Micro-Nano Materials Tester (Figure 4) was used to perform ball-on-disk sliding friction tests on specimens. Several pre-tests were performed with different loading conditions to find better test parameters for the target tests. As a result, the most purposeful testing conditions were defined and the experimental wear tests were carried out with the following variables:

− Normal load, F = 10 N;
− Time, t = 180 min;
− Sliding velocity, v = 25 mm/s;
− Rotational speed, n= 79.6 1/min.

Figure 4 – CETR – UNMT1 Universal Micro-Nano Materials Tester

Compression test

In the compression testing technique, the samples are compressed between two platens. During the test, an extensometer and load cell equipment are used for measuring displacement and force. This type of testing technique is useful to study a material or mechanical part load bearing capacity under compressive loading [18]. A schematic diagram of the compression testing machine is illustrated in Figure 5.

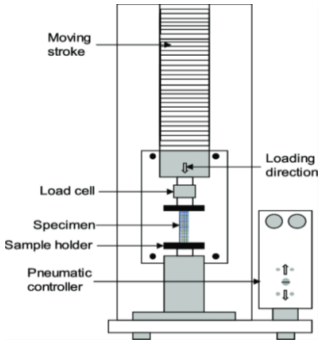

Figure 5 – Schematic diagram of the compression testing machine [19]

4. EXPERIMENTAL RESULTS AND DISCUSSION

Based on the performed ball-on-disk wear tests, the change in friction coefficient with respect to the sliding distance graphs was analyzed. Typical friction coefficient vs. sliding distance diagrams are shown in Figure 6. The diagrams show a steady-state character, i.e., the friction coefficient values are stabilized in the second half part of the total sliding distance. According to the gathered diagrams, the steady-state friction coefficient values (μ_{ss}) were determined as the average of those measured on the last 20% of the sliding distance, i.e., in the stabilized region.

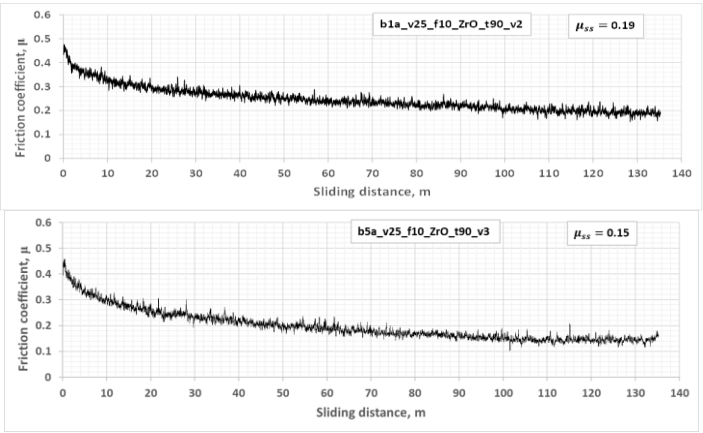

Figure 6 – Typical friction coefficient diagrams obtained during ball-on disk wear tests

The wear test results determined in the above-mentioned way, are presented in Table 3. Comparison of the measured friction coefficient data and assessing the general trend is easier by visualizing them in a diagram. While Figure 6 provides insight into the friction behaviour of the produced samples made of ABS plastics along with the whole sliding distance, Figure 7 gives information on the friction coefficient values developed at the end of the total sliding distance.

Table 3 – Steady-state friction coefficient values obtained from the ball-on-disk wear test

Material	File name (wear track)	Ball-on-disk test results			
		Final friction coefficient μ_{ss}	Average	Standard deviation, SD	Var. coeff. %
ABS	ABS_1_v1	0.168	0.181	0.019	10.5
	ABS_1_v2	0.194			
	ABS_2_v1	0.259	0.257	0.002	0.8
	ABS_2_v2	0.255			
	ABS_3_v1	0.191	0.192	0.002	0.8
	ABS_3_v2	0.193			
	ABS_4_v1	0.209	0.212	0.005	2.1
	ABS_4_v2	0.215			
	ABS_5_v2_2	0.122	0.133	0.017	12.4
	ABS_5_v3	0.145			
	ABS_6_v1	0.213	0.212	0.002	1.1
	ABS_6_v2	0.210			

By analysing the ball-on-disk experimental wear tests, the following establishments can be made regarding the influence of the technological parameters of the 3D printing on the friction behaviour of the ABS plastic samples:

- At the applied total sliding distance, the lowest friction coefficients were achieved for samples ABS_5_2_2 and ABS_5_3 and ABS_1_1, μ_{ss} = 0,122; 0,145 and 0,168 respectively.
- The less favourable friction behaviour was shown by the ABS_2_1 and ABS_2_2 samples.
- Regarding the printing parameters, the most unfavourable friction conditions occurred when the layer height was twice as high, i.e. 0.4 mm.

The friction coefficient curve for ABS_2_1 and ABS_2_2 decreases monotonically in the first half of the total sliding distance, but in the second half of the wearing test the friction coefficient values show an unusual and significant increase that is characteristic for no other samples. A possible explanation for this can be that the higher layer height adversely affected the wear behaviour, e.g., by modifying the layer structure and stiffness, making the surface layer more sensitive to damage, thus the resulting wear debris increased the value of the coefficient of friction.

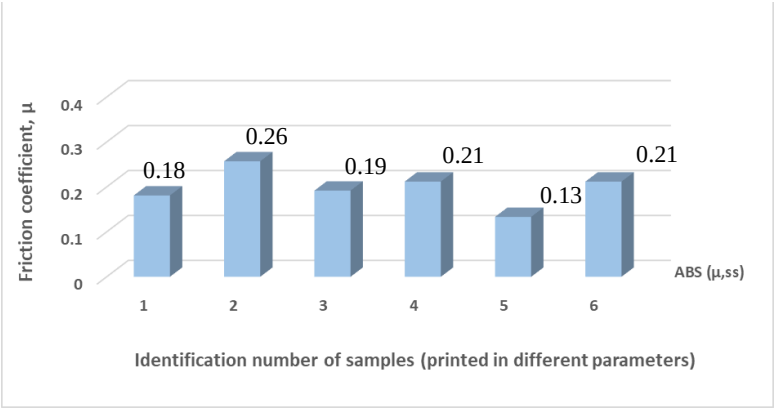

Figure 7 – Comparison of the steady state friction coefficient (μ_{ss}) values measured on the ABS samples

Based on the executed tribological tests, the processing parameters of the 3D printing, which provides the lowest friction coefficient, were determined as below.

- Temperature: 220 °C
- Layer height: 0.2 mm
- Printing speed: 50 mm/s
- Number of Contours: 2
- Base Layers: 1-3
- Top Layers: 1-3
- Infill pattern: 100%

In addition, compression laboratory tests were carried out on the 18 samples, and the maximum compressive forces were determined and summarized by calculating their average values for each sample group (illustrated in Table 4). Figure 8 shows typical force vs. displacement diagrams recorded during the compression tests to evaluate the effect of the 3D printing parameters on the test results.

Table 4 – F_1 and F_2 maximum compressive force values for ABS thermoplastics

Material	Sample No.		Compression test results			
			F_1 maximum compressive force (at 0.5 mm displace-ment or first peak point), N	Average	F_2 maximum compressive force (at the last peak point), N	Average
ABS	1.	1	5900	5600	9801	9167
		1.1	5501		9000	
		1.2	5400		8700	
	2.	2	5900	5667	8900	8501
		2.1	5700		8400	
		2.2	5400		8201	
	3.	3	5400	5567	8001	8201
		3.1	5600		8101	
		3.2	5700		8501	
	4.	4	4801	4668	9302	9234
		4.1	4602		9302	
		4.2	4601		9100	
	5.	5	2802	2735	2201	2367
		5.1	2702		2400	
		5.2	2701		2500	
	6.	6	3201	3301	3001	3767
		6.1	3400		4100	
		6.2	3301		4200	

Figure 9 was created regarding the average of the maximum compressive force values that were determined for 0.5 mm displacement or the first peak point in Figure 8. It can be clearly seen in Figure 9 that the highest average compressive force (F_1 = 5667 N) was calculated on sample group number 2 (2; 2.1; 2.2). An additional observation is that the maximum compressive forces for the sample groups number 5 and 6 decrease significantly. A possible explanation for this can be the decrement of the infill pattern parameter of the samples. The lower infill in percentage makes the structures sensitive to failure under compressive forces.

It can be established that 3D printing parameters have a significant influence on the load-bearing capacity of ABS thermoplastics. The difference between the highest and lowest average maximum compressive force values reaches 48% of the highest one.

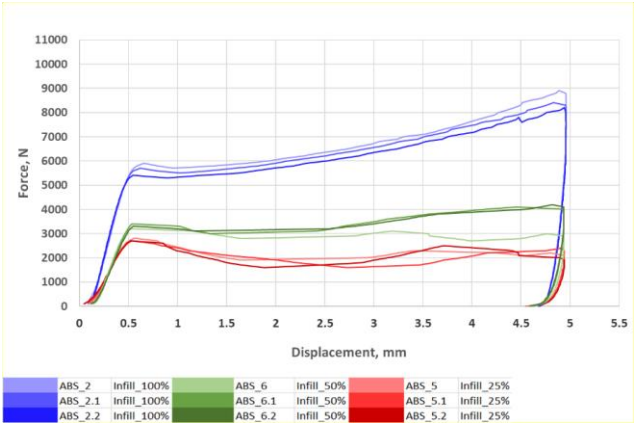

Figure 8 – The effect of "Infill pattern" parameter on load-bearing capability of samples

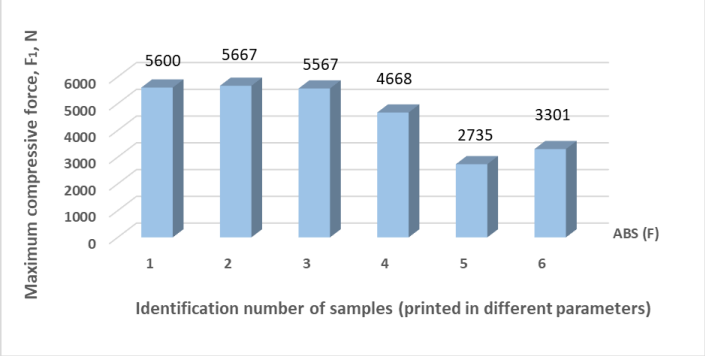

Figure 9 – Comparison of the average of F_1 maximum compressive forces

According to the compression test results, the following printing parameters presented the best results providing the highest load-bearing capabilities.

- Temperature: 220 °C
- Layer height: 0.2 mm
- Printing speed: 50 mm/s
- Number of Contours: 2
- Base Layers: 3
- Top Layers: 3
- Infill pattern: 100%

5. CONCLUSIONS

The objective of the current research work was to investigate the influence of the printing parameters on the material's behaviour of ABS polymers used for the 3D-printed gears by characterizing the material with ball-on-disk and compression tests. in order to define the load-bearing capability and wear performance.

In total, six specimens for the wear and eighteen specimens for the compression tests were printed by using the „Ultimaker Original +" 3D printer from (ABS) thermoplastic. All the specimens were printed with different printing parameter combinations to analyze their influences on the sample behaviour. For the ball-on-disk wear tests, the analyses were carried out on a variety of specimens, and the friction coefficient vs. sliding distance curve was compiled using the obtained wear test data. As a result, for the applied total sliding distance, the lowest steady state friction coefficients were achieved for sample ABS_5, $\mu_{ss} = 0.133$ as average.

Another very important factor for the gears is the load-bearing capability of the printed samples, which was investigated by the compression experimental testing method. The investigations were performed on the recorded compression test data to analyze the influence of different printing parameters on the load-bearing capabilities of printed samples. Temperature and layer height printing parameters had a measurable, but slighter influence, while the infill pattern parameter proved to have the highest effect on the load-bearing capabilities of the printed ABS polymers. According to the test results, sample group 2 could bear the highest average maximum compressive force $F_1 = 5667$ N.

As a summary, based on the executed tribological tests, the best 3D printing parameters were determined to provide the lowest friction coefficient and the highest load-bearing capacity under compressive forces for additively manufactured ABS polymer gears. These ideal 3D printing parameters are, as below:

- Temperature: 220 °C
- Layer height: 0.2 mm
- Printing speed: 50 mm/s
- Number of Contours: 2
- Base Layers: 3
- Top Layers: 3
- Infill pattern: 100%

References: 1. *M. S. A. Mote, A. v Gaur, and M. A. B. Gujale,* "Design and FEM Analysis of Helical Gear," *Journal Impact Factor*, vol. 2, p. 14, 2018. **2.** *A. Bravo, D. Koffi, L. Toubal, and F. Erchiqui,* "Life and damage mode modeling applied to plastic gears," *Eng Fail Anal*, vol. 58, pp. 113–133, 2015. **3.** *B. Polanec, F. Zupanič, T. Bončina, F. Tašner, and S. Glodež,* "Experimental investigation of the wear behaviour of coated polymer gears," *Polymers (Basel)*, vol. 13, no. 20, Oct. 2021, doi: 10.3390/polym13203588. **4.** *B. Trobentar, M. Hriberšek, S. Kulovec, S. Glodež, and A. Belšak,* "Noise Evaluation of S-Polymer Gears," *Polymers (Basel)*, vol. 14, no. 3, Feb. 2022, doi: 10.3390/polym14030438. **5.** *B. Trobentar, S. Kulovec, G. Hlebanja, and S. Glodež,* "Experimental failure analysis of S-polymer

gears," *Eng Fail Anal*, vol. 111, p. 104496, 2020. **6.** *J. R. Davis*, Gear materials, properties, and manufacture. ASM International, 2005. **7.** *K. Gupta, N. K. Jain, and R. F. Laubscher*, "Advanced gear manufacturing and finishing: classical and modern processes," 2017. **8.** *P. Varalakshmi, G. R. Kumar, D. S. Harshitha, C. Akhila, and B. Priyatham*, "Modeling and Manufacturing of Helical Gear by using 3D Printing Technology". **9.** *Z. Mehdiyev, C. Felhő, and K. P. Zoltán,* "Investigation on 3D Printing Parameters of PLA Polymers for Gear Applications," in *Vehicle and Automotive Engineering 4*, 2023, pp. 654–664. **10.** *V. Roda-Casanova and F. Sanchez-Marin*, "A 2D finite element based approach to predict the temperature field in polymer spur gear transmissions," *Mech Mach Theory*, vol. 133, pp. 195–210, 2019. **11.** *L. J. Kumar, P. M. Pandey, and D. I. Wimpenny*, 3D printing and additive manufacturing technologies, vol. 311. Springer, 2019. **12.** *J. Griffey*, 3-D printers for libraries. American Library Association, 2014. **13.** *C. Barnatt, 3D printing third edition*. CreateSpace Independent Publishing Platform, 2016. **14.** *M. Paudyal*, "A Brief Study on Three-Dimensional Printing Focusing on the Process of Fused Deposition Modeling," 2015. **15.** *P. J. Bártolo,* Stereolithography: materials, processes and applications. Springer Science & Business Media, 2011. **16.** *Ultimaker*, "Ultimaker Original+Full Specifications."; Available from: <https://ultimaker.com/3d-printers/ultimaker-original-plus> [Accessed on 14.09.2022]. **17.** *A. T. Methods*, "Standard Test Method for Wear Testing with a Pin-on-Disk Apparatus1," *Wear*, vol. 5, pp. 1–5, 2011. **18.** *Arunachalam, R. and P.K. Krishnan*, Compressive Response of Aluminum Metal Matrix Composites, in Reference Module in Materials Science and Materials Engineering. 2021, Elsevier. **19.** *A. Nazir and J.-Y. Jeng*, "Buckling behavior of additively manufactured cellular columns: Experimental and simulation validation," *Mater Des*, vol. 186, p. 108349, 2020.

Зія Мехдієв, Чаба Фельхо,
Марія Беркеш Марош, Мішкольц, Угорщина

ДОСЛІДЖЕННЯ ВИРОБНИЧИХ ПАРАМЕТРІВ АДИТИВНО ВИГОТОВЛЕНИХ АБС-ПОЛІМЕРНИХ ЗУБЧАТИХ КОЛІС

Анотація: *Величина зношування та несуча здатність є важливими факторами, що впливають на термін служби зубчастих передач. І ці чинники можуть впливати різні на параметри 3D-друку у виробництві. В останні роки адитивне виробництво вважалося ефективною технологією виробництва, і з розвитком технологій воно зайняло важливе місце у виробничому секторі процесу. Мета дослідження полягала в тому, щоб проаналізувати поведінку надрукованих акрилонітрил-бутадієн-стирольних (АБС) полімерів для зубчастих коліс залежно від виробничих параметрів. Кожен надрукований зразок тестували кілька разів і підсумовували результати, визначаючи середні значення. У той час як на зносостійкість зразків сильно впливав параметр «Висота шару», на несучу здатність друкованих зразків, сильно впливала величина виробничого параметра «Шаблон заповнення». Нарешті, на основі проведених експериментальних випробувань було прийнято рішення про ідеальні параметри 3D-друку, щоб забезпечити найвищу несучу здатність і найнижчий коефіцієнт тертя при стискаючих зусиллях для зубчастих коліс, надрукованих на 3D-принтері з АБС-пластика. Усі зразки були надруковані з різними комбінаціями параметрів друку, щоб проаналізувати вплив на поведінку зразка. В результаті, для прикладеного повного шляху ковзання найнижчі коефіцієнти стаціонарного тертя досягнуто для зразка ABS_5, μ_{ss} = 0,133 в середньому. Іншим дуже важливим фактором для зубчастих коліс є несуча здатність друкованих зразків, яка була досліджена методом експериментальних випробувань на стиск. Параметри друку температури та висоти шару мали сумірний, але менший вплив, у той час як параметр малюнка заповнення справив найбільший вплив на несучу здатність надрукованих АБС-полімерних зразків. За результатами випробувань група зразків 2 витримала найбільше середнє максимальне зусилля F_1 = 5667 Н.*

Ключові слова: *3D-друк; АБС-полімер; FDM та параметри друку.*

UDC 621.9.048 **doi: 10.20998/2078-7405.2022.97.09**

A. Mitsyk, V. Fedorovich, Kharkiv, Ukraine

THE NATURE OF THE FORMATION OF SURFACE MICRO-ROUGHNESS IN VIBRATION FINISHING AND GRINDING PROCESSING

Abstract. *The main aspects related to the nature of the formation of surface micro-roughness during vibration finishing and grinding processing are given. It is indicated that the material removal from the surface of the part occurs as a result of the combined action of micro-cutting processes, chipping of metal particles during repeated deformation of the processed surface areas, their fatigue and destruction, the formation, destruction and removal of secondary structures, and adhesion phenomena. It is noted that the real surface after vibration treatment is a set of roughnesses of a certain size, shape and direction. It is defined that the micro-roughness of the surface of the part during vibration finishing and grinding is formed in the form of traces from numerous impacts of abrasive granules on the surface of the part. The largest value of the granule penetration into the processed surface is determined, that makes it possible to characterize the trace from plastic compression in the zone of collision between the granule and the part. The technique and study of the mechanism of formation of surface microroughness is considered. An expression is determined for the normal component of the impact force, which characterizes the main effect on the mechanism of micro-roughness formation. The value of penetration of the granule into the metal of the part is determined. The study showed that the surface micro-roughness during vibration treatment is formed by impacts of granules on the part at different meeting angles. The traces from action of straight and oblique impacts are established. The average height of micro-roughness is calculated. According to the hodographs, the normal velocities of abrasive granules and parts are determined. The average value of the angle of impact of the granules with the part at any point of the trajectory of their movement is also determined. It was revealed that the velocities of granules and parts change in magnitude and direction during one period of the reservoir oscillation, reaching their limiting values, which are proportional to the reservoir movement velocities. The degree of proportionality is expressed by the similarity coefficient for the granule and the part. The average similarity coefficient was also determined by the points of the hodograph. The average values of the movement velocities of the granule and the part in the reservoir are obtained. The minimum and maximum value of the granule penetration into the surface of the part is established. The formulas for the limiting values of the granule penetration depth are given, taking into account the coefficient of ellipticity. The results of calculations for determining the height of micro-roughness of the processed part surface are presented. A formula is obtained for determining the surface micro-roughness during vibration finishing and grinding processing.*

Keywords: *vibration treatment; abrasive granule; processed part; collision between granule and processed part; collision angle; surface micro-roughness; velocity hodographs.*

1. Introduction

In vibration finishing and grinding process, as well as in other finishing methods, the processed surface in terms of geometric parameters is the intersection of the original surfaces with new processing traces, characteristic for this process [1, 2].

The nature of this intersection may be different under different processing conditions. That is, the nature of the micro-roughness of the parts surface layer during vibration treatment is the result of its deformation by granules of a free abrasive medium, as well as by the action of physicochemical processes taking place in the zone of collision of granules with the processed part [3].

In this case, the removal of material from the surface of the part occurs as a result of the combined action of such processes as micro-cutting with the part metal removal, chipping as a result of multiple deformation of the processed surface sections and their fatigue and destruction, the formation, destruction and removal of secondary structures, adhesion phenomena. The real surface after vibration treatment is a set of roughness of a certain size, shape and direction [4].

The study of traces of processing, their structure and dimensions provides information about physical phenomena in the collision zone of granules and processed parts, and also reveals the nature of the formation of micro-roughness of the newly formed surface.

2. The nature of the collision of granules with the surface of the processed part

It is known from practice that the micro-roughness of the surface of parts during finishing and grinding processing is formed in the form of traces from numerous wave impacts of abrasive granules on the processed surface of the part [5, 6].

During vibration processing, inelastic bodies collide, as a result of which the depth β of indentation of a granule into the part surface can be determined by the equality $\beta = \beta_1 + \beta_2$, where β_1, β_2 is the elastic and plastic parts of local crushing and indentation.

The elastic part β_1 of the local collapse after the rebound of the abrasive granules from the processed surface is restored to its original state. The trace left on the part is determined by the size of the local collapse.

The largest value of the penetration of the granule into the part surface is determined as,

$$\beta_{2\max} = \frac{a}{\pi D \sigma_s} P_N ,$$

where a is a constant coefficient, $a = 0.35$; D – imprint diameter; σ_s – yield strength of the material under simple tension; P_N is the normal component of the impact force in an oblique collision.

Elastic-plastic deformations of the abrasive granule in the zone of contact with the part are not taken into account due to the significant hardness of the material from which the part is made [7, 8].

Under the action of the normal component of the impact force P_N, the processed surface of the part under the granule flows and is squeezed out around its periphery, forming a trace from plastic compression.

3. Technique and study of the mechanism of formation of micro irregularity of the processed part surface

In oblique impact, the normal component of the interaction causes the penetration of the granule into the surface of the part, the tangential component causes the shear of the metal. The main action on the mechanism of formation of micro-roughness is exerted by the normal component of the impact force. It is determined by the expression:

$$P_N = \frac{2(1+k)mM\left(V_1 \sin\alpha_1 - V_2 \sin\alpha_2\right)}{\Delta T\left(m+M\right)}.$$

Hence, the value of the granule penetration into the metal is determined as:

$$\beta_2 = \frac{a(1+k)mM\left(V_1 \sin\alpha_1 - V_2 \sin\alpha_2\right)}{\pi D\sigma_s \Delta T\left(m+M\right)},$$

where k is the recovery factor; m – weight of the granule; M – mass of the part; V_1, V_2 – velocities of a granule and a part at the moment of their collision; ΔT – collision time; α_1, α_2 – angles between the direction of the velocity of the abrasive granule and the part and the normal to the line of centers of the colliding bodies; $D = \rho_x$ – grain size of the granule material; σ_s – the yield strength of the material of the part at simple tension.

Experimental studies show that the micro-roughness of the surface during vibration treatment is formed by impacts of granules at different meeting angles and has an irregular character [9]. You can determine the traces of the impact of direct and oblique impacts. There are n_1 traces from straight and n_2 traces from oblique impacts on the surface of the part with a length of l. The average height of micro-roughness, calculated on the basis of geometric constructions, is equal to:

$$H_{\text{avg}} = \frac{\left(\beta'_{2\min} + \beta'_{2\max}\right)n_1 + \left(\beta_{2\min} + \beta_{2\max}\right)n_2}{2\left(n_1 + n_2\right)},$$

where $\beta'_{2\min}$ and $\beta'_{2\max}$ – the smallest and largest depth of penetration of the granule during an oblique impact; n_1, n_2 – the number of straight and oblique impacts of the granule.

Obviously, the penetration depth is proportional to the normal component of the collision velocity, that is, $V_1 \sin\alpha_1 - V_2 \sin\alpha_2 = V_{\text{avg}}$, where V_{avg} is the average collision velocity.

The value $V_1 \sin\alpha_1$ represents the velocity of the granule directed along the line connecting the center of the colliding bodies. The value $V_2 \sin\alpha_2$ represents a similar value. These values are the velocity components V_1 and V_2 directed along the line of impact of the abrasive granule on the part.

The normal velocities of the abrasive granule and processed part can be determined from the hodographs of their velocities. By superimposing hodographs one on another, we determine the angles between their velocities at each point (Fig. 1). Then the angle between the velocities of the granule and the part at point *1* will be equal to α_1, at point 2 – α_2, at point 3 – α_3, etc.

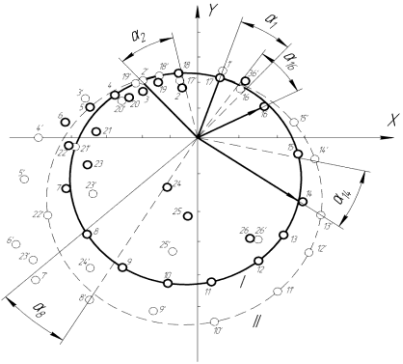

Figure 1 – Scheme for determining the angle of meeting of the granule and the part:
I – hodograph of the velocity of the part; II – hodograph of the velocity of the granule

The average value of the angle α_{avg} for the period of one oscillation is,

$$\alpha_{\text{avg}} = \frac{\alpha_1 + \alpha_2 + \alpha_3 + ... + \alpha_n}{n},$$

where n is the number of velocity measurement points along the hodograph.

Collision of granules with a part can occur at any point of their trajectory. At each point of the hodograph the angles between the velocity of the granule and the part is approximately equal to each other. Therefore, we can assume that the velocities at this moment are directed relative to each other at an angle of α_{avg}. In this case, two separate equally probable positions of the impact line O_1O_2 (Fig. 2) are possible, when the latter coincides: with the velocity V_1 of the granule (line $O_1^{'}O_2^{'}$) and with the velocity V_2 of the part (line O_1O_2).

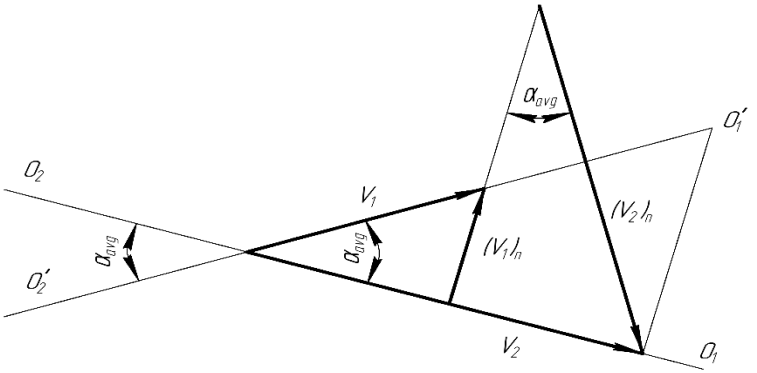

Figure 2 – Scheme for determining the collision velocity of the granule and the part: $(V_1)_n$, $(V_2)_n$ – normal components of the movement velocities of the granule and the part

Let us decompose the velocities V_1 and V_2 into normal (V_{1n} and V_{2n}) and tangential (V_{1t} and V_{2t}) components. As it was said, micro-roughness is formed due to the normal component. According to (see Fig. 2) the average velocity V_{avg} is determined as $V_{\text{avg}} = \dfrac{V_{1n} + V_{2n}}{2}$.

Since the collisions are carried out at an average angle of α_{avg}, then $\sin\alpha_1 = \sin\alpha_2$. Replacing the speed components V_{1n} and V_{2n} with their values, we get: $V_{\text{avg}} = (V_1 - V_2)\dfrac{\sin\alpha_{\text{avg}}}{2}$.

The velocities of granules and parts change in magnitude and direction during one oscillation of the reservoir, reaching their limiting values. They are

approximately proportional to the velocities of the reservoir. The degree of this proportionality is expressed by the similarity coefficients for the granule F_1 and for the part F_2.

Then the average similarity coefficient for the full period of oscillation is determined as the probable value of the individual similarity coefficients according to the hodograph points:

$$F_1 = \frac{\sum_1^n \frac{V_{1i}}{V_{ri}}}{n},$$

where n is the number of points considered on the velocity hodograph; V_{1i} – granule velocity at the i -th point; V_{ri} – reservoir velocity at the i -th point.

Similarly, we determine the coefficient of similarity of velocities for the part:

$$F_2 = \frac{\sum_1^n \frac{V_{2i}}{V_{ri}}}{n}.$$

The probable velocity of the granule is determined from the expression: $V_1 = F_1 A\omega$, where F_1 is the similarity coefficient for a granule; A – oscillation amplitude; ω – oscillation frequency.

The probable velocity of the part will be equal to: $V_2 = F_2 A\omega$ .The velocities of the granule and part vary from their location along the cross section of the reservoir. Since the force of interaction between the granule and the part is directly proportional to the velocity, the determination of the velocities over the cross section of the reservoir is proportional to the distribution of the pressure of the medium. Then the average probable value of the granule velocity in the reservoir will be equal to: $V_1 = \Delta_{\text{avg}}\, \xi_{\text{avg}}\, F_1 A\omega$, where Δ_{avg} is the average value of the power impulse damping coefficient; ξ_{avg} – coefficient of force action time.

The average value of the part velocity is equal to: $V_2 = \Delta_{\text{avg}}\, \xi_{\text{avg}}\, F_2 A\omega$.

Then the value V_{avg} of the normal component of the collision velocity of the granule and the part is equal to:

$$V_{\text{avg}} = \Delta_{\text{avg}}\, \xi_{\text{avg}}\, A\omega \frac{\sin\alpha_{\text{avg}}}{2}\left(F_1 + F_2\right).$$

The amplitude of the reservoir oscillations is not the same along the coordinate axes OX and OY. Therefore, depending on the setting of the vibrating machine, the minimum collision velocity $V_{\text{avg min}}$ corresponding to the elliptical-shaped trajectory of the reservoir $\left(K_A = \max\right)$ can be determined.

Hence, the value $\beta_{2\min}$ of the penetration of the granule into the part will be:

$$\beta_{2\min} = \frac{a\,\Delta_{\text{avg}}\,\xi_{\text{avg}}\,A\omega(1+k)\,m\,M\,(F_1+F_2)\sin\alpha_{\text{avg}}}{2\pi\rho_x\,\sigma_s\,\Delta T\,(m+M)},$$

the value of the penetration of the granule into part $\beta_{2\max}$ is equal to:

$$\beta_{2\max} = \frac{a\,\Delta_{\text{avg}}\,\xi_{\text{avg}}\,A\omega K_A(1+k)\,m\,M\,(F_1+F_2)\sin\alpha_{\text{avg}}}{2\pi\rho_x\,\sigma_s\,\Delta T\,(m+M)},$$

where k is the recovery factor; K_A – coefficient of ellipticity.

The highest normal velocities are possible at $\alpha_{\text{avg}} = 90^\circ$ and $\alpha_{\text{avg}} = 180^\circ$.

Then, for $\alpha_{\text{avg}} = 90^\circ$ we have $V_{\text{avg max}} = V_1 + V_2$. With $\alpha_{\text{avg}} = 180^\circ$ – $V_{\text{avg min}} = 0$. Average probable velocity V_{avg} will be equal to: $V_{\text{avg}} = \frac{V_1 + V_2}{2}$.

The limiting values of the depth of granule penetration, taking into account coefficient of ellipticity K_A, are determined by the formulas:

$$\beta'_{2\max} = \frac{a\,\Delta_{\text{avg}}\,\xi_{\text{avg}}\,A\omega K_A(1+k)\,m\,M\,(F_1+F_2)}{\pi\rho_x\,\sigma_s\,\Delta T\,(m+M)};$$

$$\beta'_{2\min} = \frac{a\,\Delta_{\text{avg}}\,\xi_{\text{avg}}\,A\omega(1+k)\,m\,M\,(F_1+F_2)}{\pi\rho_x\,\sigma_s\,\Delta T\,(m+M)}.$$

Carrying out transformations and substitutions, we get:

$$H_{\text{avg}} = \frac{a\,\Delta_{\text{avg}}\,\xi_{\text{avg}}\,A\omega(1+k)\,m\,M\,(F_1+F_2)}{\pi\rho_x\,\sigma_s\,\Delta T} \times \frac{\left[(1+2K_A)\,n_1 + (1+2K_A)\,n_2\sin\alpha_{\text{avg}}\right]}{4(m+M)(n_1+n_2)}.$$

The values of the coefficients in the micro-roughness formula were found empirically on serial vibrating machines.

4. The results of calculations to determine the height of the micro-roughness of the processed part surface

Velocity hodographs were used to find the meeting angles of the abrasive granule with the processed part. The research results are summarized in table 1.

Table 1 – Values of the angles of the meeting of the granule with the part along the zones of the reservoir

Angle	The zones of the reservoir						
	1	2	3	4	5	6	7
α_{min}	20	35	17	22	29	23	28
α_{max}	28	37	39	30	29	31	29
α_{avg}	24	36	28	26	29	27	28

The determination of the micro-roughness of the processed part surface was carried out taking into account the values of the angles of the meeting of the granule with the processed part, passing through the zones of the reservoir. For these calculations, the hodographs of the movement velocities of the granule and the part were used. The values of the coefficients included in the roughness formula were also used (Table 2).

Table 2 – Values of coefficients for determining the height of micro-roughness of the processed parts surface

Quantities	Notation	Value
Constant factor	α	0.35
Power impulse damping coefficient	Δ_{avg}	0.55
Similarity coefficients:		
granules	F_1	0.47
parts	F_2	0.38
Coefficient of ellipticity	K_A	1.5
Straight impacts number	n_1	
Oblique impacts number	n_2	
Collision time	ΔT	$4 \cdot 10^{-5}$
Coefficient of force action time	ξ_{avg}	0.16
Recovery factor	k	0.9
Average meeting angle	α_{avg}	28º

The calculation determined the value of the average probable meeting angle, which turned out to be equal to $\alpha_{avg} = 28^{\circ}$. Based on them, the values of the similarity coefficients were: for a granule $F_1 = 0.47$, for a part $F_2 = 0.38$.

Taking into account the obtained data, the height micro-roughness formula will take the form:

$$H_{avg} = \frac{106\eta A\omega mM}{C\sigma_s\rho_x\left(m+M\right)},$$

where η is the abrasive ability of the granule grain; C – the number of simultaneously working grains of the granule; σ_s – tensile strength of the part material; ρ_x – diameter of the penetration of abrasive grain.

5. Conclusions

Thus, based on the analysis of the direct and oblique collision of the granule and the processed part, the values of the angles of contact with the processed part, as well as taking into account the velocities of their collisions and the proportionality of the speed of the reservoir, the micro-roughness of the part surface has been determined during vibration finishing and grinding processing To check the micro-roughness formula and establish the limits of its application, experiments were carried out that showed a good 80 ... 85 % convergence of experimental and calculated data.

References: 1. *Jashhericyn P.I., Martynov A.N.* Chistovaja obrabotka detalej v mashinostroenii. Minsk: Vishjejshaja shk., 1983. 191 p. **2.** *Kartashov I.N., Shainskij M.E., Vlasov V.A.* Obrabotka detalej svobodnymi abrazivami v vibrirujushhih rezervuarah. Kyiv: Vishha shk., 1975. 188 p. **3.** *Mitsyk A.V., Fedorovich V.A., Grabchenko A.I.* Mechano-physico-chemical modeling of the process of destruction of the part surface in a free abrasive medium. *Cutting & Tools in Technological System.* Kharkiv, NTU «KhPI». 2020. № 92. pp. 62 – 67. http://doi.org/10.20998/2078–7405.2020.92.08 **4.** *Babichev A.P., Babichev I.A.* Osnovy vibracionnoj tehnologii: monografija. Rostov-na-Donu: Izd-vo DGTU, 2008. 694 p. **5.** *Kulakov Ju.M., Hrulkov Ju.M.* Otdelochno-zachistnaja obrabotka detalej. Moskva: Mashinostroenie, 1979. 216 p. **6.** *Mitsyk A.V., Fedorovich V.A., Grabchenko A.I.* The effect of a shock wave in an oscillating working medium during vibration finishing-grinding processing. *Cutting & Tools in Technological System*. Kharkiv, NTU «KhPI». 2020. № 93. pp. 43 – 55. http://doi.org/10.20998/2078-7405.2020.93.06 **7.** *Shainskij M.E.* Issledovanie dekorativnogo shlifovanija i polirovanija stal'nyh detalej v vibrirujushhih rezervuarah: dis. … kand. tehn. nauk: 05.02.08. Lviv, 1967. 171 p. **8.** Instrument dlja obrobky detalej vil'nymy abrazyvamy: monografija / M.O. Kalmykov, T.O. Shumakova, *V.B. Strutynskyi, L.M. Lubenska.* Kyiv – Luhansk: «Noulidzh», 2010. 214 p. **9.** *Vlasov V.A.* Issledovanija mehaniki vzaimodejstvija shlifoval'nyh tel i stal'nyh detalej v vibrirujushhih rezervuarah: dis. … kand. tehn. nauk: 05.02.08. Kharkiv, 1974. 226 p.

Андрій Міцик, Володимир Федорович, Харків, Україна

ХАРАКТЕР УТВОРЕННЯ МІКРОШОРСТКОСТІ ПОВЕРХНІ ПРИ ВІБРАЦІЙНІЙ ОЗДОБЛЮВАЛЬНО-ЗАЧИЩУВАЛЬНІЙ ОБРОБЦІ

Анотація. *Наведено основні аспекти щодо характеру утворення мікрошорсткості поверхні при вібраційній оздоблювально-зачищувальній обробці. Вказано, що видалення матеріалу з поверхні деталі відбувається в результаті спільної дії процесів мікрорізання, викришування частинок металу при багаторазовому деформуванні ділянок оброблюваної поверхні, їх втоми та руйнування, утворення, руйнування та видалення вторинних структур, адгезійних явищ. Зазначено, що реальна поверхня після віброобробки є сукупністю шорсткостей певної величини, форми та напряму. Встановлено, що мікрошорсткість поверхні деталі при вібраційній оздоблювально-зачищувальній обробці утворюється у вигляді слідів від численних ударів абразивних гранул по поверхні деталі. Визначено найбільшу величину проникнення гранули в оброблювану поверхню, що дає можливість характеризувати слід від пластичного стиску в зоні зіткнення гранули та деталі. Розглянуто методику та досліджено механізм утворення мікрошорсткості поверхні. Визначено вираз для нормальної складової сили удару, що характеризує основний вплив на механізм утворення мікрошорсткості. Встановлено величину проникнення гранули у метал деталі. Дослідженнями встановлено, що мікрошорсткість поверхні при віброобробці утворена ударами гранул о деталь під різними кутами зустрічі. Визначено сліди від впливу прямого та косого ударів. Обчислена середня висота мікрошорсткості. За годографами встановлено нормальні швидкості абразивних гранул та деталей. Також визначено середнє значення кута зіткнення гранул з деталлю у будь-якій точці траєкторії їхнього руху. Виявлено, що швидкості гранул і деталей змінюються за величиною та напрямком протягом одного періоду коливання резервуара, досягаючи своїх граничних значень, які пропорційні швидкостям руху резервуара. Ступінь пропорційності виражена коефіцієнтом подібності для гранули та деталі. Також за точками годографа визначено усереднений коефіцієнт подібності. Отримано середні значення швидкостей руху гранули та деталі в резервуарі. Встановлено мінімальну та максимальну величину проникнення гранули в поверхню деталі. Наведено формули граничних значень глибини проникнення гранули з урахуванням коефіцієнта еліпсності. Наведено результати розрахунків для визначення висоти мікронерівності поверхні та оброблюваної деталі. Отримано формулу для визначення мікрошорсткості поверхні при вібраційній оздоблювально-зачищувальній обробці.*

Ключові слова: *віброобробка; абразивна гранула; оброблювана деталь; співударяння гранули та деталі; кут співударяння; мікронерівність поверхні; годографи швидкостей.*

UDC 621.9 **doi: 10.20998/2078-7405.2022.97.10**

V. Molnar, Miskolc, Hungary

ANALYSIS OF THE SBI AND SVI FUNCTIONAL INDICES IN HARD MACHINING

Abstract. *The functional requirements of precision machined parts can be expressed among others by topography parameters. In the automotive industry there is an increased need for the application of high-accuracy quantifying parameters. In this study wear resistance and the fluid retention ability-related 3D surface texture parameters are analyzed based on hard turning and grinding experiments. The less frequently applied functional parameters (Sbi and Svi) are compared to the high-accuracy volume parameters (Vmp and Vvv) to obtain information about the reliability of the former ones. It was found that the correlation between the two types of parameters are quite weak.*
Keywords: *hard machining; grinding; surface texture.*

1. INTRODUCTION

In several machining industrial application, the characterization of surface texture plays an important role in obtaining information about the functional properties and the functional operation performance of the components [1]. To increase production efficiency and therefore reduce costs, reliable control processes have to be applied. This can be reached by a high degree of precision and by ensuring the repeatability of the measurements [2]. In precision machining the need for this is increased due to the increased number of hardened components. In machining hardened surfaces grinding has been the dominant procedure for decades [3, 4]. Now, it can be substituted by e.g. hard turning, which is a more productive procedure and among certain circumstances the texture of the surfaces have the same quality as that of ground ones. Machining of hardened materials requires superhard tool materials [5] in order to reach the expected surface quality [6]. Hard turning results in a periodic surface topography, however, random topography is required, grinding has to be applied [7].

In this study some function-related 3D surface texture parameters of hard turned and ground surfaces are analyzed and compared for the two procedures. 3D texture characterization is necessary because of the increased need for exact analysis of the surfaces [8, 9] and they describe the state of the surface better that the 2D parameters [10]. The analyzed parameters are the volume parameters, peak material volume (*Vmp*) and valley void volume (*Vvv*) and the functional indices, surface bearing index (*Sbi*) and valley fluid retention index (*Svi*). They provide information about the surface peaks and through this the wear resistance and the surface valleys, and through this about the fluid-retention ability.

These tribology-related characteristics have a high importance in operation of contacting surfaces.

The functional indices were compared to the volume parameters when the latter were considered as basis due to their reliability.

The volume parameters *Vmp* and *Vvv* are exact 3D volume parameters and they measure the peak material volume and the valley void volume precisely. A lower *Vmp* value is more favorable from tribological point of view [11] and indicates higher wear resistance. Concerning the valley parameter, a higher *Vvv* indicates higher fluid-retention ability [12]. In the volume analysis the peak zone is defined as the upper 10% and the valley zone as the lower 20% of the topography.

The so-called functional indices are less frequently applied. They also characterize the wear resistance and fluid retention abilities of the surfaces [13]. The lower the surface bearing index, the higher its wear resistance, while the higher the valley fluid retention index, the better the fluid retention ability [14, 15]. It can be stated that the analyzed volume and functional parameters provide information about the same tribological properties. In the analysis the *Sbi* characterizes the upper 5% and the *Svi* characterizes the lower 20% of the topography.

2. METHODOLOGY

2.1 Experimental setup

In the experiments external cylindrical surfaces were machined by hard turning and infeed grinding. The machined material was 16MnCr5 case hardened steel used widely in the automotive industry. The hardness of the surfaces varied between 62 and 63 HRC. The carburizing was carried out at 900 °C for 8 h. The temperature of case hardening was 820 °C and its duration was 30 min. For the cooling oil was used. The chemical composition and the mechanical and physical properties are summarized in Tables 1 and 2.

The applied machine tools were a precision CNC lathe type Optiturn S600 and a universal cylindrical grinding machine type KE 250-04. In the hard turning experiment, the cutting speed and the feed rate were varied on four levels, the depth-of-cut was fixed. In the grinding experiment the infeed velocity and the workpiece revolution-per-minute (rpm) were varied on three levels, the allowance and the wheel rpm were fixed. In Table 3 the applied technological data and tool cutting specifications are summarized. Concerning the varied cutting parameters, full factorial designs of experiment were applied; all the varying parameter combinations were analyzed. This resulted in 16 setups (4*4) and 9 setups (3*3) in the cases of hard turning and grinding, respectively.

Table 1 – Physical and mechanical properties of 16MnCr5 [16]

Tensile strength	1158 MPa	**Elongation**	15 %
Yield strength	1034 MPa	**Specific heat**	500 J/kgK
Thermal conductivity	16 N/mK	**Melting temp.**	1370-1400 °C

Table 2 – Chemical composition of 16MnCr5 (DIN EN 10184:2008)

C	**Si**	**Mn**	**Cr**	**S**	**P**
0.14–0.19	<0.4	1.00–1.30	0.80–1.10	<0.035	<0.025

Table 3 – Cutting parameters cutting tools

Hard turning		**Grinding**	
depth-of-cut (a_p, mm)	0.05	allowance (Z, mm)	0.1
feed rate (f, mm/rev)	0.05; 0.1; 0.15; 0.2	wheel rpm (n_w, 1/min)	1400
cutting speed (v_c, m/min)	60; 90; 120; 150	infeed velocity (v_{fR}, mm/s)	0.007; 0.019; 0.03
CBN insert: CNGA 120408TA4 Tool holder: CLNR 2525M12		workpiece rpm (n, 1/min)	31.5; 63; 90
		Ceramic bound alumina wheel: KA32M5KE (diameter: 400 mm, width: 63 mm)	

2.2 Texture measurement and the analyzed parameters

The textures of the surfaces were scanned and analyzed by a 3D roughness tester equipment, type AltiSurf 520. An optical (chromatic confocal) sensor, type CL2, was used. The resolutions of the sensor in the x- and y-directions were 2 μm and in the z-direction 0.012 μm. The measurement range in z-direction was 0–300 μm. For the evaluation of the data λ_c = 0.25 mm cut-off and Gauss filter were applied according to the standard ISO 4288-1996. For the analysis of the parameters, the standards ISO 25178 and EUR 15178N were used. The evaluation area was 2 mm × 2 mm.

The analyzed functional parameters are defined based on the root mean square roughness value *Sq*, which is defined by Eq 1.

$$Sq = \sqrt{\frac{1}{MN}\sum_{k=0}^{M-1}\sum_{l=0}^{N-1}[z(x_k, y_l)]^2}, \quad (1)$$

where M and N are the number of points scanned in x and y directions, and *z* is the height of a topography point.

The surface bearing index is defined by Eq 2 and the valley fluid retention index by Eq 3.

$$Sbi = \frac{Sq}{z_{0.05}}, \tag{2}$$

$$Svi = \frac{1}{Sq} \cdot \frac{V_v(h_{0.08})}{(M-1)(N-1)\delta x \delta y}, \tag{3}$$

where $z_{0.05}$ is the height from the top (highest peak point) of the surface to the line designating the 5% bearing area; $h_{0.8}$ is the height from the bottom (lowest valley point) of the surface to the line designating the 80% bearing area; V_v is the volume representing the void volume [17].

These functional and volume parameters are derived from the Abbott-Firestone curve. In Fig. 1 the z parameters and the topography zones and in Fig. 2 the definitions of the analyzed volume parameters are demonstrated.

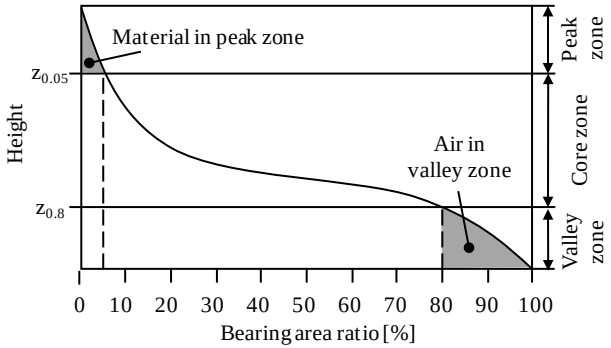

Figure 1 – Components of the *Sbi* and *Svi* indices and the topography zones [18]

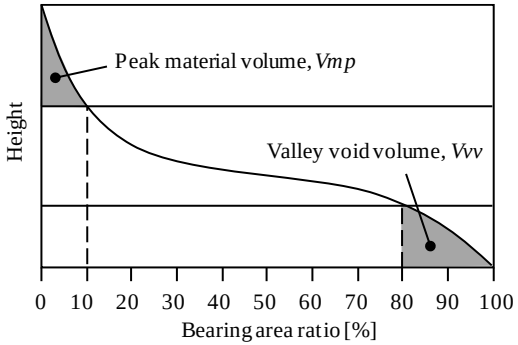

Figure 2 – Definitions of the analyzed volume parameters

3. RESULTS AND DISCUSSION

The peak material volume (*Vmp*) was compared to the surface bearing index (*Sbi*) for hard turning. It is demonstrated in Fig. 3 that the *Vvv* values show increase with the feed rate when 60 and 150 m/min cutting speed is applied. Such connection cannot be observed in the case of the *Sbi* parameter. At the same time, if only the lowest (0.05 mm/rev) and the highest (0.2 mm/rev) feed rates are considered, both the Vmp and the Sbi parameters increase with the feed rate. The two parameters theoretically are in connection with the same functional characteristics, the wear resistance and this connection can be observed in the analyzed setups, however the correlation is not obvious when all the setups are considered.

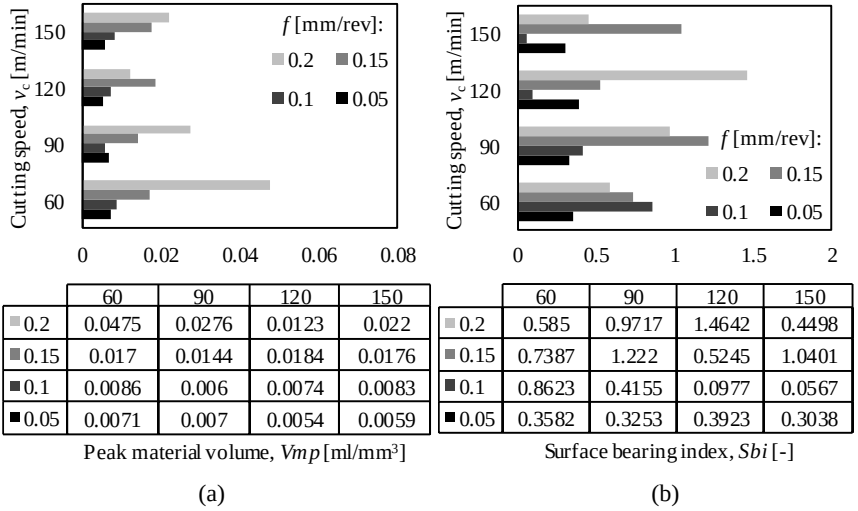

	60	90	120	150
0.2	0.0475	0.0276	0.0123	0.022
0.15	0.017	0.0144	0.0184	0.0176
0.1	0.0086	0.006	0.0074	0.0083
0.05	0.0071	0.007	0.0054	0.0059

Peak material volume, *Vmp* [ml/mm³]

	60	90	120	150
0.2	0.585	0.9717	1.4642	0.4498
0.15	0.7387	1.222	0.5245	1.0401
0.1	0.8623	0.4155	0.0977	0.0567
0.05	0.3582	0.3253	0.3923	0.3038

Surface bearing index, *Sbi* [-]

(a) (b)

Figure 3 – (a) Peak material volume (*Vmp*) and (b) Surface bearing index (*Sbi*) parameter values of the hard turned surfaces

Analyzing the fluid retention ability based on the *Vvv* and the *Svi* parameters, contradictory results were obtained (Fig 4). The higher fluid retention ability theoretically is demonstrated by higher *Vvv* and higher *Svi* values. However, this cannot be observed from the data of the analyzed surfaces and the correlation between them is negative. It also can be observed that with the increase of the feed rate the *Vvv* values increase on 60 and 90 m/min cutting speeds and the *Svi* values decrease on 90 and 120 m/min. It can be observed from the diagrams (by neglecting some datapoints) that the increase in the *Vvv* show decrease in the *Svi*

when the feed rate increases. The reason for this is the relatively high *Sq* values. While the valley volume increases the *Svi* value, the *Sq* decreases it. For example, in the case of *f*=0.05 mm/rev and v_c=60 m/min the *Vvv* divided by the *Sq*=0.155 μm results in 0.1148 ml/mm^3 *Svi* value or in the case of *f*=0.2 mm/rev, v_c=60 m/min and *Sq*=1.115 μm, the *Svi* equals to 0.0317 ml/mm^3. These *Vvv* and *Svi* values are placed in the first and fourth rows and first columns of the data tables in Fig 4 (The 0.001 and 0.003 differences of the calculated *Svi* values are resulted from the only four decimals). This result means that the values or their tendencies in the case of the *Svi* parameter do not inform uniformly or reliably about the same fluid retention ability due to the influencing effect of the incorporated *Sq* parameter. The comparison can be carried out only for surfaces whose *Sq* values are identical.

Both in the wear resistance and the fluid retention ability no clear effects can be observed based on the cutting speed values.

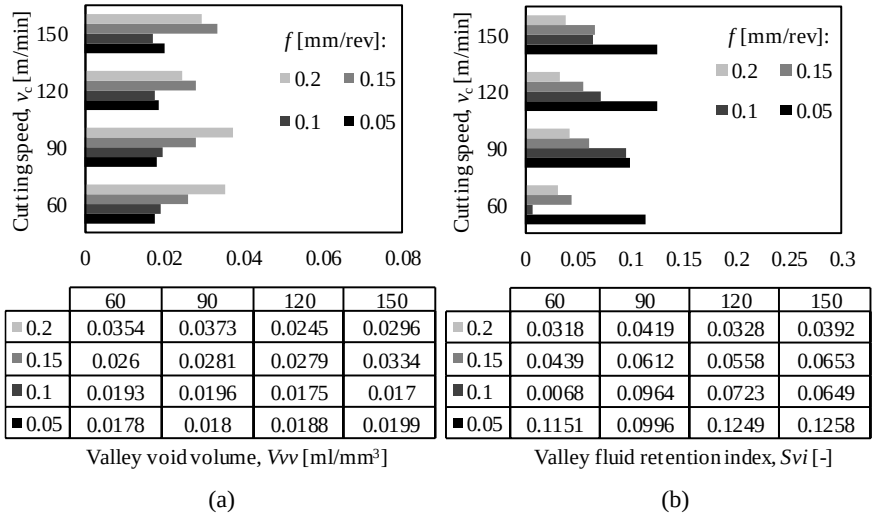

	60	90	120	150
0.2	0.0354	0.0373	0.0245	0.0296
0.15	0.026	0.0281	0.0279	0.0334
0.1	0.0193	0.0196	0.0175	0.017
0.05	0.0178	0.018	0.0188	0.0199

Valley void volume, *Vvv* [ml/mm^3]

	60	90	120	150
0.2	0.0318	0.0419	0.0328	0.0392
0.15	0.0439	0.0612	0.0558	0.0653
0.1	0.0068	0.0964	0.0723	0.0649
0.05	0.1151	0.0996	0.1249	0.1258

Valley fluid retention index, *Svi* [-]

(a) (b)

Figure 4 – (a) Valley void volume (*Vvv*) and (b) Valley fluid retention index (*Svi*) parameter values of the hard turned surfaces

In the grinding experiments the infeed velocity and the workpiece rpm were varied. The *Vmp* and *Sbi* values of the machined surfaces are demonstrated in Fig. 5. Clear tendencies cannot be observed when all the feed rates are considered. However, if neglecting the 0.019 mm/s infeed velocity, it can be stated that by the infeed velocity the *Vmp* value increases and the *Sbi* value decreases. The reason for this contradiction is similar to that between the *Vvv* and *Svi* parameters of hard turning. The *Sq* increases the *Sbi* and the $h_{0.05}$ peak zone height decreases it.

Concerning the fluid retention ability, no clear tendencies can be observed. The *Vvv* shows no unequivocal increase with both the infeed velocity and the rpm. Concerning the *Svi* parameter, it increases with the infeed velocity in the cases of 31.5 and 63 1/min rpm levels (Fig. 6). The reason for these contradictory results is the same as in the case of hard turning: the influencing effect of the scale of the *Sq* parameter.

To obtain quantitative information about the connections between the volume parameters and the functional indices, coefficients of determination were calculated. This parameter provides information about the strengths of the correlation of two variables if linear connection is supposed.

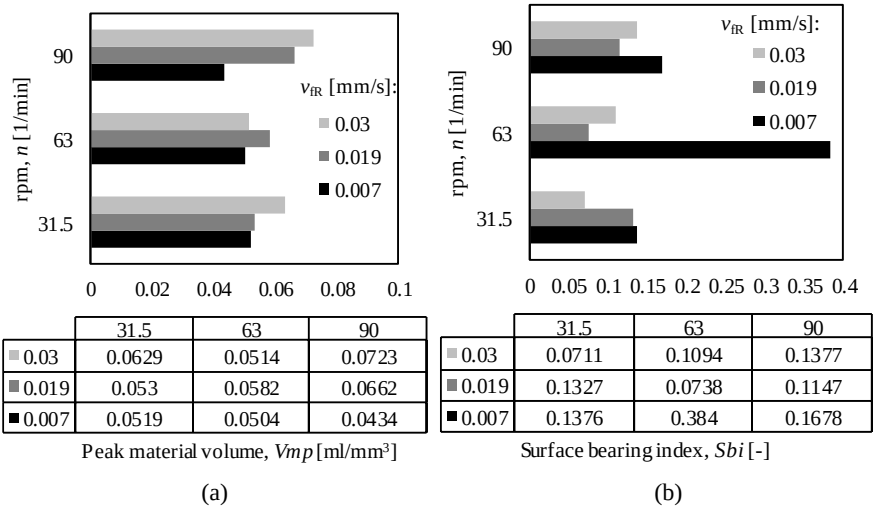

	31.5	63	90
0.03	0.0629	0.0514	0.0723
0.019	0.053	0.0582	0.0662
0.007	0.0519	0.0504	0.0434

Peak material volume, *Vmp* [ml/mm³]

(a)

	31.5	63	90
0.03	0.0711	0.1094	0.1377
0.019	0.1327	0.0738	0.1147
0.007	0.1376	0.384	0.1678

Surface bearing index, *Sbi* [-]

(b)

Figure 5 – (a) Peak material volume (*Vmp*) and (b) Surface bearing index (*Sbi*) parameter values of the ground surfaces

The coefficient of determination is calculated from the linear correlation coefficient; the former is the square of the latter. The connection is considered as extremely strong if $0.81 \leq R^2 < 1$; strong, if $0.49 \leq R^2 < 0.81$; medium, if $0.16 \leq R^2 < 0.49$; weak, if $0.04 \leq R^2 < 0.16$ and extremely weak, if $R^2 < 0.04$.

In the cases of the hard turned surfaces there is a positive weak correlation between the *Vmp* and the *Sbi* parameters and a negative medium correlation between the *Vvv* and the *Svi* parameters. In the cases of the ground surfaces there is a weak correlation between the *Vmp* and the *Sbi* parameters and an extremely weak correlation between the *Vvv* and the *Svi* parameters.

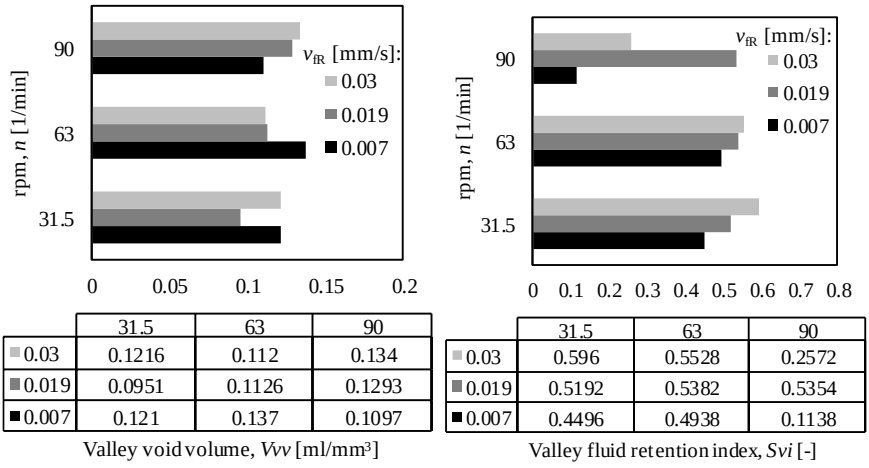

	31.5	63	90
0.03	0.1216	0.112	0.134
0.019	0.0951	0.1126	0.1293
0.007	0.121	0.137	0.1097

	31.5	63	90
0.03	0.596	0.5528	0.2572
0.019	0.5192	0.5382	0.5354
0.007	0.4496	0.4938	0.1138

Figure 6 – (a) Valley void volume (*Vvv*) and (b) Valley fluid retention index (*Svi*) parameter values of the ground surfaces

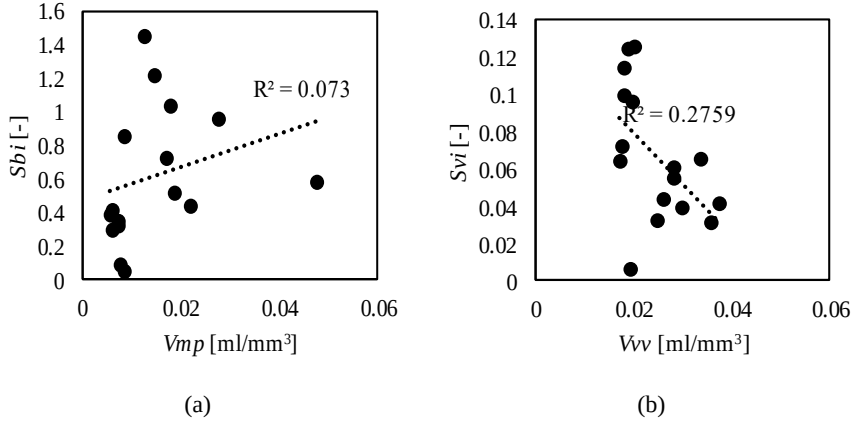

Figure 7 – Connection between the (a) *Vmp* and *Sbi* parameters and the (b) *Vvv* and *Svi* parameters of the hard turned surfaces

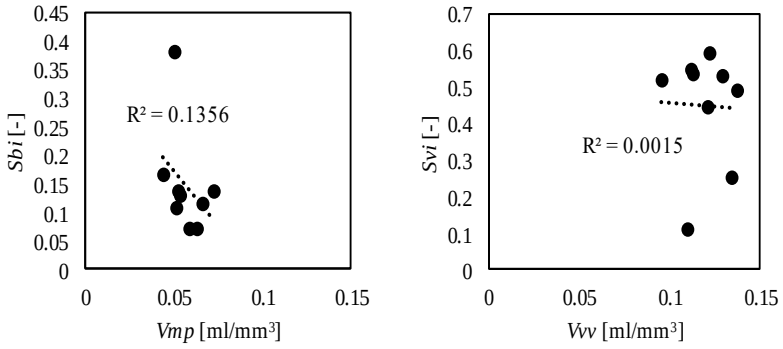

(a) (b)

Figure 8 – Connection between the (a) *Vmp* and *Sbi* parameters and the (b) *Vvv* and *Svi* parameters of the ground surfaces

The connections between the data points and the values of the coefficients of determination are demonstrated in Figs. 7 and 8 for hard turning and grinding, respectively.

CONCLUSIONS

The findings of this study were obtained based on hard machining experiments and 3D texture analysis and valid for the material grade 16MnCr5 (HRC 62–63) and for the next cutting parameters: hard turning – a_p = 0.05 mm; v_c = 60 – 150 m/min; f = 0.05 – 02. mm/rev; infeed grinding – Z = 0.1 mm; n_w = 1400 1/min; v_{fR} = 0.007 – 0.03 mm/s; n = 31.5 – 90 1/min. The followings can be stated for the reliability of the surface bearing index (*Sbi*) and the valley fluid retention index (*Svi*) when the volume parameters peak material volume (*Vmp*) and valley void volume (*Vvv*) are considered as bases:

- In hard turning the correlation between the *Vmp* and *Sbi* parameters is positive and weak (R^2 = 0.073). Considerably connection can be observed only when the feed rate values are relatively far from each other.
- In hard turning the correlation between the *Vvv* and *Svi* parameters is negative and medium (R^2 = 0.2759). The reason for the negative correlation is the relatively strong influencing effect of the *Sq* parmeter incorporated in the formula of *Svi*.
- In grinding the correlation between the *Vmp* and *Sbi* and between the *Vvv* and *Svi* parameters are weak (R^2 = 0.1356) and extremely weak (R^2 =

0.0015), respectively. The reason for there is the relatively high influencing effect of the *Sq* parameter.

References: 1. *Whitehouse, D.J.:* Handbook of surface and nanometrology, Taylor & Francis, NY, 2011. **2.** *Deltombe, R., Kubiak, K.J., Bigerelle, M.:* How to select the most relevand 3D roughness parameters of a surface, Scanning 36, pp150-160, 2014. **3.** *Mamalis, A.G., Kundrak, J., Horvath, M.:* On a Novel Tool Life Relation for Precision Cutting Tools, Journal of Manufacturing Science and Engineering 127(2), pp.328-332, 2005. **4.** *Kundrak, J., Felho, Cs.:* 3D Roughness Parameters of Surfaces Face Milled by Special Tools, Manufacturing Technology 16(3), pp.532-538, 2016. **5.** *Zawada-Tomkiewicz, A.:* Analysis of surface roughness parameters achieved by hard turning with the use of PCBN tools, Estonian Journal of Engineering 17(1), pp.88-99, 2011. **6.** *Kundrak, J., Nagy, A., Markopoulos, A.P., Karkalos, N.E.:* Investigation of surface roughness on face milled parts with round insert in planes parallel to the feed at various cutting speeds, Cutting & Tools and Technological System 91, pp.87-96, 2019, pp.87–96. **7.** *Grzesik, W., Zak, K., Kiszka, P.:* Comparison of surface textures generated in hard turning and grinding operations, Procedia CIRP 13, pp.84–89, 2014. **8.** *Przestacki, D., Majchrowski, R., Marciniak-Podsadna, L.:* Experimental research of surface roughness and surface texture after laser cladding, Applied Surface Science 388, pp.420–423, 2016. **9.** *Kumar, R., Seetharamu, S., Kamaraj, M.:* Quantitative evaluation of 3D surface roughness parameters during cavitation exposure of 16Cr–5Ni hydro turbine steel, Wear 320, pp.16–24, 2014. **10.** *Aidibe, A., Nejad, M.K., Tahan, A., Jahazi, M., Cloutier, S.G.:* A proposition for new quality 3D indexes to measure surface roughness, Procedia CIRP 46, pp.327–330, 2016. **11.** *Letocha, A., Miller, T., Kalisz,* J.: Optimization of measurement and analysis parameters of burnishing surfaces, Mechanik 11, pp.1030-1034, 2017. **12.** *Grzesik, W., Zak, K., Kiszka, P.:* Comparison of surface textures generated in hard turning and grinding operations, Procedia CIRP 13, pp.84–89, 2014. **13.** *Yu Gazizova, M., Smirnov, N.A., Kudryashov, S.I., Chen, J., Ahmadeev, Y.H., Goncharov, I.Y., Shugurov, V.V., Prokopenko, N.A.:* Correlation of the tribological properties of LIPSS on TiN surface with 3D parameters of roughness, IOP Conf. Series: Materials Science and Engineering 1014, art no 012014, 2021. **14.** *Grzesik, W.:* Prediction of the functional performance of machined components based on surface topography: state of the art, Journal of Materials Engineering and Performance 25(10), pp.4460–4468, 2016. **15.** *Suh, A.Y., Polycarpou, A.A., Conry, T.F.:* Detailed surface roughness characterization of engineering surfaces undergoing tribological testing leading to scuffing, Wear 255, pp.556–568, 2003. **16.** Longhai Special Steel. Available online: https://www.steelss.com/Carbon-steel/16mncr5.html (accessed on 10/09/2022). **17.** *Georgescu, C., Cristea, G.C., Dima, C., Deleanu, L.:* Evaluating lubricating capacity of vegetal oils using Abbott-Firestone curve, IOP Conf. Series: Materials Science and Engineering 174, art no 012057, 2017. **18.** *Deleanu, L., Cantaragiu, A., Georgescu, C., Botan M.:* Influence of measurements on 3D roughness parameters, Mechanical Testing and Diagnosis 1, pp.42-53, 2011.

Віктор Мольнар, Мішкольц, Угорщина

АНАЛІЗ ФУНКЦІОНАЛЬНИХ ПОКАЗНИКІВ SBI І SVI ПРИ ЖОРСТКІЙ МЕХАНІЧНІЙ ОБРОБЦІ

Анотація. *У цьому дослідженні деякі функціональні параметри тривимірної текстури поверхні точених та відшліфованих поверхонь аналізуються та порівнюються для двох процедур. Тривимірна характеристика текстур необхідна через збільшення потреби в точному аналізі*

поверхонь, і вони краще описують стан поверхні, ніж двовимірні параметри. Аналізованими параметрами є об'ємні параметри, піковий об'єм матеріалу (Vmp) та обсяг порожнеч у западинах (Vvv), а також функціональні індекси, індекс поверхневої несучої здатності (Sbi) та індекс утримання рідини в западинах (Svi). Вони надають інформацію про піки поверхні і, таким чином, про зносостійкість і западини поверхні, а також про здатність утримувати рідину. Ці пов'язані з трибологією характеристики, мають велике значення при експлуатації поверхонь, що контактують. Функціональні показники зіставлялися з об'ємними параметрами, коли останні бралися за основу через їх достовірність. В експериментах зовнішні циліндричні поверхні оброблялися точінням різцем із КНБ та шліфуванням з подачею. Оброблюваним матеріалом була цементована сталь, що широко використовується в автомобільній промисловості. Твердість поверхонь варіювалася від 62 до 63 HRC. Навуглерожування проводили при 900°C протягом 8 годин. Температура цементації 820 ° C, тривалість 30 хв. Для охолодження використовувалося масло. Текстури поверхонь були відсканована та проаналізовані за допомогою 3D-тестеру шорсткості типу AltiSurf 520. Використовувався оптичний (хроматичний конфокальний) датчик типу CL2. Результати дослідження були отримані на основі експериментів для наступних параметрів різання: жорстке точіння – a_p = 0,05 мм; $v_к$ = 60–150 м/хв; f = 0,05–0,2 мм/об; врізне шліфування – Z = 0,1 мм; n_w = 1400 1/хв; v_{fR} = 0,007–0,03 мм/с; n = 31,5–90 1/хв. Щодо надійності індексу несучої здатності поверхні (Sbi) та індексу утримування рідини у западині (Svi), коли об'ємні параметри пікового обсягу матеріалу (Vmp) та обсягу порожнин у западині (Vvv) розглядаються як базові, можна констатувати наступне: при жорсткому точінні, кореляція між параметрами Vmp та Sbi позитивна та слабка (R^2 = 0,073). Помітний зв'язок можна спостерігати лише тоді, коли значення швидкості подачі відносно далекі одне від одного. При жорсткому точінні кореляція між параметрами Vvv і Svi негативна і середня (R^2 = 0,2759). Причиною негативної кореляції є відносно сильний вплив параметра Sq, закладеного у формулу Svi. При шліфуванні кореляція між параметрами Vmp та Sbi та між параметрами Vvv та Svi слабка (R^2 = 0,1356) та вкрай слабка (R^2 = 0,0015) відповідно. Причиною є відносно високий ефект впливу параметра Sq.

Ключові слова: *жорстка механічна обробка; шліфування; поверхнева текстура*.

UDC 621.923 **doi: 10.20998/2078-7405.2022.97.11**

V. Fedorovich, Y. Ostroverkh, I. Pyzhov, Kharkiv, Ukraine,
V. Lavrinenko, Kyiv, Ukraine

THEORETICAL JUSTIFICATION OF RATIONAL CONDITIONS FOR PRODUCING DIAMOND WHEELS ON CERAMIC BONDS

Abstract. *The article describes the results of theoretical studies using 3D finite element modeling, which made it possible to determine the rational characteristics of diamond wheels on ceramic bonds. The influence of the parameters of the diamond-bearing layer on the change in its stress-strain state in the sintering zone of the diamond wheel has been studied. The results of finite element and microlevel 3D modeling of the sintering process of a ceramic-matrix diamond-containing composite are analyzed. The influence of the technological parameters of the process and the characteristics of the diamond wheel on the integrity of the grains during sintering was established, on the basis of which practical recommendations were given for the selection of diamond compositions with rational properties.*
Keywords: *Diamond grinding wheel; ceramic bond; diamond-bearing layer; diamond grain; grinding process; force and temperature factors; Finite element method; 3D model; diamond wheel sintering process; metal phase; equivalent stresses.*

1. Literature review

It is known that during the operation of diamond abrasive tools (DAT), the coefficient of effective use of diamond grains does not exceed 10%. The rest of the grains are destroyed even at the stage of tool manufacturing and fall out during grinding. The efficiency of diamond grinding depends largely on the characteristics of diamond wheels, and is also determined by the rational choice of the optimal technological parameters for their manufacture, which ensures the integrity of diamond grains at this stage. And this, in turn, contributes to the creation of prerequisites for their rational self-sharpening during the operation of the DAT [1, 2]. The information available in the literature on the mechanism of renewal of the cutting surfaces of grains during grinding and the conditions under which the rational self-sharpening of DAT is realized are contradictory and general, which does not contribute to the efficiency of their use. In the process of diamond abrasive processing, two cases most often take place: spontaneous uncontrolled self-sharpening of the wheel due to the tearing of grains from the bond, which leads to unjustified loss of diamonds, or its complete absence, leading to greasing of the working surface of the tool.

The choice of the composition of the diamond-bearing layer, depending on the purpose of the diamond wheel and the type of material being processed (PM), should be based on scientifically grounded recommendations for the optimal combination of concentration, grain size and strength of diamond grains, properties

and structure of the bond, as well as coatings that protect diamond from destruction during composite sintering. [3]. This approach can ensure the integrity of diamond grains in the manufacture of tools, and will contribute to the creation of prerequisites for rational self-sharpening of grains during grinding.

An equally important issue in the design of diamond wheels is the correct choice of technological parameters for the sintering of the diamond-bearing layer of the tool, taking into account the physical and chemical characteristics of the processes occurring in this case. Sintering of the diamond-bearing layer on typical ceramic bonds occurs at higher temperatures, sufficient for the graphitization of diamonds. Depending on the properties of diamond powders, their cost can differ hundreds of times. Therefore, the choice of the characteristics of the wheel, as well as the parameters of its manufacture, should not only provide the specified properties of the tool, depending on its purpose, but also take into account the production cost. To solve this problem, we used an approach based on the analysis of the results of three-dimensional modeling of the sintering process of the diamond-bearing layer, identifying the most significant factors that determine the stress level and the state of the grains during sintering of the diamond-bearing layer.

To reduce lengthy and labor-intensive experimental studies, theoretical modeling of the process of sintering the diamond-bearing layer of a grinding wheel was carried out by analyzing the stress-strain state (SSS) of the "bond-coating-diamond grain-metal phase" system using the finite element method. The *SolidWorks* software package was used to create models of a diamond-bearing layer fragment. To implement simulation experiments, the *ABAQUS* software package was used. The research task at this stage was to simulate the sintering process to determine the conditions for the formation of a diamond-bearing layer, ensuring the integrity of diamond grains in it. When carrying out model experiments, such a combination of its morphological characteristics was determined, which ensured the preservation of the integrity of diamond grains under the conditions of specified temperature and power loads.

2. Methods

To carry out simulation experiments, models of the grinding process have been developed (the system “bond - grain - metal phase - processed material”, Fig. 1).

In modeling, it was assumed that a fragment of a diamond-bearing layer in the form of a cube with a certain amount of diamond grains, bounded on all sides by a bond array [4, 5] can fully represent the diamond wheel as a whole.

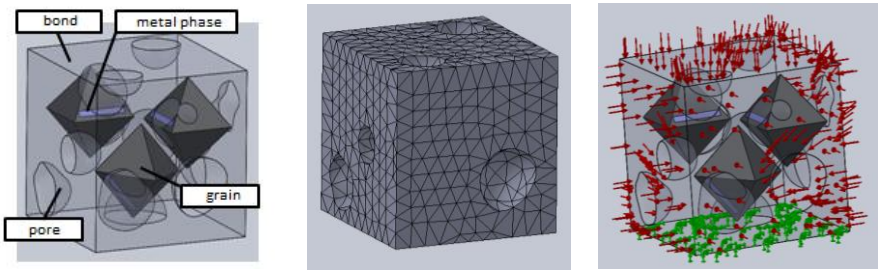

a) b) c)

Figure 1 – 3D model (a), finite element mesh (b) and loading scheme (c) in the study of the sintering processes of the diamond-bearing layer

When creating the models, the shape, dimensions and properties of its elements were taken into account, which were considered elastic solid bodies. Since the most common form of diamond crystals is the octahedron [6, 7], the grain was designed with the geometry of an octahedron. The diamond grain sizes (grain size) were as follows: 50/40, 100/80, 125/100, 200/160. Local inclusions of the metal phase in the grains were created in the form of arbitrarily oriented parallelepipeds, the volumetric content of which was set depending on the grain grade (AS4 – 7.5%, AS6 – 6%, AS15 – 2.2% and AS32 – 0.6%) [8, 9, 10]. When modeling protective coatings on a diamond grain, a shell with a thickness of 100 mass% was created.

The bond was created in the form of prismatic fragments with sizes from 250 × 250 × 125 μm to 1000 × 1000 × 500 μm, depending on the size and concentration of grains in the diamond-bearing layer. In the volume of the bond, seating surfaces for grains were randomly placed, the amount of which varied depending on the concentration of diamonds (25% – 200%), which was set as the percentage of the volume of the binder and the total volume of grains. To reproduce the natural structure of the wheel in the body of the bond, pores of arbitrary shape with sizes from 80 to 100 μm were created. The relative pore volume in the model was varied in accordance with the selected porosity values of 10, 20, and 30%.

The element of the “processed material” system was modeled in the form of prismatic fragments with sizes from 250 × 250 × 125 μm to 1000 × 1000 × 500 μm. Examples of the main three-dimensional models developed for the finite element analysis of the stress-strain state of microvolumes of the diamond-bearing layer during grinding are shown in Fig. 1.

Finite element analysis was performed using eight-node *SOLID* elements. The *ANSYS* program was used to select the type of finite elements from the package library for each component of the system, build a finite element mesh and

selectively refine it. When creating a mesh for metal phases, *Hex Dominant* and *Tetrahedron* elements were used. Thickening of the mesh was carried out in the areas where abrasive grains were embedded in the bond and in the inclusion of the metal phase, as well as on the contact surfaces of the system elements. This approach made it possible to more accurately simulate the deformation of the model fragments, taking into account the remoteness of the zones of edge effects.

Fixing the model (setting zero or other necessary displacements) was carried out using the attributes of the geometric model (points, lines, surfaces) [5]. The model was loaded with a static uniaxial uniformly distributed load in the form of the applied pressure and temperature values (Fig. 1). The choice of the boundary loading parameters was carried out taking into account the temperature and force loads accompanying the sintering of the diamond-bearing layer. So, when simulating the conditions of hot pressing or free firing of the diamond-bearing layer of the wheels, the model was subjected to a uniform temperature load from 500 to 800°C, which corresponds to the conditions for the production of DAT using ceramic (550÷800°C) bonds [11, 12, 13, 14]. The force load was varied in the range of 30–50 MPa, corresponding to the pressing pressure in the manufacture of diamond wheels [15, 16]. The analysis of the influence of the loading parameters of the models was carried out in three versions: only taking into account the effect of pressure; only taking into account the heating temperature and with the simultaneous application of pressure and temperature.

The calculation model included the following characteristics of the system elements: elastic modulus (E), bulk compression modulus (G), thermal coefficient of linear expansion (TCLE, α), Poisson's ratio (μ), yield stress (σ_0), thermal conductivity coefficient (λ). The setting of the properties of grains was carried out according to the reference data [17, 18], taking into account the information on the temperature dependences of the properties of synthetic diamond.

3. Results

The main difference between ceramic-bonded diamond wheels is the high sintering temperature of the diamond-bearing layer (700-800°C). In a number of cases (especially when using fine-grained diamond powders), this causes destruction and graphitization of grains [19–21].

Theoretical calculations made it possible to quantify the stresses in the elements of microlevel models of the "metal phase - diamond grain - bond - pore" system depending on the sintering conditions, as well as the concentration of diamonds, their size, composition and properties of the metal phase and the bond. In this case, we investigated the behavior of grains of grades AS2, AS4, characterized by an increased content of the metal phase and minimum strength properties.

Modeling the sintering process of a diamond-bearing layer on a ceramic bond made it possible to evaluate the role of temperature and force effects, both separately and during joint manifestations. In figures 2 and 3 are shown examples of stress distribution diagrams and the results of calculating the maximum equivalent stresses σ_{eq} arising in the system under conditions of power and temperature-power loads. Characteristics of the 3D model (Fig. 1, a): diamond grains AS6 125/100 (σ_{st} = 0.2 GPa); metal phase: 6% $Fe_{95}Si_5$; bond K1-01, porosity 15%.

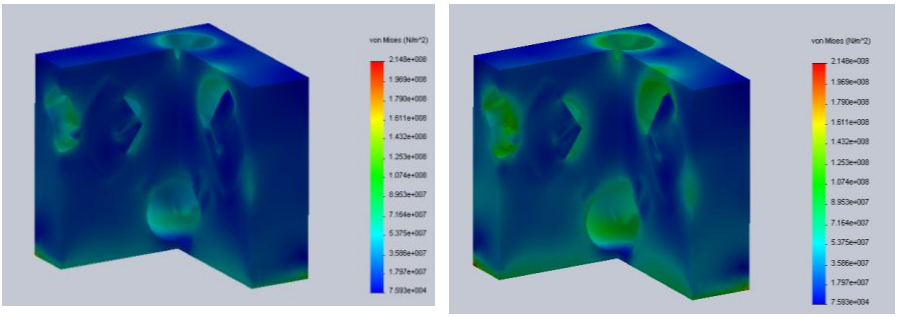

a) – σ_{eq}=3,11MPa b) – σ_{eq}=3,82MPa

Figure 2 – Stress distribution in the "metal phase - diamond grain - bond - pore" system at power loads P=30 MPa (a) and P=50 MPa (b)

Calculations have shown that loading the specified system (Fig. 1, a) only by pressure in the range of values typical for the technology of sintering wheels on ceramic bonds insignificantly affects the level of arising stresses and does not lead to a violation of the integrity of diamond grains of these grades (Fig. 3, table). This fact made it possible to conclude that the pressure (in the range of 30 – 50 MPa) from the point of view of grain integrity is an insignificant factor and practically does not cause destructive stresses.

The stresses arising during the sintering of diamond wheels under the influence of temperature are distinguished by much higher values and a characteristic distribution pattern: their increase is especially observed in the places of inclusions of the metal phase in the grain along the contour of the sphere inscribed in the octahedron. With an increase in temperature, the stresses in the system under study increase, which is explained by a significant difference in the

values of the TCLE of the metal phase and diamond, as well as the structural heterogeneity of the latter.

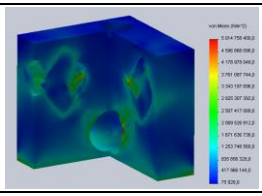

a) – T=400 ºC

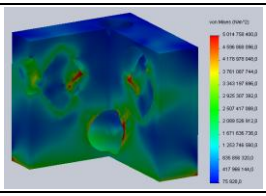

b) – T=600 ºC

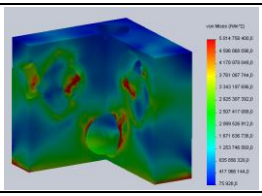

c) – T=800 ºC

Figure 3 – Distribution of stresses in the system "metal phase - diamond grain - bond - pore" at temperature and power loads

Table – Influence of temperature and power loads on equivalent stresses

Pressure	T= 400 ºC	T= 600 ºC	T= 800 ºC
P = 0 MPa	σ_{eq}=63,85 MPa	σ_{eq}=590,92 MPa	σ_{eq}=748,76 MPa
P =30MPa	σ_{eq}=64,06 MPa	σ_{eq}= 591,23 MPa	σ_{eq}=749,03 MPa
P =50MPa	σ_{eq}=64,74 MPa	σ_{eq}=591,86 MPa	σ_{eq}=749,81 MPa

This leads to a significant expansion of the inclusions of the metal phase with an increase in the sintering temperature and, as a consequence, to the appearance of internal stresses in the diamond grain, which can lead to the cracks formation in its volume and its subsequent destruction. By the nature of the distribution of the limiting values of the stress arising in the system at thermal power stresses, they are similar to the picture of thermal stresses, while their value at the same power load increases significantly. With an increase in the sintering temperature to 600°C and higher, stresses arise in the grain, localized in the region of inclusions of the metal phase, which can destroy the grain itself.

Each brand of diamond powder has characteristic performance properties, determined by the shape and morphology of grains, as well as microstructural features of their structure. It also represents the arithmetic mean of the compressive strength of all grain sizes of a given grade, expressed in newtons [22]. According to [23–24], with an increase in the strength of diamond powders, the number of metal phase inclusions in them decreases (for example, in diamonds of grades AS4, AS6, AS15, AS32, the content of the solvent alloy reaches 7.5; 6.0; 2.2 and 0, 6

wt%, respectively). The presence of inclusions of the metal phase reduces the thermal resistance of diamonds and the value of their breaking load.

Within the framework of theoretical studies, we determined the influence of the quantitative and qualitative characteristics of the metal phase (depending on the grade of diamonds and the composition of the metal catalyst) on the level of stresses arising in the grains under loads corresponding to the sintering conditions of the ceramic matrix diamond-containing layer of the tool. Since the ultimate tensile strength of diamond is lower than that of compression, the calculated values of the maximum tensile stresses were taken as a fracture criterion, which were compared with their ultimate strengths for diamonds of various grades and grain sizes [25–28]. As shown in [29, 30], stresses exceeding the ultimate strength of diamond and located at the boundaries of the metal phase inclusions cause the development of internal cracks in the grain. However, this is not a sufficient condition for grain damage, the destruction of which begins if the breaking stresses propagate in a significant volume of the grain (more than 10%).

As the reaction of the model to loading, we considered the equivalent stress at the mesh nodes belonging to the elements of the system under study (grain and metal phase). Using the *ABAQUS* software, the limiting stress value in the studied area of the system was set, in accordance with which the gradation of the equivalent stress was built on the epure and scale. According to the calculation results, the grain volume (V_{cr}) was determined, in which the stresses exceeded the ultimate tensile strength of diamonds for a given grade and grain size. Fig. 4 shows examples of epure, obtained for the case of using diamonds AS6 [σ_{st} = 0.2GPa] and AS15 [σ_{st} = 0.53GPa] with the $Fe_{95}Si_5$ metal phase and its percentage in them 4% and 2.2%, respectively.

As can be seen from the data obtained, the maximum level of equivalent stresses recorded in the areas of the metal phase in the grain differs insignificantly for diamonds of different grades (the difference is ~ 4%). At the same time, the volumes of grains in which stresses exceeding the limiting level for diamonds of the indicated grades are noted differ significantly (for diamonds of the AS6 grade this indicator is 2.5 times higher).

To obtain more complete information on the influence of the qualitative characteristics of the metal phase on the integrity of diamond grains during sintering, cases with different compositions of the metal phase containing cobalt, nickel, and iron are considered. The results of model experiments on the effect of the composition of the metal phase (content 6%) on the value of σ_{eq} in the grain are shown in Fig. 5.

Since at this stage of research, the most interesting is the analysis of the influence of the metal phase on the stresses arising in the diamond grain during sintering, the image of the bond in this illustration is hidden. Analysis of the distribution epures of stresses arising during the thermal-force loading of the model

shows that the maximum values of the equivalent stresses are fixed in the region of inclusions of the metal phase, whereas in the absence of the metal phase in the diamond grain, the maximum stresses are localized at the boundary of the contact between the diamond and the bond.

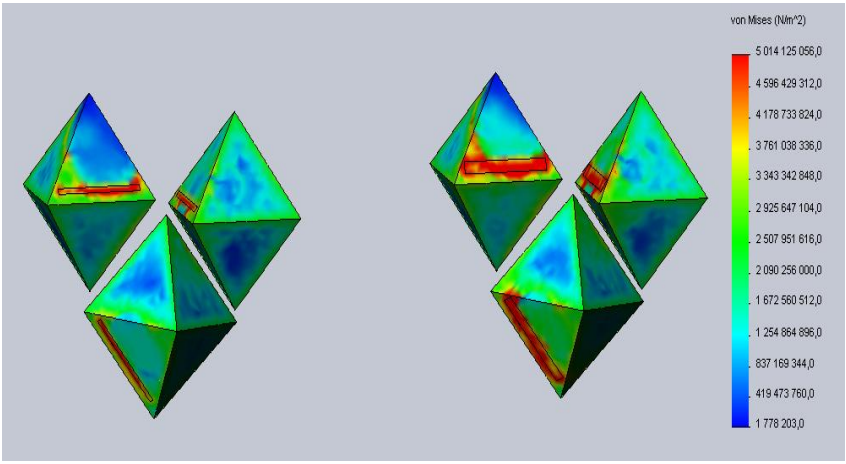

AS15, σ_{eq}= 722,37 MPa

AS6, σ_{eq}= 780,23 MPa

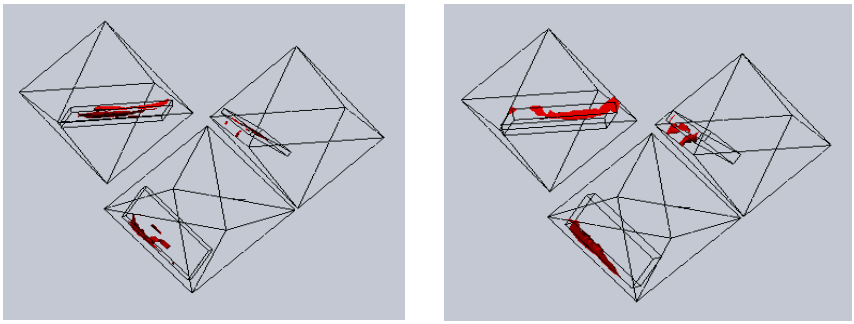

V_{cr}=4,73 %

V_{cr}=9,56 %

Figure 4 – Characteristics of the stress-strain state of the system "metal phase - diamond grain - bond - pore" during sintering of the K1–01 bond (sintering parameters P = 30 MPa; T = 700°C)

Stresses exceeding the ultimate strength of diamond grains are located along the boundary of inclusions of the metal phase, which suggests the appearance of an internal crack in the grain. At the same time, the stresses at the grain periphery are distributed in such a way that they will facilitate the separation of the protruding sections from the grain. This can cause rounding of the cutting edges of the diamond grains, which can adversely affect the cutting ability of the diamond wheel.

The calculation results indicate (Fig. 6) that, with an increase in temperature loads from 500 to 800°C (at a constant pressure of 30 MPa) in grains of grade AS6 125/100, an increase in maximum stresses from $\sigma_{600°C}$ = 703.22 MPa is observed up to $\sigma_{800°C}$ = 1721.5 MPa (for the metal phase of composition $Ni_{39.6}Mn_{59.6}(Cr_3C_2)_{0.8}$) and from $\sigma_{600°C}$ = 526.06 MPa to $\sigma_{800°C}$ = 999.65 MPa (for the metal phase of composition $Fe_{44}Co_{44}(Cr_3C_2)_{12}$).

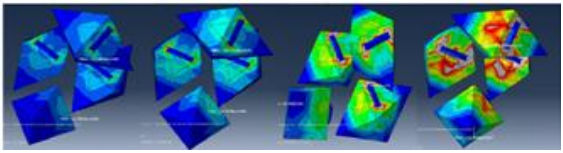

500^{0}C 600^{0}C 700^{0}C 800^{0}C

a) – metal phase $Fe_{44}Co_{44}(Cr_3C_2)_{12}$, σ_{eq} = 612,55 MPa

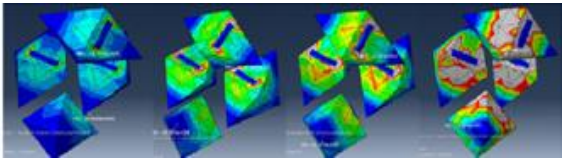

500^{0}C 600^{0}C 700^{0}C 800^{0}C

b) – metal phase $Fe_{95}Si_5$, σ_{eq} = 725,16 MPa

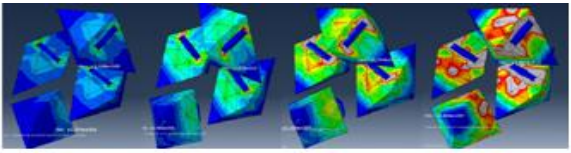

500^{0}C 600^{0}C 700^{0}C 800^{0}C

c) – metal phase $Ni_{39,6}Mn_{59,6}(Cr_3C_2)_{0,8}$, σ_{eq} = 835,63 MPa

Figure 5 – Epures of stress distribution in grain during sintering
(sintering parameters: K1-01 bond with 15% porosity; P = 30 MPa; T = 700°C)

The different level of the arising stresses is due to the significant difference (more than 2 times) in the TCLE of the indicated metal phases containing different amounts of cobalt, nickel and iron. At the sintering temperature of diamond wheels on a ceramic bond K1-01 (~ 750°C), stresses arise in the grains of AS6 125/100 powder that exceed the ultimate tensile strength of diamonds (0.2 GPa). It follows from this that when using diamonds of low strength grades (contaminated with metal inclusions), the sintering temperature should not exceed 550 ° C.

For diamond grains AS15 125/00 in the absence of nickel in the composition of the metal phase, the maximum sintering temperature can reach 650°C. Otherwise, the sintering temperature must be reduced to 600°C. Compliance with these conditions will ensure the integrity of the grains at the stage of manufacturing diamond wheels when using synthetic diamonds of low grades.

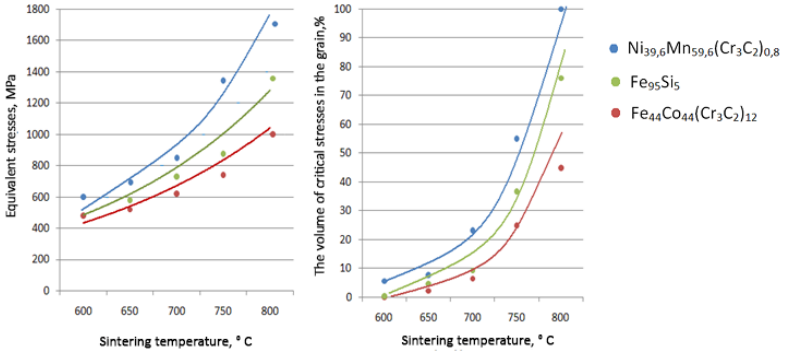

a) b)

Figure 6 – Temperature dependences of equivalent stresses (a) and volumes of critical stresses in a grain (b) for AS6 125/100 diamonds containing a metal phase of different composition

In the case of using synthetic diamonds, the choice of catalyst metals should be based on the observance of two conditions: low thermal conductivity and minimum TCLE while maintaining a high elastic modulus. This conclusion is explained by the fact that a decrease in thermal conductivity will lead to a slowdown in the heating of metal inclusions, and, as a consequence, a decrease in their thermal expansion, which, in turn, will contribute to a decrease in stresses in the system. An increase in the elastic modulus of the metal phase increases its tensile strength; however, the nature of the temperature dependence of the elastic modulus for various catalyst metals (as well as the features of the temperature dependences of thermal conductivity and TCLE) significantly reduce this effect.

Based on the foregoing, it is advisable to use iron-based solvent alloys as catalysts in the synthesis of diamonds, for example, $Fe_{44}Co_{44}(Cr_3C_2)_{12}$ or $Fe_{95}Si_5$, the first of which is characterized by minimal thermal conductivity and TCLE, and the second has an optimal combination of thermal conductivity and elastic modulus, which will be help to minimize the equivalent stresses in the diamond grain.

4. Summary

Adherence to the general recommendations for all diamond wheels regarding the design principles of DAT leads to grain damage already at the stage of tool manufacturing, which can be the reason for the low efficiency of diamond abrasive processing. An analysis of modern research aimed at increasing the efficiency of DAT manufacturing and the results of our own experiments indicates the efficiency of using an approach based on microlevel 3D modeling of the behavior of a diamond-bearing layer at the stage of tool manufacturing in the design of DAT on a ceramic bond. The studies carried out at this stage have led to the following conclusions:

The integrity of diamond grains at the stage of manufacturing DAT on ceramic bonds is mainly determined by the temperature factor. The force factor (pressure during workpiece molding) within the studied limits (up to 50 MPa) practically does not affect the stress distribution in the sintered diamond-bearing layer and does not cause the appearance of destructive stresses in the grain.

The role of the qualitative and quantitative characteristics of the metal phase present in synthetic diamonds in the process of their destruction during sintering of the diamond-bearing layer has been determined and their relationship with the technological parameters of the process has been revealed. It has been substantiated by calculation that the main reason for the premature destruction of grains during sintering of the diamond-bearing layer is the stresses in the grain, caused by a significant difference in the TCLE of diamond and metal phase (3.5÷8 times for different solvent alloys). With a decrease in the content of the metal phase, the thermal resistance of diamonds increases. When using diamonds of grades AS32 and higher, the sintering temperature of the diamond-bearing layer, at which the appearance of stresses destroying the grain is excluded, can be increased to the softening temperature of known ceramic bonds. When making DAT using cheaper diamonds of grades AS2 - AS15, the sintering temperature of the diamond layer should be reduced to 550÷650 ºC in order to avoid the destruction of grains. A comparative analysis of the effect of the properties of some solvent alloys on the level of stresses arising in the grain is carried out. The choice of the $Fe_{44}Co_{44}(Cr_3C_2)_{12}$ solvent-alloy is substantiated, which makes it possible to reduce the level of stresses arising in the grain during sintering of the diamond-bearing layer.

References: 1. *Mamalis AG, Grabchenko AI, Fedorovich VA, Kundrák J.:* Methodology of 3D simulation of processes in technology of diamond-composite materials/ International Journal Of Advanced Manufacturing Technology, Volume: 43, Issue: 11–12, pp.1235–1250. DOI: 10.1007/s00170-008-1802-0 Published: 2009. **2.** *Kundrák, J., Fedorenko, D.O. Fedorovich, V.O,,,Fedorenko, E.Y., Ostroverkh, E.V.* Porous diamond grinding wheels on ceramic binders: Design and manufacturing/ Manufacturing Technology 2019, Vol. 19, No. 3, pp. 446–454. **3.** *Grabchenko A.I.* 3D modeling of diamond-abrasive tools and grinding processes / Grabchenko A.I., Dobroskok V.L., Fedorovich V.A. – Kharkiv: NTU "KhPI", 2006. – 364 p. **4.** *Fedorovich V.A.* Development of scientific grounds and methods of practical realization of adaptability control at diamond grinding of superhard materials, Kharkiv DSc dissertation (2002).– 466 p. (In Russian). **5.** Principles of 3D modeling of the production and application of diamond composite materials / [A. G. Mamalis, A. I. Grabchenko, V. I. Fedorovich and oth.] // Nanotechnology perception.– Basel: Institute of advanced study. – 2012. – pp.132–139. **6**. *Epifanov V.I.* Technology of processing diamonds into brilliants / V. I. Epifanov, A. Y. Pesina, L. V. Zykov. – Moscow.: Vys'shaya shkola, 1984. – 319 p. **7.** *Rakin V. I.* Morphology of artificial diamonds / V. I. Rakin, N.N. Piskunova // Izvestia of the Komi Scientific Center of the Ural Branch of the Russian Academy of Sciences (Syktyvkar). – 2012. – Issue. 3 (11). – pp. 61-67. **8.** *Bogatyreva G.P.* Impurities and inclusions in powders of synthetic diamonds of grades AS4 and AS6 / [G. P. Bogatyreva, V.M. Maevsky, G.D. Ilnitskaya et al.] // Superhard materials. – 2006. – No. 4. – pp. 62–69. **9.** *Phaal S.* X-ray and metal inclusions in synthetic diamond / S. Phaal, G. Woolds // Nature. – 1966, 212. – pp. 1227–1229. **10.** To the question of the mechanism of softening of synthetic diamond crystals at high-temperature heating / [A. L. Maistrenko, A. I. Borimsky, L. N. Devin et al.] // Rock-cutting and metal-working tool - equipment and technology of its manufacture and application: collection of articles. scientific. tr. - Kyiv.: INM named by V.M. Bakul National Academy of Sciences of Ukraine, 2010. – Ed. 13. – pp. 272–279. **11.** *Mamalis, A.G., Grabchenko, A.I., Fedorovich, V.A., Paulmier, D., Horvath, M.* Development of an expert system of diamond grinding of superhard polycrystalline materials considering grinding wheel/International Journal of Advanced Manufacturing Technology. (2001) 17(7), pp. 498–507. **12.** *Sudnik L.V.* Diamond-containing abrasive nanocomposites / L. V. Sudnik, P. A. Vityaz, A. F. Ilyushchenko. – Minsk: Belaruskaya Navuka, 2012. – 318 p. **13.** *Reznikov A. N.* Abrasive and diamond processing of materials: Handbook / [A. N. Reznikov, E.I. Aleksentsev, Y.I. Barats and others]; ed. A.N. Reznikov. – Moscow.: Mashinostroenie, 1977. – 391 p. **14.** *Reshetnikov A.A.* Study of the influence of the thermal factor on the formation of residual stresses during grinding: 150900 – Technology of mechanical engineering: author. diss. ... master. – Samara: SSTU, 2010. – 17 p. **15.** *Yakimov A.V.* Thermophysics of mechanical processing. Textbook / A.V. Yakimov, P.T. Slobodyanik, A.V. Usov. – Kyiv.–Odessa: Lybid, 1991. – 240 p. **16.** *Yadava V.* Theoretically analysis of Thermal Stress in Electro-Discharge Diamond Grinding / V. Yadava, V. K. Jain, P. M. Dixit // Machining Science and technology. – 2004. – Vol. 8. – № 1. – pp. 119–140. **17.** Physical properties of diamond: handbook / ed. N.V. Novikova. – Kyiv: Naukova Dumka, 1987. – 188 p. **18.** The Element Six CVD Diamond Handbook, Ascot (UK): Element Six, 2015. – 27 p. https://e6cvd.com/us/diamond-book-download. **19.** *N.V. Novikov* Resistance to destruction of superhard composite materials / N.V. Novikov, A.L. Maistrenko, V.N. Kulakovsky. - K.: Naukova Dumka, 1993. -- 220 p. **20.** *Janos Kundrák, Vladimir Fedorovich, Angelos P. Markopoulos, I. Pyzhov, Natalya Kryukova*. Improvements of the Dressing Process of Super Abrasive Diamond Grinding Wheels / Manufacturing Technology December 2014, Vol. 14, №. 4 - Page. -545 – 554. Permission: MK CR E 20470 ISSN 1213–2489; **21.** *Mastyugin L. I.* Using a diamond tool with a ceramic binder / L. I. Mastyugin, V. V. Moroz, A. V. Katyuk // Journal of Optical Technology– 1994. – 61, № 2. P. 165– 166. **22.** DSTU 3292-95. Synthetic diamond powders. General technical specs. - Kyiv: Derzhspozhivstandart Ukrainy, 1997. – 151 p. **23.** *Novikov N.V.* Inclusions in crystals of synthetic diamond high-strength powders // N.V. Novikov, G.P. Bogatyreva, G.D. Ilnitskaya et al. // High Pressure Physics and Technology. – 2009. – T. 19, No. 2. – pp. 48 –53**. 24.** *Gargin V.G.* Influence of inclusions in diamonds on their strength. V.G. Gargin // Superhard materials. – 1983. – No. 4. – pp. 27–30. **25.** *Ivester R. W.* Measuring Chip Segmentation by High-Speed Microvideography and Comparison to Finite-Element Modelling Simulations / R.W. Ivester, E. Whitenton, J. Heigel // Proceedings of the 10th CIRP International Workshop on Modeling of Machining Operations.– 2007. – pp. 37–44. **26.** *Fischer C.*

Runtime and Accuracy Issues in Three Dimensional Finite Element Simulation of Machining / C. Fischer // Proceedings of the 10th CIRP International Workshop on Modeling of Machining Operations. – 2007. – pp.45–50. **27.** *Salmon S.C.* Modern Grinding Process Technology / S.C. Salmon. – New York: McGraw-Hill, Inc., 1992. – 225 p. **28.** *Malkin S.* Grinding Technology: theory and applications of machining with abrasives / S. Malkin. – NY: John Wiley & Sons, 1989. – 275p. **29.** *Watson J. H.* Compressive strength of synthetic diamond grits containing metallic nanopazticles / J. H. Watson, Z. Li, A.M. Hyde // Applied Physics Letters. – 2000. – Vol.77. – pp. 4330–4331. **30***. Maistrenko A.L.* To the question of the mechanism of softening of synthetic diamond crystals at high-temperature heating / [A. L. Maistrenko, A. I. Borimsky, L.N. Devin et al.] // Rock-cutting and metal-working tool - equipment and technology for its manufacture and application: collection of articles. scientific. tr. - Kyiv.: INM named by V.M. Bakul National Academy of Sciences of Ukraine, 2010. – Ed. 13. – pp. 272–279.

Володимир Федорович, Євгеній Островерх, Іван Пижов, Харків, Україна,
Валерій Лавриненко, Київ, Україна

ТЕОРЕТИЧНЕ ОБГРУНТУВАННЯ РАЦІОНАЛЬНИХ УМОВ ВИГОТОВЛЕННЯ АЛМАЗНИХ КРУГІВ НА КЕРАМІЧНИХ ЗВ'ЯЗКАХ

Анотація. *Аналізуються результати проведених теоретичних досліджень із застосуванням 3D моделювання методом кінцевих елементів, що дозволило визначити раціональні характеристики алмазних кругів на керамічних зв'язках. Вивчено вплив параметрів алмазоносного шару на зміну його напружено-деформованого стану в зоні спікання алмазного круга. Встановлено вплив технологічних параметрів процесу та характеристик алмазного круга на цілісність зерен при спіканні, на підставі чого надано практичні рекомендації щодо вибору алмазних композицій з раціональними властивостями. Аналіз сучасних досліджень, спрямованих на підвищення ефективності виготовлення ААІ та результатів власних експериментів, свідчить про ефективність використання при проектуванні ААІ на керамічних зв'язках підходу, заснованого на мікрорівневому 3D моделюванні поведінки алмазоносного шару на етапі виготовлення інструменту. Проведені на цьому етапі дослідження дозволили зробити висновки, що цілісність алмазних зерен на етапі виготовлення ААІ на керамічних зв'язках визначається переважно температурним фактором. Силовий фактор (тиск при формуванні заготівки) в досліджуваних межах (до 50 МПа) практично не впливає на розподіл напружень в алмазоносному шарі, що спікається, і не викликає появу руйнівних напружень у зерні. Визначено роль якісних та кількісних характеристик металофази, що присутня у синтетичних алмазах, у процесі їх руйнування при спіканні алмазоносного шару та виявлено їх взаємозв'язок з технологічними параметрами процесу. Розрахунковим шляхом обґрунтовано, що головною причиною передчасного руйнування зерен при спіканні алмазоносного шару є напруження в зерні, зумовлені суттєвою різницею КЛТР алмазу та металофази (у 3,5÷8 разів для різних сплавів-розчинників). Зі зменшенням вмісту металофази термостійкість алмазів підвищується. При використанні алмазів марок АС 32 і вище температура спікання алмазоносного шару, при якій виключена поява напружень, що руйнують зерно, може бути збільшена до температури розм'якшення відомих керамічних зв'язок. При виготовленні ААІ з використанням більш дешевих алмазів марок АС2 – АС15 температура спікання алмазоносного шару повинна бути знижена до 550÷650 ℃, щоб уникнути руйнування зерен. Проведено порівняльний аналіз впливу властивостей деяких сплавів-розчинників на рівень напружень, що виникають у зерні. Обґрунтовано вибір сплаву-розчинника $Fe_{44}Co_{44}(Cr_3C_2)_{12}$, що дозволяє знизити рівень напруження, що виникає в зерні при спіканні алмазоносного шару.*

Ключові слова: *алмазний шліфувальний круг; керамічна зв'язка; алмазоносний шар; алмазне зерно; процес шліфування; силовий та температурний фактори; метод кінцевих елементів; 3D-модель; процес спікання алмазного круга; металева фаза; еквівалентне напруження.*

UDC 621.923.5 **doi: 10.20998/2078-7405.2022.97.12**

I. Sztankovics, G. Varga, Miskolc, Hungary

FEM ANALYSIS OF THE BURNISHING PROCESS OF X5CrNi18-10 STAINLESS STEEL

Abstract. *The burnishing process can improve the surface roughness of machined parts, while having an advantageous effect on the properties of the layer below the surface. In this paper the effect of the surface speed, the feed rate and pressing force are analysed with Finite Element Method. The affected width and depth were analysed during one pass of the burnishing tool. We also examined the highest pressure and the stress distribution of the surface layer. The values of the studied parameters were chosen according to the "Design of Experiments" method. Equations determining the studied properties were also given.*
Keywords: *burnishing; design of experiments; FEM simulation.*

6. INTRODUCTION

In the development of different manufacturing processes and systems, many factors must be considered. An aim of these improvements is the increase the quality of the machined surface while decreasing the costs of manufacturing [1]. However, production engineers must consider the energy efficiency and environmental impact of different procedures during the process planning. A further aim is to improve the properties of workpieces to reduce the weight and therefor the fuel consumption [2]. The burnishing process can effectively improve the properties of the surface layer.

Diamond burnishing leads to a favourable combination of the 3D height and shape parameters for surface texture in the point of view of the wear resistance enhancement [3]. Raza et al. showed in their review work that the burnishing parameters such as force, feed, speed, number of tool passes, ball diameter and lubrication medium have a greater influence on the surface characteristics of the component [4]. The experimental results of Mohamed et al. indicate that feed, speed, burnishing force and number of passes are the most important and significant parameters to improve hardness [5]. Fedorovich et al. showed in their study that the optimal choice of the technological parameters should consider both the equivalent stress distribution in the surface layer of the products and the factors influencing the tool wear observed under a particular processing mode [6]. An effective way of increasing the depth of the hardened layer is the increase of the number of passes [7]. Yaman et al. studied the surface integrity alteration and found that the burnishing force and burnishing speed are critical parameters to make the burnishing process more effective and increase the wear resistance of parts [8]. Teimouri et al. proved in their theoretical and experimental work,

that among the process factors the burnishing depth has the greatest influence on microhardness alternation [9]. The analysis of Barahate et al. showed that the burnishing feed rate has the highest impact on the surface roughness (a contribution of 54.51% in their experiments), followed by load and burnishing speed [10]. Borysenko et al. studied the burnished surface on reverse engineering approach, where the models of the workpiece and the tool were created using 3D scanning [11]. Ferencsik et al. studied the burnishing process by the application of FEM simulation, and showed that numerical value of roughness is in a good correlation with the experimental results [12].

The values of the affected depth and width in burnishing of different materials are essential information in the process planning of the procedure. Therefore, the alteration effect of the feed, surface speed and pressure force were studied in diamond burnishing using Finite Element Method simulations in this paper. The results were evaluated using the Design of Experiment method.

7. EXPERIMENTAL METHODS AND CONDITIONS

In this paper we intended to make a study to better describe and understand the processes in the surface layer during burnishing. The aim of our study is the description of the affected depth and width in diamond burnishing by FEM analysis. The finite element simulations were done with the ThirdWave Advantedge 7.601 software.

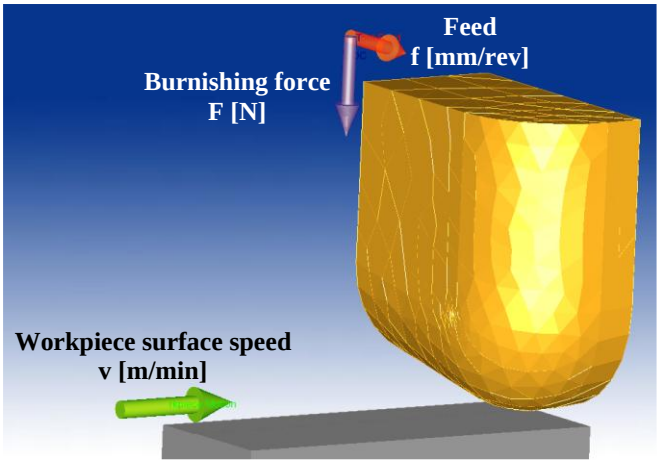

Figure 1 – Experimental setup in the FEM software

The setup of the tool, workpiece, burnishing force, feed and surface speed were shown in Figure 1. It can be seen that the burnishing of a shaft is simulated on a plane. The burnishing force were adjusted by the precise adjustment of the depth of cut parameter, where the chip removal is not occurred, and the desired load could be measured from the force perpendicular of the workpiece surface. X5CrNi18-10 grade stainless steel were selected as workpiece material. The tool material was PCD with medium conductivity. The initial temperature was 20 °C. Furthermore, minimum element size of 0.0054 mm, refined region radius of 0.026 mm, refining factor of 4, coarsening factor of 3, 6.0 grading near the cutting edge were set.

Three process parameters were analysed in our study: surface speed (*v*), feed (*f*), burnishing force *(F*). The values of these parameters were chosen according to the Full Factorial Design of Experiments method, where a high (+1) and a low (-1) value is determined for each factor, and the experimental setup is generated through the combination of these values. Table 1 shows the experimental plan for the 8 cases. The parameters were chosen according to our real experimental plan of burnishing a shaft with 50 mm diameter.

We measured 4 parameters in each setup. The first is the stress depth, which represents the depth where at least 350 MPa Mises stress occurs, which is the 1.5-fold value of the materials proof strength. The second is the Burnished depth, which measures the affected depth according to the perpendicular stress (Stress Y-Y in the program notation). The third is the Burnished width, which measures the affected width according to the shear stress (Stress Y-Z in the program notation). The final studied parameter is the maximum value of the Pressure occurring in the surface layer during burnishing.

Table 1 – Setup values of the studied process parameters

	v	*f*	*F*	*n* [1/min]	*v* [m/min]	*f* [mm/rev]	*F* [N]
1	-1	-1	-1	265	41.17	0.025	30
2	1	-1	-1	375	58.26	0.025	30
3	-1	1	-1	265	41.17	0.05	30
4	1	1	-1	375	58.26	0.05	30
5	-1	-1	1	265	41.17	0.025	40
6	1	-1	1	375	58.26	0.025	40
7	-1	1	1	265	41.17	0.05	40
8	1	1	1	375	58.26	0.05	40

8. EXPERIMENTAL RESULTS

Measurements were made on the results of the FEM simulations according to the previous conditions. Here an example is given for the better understanding of the process in case of Setup 8. The results of the measurements were shown in Table 2.

Figure 2 shows the measurement of the stress depth and burnished depth. In the former, the highest distance from the surface was taken where the Mises stress value exceeds 350 MPa, which is crucial for the elastic deformation. In the latter the highest distance of that FEM element was measured, where the perpendicular stress is different than 0.

Table 2 – Results of the FEM simulations

	Stress Depth [mm]	Burnished Depth [mm]	Burnished Width [mm]	Pressure [MPa]
1	0.0834	0.2007	0.1145	1367.37
2	0.0907	0.2061	0.1266	1321.92
3	0.1057	0.1843	0.1379	1412.23
4	0.1349	0.2249	0.1604	1372.58
5	0.0913	0.2178	0.1092	1625.49
6	0.1177	0.1835	0.1123	1672.84
7	0.1141	0.2978	0.1810	1652.82
8	0.1412	0.2960	0.2115	1612.35

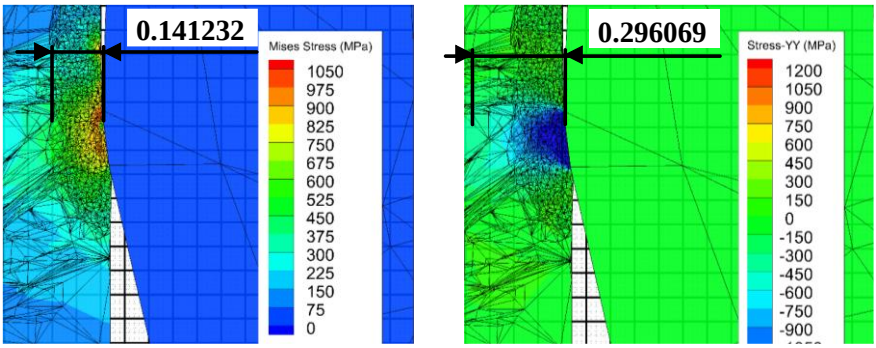

a) b)

Figure 2 – Measurement of the Stress depth (a) and Burnished depth (b), Setup 8

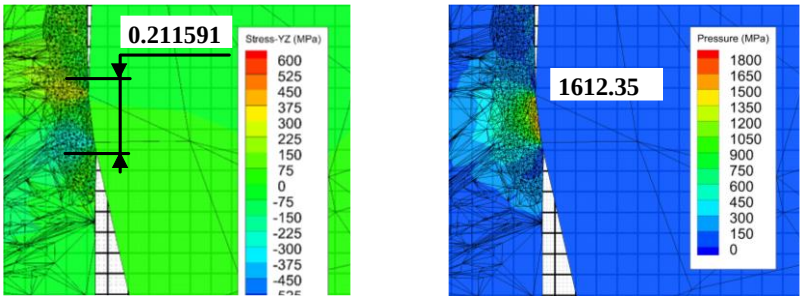

a) b)

Figure 3 – Measurement of the Burnished width (a) and Pressure (b), Setup 8

The measurement of burnished width and pressure can be seen in Figure 3. To measure the affected width, we measured the distance between the occurring shear stresses. The highest value of the pressure occurring in the surface layer was provided by the FEM software.

A further aim of our study was to provide equations for the calculation of the studied attributes. These were determined in the form of Equation 1, where the k_i are the constant of the different factors.

$$y(v,f,F) = k_0 + k_1 v + k_2 f + k_3 F + k_{12} vf + k_{13} vF + k_{23} fF + k_{123} vfF \quad (1)$$

The k_i constants were determined for the studied parameters. The results can be seen for the Stress depth (y_1) in Equation 2, for the Burnished depth (y_2) in Equation 3, for the Burnished width (y_3) in Equation 4 and for the Pressure (y_4) in Equation 5.

$$y_1(v,f,F) = 0.3641 - 7.912 \cdot 10^{-3} v - 7.369 f - 8.933 \cdot 10^{-3} F + 0.2 vf + 2.354 \cdot 10^{-4} vF + 0.205 fF - 4.948 \cdot 10^{-3} vfF \quad (2)$$

$$y_2(v,f,F) = 0.2586 - 4.772 \cdot 10^{-3} v - 16.39 f - 1.006 \cdot 10^{-3} F + 0.101 vf - 2.171 \cdot 10^{-4} vF + 0.4110 fF - 6.258 \cdot 10^{-4} vfF \quad (3)$$

$$y_3(v,f,F) = 0.0609 - 4.644 \cdot 10^{-3} v - 0.991 f - 8.763 \cdot 10^{-4} F + 0.094 vf - 1.517 \cdot 10^{-4} vF + 0.031 fF \quad (4)$$

$$-3.963 \cdot 10^{-3} vfF$$

$$y_4(v,f,F) = 1.966 - 35.722v - 2.373 \cdot 10^4 f - 17.345F + 670.927vf - 1.091vF + 832.037fF - 21.912vfF \quad (5)$$

9. DISCUSSION

Equation 2-5 were drawn as a function of the surface speed (*v*) and feed (*f*) for the two levels of the burnishing force.

Figure 4 shows the effect of these parameters on the Stress depth and Burnished depth. We conclude that the increase of the perpendicular force has an increasing effect on these parameters, however a larger increase can be seen in the affected depth than the stress depth. Increasing the surface speed led to an interesting finding. While the 1.5-fold increase of the speed led to an average of 1.2-fold increase in the stress depth, the affected depth remained the same. Doubling the feed leads to an average 1.25 increase in the stress depth, while the affected depth only increases in the higher load setups, and it remains nearly the same if the burnishing force was adjusted to 30 *N*.

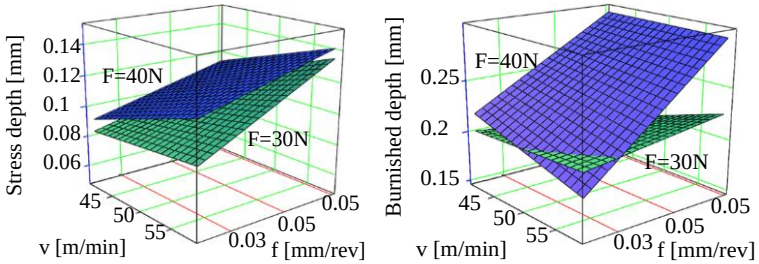

Figure 4 – Stress depth and burnished depth as a function of the studied parameters

The alteration of the burnished width and the pressure is presented in Figure 5.. The alteration of the surface speed has a very low effect on these parameters (0-16% change). However increasing the feed has a significant impact on the affected width. By the 1.5-fold incrase of the feed, a 1.2-1.8-fold increase can be observed in the affected width. The effect of burnishing force alteration depends on the feed value. As expected, the highest pressure value increases by the increase of the burnishing force: 1.33-fold increase of the latter leads to an 1.2 higher pressure on avarage. The surface speed and the feed has almost no effect on this studied parameter.

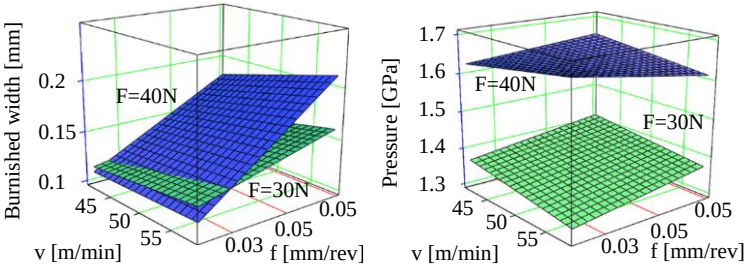

Figure 5 – Burnished width and pressure as a function of the studied parameters

SUMMARY

The burnishing process of X5CrNi18-10 grade stainless steel material was studied in this paper by the application of FEM simulations. The analysed parameters were selected according to the Design of Experiments method. The stress depth, the affected depth and width and the pressure were measured and further analysed. Equations were given for the calculation of these parameters in the studied range. The effect of the surface speed, feed and burnishing force were analysed. It is found that the increase of the burnishing force has the highest effect, followed by the feed.

ACKNOWLEDGEMENTS

Project no. NKFI-125117 has been implemented with the support provided from the National Research, Development and Innovation Fund of Hungary, financed under the K_17 funding scheme.

References: 1. *Grewal S.* Manufacturing process design and costing an integrated approach (1st ed. 2011). Springer London : Imprint: Springer. **2.** *Kovács, Gy.*: Optimization of structural elements of transport vehicles in order to reduce weight and fuel consumption. STRUCTURAL ENGINEERING AND MECHANICS 71 : 3 pp. 283-290. , 8 p. 2019. **3.** *Duncheva, G.V., Maximov, J.T., Anchev, A.P., Dunchev, V.P., Argirov, Y.B., Kandeva-Ivanova, M.:* Enhancement of the wear resistance of CuAl9Fe4 sliding bearing bushings via diamond burnishing. Wear, Volumes 510–511, 204491, 2022. **4.** *Raza, A., Kumar, S.*: A critical review of tool design in burnishing process. Tribology International, Volume 174, 107717, 2022. **5.** *Mohamed, T., Hamid, H., Salah, A. and Salim B.*:"Effect of Roller Burnishing Parameters on Roughness Surface and Hardness of Unalloyed S 355 J0 Steel by Using Response Surface Methodology. Manufacturing Technology, vol. 17, pp. 602-10, 2017. **6.** *Fedorovich, V., Pyzhov, I., Kundrak, J., Pupan, L., & Voloshkina, I.*: Simulation methodology of diamond burnishing. In Design, Simulation, Manufacturing: The Innovation Exchange (pp. 363-372). Springer, Cham. 2021. **7.** *Attabi, S., Himour, A., Laouar, L., Motallebzadeh, A.:* Mechanical and wear behaviors of 316L stainless steel after ball burnishing treatment. Journal of Materials Research and Technology, Volume 15, Pages 3255-3267, 2021. **8.** *Yaman, N., Sunay, N., Kaya, M., Kaynak, Y.:* Enhancing Surface Integrity of Additively Manufactured Inconel 718 by Roller Burnishing Process, Procedia CIRP, Volume 108, Pages 681-686, 2022. **9.** *Teimouri, R., Grabowski, M., Bogucki, R., Ślusarczyk, Ł.,*

Skoczypiec, S.: Modeling of strengthening mechanisms of surface layers in burnishing process. Materials & Design, Volume 223, 111114, 2022. **10.** *Barahate, V., Govande, A. R., Tiwari, G., Sunil, B. R., Dumpala, R.:* Parameter optimization during single roller burnishing of AA6061-T6 alloy by design of experiments. Materials Today: Proceedings, Volume 50, Part 5, pp 1967-1970, 2022. **11.** *Borysenko, D., Welzel, F., Karpuschewski, B., Kundrák, J., Voropai, V:* Simulation of the burnishing process on real surface structures. Precision Engineering, Volume 68, Pages 166-173, 2021. **12.** *Ferencsik, V. and Gál, V.*: FE Investigation of Surface Burnishing Technology. Cutting & Tools in Technological System, (93), pp.3-8. 2020

Іштван Станкович, Дьюла Варга, Мішкольц, Угорщина

АНАЛІЗ ПРОЦЕСУ ВИГЛАДЖУВАННЯ НЕРЖАВІЮЧОЇ СТАЛІ X5CrNi18-10 МЕТОДОМ КІНЦЕВИХ ЕЛЕМЕНТІВ

Анотація. *Алмазне вигладжування призводить до сприятливого поєднання тривимірних параметрів висоти та форми текстури поверхні з точки зору підвищення зносостійкості. Значення порушеної глибини та ширини при вигладжуванні різних матеріалів є важливою інформацією під час планування процесу. Метою даного дослідження є опис методом МКЕ глибини, що порушується, і ширини при вигладжуванні алмазним індентором. Моделювання шляхом кінцевих елементів було виконано за допомогою програмного забезпечення ThirdWave Advantedge 7.601. Вигладжування валу моделювалося на площині. Сила вигладжування регулювалася точним регулюванням параметра глибини різання, при якому видалення стружки не відбувалося, а бажане навантаження могло бути виміряне за силою, що перпендикулярна поверхні заготовки. Як матеріал заготівки була обрана нержавіюча сталь марки X5XH18-10. У цьому дослідженні проаналізовано три параметри процесу: швидкість (v), подача (f), сила вигладжування (F). Значення цих параметрів було обрано відповідно до методу повного факторного планування експериментів. У цьому дослідженні вимірювали 4 параметри у кожній установці. Перший – це глибина напруження, що є глибиною, на якій виникає напруження по Мізесу не менше 350 МПа, що в 1,5 рази перевищує межу міцності матеріалу. Другий – глибина вигладжування, яка вимірює порушену глибину відповідно до перпендикулярного напруження (напруження Y-Y в позначеннях програми). Третє значення – ширина полірування, яка вимірює задіяну ширину відповідно до напруження зсуву (напруження Y-Z в позначенні програми). Останнім параметром, що вивчався, є максимальне значення тиску, що виникає в поверхневому шарі при вигладжуванні. Автори дійшли висновку, що збільшення перпендикулярної сили дає зростаючу дію на ці параметри, проте можна побачити більше збільшення глибини впливу, ніж глибини напруження. Збільшення поверхневої швидкості призвело до цікавого відкриття. У той час як збільшення швидкості в 1,5 раза призвело до збільшення глибини напружень в середньому в 1,2 раза, глибина впливу залишилася незмінною. Подвоєння подачі призводить до збільшення глибини напружень в середньому в 1,25 рази, у той час як глибина впливу збільшується тільки при більш високих налаштуваннях навантаження і залишається майже незмінною, якщо зусилля вигладжування було відрегульовано до 30 Н. Зміна поверхневої швидкості дуже слабко впливає на ці параметри (зміна 0–16%). Однак збільшення подачі значно впливає на порушену ширину. При збільшенні подачі 1,5 разу спостерігається збільшення ураженої ширини в 1,2–1,8 рази. Ефект зміни сили вигладжування залежить від величини подачі. Як і очікувалося, максимальне значення тиску збільшується зі збільшенням сили вигладжування: збільшення останньої в 1,33 рази призводить до збільшення середнього тиску в 1,2 рази.*

Ключові слова: *вигладжування; план експерименту; МКЕ-моделювання.*

UDC 621.914.1 **doi: 10.20998/2078-7405.2022.97.13**

T. Makkai**,** Miskolc, Hungary

FACE MILLING OF STEEL WITH OCTAGONAL INSERT

Abstract. *Face milling is often used to create flat surfaces, since when used as finishing, a suitable surface roughness can be achieved by fulfilling the specified dimension and tolerance requirements. In addition, high productivity can be reached by choosing the appropriate parameters of the cutting process. The cutting data also affect the cutting force and the wear of the tool, and another consideration is that the resulting vibrations can deteriorate the microgeometry of the surface. Several insert shapes are available for face milling. Experiments were carried out with a milling head equipped with a single octagonal insert. The effect of increasing the feed per tooth was examined through the cutting force components, while keeping the cutting speed and depth of cut fixed. The changes in the specific cutting force components were also analysed.*
Keywords: *face milling; octagonal insert; feed per tooth; cutting forces; specific cutting forces.*

1. INTRODUCTION

Workpiece surfaces machined with face milling are characterized by a high degree of precision and good surface quality, that is why face milling is well liked as a machining process. The productivity of face milling can be increased by increasing the feed rate [1,2]. This can be achieved by increasing two technological parameters, the spindle speed and the feed per tooth [3]. The effect of the forces arising during cutting not only appears on the workpiece (when the chip is being formed); the cutting force also loads the tool, the clamping devices and the machine. The magnitude of the cutting force and its prediction are important from the point of view of the entire machining system.

A novel approach to the theoretical modelling of cutting forces was presented by Zheng et al. in face milling [4]. The operation of the cutter was modelled as the simultaneous operation of several single-edged cutting tools. Subramanian et al. developed a statistical model that predicts cutting force based on cutting speed, feed, and axial depth of cut [5]. They found that cutting speed was the dominant factor in the second-order models, followed by feed and axial depth of cut. Higher cutting speed, lower feed and smaller axial depth of cut resulted in lower cutting force. Čekić et al. investigated the effect of cutting parameters [6]. They found that increasing the cutting speed causes a decrease in the cutting forces, and the feed per tooth has a significant effect on the value of the cutting forces. Chuangwen et al. performed milling experiments under different process conditions with a coated carbide end mill insert on stainless steel [7]. It was found that among the process factors, tool wear and depth of cut significantly affect the cutting force and vibration. Ghorbani and Moetakef-Imani presented a new method for determining specific cutting force coefficients for face milling with circular inserts [8].

An inverse method was proposed to solve the equations of the mechanical force model using a genetic algorithm. The interaction of the cutting speed, the feed per tooth and the depth of cut with the changes in the tangential and radial coefficients of the specific cutting force were examined. They found that, under given cutting conditions, the edge geometry of the circular insert significantly affects the value of the coefficients. Nguyen presents a cutting force modelling method and a combined approach of theoretical and experimental methods in the face milling process with a parallelogram insert [9]. Kundrák et al. examined the effect of different insert geometry characteristics on the cutting force and the values of the specific cutting force components in the case of face milling [10]. The aim was to determine the insert with the appropriate cutting edge geometry that results in the lowest energy consumption for the same material volume removed. Kundrák et al. studied the energetic characteristics of milling with special attention to the shape of the cross-section removed by the tool [11]. It was found that it is advantageous from an energetic point of view if the applied chip ratio is as small as possible. Felhő presented a study about the finite element modelling of cutting force components acting on the workpiece in face milling [12], introducing a method for measuring the cutting edge radius of an insert using an optical method. The simulated cutting force values and real measurement data were compared and good correlation was found.

In this paper, the effect of feed per tooth on the cutting force components was investigated during face milling with an octagonal milling insert. The change in the specific cutting force components which characterizes the specific energy consumption, was also examined.

2. METHODOLOGY

In the cutting experiment presented in this paper, the change in the cutting force during face milling of C45 carbon steel was examined. A single octagonal coated carbide milling insert was clamped in the milling head. The reason for this was that the cutting force could be measured without the interaction of the other inserts, because only one insert was working at a time. The devices used in the experiment are summarized in Figure 1.

The face milling experiments were performed by setting a constant cutting speed and a constant depth of cut. The variable parameter was the feed per tooth, which was set to six values between 0.1 and 1.6 mm/tooth. The workpiece was fixed to the dynamometer on the table of the milling machine with screws. According to the spatial Cartesian coordinate system, the dynamometer generated the cutting force signals in three directions (x – the same direction as the feed direction, y – the direction perpendicular to the feed direction, z – the direction perpendicular to the x and y directions), which were amplified by the three charge amplifiers and then transmitted by the data collection unit to the computer. The

special measuring software running on the computer was written in the LabVIEW system-design platform, which was used to obtain the measurement data for evaluation.

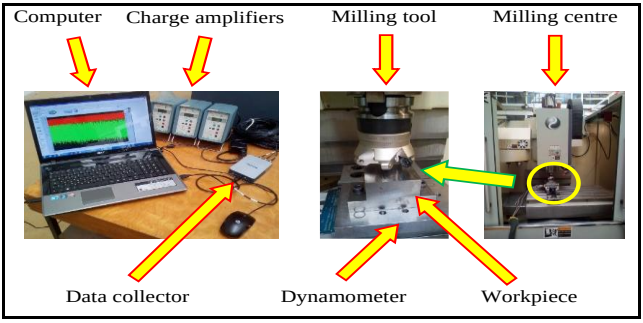

Figure 1 – Experimental equipment [13]

Table 1 – Types and characteristic parameters of experimental devices

Machine tool	
Vertical machining centre	Perfect Jet MCV-M8
Tool	
Milling head	ATORN 10612120 (D=80 mm, κ_r=43°)
Insert	ATORN OCKX 0606-AD-TR HC4640 (γ_o=25°; α_o=7°; r_ε=0.5 mm)
Workpiece	
Material	C45 (1.0503) carbon steel, normalized, hardness HB180
Dimension	cutting width 58 mm, cutting length 50 mm
Cutting force measuring equipment	
Dynamometer	Kistler 9257A
Charge amplifiers	Kistler 5011A (3 pcs)
Data collector	CompactDAQ-9171 (National Instruments)

The specifications of the milling machine, milling tool, workpiece and the elements of the force measuring system used in the experiment can be seen in

Table 1. The path of the tool was programmed in relation to the workpiece in such a way as to realize symmetrical milling.

The cutting data of the face milling experiments were chosen in such a way that the effect of the feed change on the cutting force could be examined and analysed. Additional setting parameters affecting the cutting force (cutting speed and depth of cut) were set at a constant value in the range of parameters recommended by the manufacturer of the milling insert. Table 2 summarizes the cutting data set on the milling machine during the experiments.

Table 2 – Summarized cutting data

Cutting data		
Cutting speed	v_c	200 m/min
Spindle speed	n	901.4 rev/min
Feed per tooth	f_z	0.1, 0.2, 0.4, 0.8, 1.2, 1.6 mm/tooth
Depth of cut	a_p	0.4 mm

3. RESULTS AND DISCUSSION

The experimental data were processed. From the measured forces F_x, F_y, F_z (acting on the workpiece) the load on the tool was calculated with the values of F_c (tangential), F_f (radial) and F_p (perpendicular to F_c and F_f, also known as passive) force components operating in the coordinate system rotating with the tool. The values of the measured and calculated force components are illustrated in Table 3.

By showing the values in Table 3 in a diagram, the change in the components of the cutting force becomes clearer. The change in the cutting force components acting on the workpiece (measured values) is shown in Figure 2, and the change in the cutting force components acting on the tool (calculated values) is shown in Figure 3. In both figures, it can be observed that the value of each force component increases with increasing feed per tooth, but it is also clear that the growth is not directly proportional: doubling the feed per tooth shows a smaller increase in each force component, and the force components also change differently compared to each other.

This finding is even more illustrative if the minimum and maximum values of the test range are highlighted. A 16-fold increase in the feed per tooth (from f_z=0.1 to 1.6 mm/tooth) causes a 5.6-fold increase in the force component F_x (from 117 *N* to 657 *N*), a 7.7-fold increase in the force component F_y (from 147 *N* to 1138 *N*), a 4.4-fold increase in the force component F_z (from 119 *N* to 522 *N*), a 8.6-fold increase in the force component F_c (from 128 *N* to 1091 *N*), a 4.2-fold increase in

the force component F_f (from 86 *N* to 356 to *N*) and a 4.4-fold increase in the force component F_p (from 119 *N* to 522 *N*).

Table 3 – Values of measured and calculated force components

Feed per tooth	Force components					
	Measured			Calculated		
f_z	F_x	F_y	F_z	F_c	F_f	F_p
mm/tooth	*N*	*N*	*N*	*N*	*N*	*N*
0.1	117	147	119	128	86	119
0.2	166	221	152	201	108	152
0.4	247	361	207	337	148	207
0.8	385	616	300	589	209	300
1.2	512	874	398	838	269	398
1.6	657	1138	522	1091	356	522

In the following, the effect of increasing feed per tooth on the change in the components of the specific cutting force also was examined. The specific cutting force gives the energy required to remove a unit volume of chips, so the relationship between the feed per tooth and the energy requirement of face milling can also be explored. The specific cutting force can be calculated as the ratio of the cutting force and the cross section of the chip. The results of the calculations are shown in Figures 4 and 5.

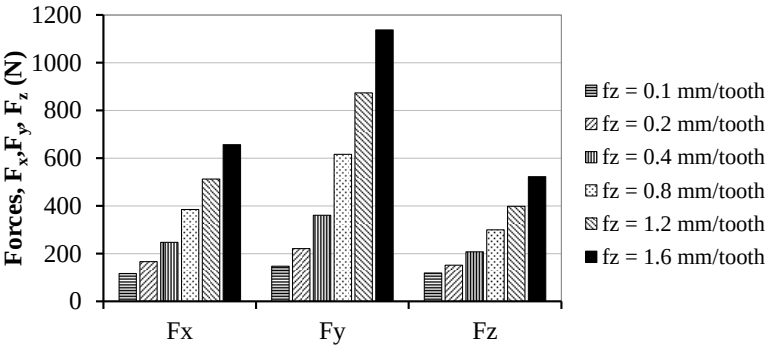

Figure 2 – Measured cutting force components at different feed rates

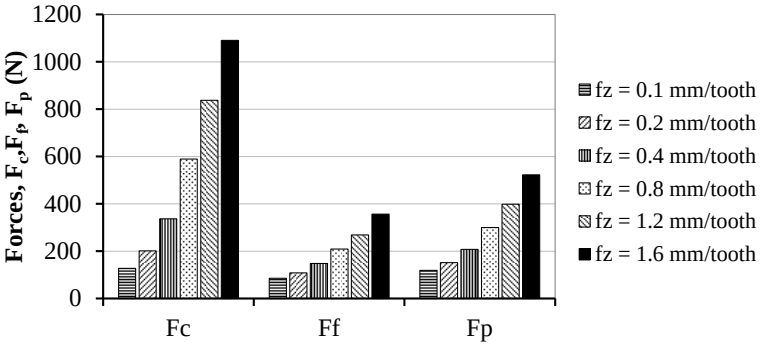

Figure 3 – Calculated cutting force components at different feed rates

From the figures, it can be observed that the value of all specific cutting force components decreases with increasing feed per tooth. Another characteristic of the diagrams is that in the case of f_z<0.4 mm/tooth, this decrease is exponential, while in the case of f_z>0.4 mm/tooth, it can be considered almost linear. Numerically, based on the diagrams, it was found, taking into account the minimum and maximum values of the test range, increasing the feed per tooth by a factor of 16 (from f_z=0.1 to 1.6 mm/tooth) decreased the specific force component k_x to 35% (from 2914 N/mm^2 to 1026 N/mm^2), the specific force component k_y to 48% (from 3677 N/mm^2 to 1777 N/mm^2), the specific force component k_z to 27% (from 2970 N/mm^2 to 816 N/mm^2), the specific force component k_c to 53% (from 3188 N/mm^2 to 1704 N/mm^2), the specific force component k_f to 26% (from 2145 N/mm^2 to 557 N/mm^2) and the specific force component k_p to 27% (from 2970 N/mm^2 to 816 N/mm^2). Also it was found that increasing the feed per tooth causes a decrease in the specific energy requirement. An additional advantage of increasing some cutting parameter values, e.g. the feed rate [14], results in the increasing productivity, which is the major objective of manufacturing processes in the automotive industry [15].

Using our previous research results [16], the effect of the change in the chip cross-section on the force components was examined. In our previous research, the chip cross-section could be determined according to the relation $A_c=a_p \cdot f_z=0.8 \cdot f_z$, in our current research it is $A_c=a_p \cdot f_z=0.4 \cdot f_z$. During the examination of the force components and the specific force components, a ratio number was created, which can be calculated as the ratio of the force values corresponding to the depth of cut a_p=0.8 mm and the force corresponding to the depth of cut a_p=0.4 mm. The results of the calculations are presented in Figures 6 and 7.

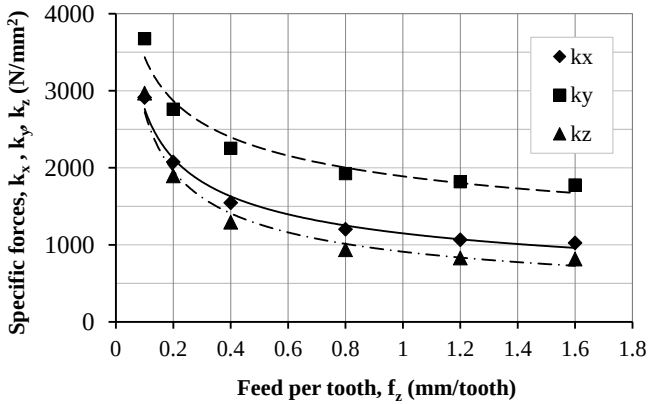

Figure 4 – Specific cutting forces k_x, k_y and k_z at different feed rates

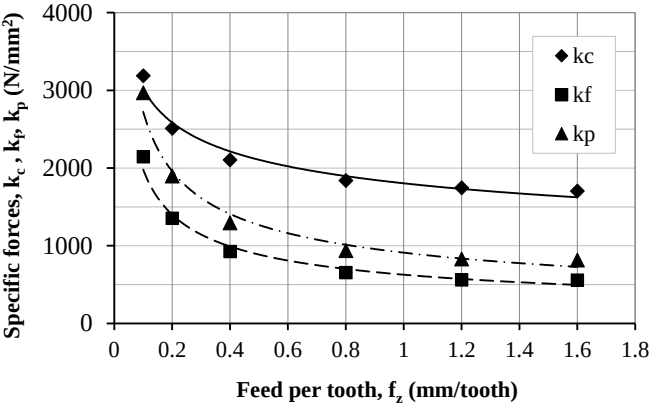

Figure 5 – Specific cutting forces k_c, k_f and k_p at different feed rates

The theoretical chip cross-section doubles are due to the double depth of cut; theoretically, the increase in force is also proportional to this. Based on the experiments, it was found that the ratio for the F_x, F_y and F_c force components is 166–188%, for the F_f force component it is approximately double (197–213%), and for the F_z (which is the same as F_p) force component it is significantly higher (257–304%). It was found that in the case of the tested feed per tooth values, F_x, F_y and F_c force components were 12–34% lower than the theoretical values, and the effect of feed per tooth is not significant. In the case of the ratio of the F_z force component, however, a significant increase was experienced, which decreases with the increase in feed per tooth. Examining the specific force components, higher

values can also be observed in the case of the ratio of the k_z component (129–152%). An increase in feed per tooth caused a decrease in the ratio of the specific force component.

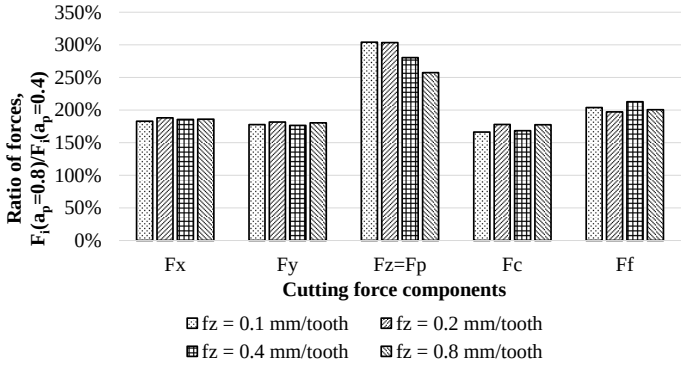

Figure 6 – Ratio of force components at different feed rates

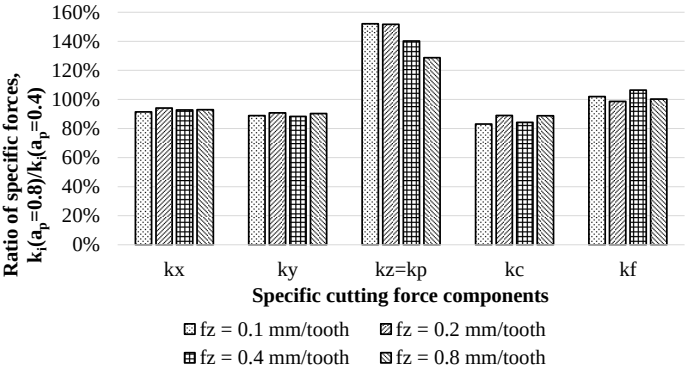

Figure 7 – Ratio of specific force components at different feed rates

4. CONCLUSIONS

In this study, a face milling experiment with an octagonal insert and its results were presented. Among the cutting data, only the feed per tooth was changed and six different values were set between 0.1 and 1.6 mm/tooth. After evaluating the experimental results, the following conclusions were made:

- By increasing the feed per tooth, the value of each force component increased.
- This increase is not directly proportional. Doubling the feed per tooth showed a smaller increase in each force component.
- The force components also changed differently compared to each other.
- Increasing the feed per tooth by 16-fold (from f_z=0.1 to 1.6 mm/tooth) caused a 4.2–8.6-fold increase in the force components.
- By increasing the feed per tooth, the value of the specific cutting force components decreased. This decrease is exponential in the case of f_z<0.4 mm/tooth, while it can be considered almost linear in the case of f_z>0.4 mm/tooth.
- Increasing the feed per tooth by 16-fold caused a decrease in the specific force components to 26–53%, that is, increasing the feed per tooth caused a decrease in the specific energy requirement.
- Using our previous research results, it was found in the test range that for the F_x, F_y and F_c force components, the values of the depth of cut were 12–34% smaller than the theoretical double values, and the effect of the feed per tooth is not significant. In the case of the ratio of the F_z force component, on the other hand, there was a significant increase, which decreased with the increase in feed per tooth. In terms of specific force components, a higher ratio (129-152%) in the case of the k_z component was also observed. An increase in feed per tooth caused a decrease in the ratio of the specific force component.

References: 1. *Karpuschewski, B., Kundrák, J., Emmer, T., Borysenko, D.*: A new strategy in face milling - inverse cutting technology, Solid State Phenomena, 261, pp. 331-338, 2017. **2.** *Borysenko, D., Karpuschewski, B., Welzel, F., Kundrák, J., Felhő, C.*: Influence of cutting ratio and tool macro geometry on process characteristics and workpiece conditions in face milling, CIRP Journal of Manufacturing Science and Technology, 24, pp. 1-5, 2019. **3.** *Karpuschewski, B., Kundrák, J., Felhő, C., Varga, G., Sztankovics, I., Makkai, T.*: Preliminary investigations for the effect of cutting tool edge geometry in high-feed face milling, Vehicle and Automotive Engineering 2, pp. 241-254, 2018. **4.** *Zheng, H. Q., Li, X. P., Wong, Y. S., Nee, A. Y. C.*: Theoretical modelling and simulation of cutting forces in face milling with cutter runout, International Journal of Machine Tools and Manufacture, 39 (12), pp. 2003-2018, 1999. **5.** *Subramanian, M., Sakthivel, M., Sooryaprakash, K., Sudhakaran, R.*: Optimization of cutting parameters for cutting force in shoulder milling of Al7075-T6 using response surface methodology and genetic algorithm, Procedia Engineering, 64, pp. 690-700, 2013. **6.** *Čekić, A., Begić-Hajdarević, Đ. & Kulenović, M.*: Effect of the cutting parameters on cutting forces in high speed face milling, Tehnicki Vjesnik, 20 (5), pp. 775-780, 2013. **7.** *Chuangwen, X., Jianming, D., Yuzhen, C., Huaiyuan, L., Zhicheng, S., Jing, X.*: The relationships between cutting parameters, tool wear, cutting force and vibration, Advances in Mechanical Engineering, 10 (1), pp. 1-14, 2018. **8.** *Ghorbani, H., Moetakef-Imani, B.*: Specific cutting force and cutting condition interaction modeling for round insert face milling operation, International Journal of Advanced Manufacturing Technology, 84 (5-8), pp. 1705-1715, 2016. **9.** *Nguyen, N.-T.*: A development method of cutting force coefficients in face milling process using parallelogram insert, EUREKA: Physics and Engineering, 5, pp. 36-52, 2021. **10.** *Kundrák, J., Markopoulos, A. P., Makkai, T., Karkalos, N. E.*: Effect of edge geometry on cutting forces in face milling with different feed rates, Manufacturing Technology, 19 (6), pp. 984-992, 2019. **11.** *Kundrák, J., Karpuschewski, B., Pálmai, Z., Felhő, C., Makkai, T., Borysenko, D.*: The energetic

characteristics of milling with changing cross-section in the definition of specific cutting force by FEM method, CIRP Journal of Manufacturing Science and Technology, 32, pp. 61-69, 2021. **12.** *Felhő, C.*: Finite element modelling of cutting force components in face milling, Multidiszciplináris tudományok, 10 (1), pp. 119-128, 2020. **13.** *Makkai, T.*: A forgácsolóerő vizsgálata nyolcszögletű lapkával végzett homlokmarásnál, Multidiszciplináris tudományok, 10 (3), pp. 285-293, 2020. **14.** *Kundrák, J., Molnár, V., Deszpoth, I., Makkai, T.*: Effect of cutting data selection on productivity in face milling, Cutting & Tools in Technological System, 88, pp. 101-106, 2018. **15.** *Molnár, V., Deszpoth, I., Kundrák, J., Markopoulos, A. P.*: Efficiency of material removal and machining in cutting, Cutting & Tools in Technological System, 92, pp. 35-47, 2020. **16.** *Makkai, T.*: Oktagonális lapka alkalmazása során mért forgácsolóerő vizsgálata és összehasonlítása más lapka geometriákkal homlokmarás esetén, Multidiszciplináris tudományok, 10 (4), pp. 292-301, 2020.

Тамаш Маккай, Мішкольц, Угорщина

ТОРЦЕВЕ ФРЕЗУВАННЯ СТАЛІ ВОСЬМИГРАННОЮ ПЛАСТИНОЮ

Анотація. *Торцеве фрезерування часто використовується для створення плоских поверхонь, тому що при використанні його в якості чистової обробки можна досягти відповідної шорсткості поверхні, виконавши зазначені вимоги до розмірів та допусків. Крім того, висока продуктивність може бути досягнута за рахунок вибору відповідних параметрів процесу різання. Режими різання також впливають на силу різання та знос інструменту, і ще одне міркування полягає в тому, що вібрації, що виникають, можуть погіршити мікрогеометрію поверхні. Для торцевого фрезерування доступні пластини кількох форм. Експерименти проводилися з фрезерною головкою, оснащеною одинарною восьмигранною пластиною-вставкою. Ефект збільшення подачі на зуб досліджувався через компоненти сили різання при фіксованих швидкості та глибині різання. Додаткові параметри налаштування, що впливають на силу різання (швидкість різання та глибина різання), задавалися постійними в діапазоні параметрів, рекомендованих виробником фрезерної пластини. З експериментів встановлено, що за рахунок збільшення подачі на зуб збільшувалося значення кожної складової зусилля. Це збільшення не є прямо пропорційним. Подвоєння подачі на зуб показало менше збільшення кожної складової зусилля. Складові сили по-різному змінювалися в порівнянні один з одним. Збільшення подачі на зуб у 16 разів (від f_z=0,1 до 1,6 мм/зуб) призвело до збільшення складових зусиль у 4,2–8,6 разів. При збільшенні подачі на зуб зменшувалась величина питомих складових сили різання. Це зменшення носить експоненційний характер у разі f_z<0,4 мм/зуб, тоді як у випадку f_z>0,4 мм/зуб його вважатимуться практично лінійним. Збільшення подачі на зуб у 16 разів спричинило зниження питомих складових сили до 26–53 %, тобто збільшення подачі на зуб спричинило зниження питомої енергоємності. Використовуючи результати попередніх досліджень, у діапазоні випробувань було встановлено, що для силових складових F_x, F_y та F_c значення глибини різання були на 12–34 % меншими від теоретичних подвійних значень, а вплив подачі на зуб значення не має. З іншого боку, у разі складової сили F_z спостерігалося значне збільшення, яке зменшувалося із збільшенням подачі на зуб. За питомою складовою сили також спостерігалося більш високе співвідношення (129-152 %) у разі k_z-складової. Збільшення подачі на зуб викликало зменшення відношення питомої складової сили різання.*

Ключові слова: *торцеве фрезерування; восьмикутна вставка; подача на зуб; сили різання; питомі сили різання.*

UDC 621.91.01 **doi: 10.20998/2078-7405.2022.97.14**

I. Sztankovics, I. Pásztor**,** Miskolc, Hungary

PRELIMINARY ANALYSIS OF SURFACE TOPOGRAPHY IN TANGENTIAL TURNING

Abstract. *Among the productivity-increasing high feed turning procedures, the tangential turning is studied in this paper. Our main focus was a preliminary analysis of the machined surface topography by the DoE method. To achieve this goal 2 kinds of cutting speed, feed and depth of cut were chosen as factors which are influence the surface topography, resulting in 8 experimental setups. After the cutting experiments 2D profile measurements and shape error measurements were done. In this paper the Ra, Rz parameters of the roughness profile, Wa, Wz parameters of the waviness profile and the straightness error were analysed in more depth. We determined their alteration as a function of the studied parameters and designated our further research directions.*
Keywords: *design of experiments; roughness; straightness; tangential turning; waviness.*

10. INTRODUCTION

Different goals can be achieved by the researchers and development engineers by studying and adjusting the manufacturing processes and systems. An important aim in the automotive engineering is to alter the properties the workpieces in that way which results in the weight reduction and less fuel consumption [1]. Production engineers tend to emphasize the better surface quality and cost reduction [2]. The productivity can be increased by procedures, where high feeds can be adjusted while maintaining the good surface quality [3]

In machining of outer cylindrical surfaces, various procedures and variants could produce surfaces with high feed [4]. Among these we analyse the tangential turning in this paper [5], where the design of the cutting tool and the machining kinematic are both differ from the traditional longitudinal turning (Figure 1). The tool moves on a course which is tangential to the workpiece and the linear cutting edge is inclined to the feeding motion (usually 30-60°).

Tangential turning is capable to machine rotationally symmetric shaped surfaces with a proper edge profile, among the production of outer cylindrical surfaces. In the former case, calculations must be done based on the workpiece profile to describe the cutting edge. Though, a straight cutting edge is sufficient in the latter. However, this edge should be inclined to the feed motion to achieve better cutting conditions and lower loads. Tool life is significantly better than in traditional turning [7] due to the different geometry and kinematics. Tool wear occurs on the whole cutting edge, a concentration point can not be observed. Due to the many differences, machine tools have different requirements like higher rigidity [8].

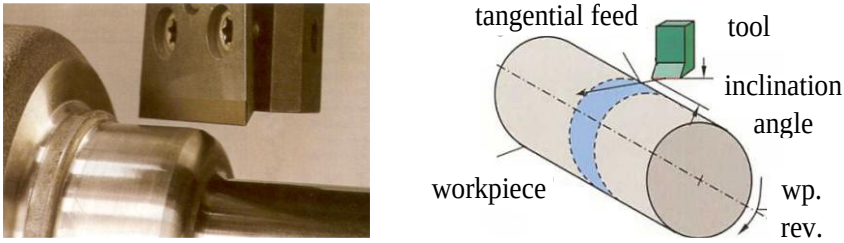

Figure 1 – Tangential turning and its kinematic scheme [6]

The main reason of this is the alteration of the ratios and values of the cutting force components due to the modification of the feed movement and the increased danger of vibration due to the increased chip width. Machining accuracy depends on many factors in this procedure as well [9], for example the value of the inclination angle, the tangential feed, or the depth of cut. Twist-free surfaces can be produced [6] because the cutting edge touches the coating cylinder of the workpiece machined surface throughout the machining process, so a very small groove depth can be achieved. Leichner et al. have promising results in the tool wear, oil leakage and cost reduction when sealing surfaces are machined by tangential turning in their study [10]. Developments are being carried out for the application of this procedure in the machining of hardened surfaces [11], the EMAG machine tool manufacturing company also has such a solution among others [12].

Analysis of the surface topography is important describe the tribological properties of the machined parts [13]. It is usually followed by the study of the surface layer [14,15] due to the life-time prediction, but the geometric properties of the machined parts have a higher impact on the working conditions. Therefore, we carried out a preliminary analysis of the surface topography in tangential turning of hardened surfaces in this paper. We analysed several parameters of the 2D roughness and waviness profiles and the straightness error.

11. EXPERIMENTAL CONDITIONS

The study consisted of two parts: cutting experiments and determining the equations describing the analysed process. The former was completed on a machine tool capable of producing the tangential feed motion, the letter was accomplished by Design of Experiments method.

The cutting experiments were carried out on an EMAG VSC 400 DS hard machining centre. The machined workpieces were 42CrMo4 grade alloyed steels which were hardened to 60 HRc. The machined diameter was 70 mm. The tangential turning tool was made by HORN Cutting Tools Ltd. and had an

inclination angle of 45° (holder code: H117.2530.4132). A S117.0032.00 coded MG12 type uncoated carbide insert was fixed into the holder.
Our aim was to study the effects of the alteration of the cutting speed (v_c), the feed per workpiece revolutions (f) and the depth of cut on the tangential turning process. Therefore (taking into consideration the principles of the Full Factorial DoE method) 2 kinds of each variable were chosen for the experiments, resulting in 8 experimental setups. In this preliminary study we aimed to analyse the process on lower and higher cutting speeds, therefore 100 m/min and 200 m/min values were adjusted. The feed was chosen to 0.3 mm/rev and 0.6 mm/rev and the depth of cut was adjusted to 0.1 mm and 0.2 mm from a similar consideration. The resulted setups can be seen in Table 1.

Table 1 – Experimental setups

Setup	**1**	**2**	**3**	**4**	**5**	**6**	**7**	**8**
v_c [m/min]	100	200	100	200	100	200	100	200
f [mm/rev]	0.3	0.3	0.6	0.6	0.3	0.3	0.6	0.6
a [mm]	0.1	0.1	0.1	0.1	0.2	0.2	0.2	0.2

The necessary measurements were carried out after the experiments. In this paper we intended to analyse the roughness and waviness profiles and the straightness error, because these values describe well the accuracy of a generatrix of the cylindrical surface.
The analysed parameters were (ISO 4287:1997 and ISO 4287:1997):

- R_a – Arithmetical mean height of the roughness profile [μm]
- R_z – Maximum height of the roughness profile [μm]
- W_a – Arithmetical mean height of the waviness profile [μm]
- W_z – Maximum height of the waviness profile [μm]
- *STRt* – straightness error [μm]

The surface roughness was measured with an AltiSurf 520 three-dimensional topography measuring instrument using a confocal chromatic probe. The shape error was measured with a Talyrond 365 accuracy measuring equipment. The variables of the measurement were chosen according to ISO 4288:1996 standard.

The gathered results were evaluated by the Design of Experiments method. By using this we were able to give equations, which are capable to calculate and present the parameters on the studied parameter intervals. These equations were determined in a polynomial form as can be seen in Equation 1, where the k_i are the constant of the different factors.

$$y(v_c, f, a) = k_0 + k_1 v_c + k_2 f + k_3 a + k_{12} v_c f + k_{13} v_c a + k_{23} f a + k_{123} v_c f a \quad (1)$$

12. EXPERIMENTAL RESULTS

The measurements were carried out on the workpieces after the cutting experiments as described in Section 2. The roughness and waviness parameters were measured in 3 profiles on each surface, while the straightness error was measured on 2 opposite generatrix of the machined cylindrical workpiece. The average values of the measured values were calculated. The result of the measurements and the calculations can be seen in Table 2.

Table 2 – Measured results and calculated averages

			1	2	3	4	5	6	7	8
R_z [µm]		1	14.13	3.61	7.63	3.37	9.56	2.60	15.09	3.70
		2	12.41	3.80	9.02	3.20	7.97	2.48	15.75	3.59
		3	15.75	3.86	7.37	3.54	8.16	2.39	17.68	3.89
		Avg.	14.10	3.75	8.01	3.37	8.56	2.49	16.17	3.73
R_a [µm]		1	2.38	0.43	1.22	0.45	1.61	0.30	2.64	0.41
		2	2.14	0.40	1.17	0.43	1.42	0.29	2.83	0.42
		3	2.31	0.43	1.10	0.44	1.43	0.29	2.40	0.42
		Avg.	2.28	0.42	1.17	0.44	1.48	0.29	2.62	0.42
W_z [µm]		1	2.75	0.35	0.15	0.26	1.48	0.57	3.03	0.27
		2	2.23	0.32	0.73	0.34	1.17	0.65	1.84	0.21
		3	1.73	0.41	0.41	0.41	0.94	0.52	2.49	0.27
		Avg.	2.23	0.36	0.43	0.34	1.20	0.58	2.45	0.25
W_a [µm]		1	0.98	0.26	0.13	0.09	0.60	0.42	0.93	0.10
		2	0.91	0.25	0.24	0.14	0.44	0.45	0.56	0.06
		3	0.68	0.27	0.15	0.16	0.40	0.43	0.84	0.08
		Avg.	0.85	0.26	0.18	0.13	0.48	0.43	0.78	0.08
STRt [µm]		1	0.27	0.56	0.58	0.43	0.64	0.61	1.71	0.66
		2	0.54	0.52	0.36	0.61	0.54	0.71	1.83	0.56
		Avg.	0.41	0.54	0.47	0.52	0.59	0.66	1.77	0.61

The evaluation of the results continued by the determination of the equations of the different parameters. Equation 2 presents the calculation of the Arithmetical mean height of the roughness profile; Equation 3 shows the function of the Maximum height of the roughness profile. The equation of the Arithmetical mean height and the Maximum height of the waviness profile can be seen in Equations 4 and 5. Finally, the resulted function of the straightness error is shown in Equation 6.

$$R_a(v_c, f, a) = 12.22 - 0.0579v_c - 22.10f - 58.45a + 0.109v_cf + 0.2805v_ca + 146.3fa - 0.7136v_cfa \quad (2)$$

$$R_z(v_c, f, a) = 71.83 - 0.3240v_c - 125.3f - 355.9a + 0593v_cf + 1.635v_ca + 859.4fa - 4.027v_cfa \quad (3)$$

$$W_a(v_c, f, a) = 5.78 - 0.0289v_c - 11.37f - 31.07a + 0.058v_cf + 0.1751v_ca + 72.78fa - 0.4011v_cfa \quad (4)$$

$$W_z(v_c, f, a) = 16.42 - 0.0828v_c - 33.38f - 87.22a + 0.171v_cf + 0.4624v_ca + 214.2fa - 1.122v_cfa \quad (5)$$

$$STRt(v_c, f, a) = -0.130 - 0.0027v_c - 0.5f - 2.5a + 0.0023v_cf + 0.005v_ca + 7.4 \cdot 10^{-15}fa - 0.0056v_cfa \quad (6)$$

13. DISCUSSION

The experimental results presented in Section 3 are shown in surface diagrams in Figures 2, 4 and 5. Based on these we drew the following conclusions. The cutting speed has a significant impact in the studied range on the Arithmetical mean height of the roughness profile (Figure 2). This proves our initial opinion, that higher cutting speed is needed to achieve smoother surfaces with tangential turning, which phenomenon caused by the chip removal mechanism. Two times higher cutting speed resulted in 2-4-fold lower R_a. The alteration of the feed rate showed less significant change in the surface roughness. This caused by the change in the generation method of the tool marks. At 0.6 mm/rev feed the geometry of the tool can be observed on the profile, while at 0.3 mm/rev the roughness is generated through different phenomenon (chip formation, vibration, etc.). The surface roughness is least affected by the difference in the depth of cut.

The measured profiles of Setups 4, 6, 7 and 8 are presented in Figure 3, where we show the alteration, when one of the studied parameters is halved. The described observation from Figure 2 can also be seen in Figure 3. We can see, that halving the depth of cut does not show any change in the roughness profile. While halving the cutting speed and feed rate in the studied range results in different profiles, which means that a different surface generation method must come to the fore.

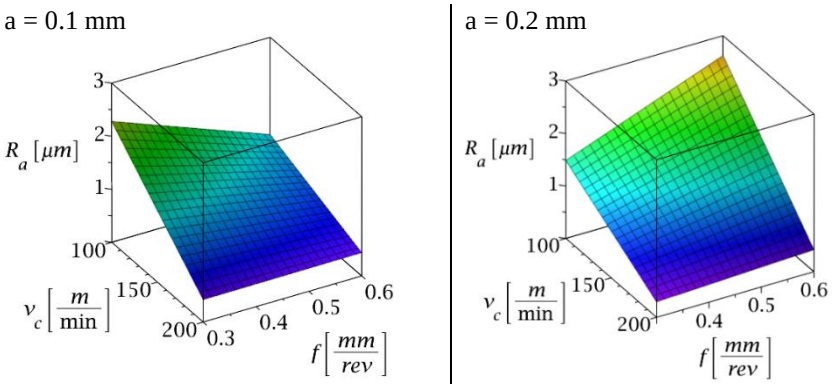

Figure 2 – Visualization of Equation 2 with depth of cut of 0.1 mm and 0.2 mm

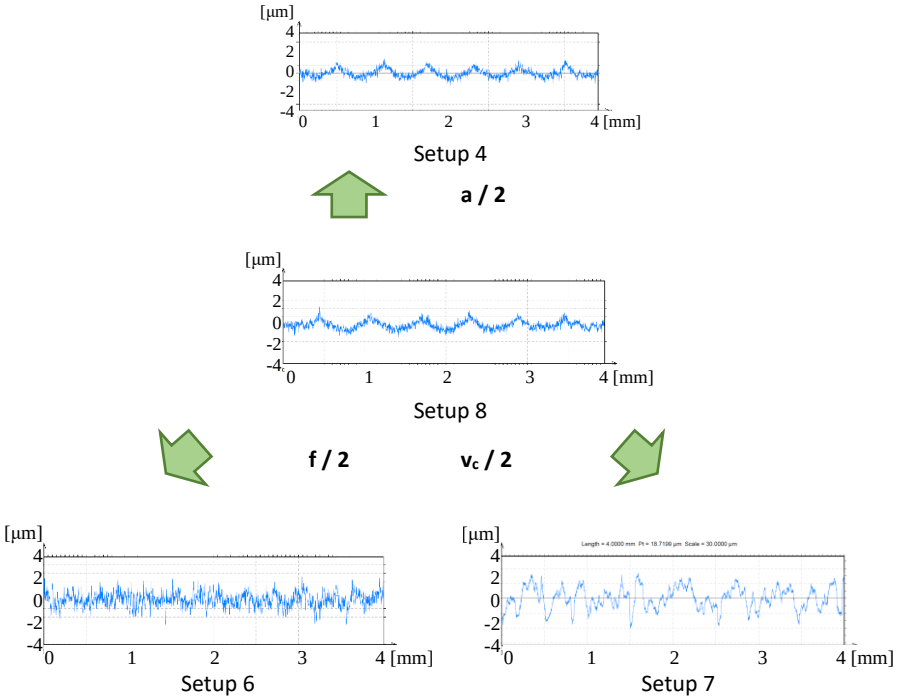

Figure 3 – Alteration from the roughness profile of Setup 8 when halving the studied technological parameters (a, f, v_c)

Figure 4 shows the alteration of the surface waviness. This parameter can indicate a vibration in the machining system, which can easily occur in tangential turning. It can be concluded from the picture that higher feed and cutting speed results in lower waviness. Increasing the feed is good for the cutting, because it stretches the cross-sectional area of the chip by increasing the chip width, which results in higher cutting forces stabilizing the process. Furthermore, it has a beneficial effect on the average chip thickness, which is crucial to be higher than a given value (minimal undeformed chip thickness). Higher cutting speed results in better material removal mechanism, which is discussed earlier. This also lowers the occurring vibrations. Higher depth of cut mostly results in lower waviness. This is caused by the stabilization effect of the increased cutting forces and the direct increasing effect on the chip thickness.

The alteration of the straightness error can be seen in Figure 5. The first conclusion, which can be drawn from the graphs, is the effect of the depth of cut. A two-fold increase of this variable results in a 20% increase of STRt. Furthermore, lower cutting speed and higher feed resulted mostly with lower straightness error.

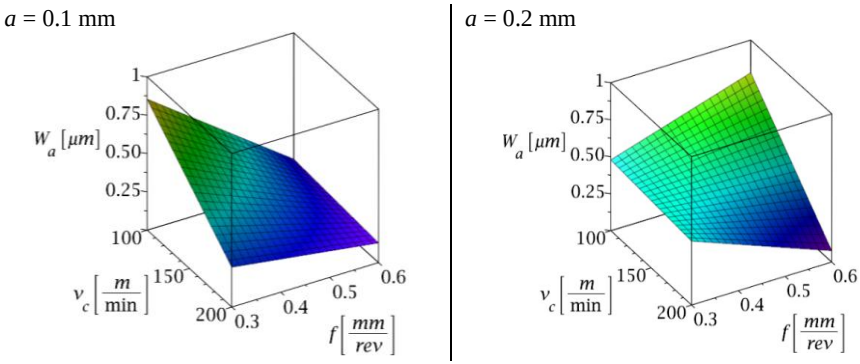

Figure 4 –Visualization of Equation 4 with depth of cut of 0.1 mm and 0.2 mm

The following conclusions can be drawn from the study:

- Higher feed and cutting speed in the analysed range resulted in better surface roughness while it lowered the machining time.
- The depth of cut affects mostly the shape accuracy.
- Other shape error parameters (e. g. cylindricity error) should be studied.
- Further experiments are needed on higher cutting speeds and feeds.

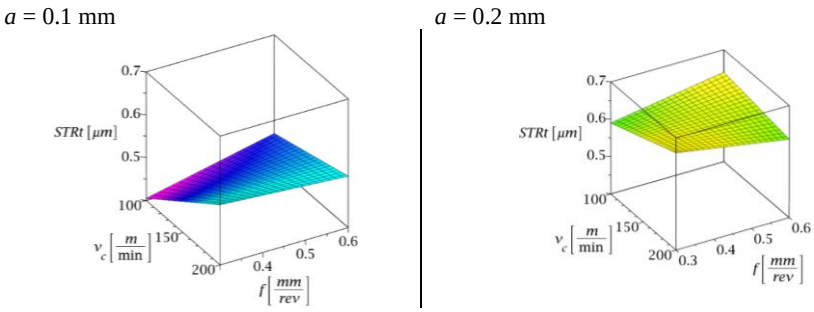

Figure 5 – Visualization of Equation 5 with depth of cut of 0.1 mm and 0.2 mm

SUMMARY

The analysis of the machined surface roughness and shape accuracy is important in finishing procedures. We studied the surface straightness and roughness of tangentially turned outer cylindrical hardened surfaces at different cutting speeds, feeds and depth of cuts. Equations for the calculation of given roughness, waviness and straightness parameters were determined using the Design of Experiments method. In our analysis we determined in detail the alteration of R_a, W_a and *STRt* parameters. The advantage of the application of high feed and cutting speed is shown as well as the increasing effect on the shape error of the depth of cut. In the end of our preliminary study, we determined our further goals in the analysis of tangential turning

ACKNOWLEDGEMENT

Project no. NKFI-125117 has been implemented with the support provided from the National Research, Development and Innovation Fund of Hungary, financed under the K_17 funding scheme.

References: 1. *Kovács, Gy.*: Optimization of structural elements of transport vehicles in order to reduce weight and fuel consumption. STRUCTURAL ENGINEERING AND MECHANICS 71:3 pp. 283-290., 8p. 2019. **2.** *Grewal S.:* Manufacturing process design and costing an integrated approach (1st ed. 2011). Springer London: Imprint: Springer. **3.** *Kundrák, J., Markopoulos, A. P., Makkai, T, Deszpoth, I., Nagy, A.:* Analysis of the Effect of Feed on Chip Size Ratio and Cutting Forces in Face Milling for Various Cutting Speeds. Manufacturing Technology 18/3 pp. 431-438. 2018. **4.** *Kundrák, J., Gyáni, K., Deszpoth, I.:* Precision Hard Turning of External Cylindrical Surfaces by Rotation Procedure. Cutting & Tool in Technological Systems, vol. 77, pp. 108-117, 2011. **5.** *Schreiber, L., Trott, K.:* Verfahren zur drallfreien spanenden Bearbeitung von rotationssymmetrischen Flächen. Patent DE19963897A1, 1999. **6.** *Schneider, J., Schreiber, L.*: Mit dem Tangentialdrehen zu drallfreien Oberflächen. Werkstatt und Betrieb, vol. 6, pp. 40-45, 2002. **7.** *Felho, C., Varga, G.*: Theoretical Roughness Modeling of Hard

Turned Surfaces Considering Tool Wear. Machines. 10(3):188. 2022. **8.** *Fine, L.*: Off centre turning, International Journal of Machine Tool Design and Research. vol. 10, no. 1, pp. 15-24, 1970. **9.** *Nee, A. Y. C., Venkatesh, V. C.:* Form Accuracy of Tangentially Skived Workpieces. CIRP Annals-Manufacturing Tech., vol. 34, no. 1, pp. 121-124, 1985. **10.** *Leichner, T., Franke, V., Sauer, B., Aurich, J. C.:* Investigation of the tribological behavior of radial shaft rings and soft turned shafts under the influence of abrasive particles. Production Engineering, vol. 5, no. 5, p. 531–538, 2011. **11.** *Schubert, A., Zhang, R., Steinert, P.:* Manufacturing of Twist-Free Surfaces by Hard Turning. Procedia CIRP, vol. 7, pp. 294-298, 2013. **12**. *EMAG*: Scroll-Free Turning from EMAG: Fast, Precise, Reliable. EMAG GmbH & Co. KG, [Online]. Available: https://www.emag.com/technologies/scroll-free-turning.html. [Accessed 16. 02. 2021.]. **13.** *Molnar, V.*: Tribological Properties and 3D Topographic Parameters of Hard Turned and Ground Surfaces. Materials.; 15(7):2505, 2022. **14.** *Kundrak, J., Mamalis, AG., Gyani, K., Bana, V.:* Surface layer microhardness changes with high-speed turning of hardened steels. International Journal Of Advanced Manufacturing Technology 53 : 1-4 pp. 105-112. , 8 p. 2011. **15.** *Varga, G., Ferencsik, V.:* Analysis of Surface Microhardness on Diamond Burnished Cylindrical Components. Rezanie I Instrumenty V Tekhnologicheskih Sistemah 90 : 1 pp. 146-152. , 7 p. 2019.

Іштван Станкович, Іштван Пастор, Мішкольц, Угорщина

ПОПЕРЕДНИЙ АНАЛІЗ ТОПОГРАФІЇ ПОВЕРХНІ ПРИ ТАНГЕНЦІЙНОМУ ТОЧІННІ

Анотація. *Різні цілі можуть бути досягнуті дослідниками та інженерами-розробниками шляхом вивчення та коригування виробничих процесів та систем. При обробці зовнішніх циліндричних поверхонь різними методами та варіантами можна отримати поверхні з використанням великих подач. Серед них у цій статті аналізується тангенціальне точіння, де конструкція ріжучого інструменту та кінематика обробки відрізняються від традиційного поздовжнього точіння. Інструмент рухається по дотичній до заготівки, а лінійна ріжуча кромка нахилена до руху подачі (зазвичай 30-60 °). Тангенціальне точіння дозволяє обробляти обертально-симетричні фасонні поверхні з правильним профілем крайки, у тому числі під час виготовлення зовнішніх циліндричних поверхонь. Стійкість інструменту значно вища, ніж при традиційній токарній обробці завдяки іншій геометрії та кінематиці. Зношування інструменту відбувається по всій ріжучій крайці. Дослідження складалося з двох частин: експериментів з різання та визначення рівнянь, що описують аналізований процес. Робота виконувалася на верстаті, здатному виробляти тангенціальний рух подачі, з використанням методів планування експериментів. Після експериментів було проведено необхідні виміри. У цій роботі автори мали намір проаналізувати профілі шорсткості і хвилястості, і навіть помилку прямолінійності, оскільки ці величини добре описують точність циліндричної поверхні. Дослідження показали, що зменшення вдвічі глибини різання не показує жодних змін у профілі шорсткості. Зменшення вдвічі швидкості різання та подачі у досліджуваному діапазоні призводить до різних профілів, а це означає, що на перший план має вийти інший метод формування поверхні. Зміна швидкості подачі показала менш значну зміну шорсткості поверхні. Це спричинено зміною методу генерації слідів інструменту. Вища подача та швидкість різання призводять до меншої хвилястості. За результатами дослідження автори зробили такі висновки: більш висока швидкість подачі та швидкість різання в аналізованому діапазоні призвели до поліпшення шорсткості поверхні та скорочення часу обробки. Глибина різання переважно впливає на точність форми. Слід вивчити інші параметри помилки форми (наприклад, похибка циліндричності). Необхідні подальші експерименти з вищими швидкостями різання та подачею.*
Ключові слова: *планування експериментів; шорсткість поверхні; прямолінійність; тангенційне точіння; хвилястість.*

UDC 621.7 **doi: 10.20998/2078–7405.2022.97.15**

Ya. Garashchenko, O. Harashchenko, Kharkiv, Ukraine

INFLUENCE OF DETERMINATION ACCURACY OF THE BUILD STEP ON THE EFFICIENCY OF ADAPTIVE SLICING GROUP OF PRODUCTS FOR LAYERED MANUFACTURING

Abstract. *Research results on improving the efficiency of the developed algorithm for adaptive layer-by-layer dissection are presented on the example of 3D models group placed in the workspace of an additive setup. This algorithm for 3D model adaptive cutting allows you to increase the productivity of the process and adjust the accuracy of manufacturing products, taking into account their geometry, by setting a rational value of the variable building step for each individual lowering of the work platform. Building step is calculated taking into account the distribution of the direction of surfaces normal of products group (relative to the construction direction) that fall into the current layer. The developed algorithm provides for some truncation of this distribution, which makes it possible to further increase the building step and, accordingly, reduce the number of layers. Thus, conditions can be created for rational support and given reduction in building time. This achieves a reduction in building time compared to existing strategies for variable dissection. Estimate of efficiency of adaptive layer-by-layer dissection was carried out taking into account the accuracy of determining (setting) building step in relation to 5 options for placing 3D models of industrial products in workspace. Comparative analysis of dissection options was performed by the number of layers and assessment of deviations from of surfaces correct shape. Increase in the efficiency of layer-by-layer shaping process with increased accuracy in determining variable step of building a group of complex products placed in workspace of installation has been revealed. This research was developed at the Department of "Integrated Technologies of Mechanical Engineering" named after M. Semko of NTU "KhPI".*

Keywords: *technology planning; additive manufacturing; triangulated model; layered slicing, packing, shaping accuracy.*

Introduction. In planning the additive manufacturing processes, one of the main tasks is layer-by-layer slicing of 3D models of products placed in the installation workspace [1]. The task of slicing quite significantly determines the efficiency of implementing layer-by-layer building processes. For example, the number of layers affects the build time. According to layered building, the product surface has a “stepped” appearance. In this case, the error mainly depends on the layer thickness and the surface orientation relative to the coordinate axis O_Z, i.e. building direction [2].

The result of 3D model separation procedure is a set of section contours and layer thicknesses. A single slice of a polygonal 3D model is formed by crossing the *XY* plane. The solution of this task has two problems: the first is determination of layer thickness, and the second is associated with determination of closed contour geometry or several contours without self-intersections.

Usual cutting strategy is carried out at a given constant building step, i.e. with the same thickness of all layers [3]. This approach does not take into account the

features of the product geometry and therefore leads to a decrease in the accuracy of resulting surfaces or manufacturing productivity. In some cases, ensuring a rational balance between the productivity of layered manufacturing and the accuracy of product surfaces is possible using adaptive slicing 3D models (with a variable building step). In this case, the step is determined based on the analysis of 3D model surface in the current layer according to the given criterion [4].

Literature analysis. In a scientific work [5], comparative analysis of known methods (two main groups: planar and nonplanar) of adaptive slicing 3D models placed in the workspace according to the surface quality, build time, support structure, and mechanical properties of 3D printed products was performed. Planar slicing methods create planar layers, non-planar algorithms create curved and non-planar layers, increasing build speed, eliminating support structures, smoothing the outer surface and improving mechanical properties. Planar algorithms are divided into single-axis and multi-axis (direction of building vector is changed for different layers). Conventional 3D printers provide uniaxial flat layering and are among the absolute majority in additive technology market.

To date, a large number of strategies have been developed for slicing: uniform slicing by set of planes [6], adaptive slicing with description of the section contour by piecewise linear curves [7, 8], piecewise linear approximation [9–12], curved lines [13-15].

Calculation of the adaptive step can be performed together with the correction of the layer contour to minimize the build error [16]. In [17] presents an adaptive slicing, which is based on the extracted amount of candidate feature points for the part model in different areas.

Often, the optimization task of determining the building step for adaptive slicing is performed together with the rational orientation of the product in a workspace [18, 19].

The main problem is that in existing scientific works, the construction step optimization can be carried out according to various criteria. This is due to the multifactorial nature of processes occurring during layer-by-layer construction, which affect their output characteristics, such as productivity and quality of resulting surfaces. But this does not take into account the non-determinism of layer-by-layer construction processes. Hypothetically, this problem can be solved better by taking into account the nature of distribution of values of the selected parameter. In this case, the choice of a parameter as a criterion is not so important. The most important thing when solving the optimization problem is to ensure in the objective function the dependence of the selected criterion on building step and the angle between building direction vector and the surface normal φ_{NZ}, which fall into the cutting plane of layer. Therefore, this problem should be considered based on the distribution density of the angles φ_{NZ} over their relative area [4].

As a rule, to ensure higher efficiency of using additive installation, products are manufactured not individually, but in a group for one or more installation loadings. Therefore, it is interesting to consider the possibilities of an adaptive slicing products group in the workspace.

This article presents the results of an additional study of adaptive slicing effectiveness of 3D models group placed in the workspace based on a statistical analysis of distribution of the angles φ_{NZ}, taking into account the relative surface area, to reasonably determine the step to ensure the specified accuracy and reduce the building time for a batch of complex products.

Purpose and objectives. This article purpose to identify the possibilities of adaptive slicing products group, provided that specified accuracy of shaping is ensured, taking into account the step (discreteness) of setting the layer thickness (i.e., the rounding error of calculated value).

To achieve this goal, the following tasks were solved:

- adaptive slicing 3D models group depending on their orientation and packing in the workspace;
- comparative analysis of options for slicing 3D models group depending on orientation and placement in the workspace, and also the discreteness of setting the layer thickness (building step);
- statistical analysis of deviations distribution from the correct form for various slicing with constant and variable building steps.

Research methodology. The research was carried out using the system of technological preparation for materialization of complex products by additive manufacturing, developed at the Department of Integrated Mechanical Engineering Technologies of NTU "Kharkiv Polytechnic Institute" [4, 19]. This system allows you to evaluate the effectiveness of solving optimization problems of planning additive manufacturing processes based on statistical analysis of studied features of polygonal, voxel and layered 3D model of products placed in the workspace.

One of the most common approaches for determining the building step h_i is to perform a calculation based on given limit Δ_{Limit} for deviations from the correct shape of surfaces specified by 3D model (as a result of the formation of step effect on the surface from layer-by-layer building process) [20, 21]:

$$h_i = \frac{\Delta_{Limit}}{cos\,\varphi_{NZ\,min}},$$

where $\varphi_{NZ\,min}$ is the minimum value of the angles between *Z*-axis (construction direction) and the normals of faces included in current layer.

Research works [4, 19] presented and developed an adaptive strategy for slicing 3D models made individually and by joint group. This research of capabilities of developed algorithm for adaptive slicing was carried out using

examples of loading group of sufficiently large number (more than 20 pcs.) of test 3D models of complex-shaped products, shown in Fig. 1.

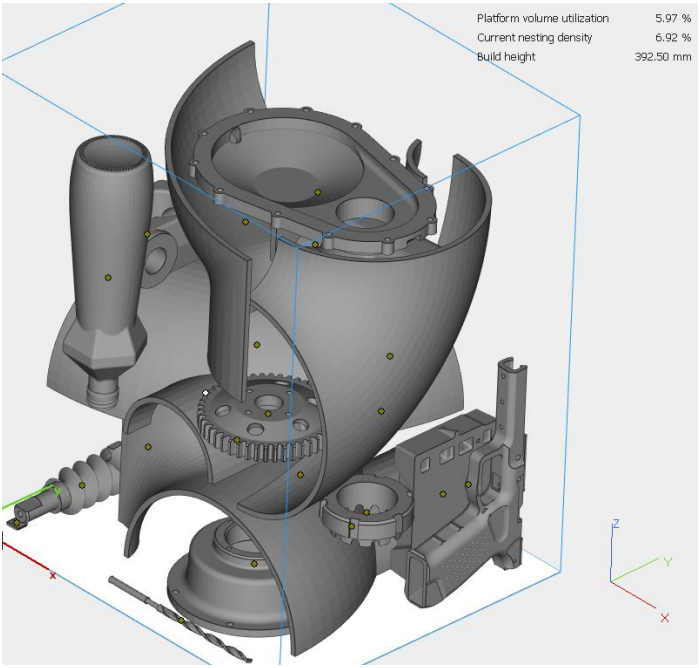

Figure 1 – A group of test 3D models placed in the workspace

Research of the influence of step discreteness of setting the layer thickness on efficiency of using adaptive slicing. In the research, to provide a comparative analysis, a group of test 3D models was dissected for 5 options for their orientation and placement in the workspace according to strategies with constant and variable construction steps. Placement options for 3D models were created in the Materialize Magics system using the EOSPACE automatic placement module. Strategy with constant step was carried out at h_i = {0.05; 0.1} mm. Strategy with variable step at $\{h_i\}_{\min}$ = {0.05; 0.1} mm, $\{h_i\}_{\max}$ = 0.3 mm, and allowable (maximum) error of surface formation Δ_{Limit} = {0.05; 0.1; 0.2} mm. The selected build steps range is wide enough for recommended steps when using SLA setups. The proposed adaptive cutting strategy was performed with a 5% truncation of the angle distribution (this truncation is the optimal value [4, 19]). Based on the results of model calculations, the range diagrams are in Fig. 2.

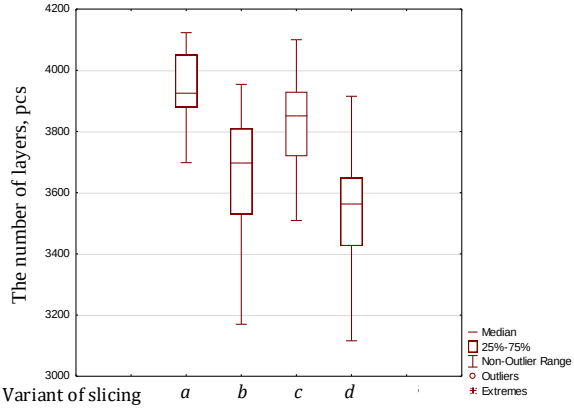

a) *constant; b*) *simpleVariable; c*) *variableNoTrim; d*) *variableTrim*

Figure 2 – Statistical comparative analysis of variants of layer-by-layer slicing with the following parameters: $\{h_i\}_{\min}$ = 0.1 mm, $\{h_i\}_{\max}$ = 0.3 mm and Δ_{Limit} = 0.1 mm

Fig. 2 shows the distribution of layers number with the same load of large batch of products that differ in orientation and packing in the workspace for four cutting strategies: *a* – uniform with a constant step; *b* – adaptive slicing according to analysis in the cutting plane; *c*, *d* – adaptive slicing with preliminary analysis of the surface by microsections (with 0 and 5% truncation of the shaping error distribution, accordingly). The variants of slicing in Fig. 2*a* and Fig. 2*c*. Other variants (Fig. 2*b*, Fig. 2*d*) of adaptive slicing are more demanding on allotting of orientation and packing strategy. But at the same time, the last option related to the developed strategy can provide the least number of layers (accordingly, the building time is minimal). This becomes possible with the rational selection of orientation and products packing in the workspace.

Comparative analysis of the number of layers for all studied options for packing 3D models (Fig. 2) confirms the previously justified [4] advantage of strategies with a variable step (Fig. 2*b*-*d*) compared to constant step (Fig. 2*a*) by 0.1-19.2%.

Adaptive slicing performed without preliminary analysis of the surface by microsection (such adaptive strategy is known from publications [22]) is shown in Fig. 2*b*. It makes it possible to reduce the number of layers relative to dissection with a constant step h_i = 0.1 mm by 19% at best. The developed strategy of dissection (Fig. 2*d*) allows to reduce in different cases from 1.8% to 15.7%, which indicates the importance of joint solution of several tasks of technological preparation. If we compare the number of layers of "VariableTrim" strategy (Fig. 2*d*) concerning "simpleVariable" (Fig. 2*b*), then it is from -11.6% to 11.7%.

The explanation for this result is a more detailed analysis of the geometry of the product surface, which in some cases requires a larger number of layers. Ancillary ambiguity in the results obtained gives the influence of orientation and relative position of the products. In the vast majority of cases (this is 84%), it is possible to obtain better results in terms of the number of layers.

Relative change in the number of layers for different building strategies changes strongly when lower accuracy requirements are set, i.e., when the permissible error doubles (corresponding range diagrams are shown in Fig. 3).

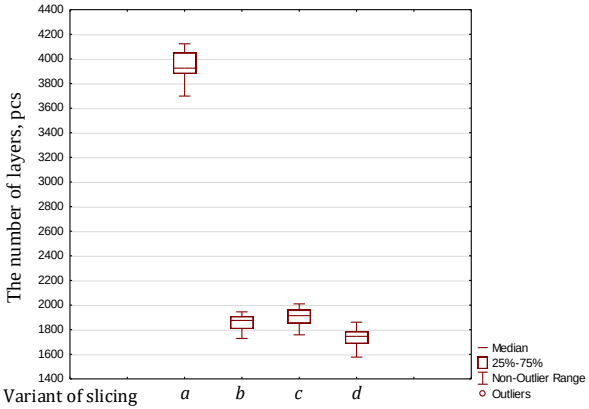

a) constant; b) simpleVariable; c) variableNoTrim; d) variableTrim

Figure 3 – Statistical comparative analysis of options for layered slicing with the following parameters $\{h_i\}_{\min}$ = 0.1 mm, $\{h_i\}_{\max}$ = 0.3 mm and Δ_{Limit} = 0.2 mm

Setting the limit of deviations value Δ_{Limit} = 0.2 mm (Fig. 3) makes it possible to reduce the number of building layers by 50-58%. At the same time, the differences between strategies of adaptive slicing are not so significant - 3.9-9.4%. It is also reasonable (according to the results in Fig. 3 in ratio to the data presented in Fig. 2), we can conclude that when requirements for building accuracy are lowered, the problem of orientation and packing problems is leveled.

In addition, the individual parameters influence on the efficiency of adaptive slicing was considered. With a strong decrease in the minimum building step to $\{h_i\}_{min}$ = 0.05 mm, no fundamental change in the number of layers was observed (within the range from -2.6% to +7.1%). While a decrease in the allowable value of deviations from the correct surface shape Δ_{Limit} = 0.05 mm leads to a change in the number of layers in the range from +62.6% to +108.1%. Therefore, we can conclude that it is necessary to rationally select two parameters $\{h_i\}_{min}$ and Δ_{Limit}.

Concerning the group of test 3D models taken in this study, the rational ratio of these parameters is their equality $\{h_i\}_{min} = \Delta_{Limit}$.

Statistical layered analysis of deviations from the correct surface shape. The use of adaptive slicing implies the provision of a given deviation from the correct shape of resulting product surfaces. Therefore, a layered assessment of deviations from the correct form Δ_S was also carried out according to the arithmetic mean value $\overline{\Delta_S}$. Predicted deviation from the correct shape was taken from the surface asperity formed on the surface as a result of the step effect by layered building [22].

Fig. 4 shows the box-whiskers distributions $\overline{\Delta_S}$ for comparing strategies with a constant step $h_i = 0.10$ mm, and with variable step $\{h_i\}_{min} = 0.1$ mm, $\{h_i\}_{max} = 0.3$ mm and allowable error $\Delta_{Limit} = \{0.1; 0.2\}$ mm at $\Delta\varphi_{NZ} = 5\%$.

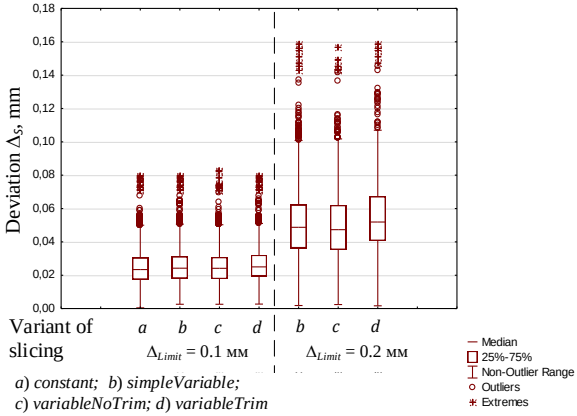

Figure 4 – Results of statistical layer-by-layer analysis of the arithmetic mean deviation from correct surface shape Δ_S

Comparative analysis of statistical layer-by-layer analysis (the result is shown in Fig. 4) was performed on the example of one variant of test 3D models placement. This analysis showed that there were no significant differences in the slicing with variable step, i.e. slicing strategy does not greatly affect the nature of distribution. For most packing options, resulting distribution for a slicing with variable step approximately corresponds to a slicing with constant step $h_i = \{h_i\}_{min}$. Statistical characteristics for Δ_S are mainly determined by the set limit value Δ_{Limit}.

Conclusions. Adaptive slicing 3D models using a statistical analysis of the distribution of angles between the *Z*-axis and the normals of surfaces that fall into

the layer section, taking into account their relative area, taking into account rational orientation and packing can significantly increase the performance of layer-by-layer building.

Adaptive slicing, taking into account an insignificant reduction in the distribution of angles between the *Z*-axis and surface normals by $\Delta\varphi_{NZ}$ = 5%, with high requirements for construction accuracy, it is rational to set the minimum building step equal to the required maximum deviation from the correct shape of resulting product surfaces.

Further research should be directed to the joint solution of technological preparation problems: orientation, packing of products in the workspace, and their adaptive slicing.

References: 1. *Huang J., Qin Q., Wen C., Chen Z., Huang K., Fang X., Wang J.* A dynamic slicing algorithm for conformal additive manufacturing. Additive Manufacturing, 51, 2022, 102622. **2.** *Lin J.Q., Wang Y.B., Jing X., Gu Y.* Research on adaptive slicing algorithm of STL model in additive manufacturing. Machinery Design & Manufacture, 2(2), 2018, 51-53. **3.** *Gibson I., Rosen D., Stucker B., Khorasani M.* Additive manufacturing technologies. Cham (Switzerland): Springer Nature Switzerland AG, 2021, 675 pp. doi: 10.1007/978-3-030-56127-7. **4.** *Garashchenko Y., Zubkova N.* Adaptive slicing in the additive manufacturing process using the statistical layered analysis. Advances in Design, Simulation and Manufacturing III. DSMIE 2020. Lecture Notes in Mechanical Engineering. Springer, Cham. 2020, pp. 253-263. doi: 10.1007/978-3-030-50794-7_25. **5.** *Nayyeri P., Zareinia K., Bougherara H.* Planar and nonplanar slicing algorithms for fused deposition modeling technology: a critical review. Int J Adv Manuf Technol 119, 2022, 2785–2810, doi: 10.1007/s00170-021-08347-x. **6.** *Chalasani K.L., Grogan B.N., Bagchi A., Jara-Almonte C.C., Ogale A.A., Dooley R.L.* An algorithm to slice 3D shapes for reconstruction in prototyping systems, Proceedings of the 1991 ASME Computers in Engineering Conference, 1991, pp. 209-216. **7.** *Dolenc A., Makela I.* Slicing procedures for layered manufacturing techniques, Computer-Aided Design, Vol. 26 No. 2, 1994. pp. 119-126. doi: 10.1016/0010-4485(94)90032-9. **8.** *Sabourin E., Houser S.A., Bohn J.H.* Adaptive slicing using stepwise uniform refinement, Rapid Prototyping Journal, Vol. 2 No. 4, 1996, pp. 20-26. doi: 10.1108/13552549610153370. **9.** *Chen X., Wang C., Ye X. and other*. Direct slicing from PowerSHAPE models for Rapid Prototyping. The International Journal of Advanced Manufacturing Technology, Vol. 17, No. 7, 2001, pp. 543-547. doi: 10.1007/s001700170156. **10.** *Sun S.H., Chiang H.W., Lee M.I.* Adaptive direct slicing of a commercial CAD model for use in rapid prototyping. The International Journal of Advanced Manufacturing Technology, Vol. 34, Nos. 7-8, 2007, pp. 689-701. doi: 10.1007/s00170-006-0651-y. **11.** *Jamieson R., Hacker H.* Direct slicing of CAD models for rapid prototyping. Rapid Prototyping Journal, Vol. 1 No. 2, 1995, pp. 4-12. doi: 10.1108/13552549510086826. **12.** *Sikder S., Barari A., Kishawy H.A.* Global adaptive slicing of NURBS based sculptured surface for minimum texture error in rapid prototyping. Rapid Prototyping Journal, 21(6), 2015, 649–661. doi: 10.1108/rpj-09-2013-0090. **13.** *Cao W., Miyamoto Y.* Direct slicing from AutoCAD solid models for rapid prototyping. The International Journal of Advanced Manufacturing Technology, Vol. 21, Nos. 10-11, 2003. pp. 739–742. doi: 10.1007/s00170-002-1316-0. **14.** *Zhou M.Y., Xi J.T., Yan J.Q.* Adaptive direct slicing with non-uniform cusp heights for rapid prototyping. The International Journal of Advanced Manufacturing Technology, Vol. 23, Issue 1-2, 2004, pp. 20-27. doi: 10.1007/s00170-002-1523-8. **15.** *Jin G.Q., Li W.D., Gao L.* An adaptive process planning approach of rapid prototyping and manufacturing. Robotics and Computer-Integrated Manufacturing, 29(1), 2013, pp. 23–38. doi: 10.1016/j.rcim.2012.07.001. **16.** *Gohari H., Kishawy H., Barari A.* Adaptive variable layer thickness and perimetral offset planning for layer-based additive manufacturing processes. International Journal of Computer Integrated Manufacturing, 34(9), 2021, pp.

964–974. doi: 10.1080/0951192x.2021.1946854. **17.** *Hu B., Jin G., Sun L.* A Novel Adaptive Slicing Method for Additive Manufacturing. 2018 IEEE 22nd International Conference on Computer Supported Cooperative Work in Design. 2018, doi: 10.1109/cscwd.2018.8465247. **18.** *Sheng H., Xu J., Zhang S. et al.* Build orientation optimization for extrusion-based additive manufacturing coupling with adaptive slicing. Int. J. Adv. Manuf. Technol. 2022, doi: 10.1007/s00170-022-10237-9. **19.** *Garashchenko Y., Dasic P.* The Efficiency of Adaptive Slicing Group of Rationally Oriented Products for Layered Manufacturing. Advanced Manufacturing Processes IV. InterPartner 2022. Lecture Notes in Mechanical Engineering. Springer, Cham. 2023, doi: 10.1007/978-3-031-16651-8_10. **20.** *Chen Q., Xu J., Zhang S.* Cylindricity and flatness optimization for mechanical parts in additive manufacturing based on tolerance adaptive slicing. The International Journal of Advanced Manufacturing Technology, 115(11-12), 2021, pp. 3839–3857. doi: 10.1007/s00170-021-07271-4. **21.** *Abdurajimov L.* "Adaptivnoe razdelenie na sloi ishodnoj 3D modeli izdelija v tehnologijah bystrogo prototipirovanija i izgotovlenija [Adaptive slicing of product 3D-model in technology of rapid prototyping and manufacturing]". "Uchenye zapiski Krymskogo inzhenerno-pedagogicheskogo universiteta. Tehnicheskie nauki [Scientific notes of the Crimean Engineering and Pedagogical University. Technical science]", Simferopol: SC CEPU, № 18. 2009, pp. 15-20.

Ярослав Гаращенко, Олена Гаращенко, Харків, Україна

ВПЛИВ ТОЧНОСТІ ВИЗНАЧЕННЯ КРОКУ ПОБУДОВИ НА ЕФЕКТИВНІСТЬ АДАПТИВНОГО РОЗСІЧЕННЯ ГРУПИ ВИРОБІВ ДЛЯ АДИТИВНИХ ТЕХНОЛОГІЙ

Анотація. *Представлено результати дослідження щодо підвищення ефективності розробленого алгоритму для адаптивного пошарового розсічення на прикладі групи 3D моделей, розміщених у робочому просторі адитивної установки. Даний алгоритм адаптивного розсічення 3D моделі дозволяє підвищити продуктивність процесу та регулювати точність виготовлення виробів, з урахуванням їхньої геометрії, за допомогою завдання раціональної величини змінного кроку побудови для кожного окремого опускання робочої платформи. Крок побудови розраховується з урахуванням розподілу напрямку нормалі поверхонь групи виробів, що потрапили до поточного шару. Розроблений алгоритм передбачає деяке усічення даного розподілу, що дозволяє додатково збільшити крок побудови, а відповідно зменшити кількість шарів. Таким чином створюються умови для раціонального забезпечення та заданого зниження часу побудови. При цьому зазвичай одержуючи зменшення часу побудови у порівнянні з традиційною стратегією з постійним кроком побудови та існуючими стратегіями адаптивного розсічення з змінним кроком. Оцінка ефективності адаптивного пошарового розсічення виконувалась з урахуванням точності визначення (завдання) кроку побудови стосовно 5 варіантів розміщення 3D-моделей промислових виробів у робочому просторі. Порівняльний аналіз варіантів розсічення виконувався за кількістю шарів та оцінкою відхилень від правильної форми поверхонь. Виявлено покращення ефективності процесу пошарового формоутворення з підвищенням точності визначення змінного кроку побудови групи складних виробів, розміщених у робочому просторі установки Vanguard SLS (виробництва 3D Systems). Розроблений алгоритм адаптивного розсічення при раціональних параметрах дозволив зменшити кількість шарів побудови при забезпеченні заданих вимог щодо допустимих відхилень від правильної форми поверхонь. Дослідження виконувалося з використанням системи "Технологічна підготовка матеріалізації складних виробів адитивними методами" розробленої на кафедрі «Інтегровані технології машинобудування» НТУ «ХПІ».*

Ключові слова: *технологічна підготовка; адитивні технології; тріангуляційна модель; пошарове розсічення; розміщення групи виробів; точність формоутворення.*

CONTENT

Наукове видання

РІЗАННЯ ТА ІНСТРУМЕНТИ
в технологічних системах

Міжнародний науково-технічний збірник

Випуск № 97

Укладач *д.т.н., проф. І.М.Пижов*
Оригинал-макет *А.М. Борзенко*
Відп. за випуск *к.т.н., проф. Є.В. Островерх*

В авторській редакції

Матеріали відтворено з авторських оригіналів

Підп. до друку 12.12.2022.Формат 60х84 1/16. ПапірСоруРарег.
Друк - ризографія. Гарнитура Таймс. Умов.друк.арк. 10,93. Облік.вид.арк. 11,0. Наклад 30 прим.
1-й завод 1-100. Зам. № 1149. Ціна договірна.

Видавничий центр НТУ «ХПІ»
Свідоцтво про державну реєстрацію ДК № 116 від 10.07.2000 р.
61002, Харків, вул. Кирпичова, 2